

Inaugural dissertation
for
obtaining the doctoral degree
of the
Combined Faculty of Mathematics, Engineering and Natural Sciences
of the
Ruprecht - Karls - University
Heidelberg

Presented by

Fabiola Helena Garcia Cortizo, M.Sc.

Born in: Caracas, Venezuela

Oral examination:

**Regulation of Glo1 activity via tyrosine
phosphorylation and the impact of methylglyoxal on
cellular metabolism**

Referees:

Prof. Dr. Marc Freichel

Prof. Dr. Aurelio Teleman

Table of Contents

List of Figures	V
List of Tables	IX
Summary	XI
Zusammenfassung	XIII
1. Introduction	1
1.1 Glucose metabolism in diabetes.....	1
1.2 Lactate metabolism in diabetes	5
1.3 Structure and function of pyruvate dehydrogenase complex	5
1.4 PDH regulation and diabetes.....	9
1.5 The role of methylglyoxal in protein modifications	12
1.6 MG acts as a signaling molecule.....	16
1.7 The role of MG in diabetes	17
1.8 The Glyoxalase system as a protective mechanism against diabetes.....	19
1.9 Glo1 structure and regulation.....	22
1.10 Alternative pathways of MG detoxification.....	24
2. Aim of the study	27
3. Results	29
3.1 The regulation of Glo1 activity via its phosphorylation	29
3.1.1 Generation of Glo1 KO HeLa and HEK293T cell lines	29
3.1.2 Role of Y136 phosphorylation of Glo1 in stability and activity.....	29
3.1.3 Generation and validation of an antibody against pY136 of Glo1	32
3.1.4 Identification of the kinase responsible for Y136 phosphorylation of Glo1.....	36
3.1.5 Phosphorylation of Glo1(Y136) increases its activity	40
3.1.6 Cellular conditions that regulate Glo1(Y136) phosphorylation in cell culture.....	41
3.1.7 Assessment of Glo1 phosphorylation levels in tissues from diabetic and healthy mice	43
3.2 The impact of MG on cellular metabolism	46
3.2.1 Strategies for the study of MG impact on cellular metabolism	46
3.2.2 MG increases L-lactate production	52
3.2.3 Impact of MG on glucose metabolism.....	55
3.2.4 Impact of MG on PDH activity.....	56
3.2.5 Regulation of PDH activity by MG is not mediated via canonical mechanisms ..	61

3.2.6	MG interacts with several PDH subunits	62
3.2.7	MG modifies PDHA via a CEL adduct	68
3.2.8	MG triggers the oligomerization of DLAT.....	70
3.2.9	MG causes a redox sensitive modification on DLAT.....	76
3.2.10	Impact of MG on mitochondrial respiration	79
3.2.11	MG does not impact the activity of other metabolic enzymes.....	83
3.2.12	MG does not impair PDH activity in kidneys of HGHCi mice	85
3.2.13	MG impairs PDH activity in livers of HGHCi mice.....	86
3.2.14	Low Glo1 expression correlates with decreased PDH activity in Ins2Akita mice	89
4.	Discussion	93
4.1	Glo1 KO cells have higher levels of MG.....	93
4.2	MG regulates its own production.....	94
4.3	Glo1 activity is regulated via glucose sensitive phosphorylation of Y136.....	95
4.4	Redundancy in the mechanism of Glo1 phosphorylation	99
4.5	MG-dependent L-lactate production as a mediator of metabolic syndrome.....	99
4.6	MG decreases PDH activity with important metabolic repercussions.....	101
4.7	Decreased PDH activity caused by MG is not mediated via canonical mechanism	102
4.8	MG triggers important metabolic changes that could lead to diabetes	104
5.	Material and Methods	107
5.1	Antibodies	107
5.2	Generation of the phospho-Glo1(Y136) antibody	108
5.3	Cell culture conditions and treatments.....	108
5.4	RNA extraction, reverse transcription, and qPCR	109
5.5	Plasmids	109
5.6	Plasmids transfections and siRNA knockdowns.....	109
5.7	Generation of Glo1 knockout cells and HEK293T stably transfected cell lines	110
5.8	CRISPR-CAS9 screening	110
5.9	Recombinant human Glo1 protein purification	110
5.10	Cell lysis, immunoblots, and immunoprecipitations.....	111
5.11	Chloroform methanol precipitation.....	112
5.12	Cellular fractionation	112

5.13 Sources of mouse tissue samples, tissue lysis, and tissue mitochondrial fraction purifications	112
5.14 Enzymatic Assays	113
5.15 Measurements of glucose, lactate, and acetyl-CoA	114
5.16 Acyl-PEG assay	115
5.17 Metabolic characterization by Seahorse XF assays	116
5.18 Click chemistry	116
5.19 Statistical analysis	117
6. Abbreviations	127
7. References	129
8. Own publications	145
9. Acknowledgements	147

List of figures

Fig. 1: The glycolytic pathway.....	3
Fig. 2: Pyruvate and NADH link fermentation and cellular respiration with glycolysis.....	4
Fig. 3: Schematic representation of PDH structure.....	8
Fig. 4: Catalytic mechanism of PDH reaction and the lipoyl group cycle.....	8
Fig. 5: Pathways that feed the production of MG.....	14
Fig. 6: Methylglyoxal advanced glycation end products.....	15
Fig. 7: Detoxification mechanisms of methylglyoxal.....	20
Fig. 8: Potential role of Glo1 in diabetes.....	23
Fig. 9: Molecular characterization of the Glo1 KO HeLa and HEK293T cells.....	30
Fig. 10: Glo1 KO cells do not possess Glo1 protein nor activity.....	31
Fig. 11: Mutation of tyrosine 136 to alanine decreases Glo1 activity.....	33
Fig. 12: Mutation of tyrosine 136 to phenylalanine reduces Glo1 activity but has no effect on protein stability.....	34
Fig. 13: Validation of pGlo1(Y136) antibody.....	35
Fig. 14: Identification of the kinases responsible for Y136 phosphorylation of Glo1 by CRISPR-CAS9 screen.....	37
Fig. 15: Glo1 Y136 is phosphorylated by multiple different kinases including all members of the Src family.....	38
Fig. 16: Validation of Src kinase family as responsible for Glo1(Y136) phosphorylation.....	39
Fig. 17: Phosphorylation of Glo1 on Y136 by Src kinases increases its activity.....	40
Fig. 18: Glo1(Y136) phosphorylation does not respond to MG in HeLa or HepG2.....	41
Fig. 19: Glo1(Y136) phosphorylation is sensitive to Glc in HepG2 and U-937 but not HeLa cells.....	42
Fig. 20: Glo1 activity is decreased in hyperglycemic conditions in HepG2 and U-937.....	43
Fig. 21: Glo1(Y136) phosphorylation is decreased in STZ mice.....	44
Fig. 22: Glo1(Y136) phosphorylation is decreased in Ins2Akita mice.....	45
Fig. 23: Glo1(Y136) phosphorylation is decreased in HGHCi mice and possibly in HFD mice.....	46
Fig. 24: Free intracellular MG is not increased in Glo1 KO cells.....	47
Fig. 25: Increased levels of MG adducts in mitochondrial and nuclear fraction of Glo1 KO HeLa cells.....	48

Fig. 26: Increased levels of MG adducts in mitochondrial and nuclear fraction of Glo1 KO HEK293T cells.....	49
Fig. 27: ROS levels are increased in Glo1 KO HeLa and HEK293T cells.....	50
Fig. 28: Optimization of experimental conditions to generate a transient MG increase.....	51
Fig. 29: MG treatment of HEK293T causes an increase in MG adducts.....	52
Fig. 30: L-lactate production is increased in Glo1 KO cells.....	53
Fig. 31: MG treatment increases L-lactate production in WT HeLa cells.....	54
Fig. 32: MG treatment increases L-lactate production in HEK293T cells.....	55
Fig. 33: Glo1 is necessary for normal glucose uptake	57
Fig. 34: Loss of Glo1 increases LDH activity.....	57
Fig. 35: Loss of Glo1 decreases PDH activity	58
Fig. 36: Characterization of WT or CI Glo1 stably transfected HEK293T	58
Fig. 37: PDH activity is decreased in Glo1 knockdown HeLa and HEK293T cells.....	59
Fig. 38: MG inhibits PDH activity in vivo and to a lesser degree in vitro.....	60
Fig. 39: Low glucose condition causes an increase in PDH activity in WT but not in Glo1 KO HEK293T cells.....	60
Fig. 40: MG does not affect PDHA1 phosphorylation	61
Fig. 41: MG does not affect the expression of PDH subunits.....	62
Fig. 42: MG interacts with PDH causing a mixed inhibition effect.....	63
Fig. 43: Schematic representation of MG click chemistry based pull down	65
Fig. 44: MG interacts with different components of PDH complex	66
Fig. 45: MG does not interact with all proteins	67
Fig. 46: MG click it interactions with proteins depend on number of arginine, cysteine, and lysine residues	67
Fig. 47: Flag-PDHA immunoprecipitation pulled down all PDH components	69
Fig. 48: Levels of MG CEL adduct of PDHA are increased in Glo1 KO HEK293T cells.....	70
Fig. 49: MG does not cause stabilizing interactions between PDHA and the E2 subunit component DLAT and E3BP	71
Fig. 50: MG causes oligomerization of DLAT	72
Fig. 51: MG does not crosslink DLAT and E3BP	73
Fig. 52: DLAT antibody specifically recognized the formation of DLAT oligomers	74
Fig. 53: DLAT oligomerization is DTT sensitive	75
Fig. 54: DLAT oligomerization in Flag-tagged WT and CI Glo1-expressing cells shows contradicting results	75

Fig. 55: Acyl-PEG exchange assay.	76
Fig. 56: DLAT shows a DTT sensitive cysteine modifications in Glo1 KO cells.	77
Fig. 57: Other PDH subunits do not show DTT sensitive modifications.	77
Fig. 58: DTT treatment partially rescues the decrease in PDH activity in Glo1 KO HEK293T cells.	78
Fig. 59: Glo1 KO HeLa cells produced more Acetyl-CoA.	80
Fig. 60: Glo1 KO HeLa cells are metabolically more active.	81
Fig. 61: Glo1 KO HeLa cells are incapable of using Palmitate as substrate for respiration...	82
Fig. 62: GAPDH and KGDH activities are unchanged in Glo1 KO HEK293T cells.	84
Fig. 63: Kidneys of Glo1 KO mice show a trend towards decreased PDH activity.	86
Fig. 64: HGHCi kidney samples show decreased PDH activity due to increased phosphorylation of PDHA.	87
Fig. 65: Loss of Glo1 in livers of HGHCi mice causes decreased PDH activity independently of PDHA phosphorylation.	88
Fig. 66: Lack of Glo1 in liver from HGHCi mice causes an increase in the expression of PDHA and PDHB subunits.	89
Fig. 67: Low Glo1 expression correlates with decreased PDH activity in Ins2Akita mice.	90
Fig. 68: PDH activity decrease in kidneys of 6-month old Ins2Akita mice is not due to increased PDHA phosphorylation.	91
Fig. 69: Location of Y136 in Glo1.	96
Fig. 70: Schematic diagram of the positive feedback loop between MG and glucose.	98
Fig. 71: MG production leads to diabetes by mediating important changes in cellular metabolism.	105

List of tables

Tab. 1: Residues of Glo1 reported to be phosphorylated or acetylated in publicly available database	32
Tab. 2: Protein with click it/input ratio and number of arginine, cysteine, and lysine residues present	68
Tab. 3: PDHA1 and DLAT are modified by MG in Glo1 KO HEK293T cell	69
Tab. 4: List of commercial primary antibodies	107
Tab. 5: Oligonucleotides	117
Tab. 6: List of kinase KOs in CRISPR-CAS9 screen	125

Summary

Methylglyoxal (MG) is a byproduct of glucose metabolism that displays high reactivity with many biological macromolecules, in particular proteins, giving rise to adducts known as advanced glycation end products (AGEs). Increased MG and AGEs are commonly observed in diabetes and, among diabetic patients, those affected by diabetic complications show the highest levels of MG and MG-adducts, raising the possibility that, besides hyperglycemia, a buildup of MG could play a direct causative role in the development of diabetes and its complications. Indeed, findings in *Drosophila melanogaster* and *Danio rerio* showed that disruption of glyoxalase I (Glo1), the rate limiting enzyme for MG detoxification, causes features of type 2 diabetes such as insulin resistance, hyperglycemia and obesity. Understanding how the activity of Glo1 is regulated and how exactly MG affects cellular metabolism is thus of the utmost importance to determine how MG detoxification goes awry in diabetes and how the ensuing MG accumulation contributes to the metabolic alterations typical of this disease. To this end, I worked on two complementary lines of investigation aimed at (1) assessing the role of post-translational modifications in the regulation of Glo1 activity and (2) studying which metabolic pathways are affected by high levels of MG in vitro and in mouse models of diabetes. My results show that phosphorylation of Glo1 at Y136 by multiple kinases, including those belonging to the Src family, promotes Glo1 activity. Consistent with impaired detoxification of MG in the pathogenesis of diabetes, I observed that phosphorylation at this residue and overall Glo1 activity are decreased when cells are cultured in high glucose (25 mM), as well as in diabetic mouse models. To study the metabolic alterations caused by MG, I generated cell lines knockout for Glo1 or acutely treated control cells with MG. Interestingly, chronic or acute exposure to MG was sufficient to increase glucose uptake, lactate production and impair fatty acid β -oxidation. I found that MG inhibits the activity of pyruvate dehydrogenase (PDH), probably accounting for the increased glucose uptake and lactate production. The effect of MG on PDH activity is not mediated by altered phosphorylation of PDH, a well-established mode of regulating PDH activity, but rather by direct interaction of MG with the pyruvate dehydrogenase α (PDHA) subunit of PDH, together with formation of a DTT-sensitive modification on the PDH subunit dihydrolipoamide acetyltransferase (DLAT). I also observed decreased PDH activity in mouse models of diabetes, further strengthening the link between accumulation of MG and impaired PDH activity. Overall, my data point to a deleterious positive feedback loop whereby hyperglycemia leads to reduced Y136 Glo1 phosphorylation and activity, contributing to elevated MG levels,

inhibition of PDH and changes of cellular metabolism to promote hyperglycemia and thus further production of MG.

Zusammenfassung

Methylglyoxal (MG) ist ein Nebenprodukt des Glukosestoffwechsels, welches eine hohe Reaktivität mit vielen biologischen Makromolekülen, insbesondere Proteinen, aufweist. Dadurch entstehende Addukte werden als fortgeschrittene Glykationsendprodukte (AGEs) bezeichnet. Erhöhte Konzentrationen von MG und AGE werden häufig bei Diabetes beobachtet. Diabetiker, die von diabetischen Komplikationen betroffen sind, weisen dabei die höchste Menge an MG und MG-Addukten auf. Diese Beobachtungen deuten darauf hin, dass neben Hyperglykämie ein Anstieg von MG eine direkte Rolle bei der Entwicklung von Diabetes und seinen Komplikationen spielen könnte. Studien mit *Drosophila melanogaster* und *Danio rerio* zeigten, dass die Störung von Glyoxalase I (Glo1), dem geschwindigkeitsbestimmenden Enzym für die MG-Entgiftung, zum Auftreten von Merkmalen von Typ-2-Diabetes wie Insulinresistenz, Hyperglykämie und Fettleibigkeit führt. Es ist daher wichtig zu verstehen, wie die Aktivität von Glo1 reguliert wird und wie genau MG den Zellstoffwechsel beeinflusst, um festzustellen, inwiefern die MG-Entgiftung in Diabetes beeinträchtigt ist und wie die daraus resultierende MG-Akkumulation zu den für diese Krankheit typischen Stoffwechselveränderungen beiträgt. Zu diesem Zweck habe ich in meiner Doktorarbeit an zwei komplementären Ansätzen gearbeitet, die darauf abzielten, (1) die Rolle posttranslationaler Modifikationen bei der Regulation der Glo1-Aktivität festzustellen und (2) zu untersuchen, welche Stoffwechselwege von akuten oder chronisch hohen MG-Spiegeln *in vitro* und in Diabetes-Mausmodellen betroffen sind. Meine Ergebnisse zeigen, dass die Phosphorylierung von Glo1 an Y136 durch mehrere Kinasen, einschließlich Mitglieder der Src-Familie, die Enzymaktivität steigern. In Übereinstimmung mit der beeinträchtigten Entgiftung von MG in der Pathogenese von Diabetes konnte ich zeigen, dass diese Glo1 Phosphorylierung und Glo1-Aktivität in Diabetes-Mausmodellen verringert sind und wenn Zellen in Medium mit hoher Glukose Konzentration (25 mM) kultiviert werden. Um die durch MG verursachten metabolischen Veränderungen zu untersuchen, generierte ich Knockout-Zelllinien für Glo1 oder behandelte Zellen akut mit MG. Interessanterweise reichte eine chronische oder akute Exposition von Zellen mit MG aus, um die Glukoseaufnahme und die Laktatproduktion zu erhöhen und die β -Oxidation von Fettsäuren zu beeinträchtigen. Ich fand heraus, dass MG die Aktivität der Pyruvatdehydrogenase (PDH) hemmt, was vermutlich für die erhöhte Glukoseaufnahme und Laktatproduktion verantwortlich ist. Die Wirkung von MG auf die PDH-Aktivität wird dabei wahrscheinlich nicht durch eine veränderte Phosphorylierung von PDH verursacht, einem gut beschriebenen Mechanismus zur

Regulierung der PDH-Aktivität, sondern vielmehr durch eine direkte Wechselwirkung von MG mit der PDH Untereinheit Pyruvatdehydrogenase α (PDHA) zusammen mit der Bildung einer DTT-empfindlichen Modifikation auf der PDH Untereinheit Dihydrolipoamidacetyltransferase (DLAT). Weiterhin habe ich eine verringerte PDH-Aktivität in Mausmodellen für Diabetes beobachtet, was die Verbindung zwischen der Akkumulation von MG und einer beeinträchtigten PDH-Aktivität weiter verstärkte. Insgesamt weisen meine Daten auf eine schädliche, positive Rückkopplungsschleife hin, bei der Hyperglykämie zu einer verringerten Y136-Glo1-Phosphorylierung und daher Glo1-Aktivität führt, was wiederum zu einer erhöhten MG Konzentration, zu einer Inhibierung von PDH und letztendlich zu einer Veränderungen des Zellstoffwechsels führt. Dies fördert Hyperglykämie und damit erneut eine verstärkte Produktion von MG.

1. Introduction

1.1. Glucose metabolism in diabetes

Diabetes mellitus is a chronic disease defined as a metabolic disorder where high blood glucose levels and hyperglycemia are a consequence of insulin insufficiency, impairment of insulin action, or both [1]. The two most important classes of diabetes are type 1 and type 2. Type 1 diabetes is characterized by the absence of insulin due to the β cells that produce insulin being attacked by the immune system. While, type 2 diabetes is considered a systemic dysfunctional metabolic disease in which insulin resistance and/or insufficiency are usually present [1, 2]. Diabetes mellitus has a high prevalence in the worldwide population and individuals with diabetes suffer from a considerable reduction in their quality of life due to the development of diabetes complications [1, 3]. The fast growth, high healthcare cost, and high mortality rates of diabetes make its study of great importance [1, 3].

When diabetes is studied, glucose metabolism needs to be considered, especially glycolysis. Glycolysis is a ten-step process which provides energy and metabolic intermediates to the cells. The first five steps of glycolysis involve the breakdown of the 6-carbon glucose into two 3-carbon molecules. Since this conversion requires energy, this part of glycolysis is known as the preparatory phase [4, 5]. The last five steps are called the payoff phase because four adenosine triphosphate (ATP) molecules are generated during the production of two pyruvate molecules. As two ATP molecules are consumed in the preparatory phase of glycolysis, the net ATP production of the pathway is two (Figure 1) [6].

Glycolysis plays a key role in glucose metabolism at the organismal level, regulating glucose consumption by muscle, and hepatic glucose production via gluconeogenesis [7-9]. Additionally, in pancreatic β cells, glycolysis is essential for the proper function of the glucose-stimulated insulin secretion process [10, 11], thus glycolysis also plays a role in regulating circulating insulin levels. Hence, disturbances in glycolysis have important repercussions in the blood glucose levels of mammals, leading to long-term hyperglycemia and diabetes [12, 13]. In sum, glycolysis is an essential pathway that needs to be efficiently regulated to avoid defects in glucose metabolism and the development of diabetes.

The first irreversible step of glycolysis is catalyzed by hexokinase in a reaction where glucose is phosphorylated to glucose-6-phosphate. This phosphorylation modifies the charge of the

molecule and prevents it from diffusing out of the cell [14]. The second key and irreversible step of glycolysis is the phosphorylation of fructose-6-phosphate to fructose-1,6-biphosphate, catalyzed by phosphofructokinase (PK). It is considered the no-return point for glycolysis and once the reaction takes place the entire glycolytic pathway should continue [5]. In experiments performed in mouse cells, the overexpression of either hexokinase or phosphofructokinase, but not other enzymes, increased the glycolytic flux, suggesting that these are the only enzymes able to control the rate of glycolysis [15]. Additionally, high expression of hexokinase 2 has recently been reported as a feature of chronic hyperglycemia, causing what is now called “unscheduled glycolysis” because it happens when the glycolytic control is impaired. The unscheduled glycolysis process leads to an overload of downstream glycolytic intermediates, triggering detrimental processes such as oxidative and dicarbonyl stress [16-18]. Therefore, dysregulation of hexokinase and phosphofructokinase can impact the rate of glycolysis and might lead to diabetes.

Glycolysis also produces important metabolic intermediates such as reduced nicotinamide adenine dinucleotide (NADH) and pyruvate. These two molecules can be further metabolized either through fermentation or cellular respiration, linking glycolysis with other metabolic pathways. During fermentation, pyruvate is converted to L-lactate by lactate dehydrogenase (LDH) in a reaction that consumes NADH but does not require oxygen (Figure 2). Hence, the net yield of glucose metabolized via fermentation is two ATP and two lactate molecules per molecule of glucose [19]. On the other hand, during cellular respiration pyruvate is transported into mitochondria where the pyruvate dehydrogenase complex (PDH) catalyzes its oxidation to acetyl-CoA, which is then used for ATP production in an oxygen-dependent manner. This process involves the tricarboxylic acid (TCA) cycle and oxidative phosphorylation (OXPHOS) (Figure 2), and the total yield of respiration is between 30 to 32 ATP molecules per glucose [20]. Both, a decrease in cellular respiration and an increase in fermentation, are observed in diabetic patients [21-24]. The link between dysregulations in these pathways and diabetes will be discussed in separate sections below.

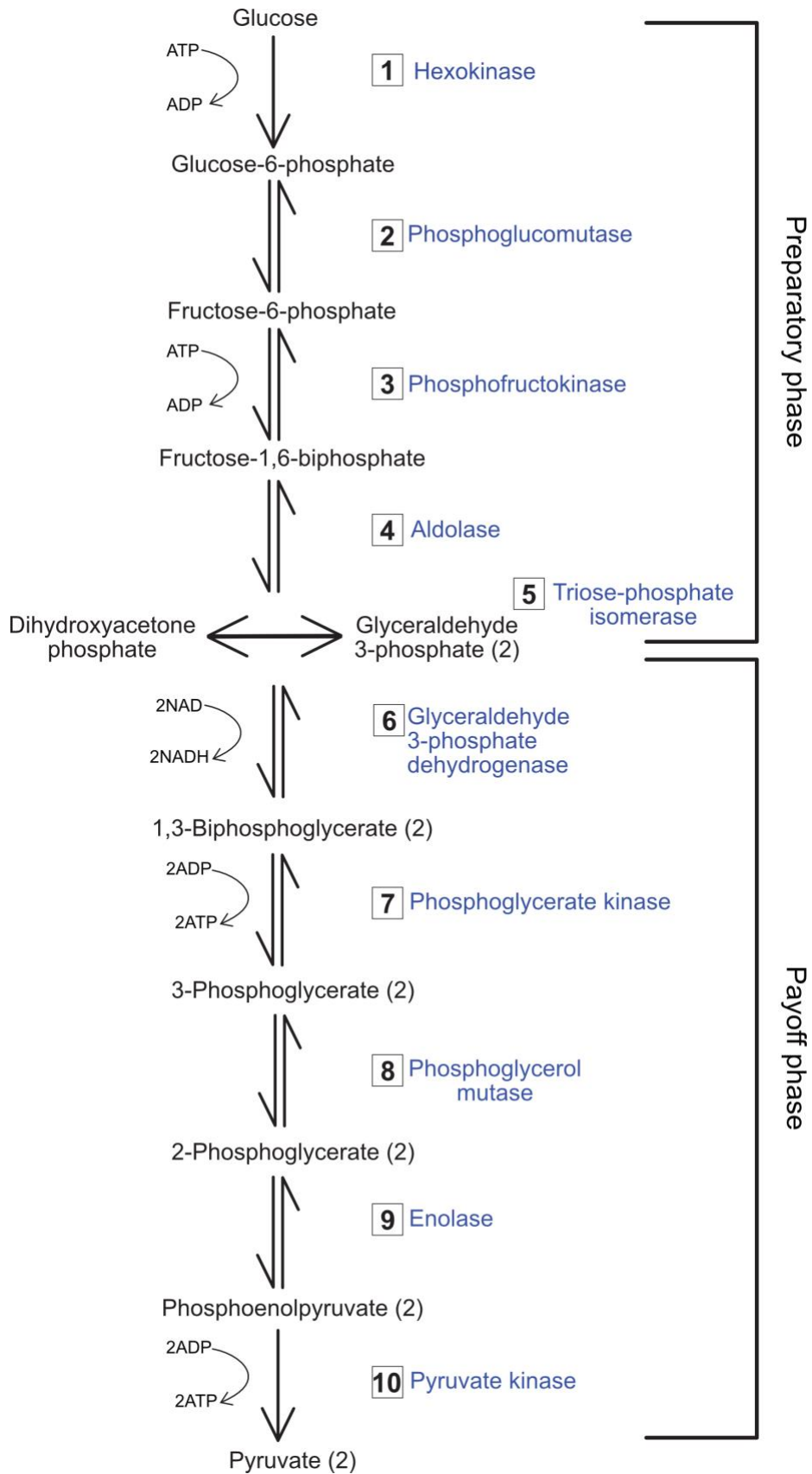


Figure 1. The glycolytic pathway. During glycolysis, a 10-step process, one molecule of glucose is broken down into two molecules of pyruvate. It can be separated into two phases, an energy-consuming preparatory phase (ATP) and an energy-producing payoff phase, during which 4 molecules of ATP are generated.

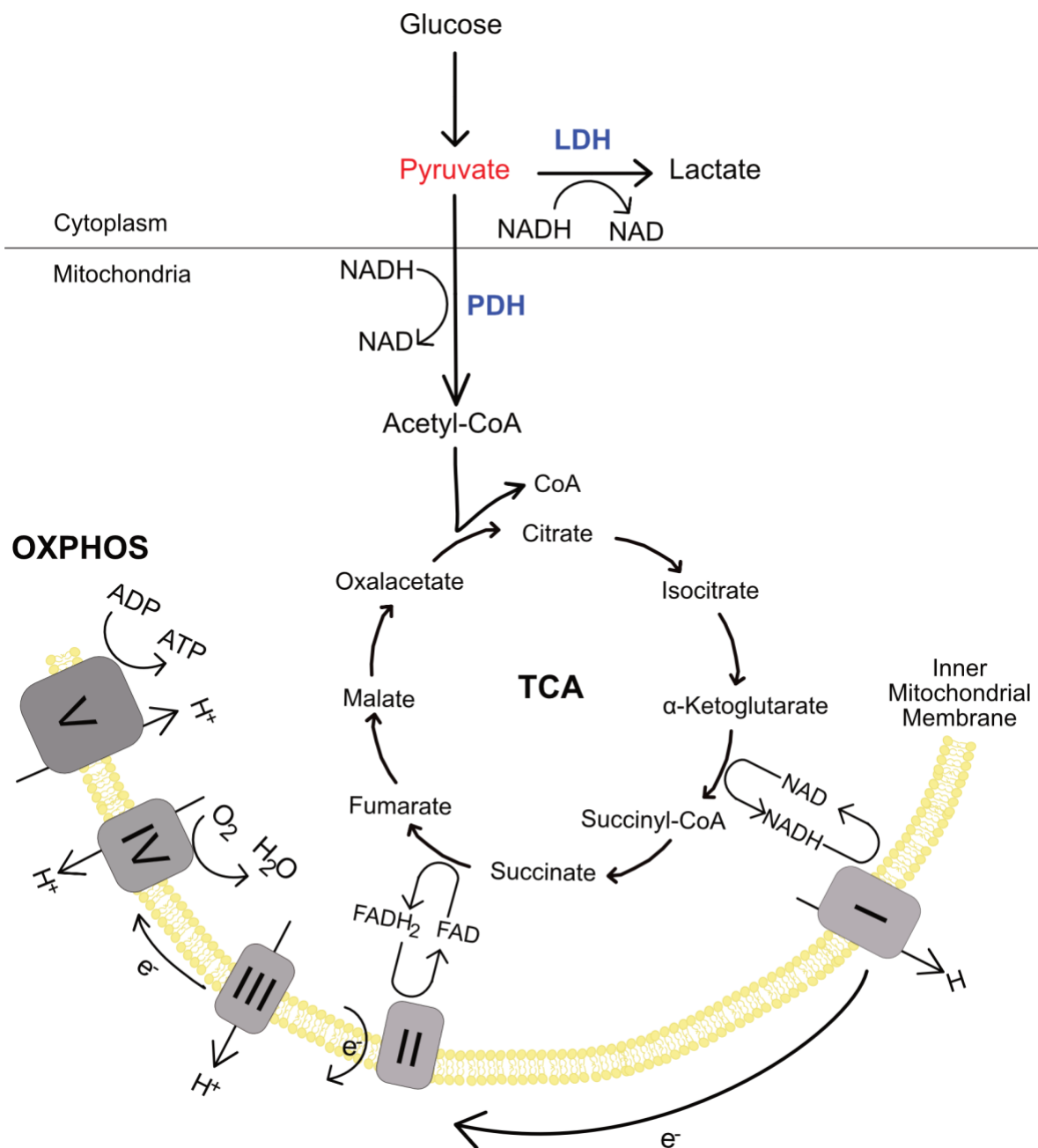


Figure 2. Pyruvate and NADH link fermentation and cellular respiration with glycolysis. Pyruvate and NADH generated in glycolysis can be used either for fermentation or cellular respiration. Fermentation produces lactate and NAD from pyruvate. While cellular respiration involves the oxidation of pyruvate to acetyl-CoA in mitochondria, which, in turn, is used to fuel the TCA cycle. The TCA cycle is required to generate reducing equivalents for the electron transport chain. Electrons provided by the reducing equivalents are channeled through 5 different complexes located in the inner mitochondrial membrane using oxygen as a final electron acceptor. This electron transfer is used to generate a proton gradient, that is consequently used to generate ATP.

1.2. Lactate metabolism in diabetes

Initially, lactate was seen as a waste or inert product of anaerobic glycolysis, but this was soon proven to be incorrect. First, lactate produced in muscle is transported to the liver in order to produce glucose via gluconeogenesis, the so-called Cori cycle [25]. There is also evidence that lactate excreted for fermenting cells can be oxidized by surrounding cells [26, 27] or tissues; skeletal muscle, heart, brain, liver, and kidneys [28]. Moreover, in a recent study by Hui *et al.*, the metabolic fluxes of different circulating metabolites were assessed in mice, and they identified lactate as the main carbon source for the TCA cycle, linking lactate usage with mitochondrial function [29]. Hence, lactate is clearly an important metabolite involved in diverse metabolic processes. Additionally, diabetic and obese patients have high blood lactate levels, suggesting that disturbances in lactate production or usage could be related to the development of diabetes [21, 22].

Miller *et al.*, also proposed that lactate is playing an important regulatory role in lipid metabolism. They observed that infusing running dogs with lactate caused a decrease in circulating free fatty acids [30]. Similar results were observed during intensive exercise in humans, suggesting that lactate regulates lipid metabolism [31, 32]. Moreover, lactate activates the G protein-coupled receptor 81 (GPR18) which is highly expressed in adipocytes and cancer cells [33-35]. This receptor mediates its antilipolytic effects through G protein-dependent inhibition of adenylyl cyclase and lipolytic enzymes [33]. Ahmed *et al.* showed that an increased plasma concentration of lactate reduced free fatty acids in WT but not in GPR18 KO mice, suggesting that the antilipolytic effect of lactate is mediated via GPR18 [33]. Therefore, lactate is also playing an important role in regulating lipolysis via GPR18, and imbalances in lactate levels might have important repercussions in lipid metabolism, leading to obesity, a well-known feature of diabetes.

1.3. Structure and function of pyruvate dehydrogenase complex

As described in more detail below, pyruvate dehydrogenase complex (PDH) plays an important role in diabetes and diabetic complications. Thus, I will first introduce the structure and function of PDH. PDH is an important metabolic control point, where the fate of the glycolytic end products is decided. Under aerobic conditions PDH converts pyruvate into acetyl coenzyme A (acetyl-CoA) through oxidative decarboxylation in mitochondria, funneling

pyruvate into the TCA cycle and, hence, towards OXPHOS (Figure 2). There are no pathways that allow the conversion of acetyl-CoA back to glucose, as a consequence inhibition of PDH activity is important to conserve glucose in conditions of scarcity, like fasting in mammals [36].

Structurally, PDH in eukaryotes consists of multiples copies of several proteins; namely pyruvate dehydrogenase α (PDHA) and β (PDHB), dihydrolipoamide acetyltransferase (DLAT), E3-binding protein (E3BP), dihydrolipoamide dehydrogenase (DLD), pyruvate dehydrogenase kinases (PDKs) and pyruvate dehydrogenase phosphatases (PDPs) (Figure 3A) [37, 38]. Eukaryotic PDH is very large with a size in the range of megadaltons, making it one of the largest complexes known today, which has complicated the study of its structure [39].

PDH is divided in three subunit, E1, E2 and E3 subunit. PDHA and PDHB together form the E1 subunit of PDH. PDH E1, consists of a heterotetramer of two 41 kDa PDHA subunits and two 36 kDa PDHB subunits. The sequence similarity between PDHA and PDHB is low and they only share a conserved thiamine pyrophosphate (TPP) motif which is essential for PDH activity. Amino acid residues that bind the TPP and are therefore essential for PDH activity have been extensively studied. So far, it is clear that W135 in PDHB and C62 in PDHA play an important role in interacting with TPP and point mutations of either of them by site direct mutagenesis affects PDH E1 activity [40-43].

The PDH E2 subunit is formed from trimers of DLAT and E3BP, but the exact composition of this trimer is still controversial. There are currently two hypotheses regarding the composition - either it consists of two 69 kDa DLAT and one 54 kDa E3BP (DLAT₂:E3BP₁) or a combination of different trimers (DLAT₃, DLAT₂:E3BP₁ and DLAT₁:E3BP₂) [32, 39, 44]. DLAT and E3BP are similar in sequence; they both possess one or two lipoyl domains, a subunit domain and an inner domain [45]. But they differ in three features: (I) E3BP has only one lipoyl domain, while DLAT possesses two, (II) DLAT binds the E1 subunit, whereas E3BP binds the E3 subunit, and (III) the catalytic domain present in E3BP is thought to be inactive due to the change of an important, conserved histidine to a serine [45-49].

The E3 component of PDH, DLD, catalyzes the re-oxidation of the reduced lipoyl motives [43]. The PDH E3 subunit is formed from a homodimer of the 53 kDa DLD protein. Each DLD has four important domains: a FAD-binding domain, an NAD⁺-binding domain, the central

domain, and the interface domain. E3 interacts with two E3BP at the same time and plays an important role linking two DLAT:E3BP heterotrimers together [50]. Additionally, DLD is present in two other enzymatic complexes, namely the α -ketoglutarate dehydrogenase (KGDH) and the branched-chain α -ketoacid dehydrogenase (BCKDC). Therefore, dysregulation of this subunit has repercussion also on the TCA cycle and on the metabolism of leucine, isoleucine, and valine [51].

Pyruvate dehydrogenase kinases (PDK) and pyruvate dehydrogenase phosphatases (PDP) are also part of PDH and they regulate the phosphorylation of PDHA subunit. There are 4 isoforms, PDK1-4, each consisting of a 46 to 49 kDa homodimer [52-54]. While in mammals only two PDPs have been identified, PDP1 and PDP2, both of which require Mg^{2+} for their enzymatic function [55]. PDPs are heterodimers composed of a 56 kDa catalytic and a 96 kDa regulatory subunit [47, 56].

Currently, there are only two X-ray crystallography structures of PDH. Both are from the prokaryote enzyme due to its simpler structure [57, 58]. For the eukaryotic PDH, only low-resolution studies have been performed, of which most were based on electron microscopy [59, 60]. Thus, there are still some open questions regarding the exact structure, as well as the stoichiometry of PDH. However, it is known that the symmetry of PDH is icosahedral, with adjacent trimers of DLAT and E3BP binding each other through the C-terminal domain of the adjacent trimer. It was furthermore shown that DLAT and E3BP proteins form the core of the complex, while the other subunits are attached non-covalently to them (Figure 3B). Specifically, one complex consists of 20 to 30 heterotetramers of E1 binding DLAT; 6 to 12 homodimers of E3 binding E3BP; 1 to 3 copies of PDK and 2 to 3 copies of PDP binding DLAT and/or E3BP [39, 61].

The catalysis mechanism of PDH possesses an important feature - it is able to covalently transfer substrate intermediates between the active sites of its three components. This process is known as substrate channeling and is highly depended on the lipoyl groups present in DLAT and E3BP (Figure 4) [62]. First, the E1 subunit decarboxylates pyruvate using TPP as a cofactor, generating a hydroxyethyl group and CO_2 . Then, the lipoyl group of E2 oxidizes the hydroxyethyl group to an acetyl group allowing TPP to be freed. Then, the E2 subunit catalyzes the transfer of the acetyl group to coenzyme A (CoA) generating acetyl-CoA. Lastly,

the E3 subunit re-oxidizes the reduced lipionic acid using FAD, and then NAD is reduced to NADH to generate FADH₂ again [43, 62, 63].

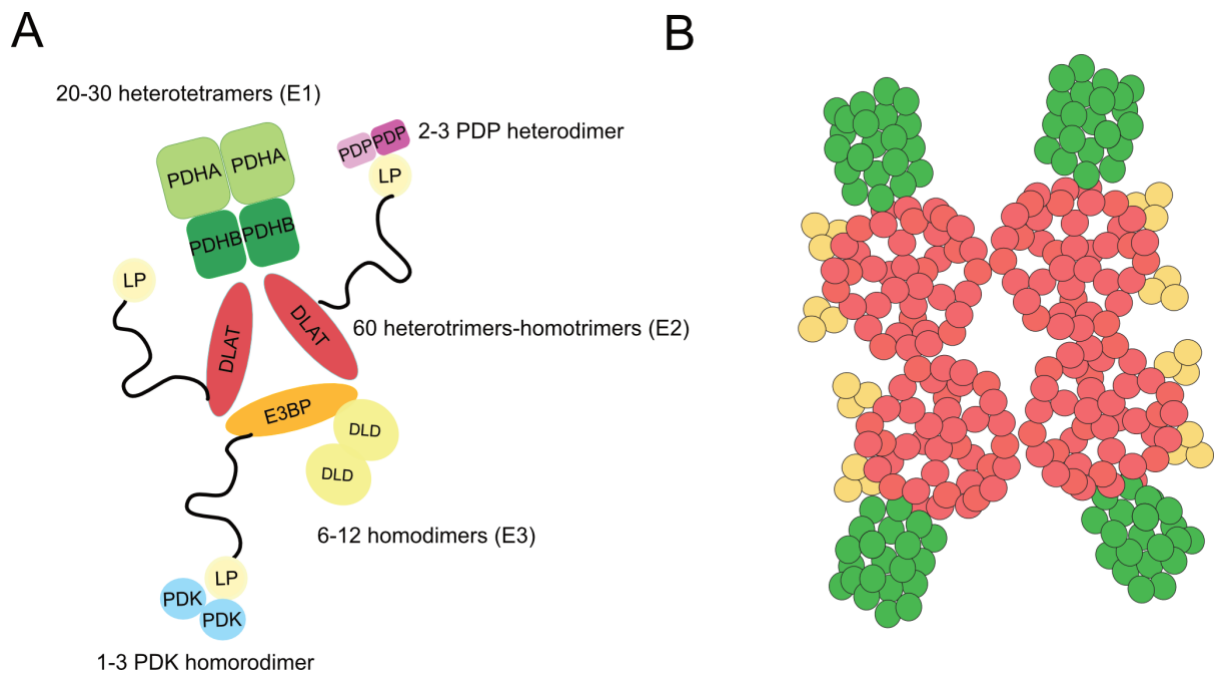


Figure 3. Schematic representation of the PDH structure. (A) Schematic representation of the (A) composition and (B) structural arrangement of PDH and subunits. The PDH core is composed of E2:E3BP (red) and its outer shell of E1 (green) and E3 subunits (yellow).

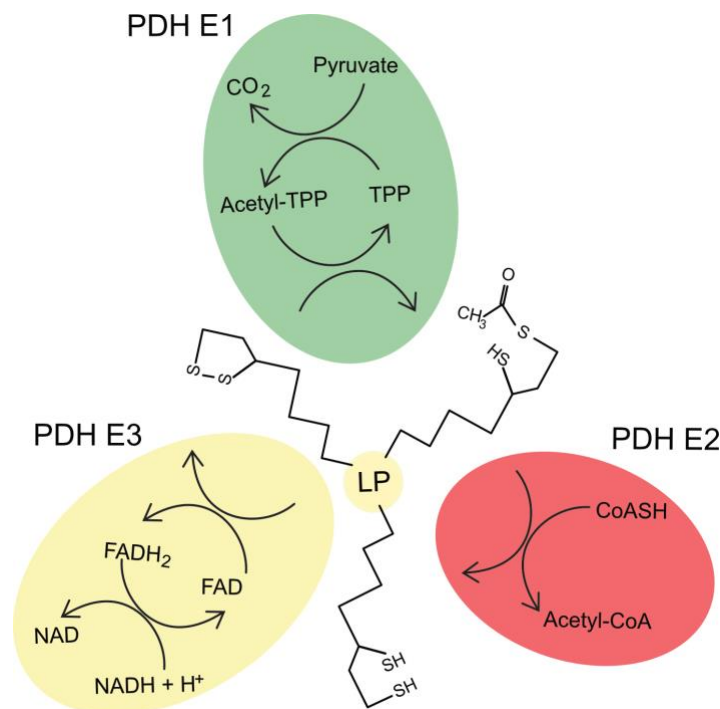


Figure 4. Catalytic mechanism of PDH reaction and the lipoyl group cycle. Schematic representation of the sequential reactions catalyzed by E1 (green), E2 (red), and E3 subunit (yellow). The lipoyl group (LP) plays a key role in the catalytic mechanism of PDH.

1.4. PDH regulation and diabetes

Impairments in PDH activity and mitochondrial disorders could cause disbalances in glucose homeostasis and lead to diabetes. In fact, patients with diabetes and obesity show insufficient oxidative capacity and reduced mitochondrial function and number [23, 24], together with a decrease in genes associated with oxidative phosphorylation and mitochondrial function [64-66]. Moreover, a decline of pyruvate entry into the TCA cycle leads to decreased OXPHOS and impaired insulin secretion [67]. Glucose stimulated-insulin secretion is highly dependent on mitochondrial function. In pancreatic β cells elevated ratios of ATP/ADP trigger the closure of ATP-sensitive potassium channels, leading to depolarization of the plasma membrane and a rise in cytoplasmic calcium necessary for exocytosis of insulin granules. When the PDH complex is inhibited, less acetyl-CoA is produced, decreasing OXPHOS, the ATP/ADP ratio, and the exocytosis of insulin granules [68, 69].

Additionally, proper regulation of metabolism is crucial for cells and organisms, as the inability to respond and adapt to nutritional changes, increases incidence of pathologies such as diabetes [70]. PDH does not only link glycolysis and the TCA cycle but also influences other metabolic pathways. Increased PDH activity leads to higher levels of acetyl-CoA and, in turn, more malonyl-CoA. Consequently, malonyl-CoA inhibits carnitine palmitoyl transferase 1 (CPT1), the mitochondrial long chain fatty acid transporter. As CPT1 is the rate limiting step of β -oxidation, inhibition of the transporter decreases long chain fatty acid oxidation [71-73]. Hence, PDH influences also lipid metabolism, making this enzyme an important metabolic node that needs to be tightly regulated for proper metabolic and, hence, cellular function.

PDH activity is primarily regulated via phosphorylation of PDHA. There are mainly three residues phosphorylated; S293, S300, and S232 [74, 75]. Site-direct mutagenesis of the phosphorylation sites on PDHA to alanine, in combinations of single, double or triple mutations, revealed that phosphorylation of any of the serine residues is enough to inactivate PDH [75]. Nonetheless, the rate of phosphorylation of the residues differ, as determined in studies performed in purified rat skeletal muscle mitochondrial by ^{32}P -phosphate incorporation [76]. S293 showed the fastest ^{32}P -phosphate incorporation, while S232 the slowest, hinting towards S293 playing a crucial role under conditions where fast regulation is necessary [75, 76].

Additionally, PDH activity can be regulated by tyrosine phosphorylation of PDHA. When GST-tagged PDHA was co-expressed with WT fibroblast growth factor receptor 1 (FGFR1) but not a kinase-dead mutant, phosphorylation of PDHA was observed by WB with a total phospho-tyrosine antibody. The phosphorylation site was identified as Y301 as site-directed mutagenesis abolishes phosphorylation. Similar results were observed when the activity of the enzyme was assessed. WT PDHA incubated with FGFR1 showed a decrease in activity that was prevented in a Y301F mutant. Additionally, the expression of the Y301F mutant in several cancer cells increased OXPHOS and decreased proliferation under hypoxic conditions, hinting that the tyrosine phosphorylation could impact the Warburg effect. Structurally, the position of Y301 in PDHA in the proximity of the active site suggests that phosphorylation of this residue could reduce the accessibility of pyruvate [77].

PDH activity is regulated by the combinatorial effect of PDK and PDP activity or their differential expression. For example, PDK4 levels are elevated during starvation and diabetes, while PDP2 levels are decreased under the same conditions [78-80]. Additionally, the interaction of PDKs with the lipoyl domain of DLAT or E3BP affects their activity. Specifically, the reduced or acetylated form of the lipoyl group stimulates the activity of PDKs [52-54, 81]. Hence, the status of the lipoyl domain also affects PDH activity.

PDH is seen as a therapeutic target for metabolic diseases, as it regulates the fate of glucose, playing a key role in glucose homeostasis and mitochondrial function, both processes disturbed in diabetes [67, 69, 82]. In this regard, most studies are focusing on PDH regulation via its phosphorylation, relying on the use of the PDK inhibitor dichloroacetate (DCA). One study that exemplified this, was done by Katayama *et al.* using ob/ob mice, carrying a mutation in the leptin gene that causes excessive eating. They treated the mice with DCA for 3 weeks and reported that DCA caused a significant reduction in plasma levels of glucose and of the long-term predictor of glycemic control fructosamine, suggesting that PDH is essential for proper glucose homeostasis. Moreover, they also used DCA in FaO hepatoma cells incubated only with the gluconeogenic substrates lactate and pyruvate, and observed a dose dependent decrease in glucose production, hinting that PDH activity has an impact on gluconeogenesis and therefore plasma glucose levels [83].

Decreased PDH activity is especially detrimental in the heart where it has been linked to cardiopathies. Rats fed with a high fat diet (HFD) and depleted of pancreatic beta cells by

injection with streptozotocin (STZ), showed reduced glucose flux, decreased PDH activity and impaired diastolic function identified by echocardiography. When these rats were treated with DCA for twenty-eight days, the metabolic dysfunctions, as well as the impaired diastolic function were reversed, indicating that PDH activity is essential for a proper cardiac function [84]. Low PDH activity in the heart of diabetic animals is thought to be mediated via an increase in PDK4 expression as consequence of Fork head box O1 (FoxO1) hyperactivation. In fact, the heart of FoxO1 KO mice showed lower PDK4 expression and less PDHA phosphorylation at S293 and S300 [85, 86]. Furthermore, inhibition of FoxO1 with AS1842856 is known to rescue the decrease in glucose oxidation rates and diastolic dysfunction displayed by diabetic mice, but had no effect in the heart of PDH deficient diabetic mice, further validating that the protective effect is mediated via PDH [85].

Low PDH phosphorylation levels and high PDK expression have been associated also with diabetic features in both liver and muscle. Livers from the offspring of gestational diabetes (GD) mice showed higher glucose intolerance when compared with offspring from control mice. The livers also had increased PDHA phosphorylation levels, suggesting that in GD PDH activity is decreased and the risk of diabetes in the offspring is increased [87]. Moreover, nonalcoholic steatohepatitis (NASH) is a liver condition associated with insulin resistance and diabetes. In NASH mice the PDK4 KO had a protective effect against liver steatosis, indicating that an increase in PDK4 activity and a decrease in PDH activity might cause or contribute to liver steatosis[88]. On the other hand, Cummings *et al.* assessed muscle tissue of a rat model of type 2 diabetes, namely UC Davis-T2DM (UCD_T2DM). These rats were created by crossing insulin resistant Sprague-Dawley rats and Zucker diabetic fatty-lean rats with a defect in pancreatic β -cell function [89]. Specifically, they studied muscle function from UCD_T2DM or control rats by dynamic nuclear polarization and ^{13}C pyruvate or lactate incorporation. They observed increased labeling of bicarbonate and acetyl carnitine in T2DM rats compared with the control animals, suggesting lower PDH activity. In the same study, it was also shown that DCA was able to restore PDH activity in the diabetic mice. However, the response of PDH activity to DCA in the diabetic animals was 4 times slower than the control ones, suggesting other factors apart from phosphorylation could also be affecting PDH activity in T2DM rats [90].

1.5. The role of MG in protein modifications

Whereas diabetic patients are characterized by hyperglycemia, it has been shown that a good glycemic control does not protect individuals from developing diabetic complications, hinting that additional factors probably contribute to the progression of the disease. One of multiple factors suspected of playing a role in diabetes and diabetic complications, is the reactive metabolite methylglyoxal (MG) [91]. MG is an α -oxoaldehyde formed non-enzymatically in eukaryotic cells mainly by dephosphorylation of the triose-phosphate intermediates of glycolysis, dihydroxyacetone phosphate (DHAP) or glyceraldehyde 3 phosphate (GAP) (Figure 5) or in bacteria enzymatically by e.g. the MG synthase [91, 92]. In experiments were both triose phosphates were incubated with Krebs-Ringer phosphate buffer at 37°C for 2 hours, 90% of GAP and only 15% DHAP spontaneously formed MG, suggesting that GAP is the major source of MG [92]. MG synthesis from the trioses phosphates occurs both under physiological and pathological conditions. Under physiological conditions, formation of MG constitutes only 0.1% of the glucotriose flux. The rate of MG formation from DHAP and GAP has been studied in rat tissues and is around 0.1 mM per day [93]. Moreover, there are additional sources of MG, such as the sorbitol pathway, the metabolism of triacyl glycerol or the metabolism of branched amino acids (Figure 5) [94].

MG is a highly reactive metabolite that can interact with macromolecules and form advanced glycation end products (AGEs). MG is 50.000 times more reactive than glucose and even at low abundance, it accounts for most AGEs in the cell. The MG-protein interaction can be irreversible, as well as reversible, meaning that while MG is mainly found bound to macromolecules, some MG is always in a dynamic equilibrium between the free state and the bound state [95]. The interaction of MG with macromolecules changes their canonical function. For example, the formation of AGEs on lipids affect the fluidity of membranes and therefore membrane signaling [96]. Furthermore, lipid glycation by MG causes increased peroxidation and oxidative damage [97]. MG modification of DNA has detrimental effects on its stability, increasing the risk of breakages and mutations, while protein-MG interactions have repercussions in the structure and activity of the molecule [94].

MG modifications on proteins are mainly found on lysine, arginine, and cysteine residues (Figure 6) [98]. While the MG interactions with arginine and lysine residues are irreversible, the ones with cysteine are reversible. MG modifies arginine and lysine via their guanidine

group and cysteines via interaction with their thiol group. The main type of MG adducts on arginine is hydroimidazolone (hydroimidazolone 1; MG-H1) accounting for around 90% of MG adducts on arginine. The second most common arginine AGE is argpyrimidine. The MG adducts on lysine are less common and are usually 1-carboxyethyl lysine (CEL) or N-lysino-4-methylimidazolium (MOLD) [98, 99]. The reversible modification of cysteine is fast and involves the thiol group [98, 100]. Due to their unstable character cysteine-MG adducts are difficult to study. Analysis of these adducts require crosslinking techniques, like the use of a photoactivable diazirine cross-linker attached to a MG molecule, previously used in the Teleman laboratory to identify MG modifications on fatty acid synthase [101].

In 2018, a new type of MG adduct was discovered on the kelch-like ECH-associated protein 1 (KEAP1), a crosslinking posttranslational modification called mercaptomethylimidazole (MICA). Chemical inhibition of phosphoglycerate kinase (PGK) causes accumulation of MG and dimerization of KEAP1. The dimerization of KEAP1 requires the formation of an initial hemithioacetal between MG and a cysteine residue, followed by a second reaction with a proximal arginine that causes a stable crosslinking, MICA adduct (Figure 6) [102]. This raised the possibility that MICA adducts could act as a crosslinking agent and generate multimers of modified proteins, changing their function. Additionally, the diversity of MICA adducts is high, as they can form between proteins and any thiol or guanidine containing molecule, including small molecule metabolites such as glutathione, antioxidant molecules such as N-acetylcysteine, or drugs such as metformin. This suggested that an increase in these metabolites or drugs in combination with elevated level of MG could lead to MICA adduct formation and changes in signaling pathways [103].

There are two recent studies that aimed to identify the MG-modified proteome. The first was performed in HEK293T cells incubated with 131 μ M MG. They identified more than 600 MG-modified proteins by mass spectrometry, with the major adduct observed being MG-H1. Moreover, it was also shown that MG treated cells had significantly less mitochondrial proteins, indicating that MG is also able to regulate protein expression or stability [104]. In the second study, Donellan *et al.* treated WIL2-NS cells with 500 μ M MG for 24 hours, and they identified among the 500 MG-modified proteins, with glycolytic enzymes being the most affected group. Of the ten glycolytic enzymes, seven were modified by MG, hinting that MG adducts play a role in glucose homeostasis [105].

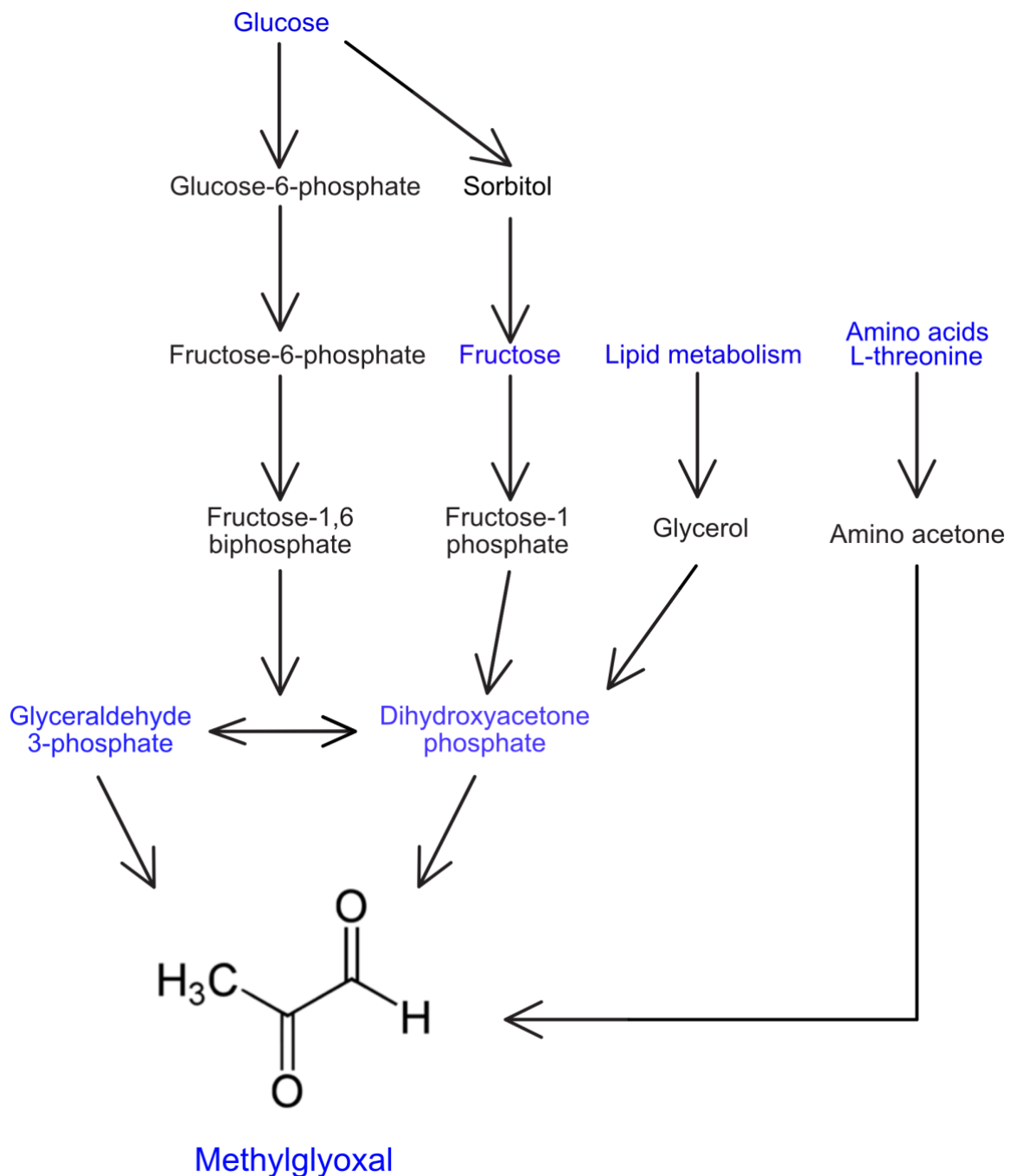


Figure 5. Pathways that feed the production of MG. Methylglyoxal (MG) can be derived from (I) glucose, (II) fructose, (III) lipid metabolism, or (IV) amino acids. (I) The trioses phosphate produced by glycolysis, GAP and DHAP, undergo spontaneous dephosphorylation to produce MG. (II) Via the sorbitol pathway, glucose can be transformed to fructose. In turn, fructose can then be used to produce fructose 1,6-biphosphate a substrate that aldolase uses for DHAP. Importantly this pathway produces DHAP from glucose while overcomes the tight regulatory controls of glycolysis. (III) Triacylglycerol can also be converted to DHAP via glycerol by the glycerol kinase and the phosphatase dehydrogenase. (IV) The metabolism of branched amino acids as L-threonine leads to the production of 2-amino-3-ketobutyrate that can spontaneous decarboxylate to amino acetone which can then be oxidized to MG by the amine oxidase.

While MG adducts on arginine and lysine residues have been documented in detail, cysteine adducts have been scarcely studied mainly due to the absence of efficient tools for their assessment. However, last year two new studies were performed with the aim of identifying the MG-modified cysteine proteome. The first study focused on MICA adducts using a newly developed technique called quantitative protein crosslinks discovered by migration analysis platform (qPC-MAP). With this approach MICA adducts were detected by a shift in their electrophoretic mobility, followed by in-gel digestion and mass spectrometry analysis. 66 new proteins were reported to bear MICA adducts, among them the inosine 5-monophosphate dehydrogenase 2 [106]. The second study was performed using iodoacetamine alkyne (IA-alkyne) in combination with mass spectrometry. IA-alkyne acts as a cysteine reactive probe, reacting with free cysteines but not with MG-modified ones. Thus, cells were incubated with MG or a control molecule in combination with IA-alkyne. Cysteines not modified by IA-alkyne anymore in the MG treated sample were identified as cysteines that reacted with MG. Particularly, several cysteines were identified in the catalytic site of acetyl-coenzyme A acetyltransferase (ACAT1), the activity of which was impaired by MG [107]. This provides further evidence that MG adducts on cysteines impact protein function.

1.6. MG acts as a signaling molecule

Elevated levels of MG and MG-protein modifications mediate cellular and metabolic changes. One example of such a mechanism was reported for the enzyme ACAT1. As was mentioned above, MG interacts with ACAT1 via its cysteine residues, thereby inhibiting its activity [107]. The enzyme catalyzes the conversion of acetoacetyl-CoA to acetyl-CoA which can be subsequently used in the TCA cycle to produce energy. However, when ACAT1 is inhibited, the acetoacetyl-CoA is metabolized to β -hydroxy β -methylglutaryl-CoA, which is further utilized for cholesterol and isoprenoid biosynthesis [108]. Consistent with this, HeLa cells treated with MG showed an accumulation of β -hydroxy β -methylglutaryl-CoA, hinting that MG inhibits ACAT1 *in vivo* [107]. These results also raise the possibility that MG might act as a signaling molecule regulating the metabolic fate of acetoacetyl- for either energy production or biosynthetic processes.

The capability of MG to modulate metabolism was also previously shown by our laboratory. Moraru *et al.* showed that MG modifies fatty acid synthase (FASN) in cells incubated with MG. In line with this result, they also observed elevated FASN activity and triglyceride levels

in glyoxalase 1 (Glo1) KO flies. These animals lacked one of the main enzymes that detoxify MG and, thus, suffered from a mild increase in MG levels. In addition, these flies were also more resistant to oxidative stress and had a higher ratio of reduced-to-oxidized glutathione compared to control animals, providing evidence that MG causes changes in different metabolic pathways [101].

Furthermore, the dimerization of KEAP1 via a MICA adduct triggers accumulation of Nfr2 and activation of the oxidative stress response [102], suggesting that MG acts as an activator of this pathway. These results together with the data mentioned above raise the possibility that MG might be acting as a signaling molecule capable of modifying specific proteins and triggering changes in the cellular state and metabolism. Additionally, changes in metabolism mediated by MG interactions with proteins could be associated with pathologies such as diabetes. Hence, further characterization of the impact of MG on cellular metabolism could contribute to the development of future therapeutic interventions against diabetes.

1.7. The role of methylglyoxal in diabetes

The formation of MG adducts on proteins can change their function and activity, which, in turn, potentially has detrimental effects on cell or organismal function. For example, an approximately 2-fold increase in MG levels in endothelial cells caused the formation of AGEs in collagen type IV, impairing its binding with integrin and consequently, leading to detachment of the cells and impairments on angiogenesis [109]. Vascular dysfunctions are one of the biggest complications in diabetic patients and MG-collagen adducts could be playing an important role in it [110, 111]. Additionally, STZ treated mice showed an early increase in MG adducts in laminin and fibronectin compared with control mice. The MG modification on laminin, an extracellular matrix protein, impaired axonal outgrowth which could explain the dysregulations in axonemal regeneration observed in diabetic neuropathy [112, 113].

As MG levels strongly depend on the glycolytic flux, the metabolic state of a cell plays an important role in AGEs formation. High glucose exposure of human aortal endothelial cells (HAECs) for six days caused an increase in the glycolytic flux and MG-protein adducts, suggesting that hyperglycemia leads to increased MG production. In the same study, MG-modified proteins were enriched in different cellular processes, including the unfolded protein response, inflammation, glycolysis, and gluconeogenesis. These results indicate that MG could

alter the function of these pathways under high glucose conditions, causing changes in the cellular state and metabolism [16]. Moreover, HeLa cells cultured in high glucose also showed high levels of AGE at lysine and arginine residues, with the major arginine modification being argpyrimidine and not MG-H1 as in previous studies [104, 105, 114]. In the same study, plasma of diabetic patients was also analyzed and MG adducts at lysine and arginine residues were detected, suggesting that hyperglycemia causes MG adducts formation *in vitro and in vivo* [114].

Increased MG levels have been associated with the development of diabetes, as well as the progression of the diseases. Diabetic patients with complications have higher MG and MG-adduct levels compared to diabetic patients without complications or healthy patients [115, 116]. This was documented in a study which measured MG levels in plasma from healthy individuals or patients with type 2 diabetes without or with nephropathy, with the latter group showing the highest levels of MG. The patients with nephropathy had 312 ± 135 nM of MG while diabetic patients without complications had 212 ± 73 nM of MG and healthy patients showed the lowest levels of MG with 147 ± 75 nM [116]. Similar results were observed in type 2 diabetic patients with or without pain. Higher plasma MG levels were documented in the first group compared to diabetics without pain or healthy patients [117]. High sensitivity to pain was caused by a modification of the sodium ion channel Na(v)1.8 by MG. The modification changed the channel activity and caused an increased in electrical excitability, which, in turn, facilitated the activation of nociceptive neurons [117].

Several studies also provided evidence that MG reduces insulin signaling. Jia *et al.* showed that insulin can be modified by MG at an arginine residue located in the beta chain, causing less efficient stimulation of glucose uptake in 3T3-L1 adipocytes and L8 skeletal muscle cells compared to unmodified insulin [118]. Additionally, L6 muscle cells treated with MG showed diminishing insulin signaling due to impairments in phosphorylation and activation of protein kinase B (PKB) and extracellular-regulated kinase 1/2 (ERK) [119]. In line with these observations, MG treatment of INS-1E pancreatic cells caused decreased phosphorylation of the insulin receptor substrate 1 and phosphoinositide 3-kinase, indicating impaired insulin signaling [120]. The above-mentioned findings show that under conditions that increase MG levels, such as hyperglycemia, insulin signaling pathways are affected via MG modifications of their components, raising the possibility that MG could lead to insulin resistance and loop back to hyperglycemia and MG production. Hence, MG could cause metabolic changes via

protein modification, and more studies are still needed to understand the impact of MG on cellular metabolism.

1.8. The glyoxalase system as a protective mechanism against diabetes

The glyoxalase pathway is considered the major detoxification pathway of MG. It is present in the cytoplasm of all cells and is evolutionary conserved among species [121]. Around 99% of MG is detoxified via the glyoxalase pathway [122]. However, there are alternative pathways for MG detoxification, such as the aldehyde dehydrogenase (ALDH) and the aldose reductase (ARK) (Figure 7). These pathways will be discussed in a latter section of this introduction [123, 124].

The glyoxalase pathway is composed of two enzymes, namely Glo1 and glyoxalase 2 (Glo2). The first step in the detoxification of MG depends on the non-enzymatic reaction between MG and reduced glutathione (GSH), yielding a hemithioacetal. Next, Glo1 further detoxifies MG to the less reactive S-lactoylglutathione. Lastly, Glo2 hydrolyses the S-lactoylglutathione producing GSH and D-lactate that can be excreted by the cell (Figure 7) [121]. Therefore, Glo1 catalyzes the most important step in the pathway, the conversion of MG into a metabolic intermediate that is no longer detrimental for the cell [125].

Over-expression of Glo1 has been reported to protect against detrimental processes like inflammation and decreased angiogenesis. In experiments using human microvascular endothelial cells transfected with Glo1, the cells were protected from loss of tube structures and angiogenesis defects associated with hyperglycemia [126]. Moreover, animal models overexpressing Glo1 have been extensively employed to assess the role of Glo1 in the development and progression of diabetes. In STZ rats, Glo1 overexpression was sufficient to prevent AGEs formation and oxidative stress [127]. In another study also using STZ rats, Glo1 overexpression impeded the development of endothelial and renal dysfunctions characteristic of diabetic nephropathy [128]. Furthermore, features of retinopathies, caused by the accumulation of AGEs in the retina, Müller glia dysfunctions, and capillary closure were also avoided by Glo1 overexpression in STZ rats [129]. Therefore, Glo1 is playing an important role *in vivo* in detoxifying MG and, consequently, protecting tissues from the repercussions of AGEs (Figure 8).

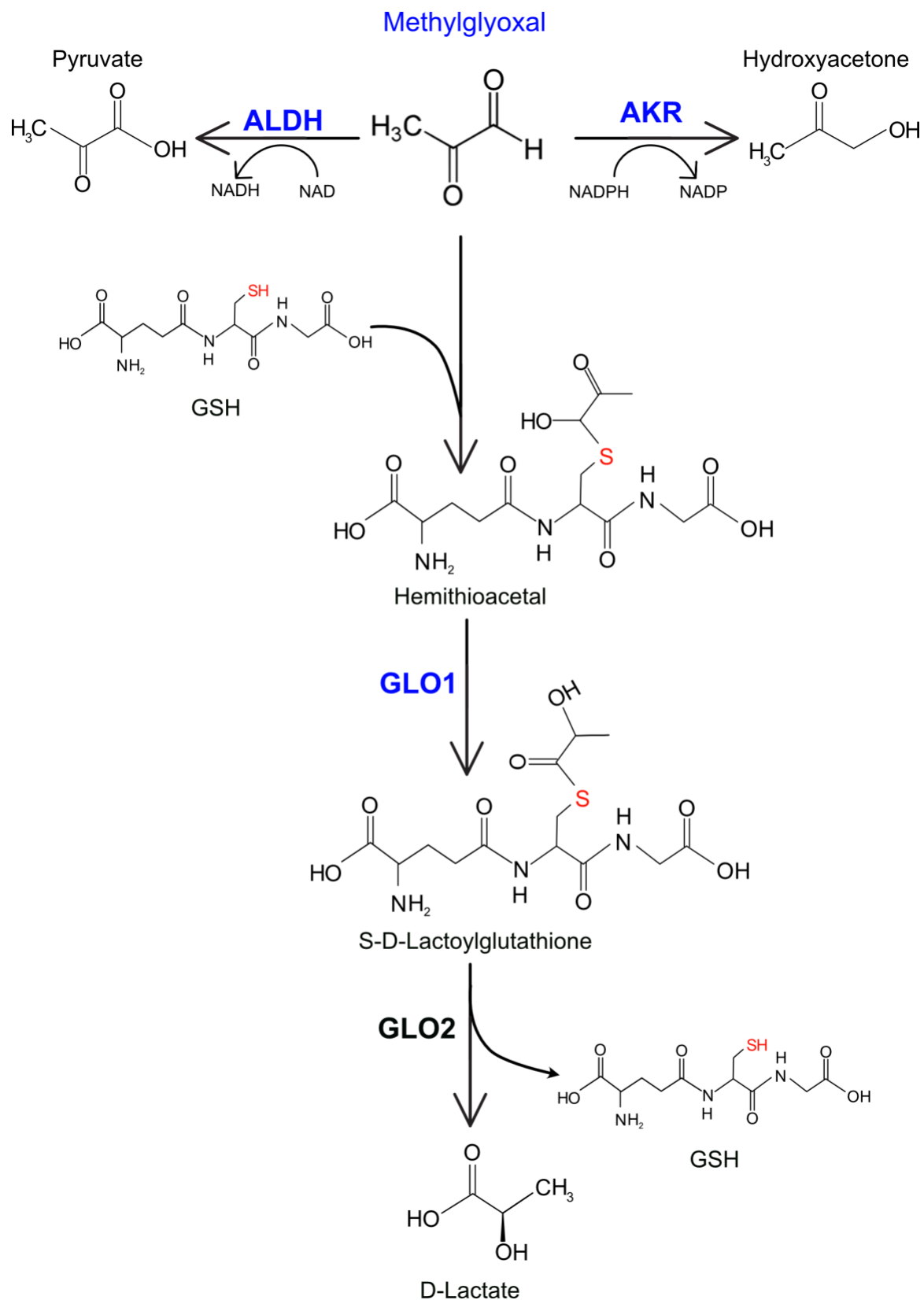


Figure 7. Detoxification mechanisms of methylglyoxal. The glyoxalase pathway, is composed of two enzymes Glo1 and Glo2 that detoxify MG into D-lactate in a reaction that is dependent on reduced glutathione. There are two additional enzymes able to detoxify MG in a GSH independent way. Aldehyde dehydrogenase (ALDH) converts MG into pyruvate in a NAD dependent mechanism and aldose reductase (ARK) produces hydroxyacetone from MG using NADPH.

On the other hand, the loss of Glo1 is associated with metabolic dysfunctions, such as obesity, insulin resistance, and hyperglycemia. KO of Glo1 in *Drosophila melanogaster* slightly elevates MG levels and even though the animals showed normal triacylglycerol levels in their juvenile stage, they gradually became obese with age. Similar results were observed regarding glucose levels in hemolymph: the animals developed hyperglycemia during adulthood [101]. Consistent with the observations in fly fruit, Glo1 KO *Danio rerio* showed impaired glucose tolerance. One hour after feeding, blood glucose of Glo1 KO zebrafish reached 118 mg/dl, almost twice the levels detected in WT animals (65 mg/dl). Additionally, when overfed, Glo1 KO zebrafishes developed high blood glucose levels also in fasting conditions [130]. These data suggest that Glo1 KO flies and fish are susceptible to develop features of diabetes and that MG could be playing an important role in the developing of diabetes and diabetic complications (Figure 8).

In mice, loss of Glo1 does not mimic the effects observed in the fly or zebra fish. Glo1 knockdown (KD) mice with a significant reduction in protein levels only showed a small, but not significant increase in MG-H1 adducts in liver, kidney, and heart. Moreover, when Glo1 KD mice were submitted to HFD for 10 weeks, only a small, but not significant increase in MG-H1 adducts and no change in body weight were detected [131]. Similar results were reported in Glo1 KO mice injected with STZ which did not show high levels of MG or MG-H1 adducts in comparison with WT STZ mice. Likewise, parameters of diabetic nephropathy (albumin creatinine ratio and glomerular filtration rate) were unchanged in Glo1 KO STZ mice compared with WT STZ mice. However, WT STZ mice showed an approximately 50% decrease in Glo1 activity in liver and kidney when compare with untreated WT mice, indicating that hyperglycemic WT mice also displayed features associated with decreased Glo1 activity. Furthermore, the Glo1 KO STZ mice showed increased expression of MG detoxification enzymes in liver and kidney, specifically ALDH was overexpressed in liver and AR in kidney [132]. This suggest a compensatory mechanism in Glo1 KO mice and future research will be necessary to fully understand the effect of Glo1 loss and high MG levels in the mouse.

The role of Glo1 in metabolic diseases such as obesity and diabetes is still not fully understood as some of the findings are contradictory or vary in different tissues. For example, in one study in which Glo1 activity was assessed in erythrocytes from diabetic patients, the activity of Glo1 was increased by approximately 40% compared with control patients [133]. However, in a different study, Glo1 activity showed the opposite effect when studied in muscle biopsies of type 2 diabetic patients compared to healthy ones: it was decreased by 80% [134]. Furthermore,

muscle tissue from diabetic patients showed an increase in protein AGEs, as well as higher levels of KEAP1, a negative regulator of Glo1 and a MICA adduct bearing protein [102, 134]. Additionally, Glo1 activity in visceral adipose tissue from pre-diabetic and diabetic obese patients was decreased compared with healthy patients [135]. These results suggest that the degree of Glo1 activity and consequently levels of MG adducts depend on the assessed organ or tissue.

The second enzyme of the glyoxalase pathway, Glo2, has been neglected so far and its role in the development of pathologies as diabetes needs to be investigated. There are only a few studies where the effect of Glo2 loss has been assessed in animal models. Similar to Glo1, mice lacking Glo2 are viable and do not show increased levels of MG or MG adducts, suggesting that this enzyme has no MG detoxification essential role or it is compensated by other enzymes. However, this study failed to perform a complete metabolic assessment of the animal model and, apart from MG levels, no other diabetic features were studied [136]. Similar results were observed in a recent study in Glo2 KO zebrafish: the animals had no defects in viability nor important metabolic dysregulation as hyperglycemia. Nevertheless, the Glo2 KO animals did show reduced uptake of hexoses in liver, while in skeletal muscles from Glo2 KO fish, the opposite was observed, an increase in hexose levels, accompanied by increased activity of several glycolytic enzymes. Nevertheless, Glo2 expression in muscle tissue is low and, as a consequence, the effect is likely a compensatory mechanism due to the reduced uptake of hexoses observed in liver [137]. These results indicate that Glo2 is an important regulator of glucose metabolism in the liver. In general, more work is necessary to fully understand the role of each component of the glyoxalase pathway *in vivo* and their role in the metabolic function of organisms.

1.9. Glo1 structure and regulation

Understanding Glo1 regulation is critical for identifying its role in the development and progression of metabolic diseases such as diabetes. Glo1 is a zinc dependent protein isomerase that, in humans, is formed a 46 kDa homodimer. The GLO1 genomic locus has an insulin and a metal response element. This was validated in a reporter assay using a GLO1 promoter controlling the alkaline phosphatase gene, which showed a two-fold increase in reporter activity in response to either insulin or Zinc [138]. Additionally, several single nucleotide polymorphisms (SNPs) in GLO1 have been associated with impaired activity. A study in which

3 common SNPs were assessed in 125 healthy individuals, 101 type 1 diabetes patients, and 102 type 2 diabetics, showed that Glo1 activity was decreased in patients carrying the SNPs rs1130534 and rs1049346 [139]. Moreover, rs1049346 is located in the 5' UTR of *GLO1* and is known to be highly prevalent for complications in type 2 diabetic patients [140].

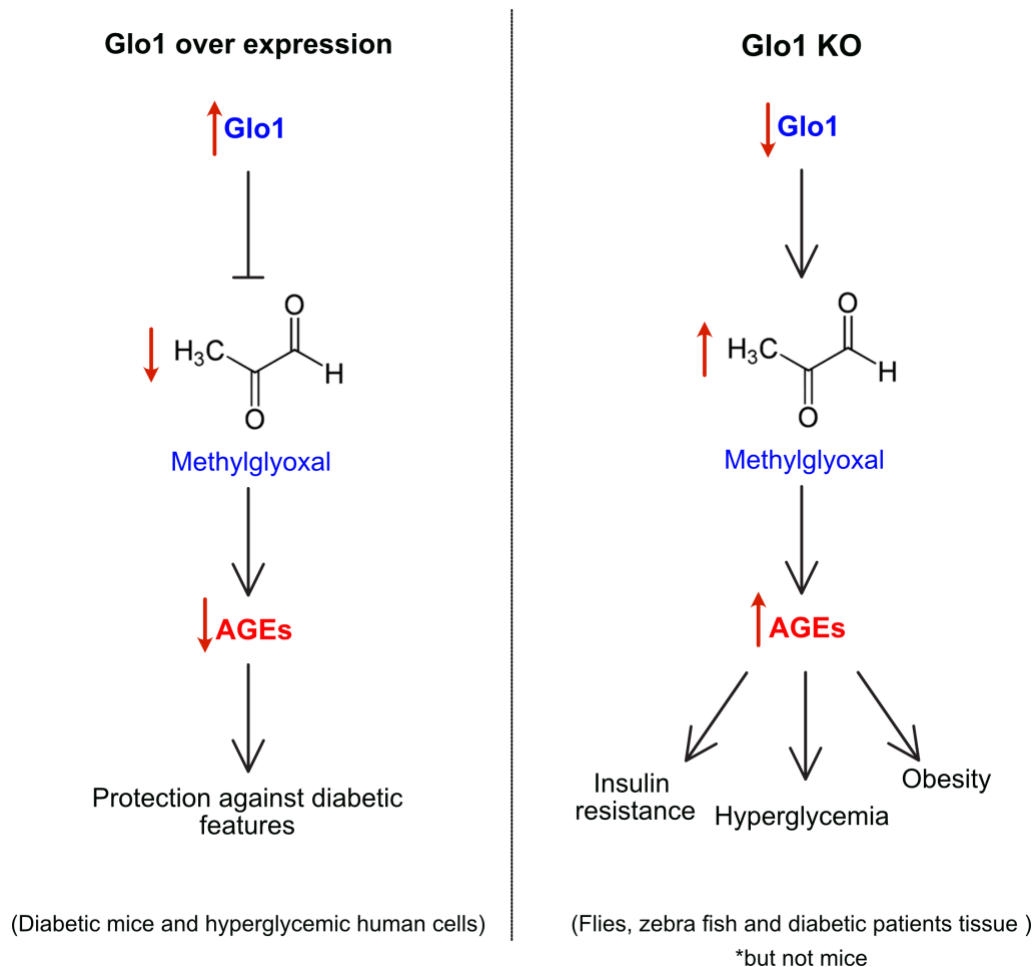


Figure 8. Potential role of Glo1 in diabetes. (Left) Overexpression of Glo1 in diabetic animals and human cells under hyperglycemic conditions prevents development of diabetic features. (Right) The loss of Glo1 in flies and zebra fish, but not in mice, causes development of diabetic features.

Glo1 activity is also regulated by posttranslational modifications. According to the phosphoSitePlus data base, there are four residues postulated to be acetylated and five to be phosphorylated in Glo1. However, only the phosphorylation of Glo1 at T107 has been extensively studied. The tumor necrosis factor (TNF) is known to induce phosphorylation of Glo1 on T107, in a mechanism required to induce cell death in L922 cells, but not related to MG detoxification [141]. Moreover, in site direct mutagenesis experiment it was also shown that CamKII has the ability to phosphorylate WT Glo1 but not the mutant T107A, implying CamKII is the kinase responsible for Glo1 phosphorylation on T107 [142]. Recently,

Morgenstern *et al.*, reported that phosphorylation of T107 increases its catalytic efficiency and delays Glo1 proteasomal degradation. Moreover, the role of CamKII on T107 phosphorylation was further assessed in 20-week old CamKII KO mice. A global decrease in MG detoxification capacity and 50% less Glo1 protein was detected in these mice when compared to WT mice, validating the role of CamKII as a Glo1 kinase and the importance of T107 phosphorylation for Glo1 stability [143].

In addition to phosphorylation, Glo1 activity is also regulated by nitric oxide (NO). It was observed that exposure of endothelial cells to NO or compounds that enhance the release of NO caused the inactivation of Glo1. Furthermore, the addition of dithiothreitol (DTT), which can act as a NO scavenger, restored Glo1 activity in endothelial cells [144]. The NO-dependent inactivation of Glo1 in endothelial cells was also prevented by the depletion of GSH, hinting rather at S-nitroso-glutathinylation (GSNO) as the modification regulating Glo1 activity [144, 145]. Site-directed mutagenesis of Glo1 identified C138 as the main residue of Glo1 being modified by GSNO [146]. C138 is located in a flexible loop of Glo1 that is opposite to the active site. Consequently, the presence of a PTM on this flexible loop could affect accessibility to the catalytic site of Glo1 and, therefore, its activity [147].

Finally, more work is still necessary to find all the residues modified in Glo1 and elucidate their role in the enzyme activity. Furthermore, the identity of the proteins responsible for the PTM on Glo1 is another factor that needs to be further addressed to comprehend the mechanism behind Glo1 regulation. All this will help identify the role Glo1 is playing in diseases like diabetes.

1.10. Alternative pathways of MG detoxification

As mentioned before, there are additional MG detoxifying enzymes besides the glyoxalase pathway, namely ALDH and AKR. AKRs catalyze the detoxification of MG to hydroxyacetone, while ALDHs generate pyruvate from MG [123, 124]. The contribution of each of these mechanism to the detoxification of MG depends on the genetic context and tissue. In a study performed in liver and kidney of WT mice, the main detoxification products of MG under normal conditions were D-lactate and hydroxyacetone, indicating AKR and Glo1 as the main detoxification enzymes in these tissues. However, when levels of MG detoxification end products were compared between Glo1 KO and WT mice, hydroxyacetone was higher in the

kidney of Glo1 KO mice, while in the liver pyruvate levels increased. Thus, ALDH would compensate for loss of Glo1 activity in the liver and AKR would do so in the kidney [132].

Compensatory mechanisms associated with loss of Glo1 have also been reported in Schwann cells. Upon Glo1 KO in Schwann cells, mRNA levels of ALDHs and AKR increased. When the activity of these enzymes was assessed in Glo1 KO cells only AKR activity was high enough to compensate for the loss of Glo1. These results suggest that AKR plays an important protective role in glia cells under conditions, in which Glo1 activity is reduced [148]. The importance of AKR for MG detoxification has also been proven in HUVEC cells under high glucose conditions, where the inhibition of AKR by sorbinil increased the levels of AGEs compared with non-treated cells. These results suggest that AKR is also important for proper MG detoxification in endothelial cells even in the presence of Glo1. Additionally, AKR1B3 KO mice injected with STZ also showed increase levels of AGEs in plasma compared with WT STZ mice, indicating the importance of AKR in MG detoxification *in vivo* [124]. Therefore, even though Glo1 is thought to be the major detoxification mechanism, AKR and ALDH play important roles depending on the tissue and the metabolic condition.

2.Aim of the study

Although disbalances in the production or detoxification of MG lead to AGE formation, and are associated with diabetes and diabetic complication in animal models and humans, little is known about the post-translational mechanisms that regulate the MG-detoxifying enzyme Glo1 nor how MG alters cellular metabolism and its links with the development or progression of diabetes. Therefore, in my research I aimed to determine the role of post-translational modifications in the regulation of Glo1 activity and identify the responsible enzymes, as well as elucidate the impact of elevated levels of MG on cellular metabolism using *in vitro* and mouse models of diabetes.

3. Results

3.1. The regulation of Glo1 activity via its phosphorylation

3.1.1. Generation of Glo1 KO HeLa and HEK293T cell lines

The main aims of my project were to determine the role of the post-translational regulation of Glo1 activity in humans and to elucidate how MG impacts cellular metabolism. For answering both biological questions I needed to generate a Glo1 KO cell line. For this purpose, I took advantage of CRISPR-Cas9 genome editing technology. I targeted GLO1 exon 1 in HeLa cells and exon 2 in HEK293T cells. For both Glo1 KO cell lines the genome editing via CRISPR-Cas9 lead to insertion of either one or six nucleotides, causing a frame-shift mutation and an early stop codon, respectively (Figure 9). Unexpectedly, I was only able to see one type of editing event in the alleles of both cell lines, hinting that both alleles suffered the same frame-shift mutation. As I validated the KO cell lines by PCR-amplification of the target genomic locus, TOPO cloning and sanger sequencing, it is possible that the 8 colonies I sequenced were insufficient to observe a second editing event happening on the other allele. To verify KO of Glo1 with a parallel approach, I also assessed the Glo1 protein levels and activity in these cells. For measuring Glo1 activity, I monitored the formation of its product S-lactoylglutathione at 235 nm. Neither the Glo1 KO HeLa cells nor the Glo1 KO HEK293T cell line had detectable Glo1 protein nor activity, hinting that both cell lines are Glo1 KO (Figure 10A-B). Therefore, I decided to use the Glo1KO HeLa and HEK293T cell lines for my study as an essential tool to answer my biological questions.

3.1.2. Role of Y136 phosphorylation of Glo1 in stability and activity

Glo1 is the main mechanism of MG detoxification and dysregulation of its activity has important repercussions on MG levels [134, 135]. Therefore, I sought to determine whether and how Glo1 is regulated by post-translational modifications (PTM). With this aim, I used publicly available databases to generate a list of residues in Glo1 reported to be acetylated or phosphorylated (Table 1). I generated 9 different Glo1 mutants by site-directed mutagenesis, changing the phosphoresidues to alanine and the acetylated residues to arginine in order to conserve the charge. I then reconstituted the Glo1 KO HeLa cell line (Figure 9) with either the WT Glo1 protein or the nine point mutant constructs (Figure 11A). In each case I calculated the specific activity of Glo1 by measuring Glo1 activity normalized to Glo1 protein levels,

determined by western blot (Figure 11B). Analysis of the activity of the different point mutants of Glo1 revealed that the tyrosine 136 to alanine (Y136A) mutant was significantly less active than WT Glo1. Since the mutation of tyrosine 136 to alanine gave the strongest and most consistent phenotype amongst the 9 mutants that I tested, I focused on this residue.

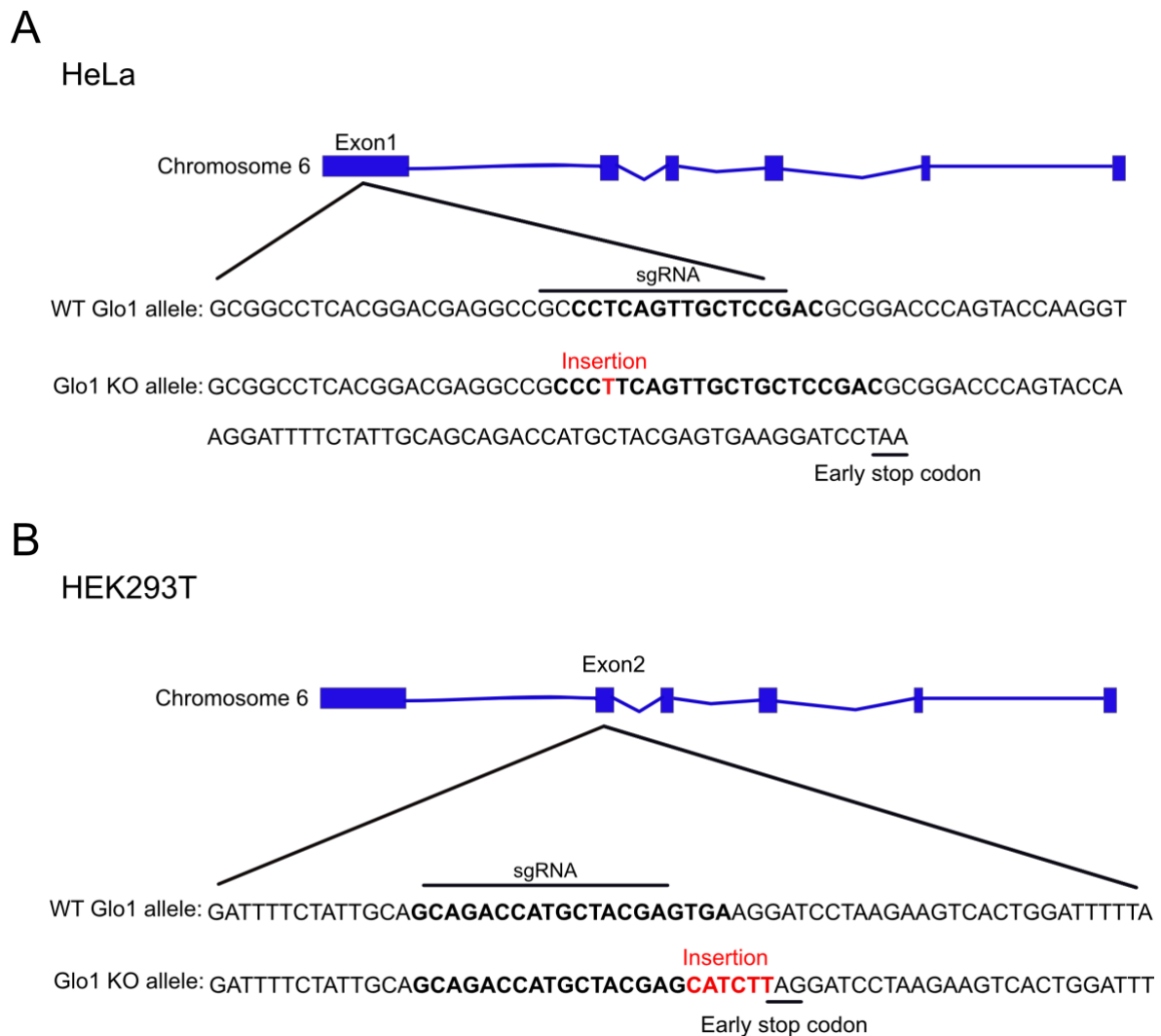


Figure 9. Molecular characterization of the Glo1 KO HeLa and HEK293T cells. Two Glo1 KO cell lines were generated by CRISPR-CAS9. (A) Molecular characterization of Glo1 KO HeLa cells and (B) Glo1 KO HEK293T cells.

To exclude that substitution of tyrosine 136 for alanine caused significant structural changes that affected Glo1 activity due to replacement of a bulky residue with a small one, I generated a second mutant where I replaced Y136 with phenylalanine. Phenylalanine differs from tyrosine by only one hydroxyl group and should cause less structural changes on Glo1. Similar to the Y136A mutant, also the Y136F mutant displayed lower activity than WT Glo1 (Figure

12A). When compared to the Y136A mutant, the Y136F mutant showed a slightly milder decrease in Glo1 activity. This is probably due to the substantial chemical difference between alanine and tyrosine.

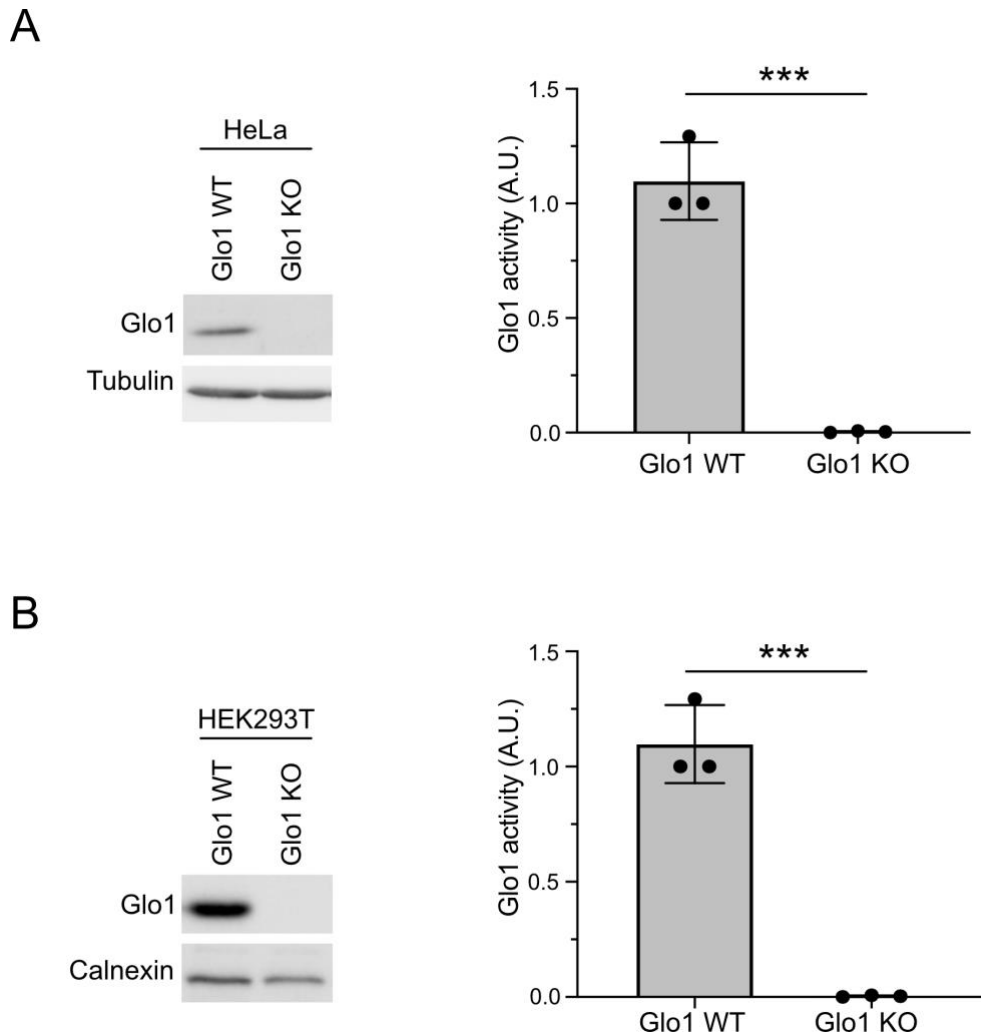


Figure 10. Glo1 KO cells do not possess Glo1 protein nor activity. I assessed Glo1 protein levels and activity on the Glo1 KO (A) HeLa and (B) HEK293T. *** $p < 0.0002$, determined by one-sided Student's t-test.

I also assessed the protein and mRNA levels of the Y136F mutant. The mutant did not show differences in protein or mRNA levels, suggesting that this PTM does not have an impact on the stability of the protein or the corresponding mRNA (Figure 12B). In order to further assess protein stability of the Y136F mutant, I incubated the cells with cycloheximide, an inhibitor of protein synthesis. Under these conditions, there was no significant difference in the rate of decrease in Glo1 protein levels between mutant and WT (Figure 12C), supporting the conclusion that this PTM only affects Glo1 activity but not stability.

Table 1. Residues of Glo1 reported to be phosphorylated or acetylated in publicly available databases.

PTM	Sequence	Residue	Database
Phosphorylation	KDFLLQQ T MLRVKD	T35	PhosphositePlus, dbPAF, PTMcode 2
Phosphorylation	RVKDPKK S LDFYTR	S45	PhosphositePlus, PHOSIDA, dbPAF
Phosphorylation	ELTHNWG T EDDETQ	T107	PhosphositePlus, UniProt, PTMcode 2
Phosphorylation	GIAVPDV Y SACKRFE	Y136	PhosphositePlus, dbPAF, PTMcode 2
Phosphorylation	IAVPDV Y SACKRFEE	S137	PhosphositePlus, dbPAF, PTMcode 2
Acetylation	PDVYSACK K RFEELGV	K140	PhosphositePlus, PTMcode 2
Acetylation	RFEELGV K FVKKPD	K148	PhosphositePlus, PHOSIDA, PTMcode 2
Acetylation	VKKPDDG K MKGLAF	K157	PhosphositePlus, PTMcode 2
Acetylation	KPDDG K MKGLAFIQ	K159	PhosphositePlus

3.1.3. Generation and validation of an antibody against pY136 of Glo1

After identifying Y136 as an important residue for Glo1 activity, I produced an antibody to specifically detect phosphorylation at this residue. To generate the phospho-Glo1(Y136) antibody, the company Seramun Diagnostica GmbH immunized rabbits with the peptide “IAVPDV(phosphoY)SA(homoalanine)KRFC” coupled to keyhole limpet hemocyanin (KLH). The use of KLH stimulates the response of the immune system due to the large size and glycosylations of this protein. Then the company harvested the hyperimmune serum and I purified the antibody using the phosphor-peptide coupled to an agarose resin. To validate the antibody, I first tested its reactivity on samples from WT and Glo1 KO HeLa cells. The pY136 antibody showed recognition of Glo1 in HeLa but not in Glo1 KO cell samples proving specificity for Glo1 (Figure 13A, first two lanes). Further validation using cells expressing only the Y136F mutant allowed me to show that the antibody detected the mutant protein far less strongly than WT Glo1 (Figure 13A, last two lanes).

As an additional control to test the antibody specificity, I purified His-tagged, human, recombinant Glo1 protein that I expressed in bacteria, which cannot phosphorylate tyrosine residues. The pY136 blot showed a substantially weaker band for the His-hGlo1 compared to WT Glo1 from HeLa cells (Figure 13B and D). These results indicate that the antibody is specific for the phosphorylated Y136 residue rather than generally recognizing the Glo1

protein. Using the pGlo1(Y136) antibody, I also observed that Glo1 is phosphorylated in various white blood cell populations (Figure 13B). It is important to mention that the pGlo1(Y136) antibody recognized some additional bands in lysates from peripheral blood mononuclear cells (PBMC), marked with ‘n.s.’, but these bands were not recognized by the antibody against total Glo1, indicating that they are unspecific (Figure 13C). Therefore, I was able to generate an antibody that recognizes GloY136 phosphorylation and it is suitable for blood cell analysis.

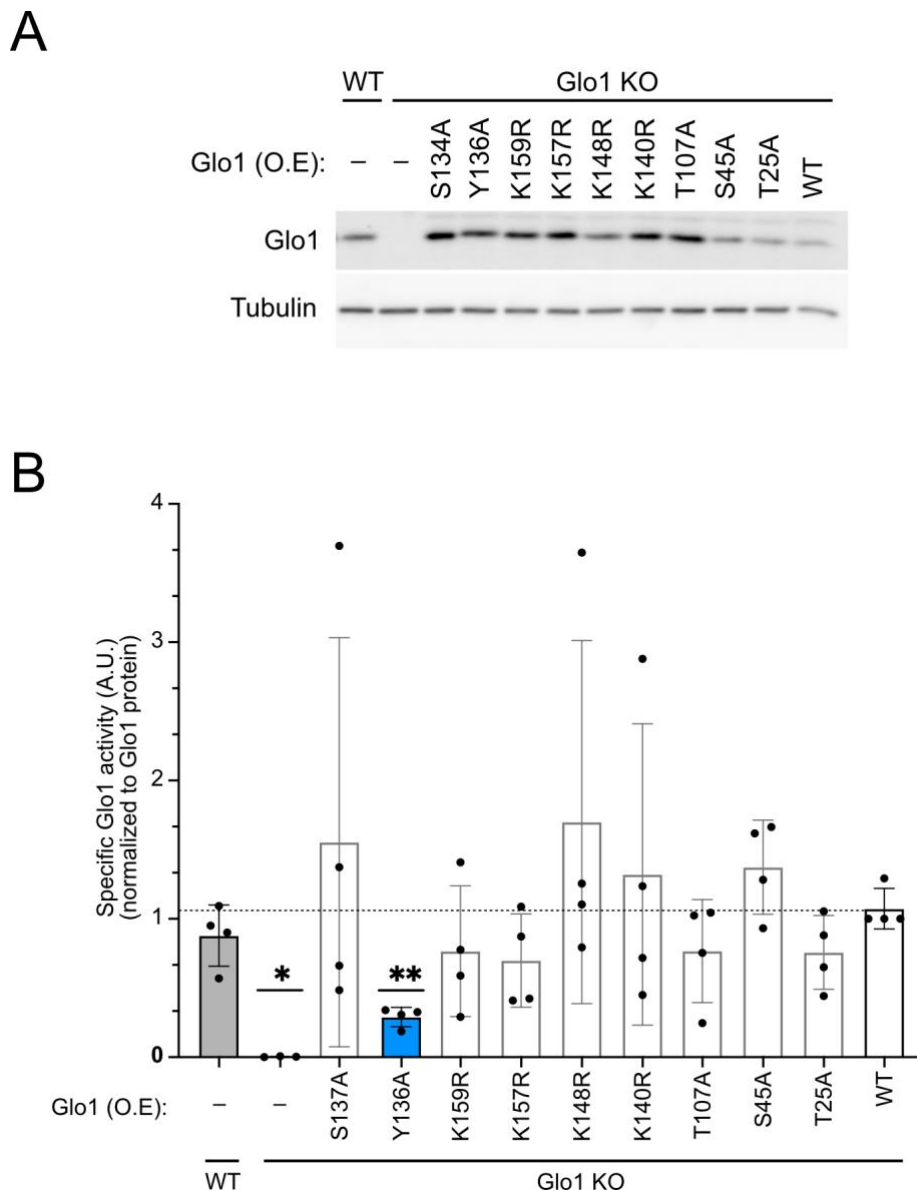


Figure 11. Mutation of tyrosine 136 to alanine decreases Glo1 activity. I used the Glo1 KO HeLa cell line to express 9 different point mutants of Glo1 and the WT protein. (A) I analyzed the expression of Glo1 by Western Blot and (B) I performed Glo1 activity assay. I quantified Glo1 protein levels by immunoblotting and I used the protein levels to normalize the Glo1 activity measurements. Biological replicates n=4, *p<0.05, **p<0.01 determined by mixed effect ANOVA (multiple comparison). Over expression (O.E). This is published data [149].

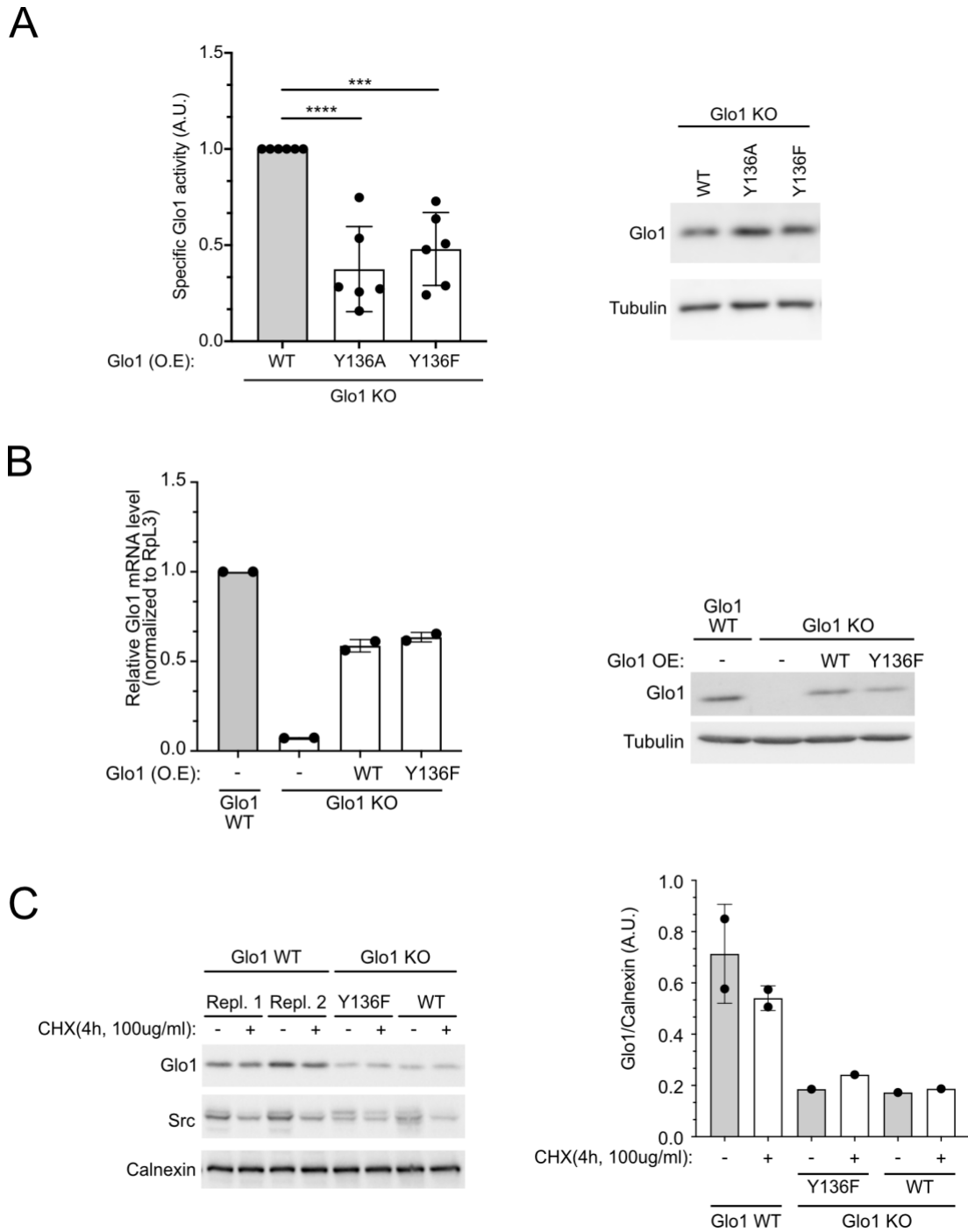


Figure 12. Mutation of tyrosine 136 to phenylalanine reduces Glo1 activity but has no effect on protein stability. (A) I transfected Glo1 knockout HeLa cells to express either wildtype or mutants Y136A or Y136F of Glo1. I quantified Glo1 protein levels by immunoblotting (right panel) and I used these values to normalize Glo1 activity measurements (left panel). Biological replicates n=6. *p<0.05, **p<0.01, determined by one-way ANOVA (multiple comparison). (B-C) Glo1 KO HeLa cells were transfected either with WT or Y136F Glo1 and (B) I assessed the stability of Glo1 mRNA and protein by immunoblot and qPCR, or (C) I incubated the cells with 100ug/ml cycloheximide (CHX) for 4 hours to assay Glo1 protein stability in the absence of de novo synthesis. For (B-C) biological replicates n=2. Over expression (O.E). This is published data [149].

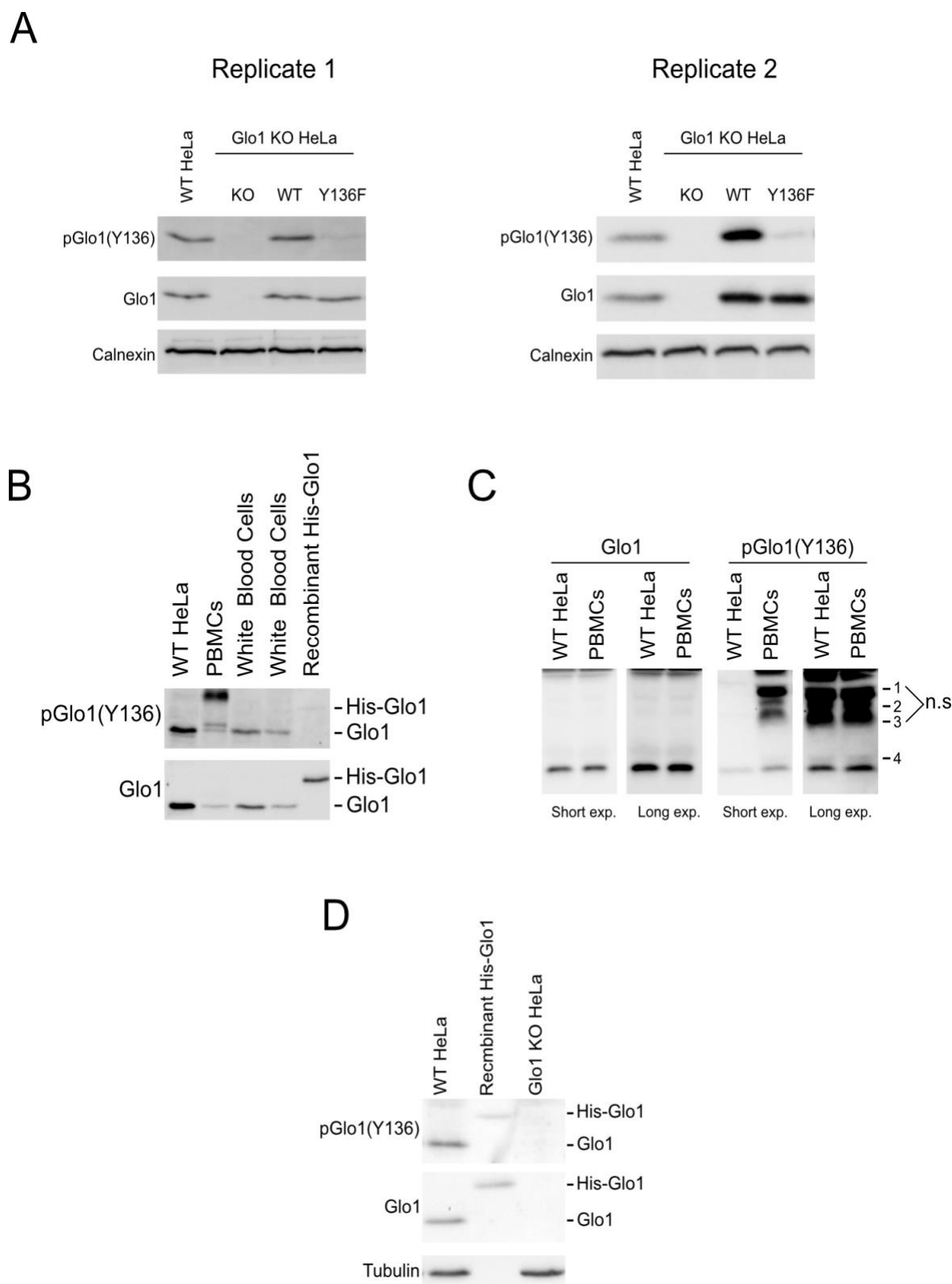


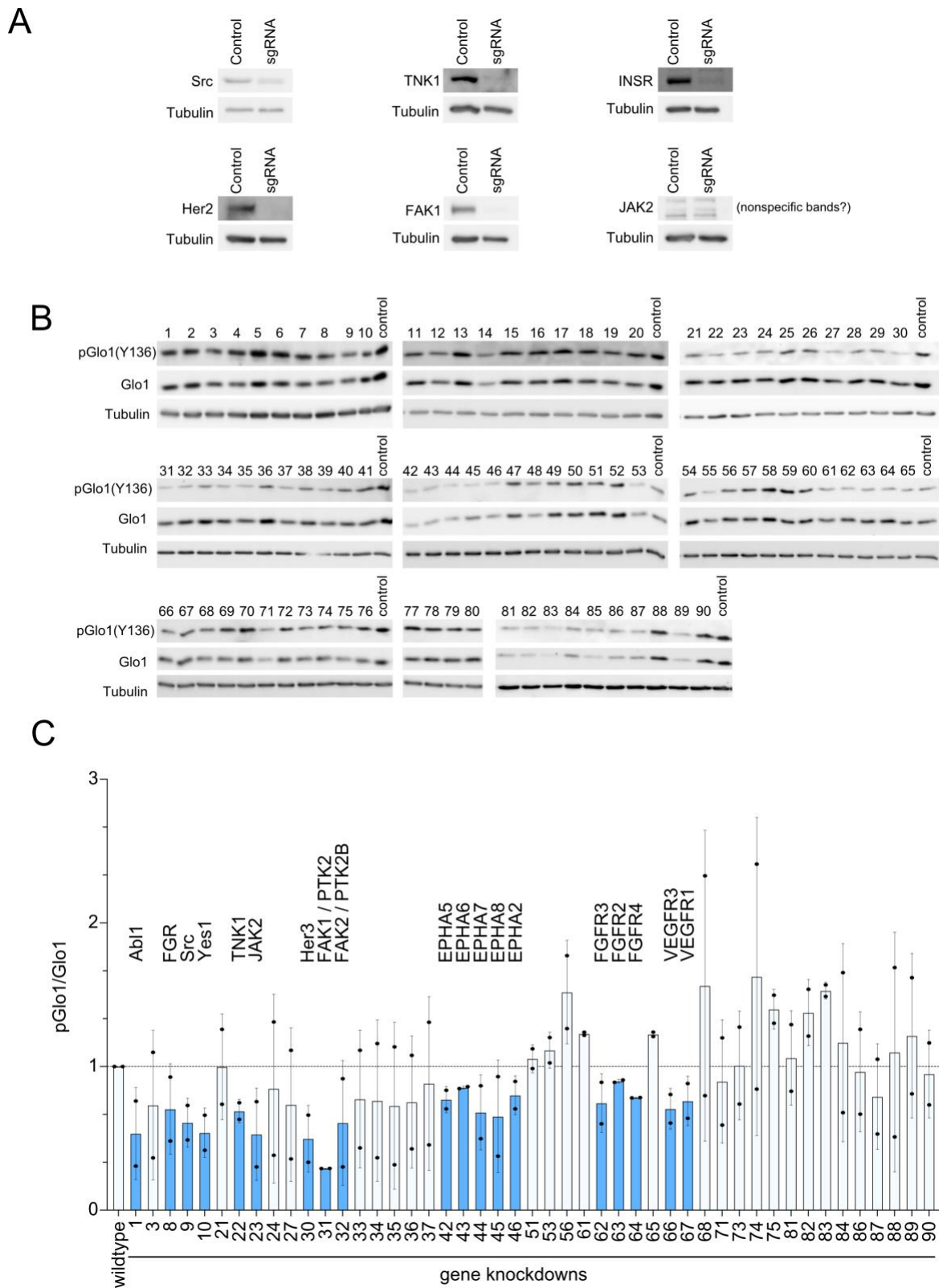
Figure 13. Validation of pGlo1(Y136) antibody. (A) I analyzed extracts from wildtype HeLa cells, or Glo1 KO cells that I transiently transfected with either WT or Y136F Glo1 by immunoblotting with the pGlo1(Y136) antibody. In (B) and (D) I used recombinant His-tagged wildtype Glo1 protein from bacteria as a control for pGlo1(Y136) antibody. (B-C) I tested lysates from different cells lines by immunoblotting. (C) in the pGlo1(Y136) immunoblot of the PBMC sample there are 4 bands that are not detected by the total Glo1 antibody. Peripheral blood mononuclear cells (PBMCs), non-specific (n.s). This is published data [149].

3.1.4. Identification of the kinase responsible for Y136 phosphorylation of Glo1

In order to identify the kinase responsible for the phosphorylation of Glo1, I carried out a CRISPR-Cas9 screen using pY136 as readout. First, I generated a sgRNA library targeting all 90 tyrosine kinases described in humans with two sgRNAs per kinase. The final library had a total of 180 CRISPR-Cas9 plasmids. I assigned numbers to each kinase as shown in table 6. Then, I assessed the efficiency of selected sgRNAs with the antibodies available in the laboratory. Out of 6 sgRNAs tested, 5 caused a substantial reduction in the protein levels of the target kinase (Figure 14A). Later, I performed the screen, first with the whole library (all 90 kinases) (Figure 14B) and then with a subset of sgRNAs to confirm promising or unclear hits. I quantified all the western blots and I used HeLa lysates as normalization control. Surprisingly, I was able to identify more than 19 tyrosine kinases whose depletion led to reduction of Glo1 phosphorylation on Y136 as compared to control HeLa sample. Among the identified kinases, I found several members of the Src family (Src, Yes1, FGR, and the related Abl1), and of the FAK, EPHA, FGFR, and VEGFR families (Figure 14C).

Since KD of a kinase affects all of its downstream targets, it is possible that the decrease in Glo1 phosphorylation I observed in the screen is an secondary, indirect effect (Figure 14). Thus, I wanted to assess which kinases could directly phosphorylate Glo1. To do so, I selected the most promising candidates and performed an *in vitro* kinase assay. The assay showed that all the members of the Src family, as well as Epha5 and VEGFR3 can phosphorylate recombinant Glo1 at Y136 (Figure 15A-B). In contrast, the kinases Fak1, Jak2, and Tnk1 were not able to phosphorylate Glo1(Y136) *in vitro* (Figure 15A), suggesting that the effect on Glo1(Y136) phosphorylation I observed in the CRISPR-Cas9 screen may be indirect for these kinases (Figure 14B-C). Therefore, Glo1 can be redundantly phosphorylated by several kinases and receptor tyrosine kinases *in vitro*.

The members of Src kinase family were especially efficient at phosphorylating Glo1(Y136). Thus, I further validated their role *in vivo*. To do so, I first knocked down Src using siRNAs. I was able to detect a decrease in Glo1(Y136) phosphorylation compared with the control siRNA targeting luciferase (Figure 16A). This result validated the findings of the screen (Figure 14C) and suggested that the reduction of Glo1(Y136) phosphorylation upon loss of Src kinase is an on-target effect. However, upon knockdown Glo1 phosphorylation was only partially decreased, hinting at the contribution of other kinases on Glo1(Y136) phosphorylation.



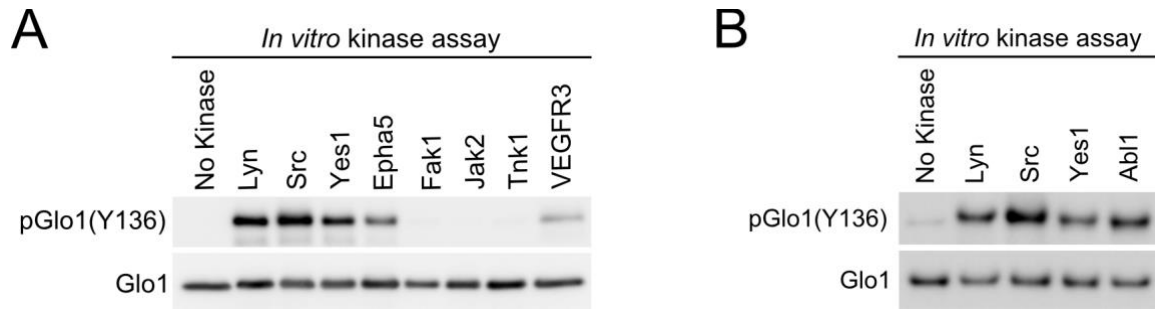


Figure 15. Glo1 Y136 is phosphorylated by multiple different kinases including all members of the Src family. (A-B) I performed an *in vitro* kinase assay with recombinant His-tagged human Glo1 (hGlo1) and multiple tyrosine kinases. This is published data [149].

The Src kinases family is composed of 9 members Src, Yes, Fyn, Fgr, Lck, Hck, Blk and Lyn. Additionally, the Abl kinases are also highly related to Src kinase family. Therefore, I decided to pharmacologically inhibit all Src kinases with the broad range inhibitors sacaratinib and dasatinib, as well as the Abl inhibitor nilotinib individually or combinations with sacaratinib (Figure 16). To assay Src inhibition, I used an antibody against an autophosphorylated residue that activates Src (pSrc(Y416)) and the phosphorylation site of a downstream target, namely pFak1(Y925). Unexpectedly, when I treated HeLa cells with either nilotinib, sacaratinib or a combination of both for 30 minutes, I observed Src inhibition but no reduction in Glo1(Y136) phosphorylation (Figure 16B). As 30 minutes incubation with saracatinib could be insufficient to cause a drop in Glo1 phosphorylation, I also incubated HeLa cells overnight with the Src family inhibitors saracatinib or dasatinib (Figure 16C). However, also under these circumstances I was not able to observed a drop in Glo1(Y136) phosphorylation. Lastly, I tried an additional inhibitor of the Src kinase family, namely PP2, which is used to broadly inhibit the Src kinase family, especially Fyn and LcK. I incubated HeLa cells overnight with either PP2 or its inactive analog PP3. But, once more there was no decreased Glo1(Y136) phosphorylation (Figure 16D). These results highlight an incongruity between the genetic and the pharmacological inhibition. It is possible that the contribution of each kinase to Glo1(Y136) phosphorylation is mediated by additional factors that differ between the genetic and pharmacological inhibition experiment, for example levels of growth factor or metabolites in the medium at the time of cell lysis. Further studies are still required to fully understand if the Src kinase family is responsible of Glo1 phosphorylation *in vivo*.

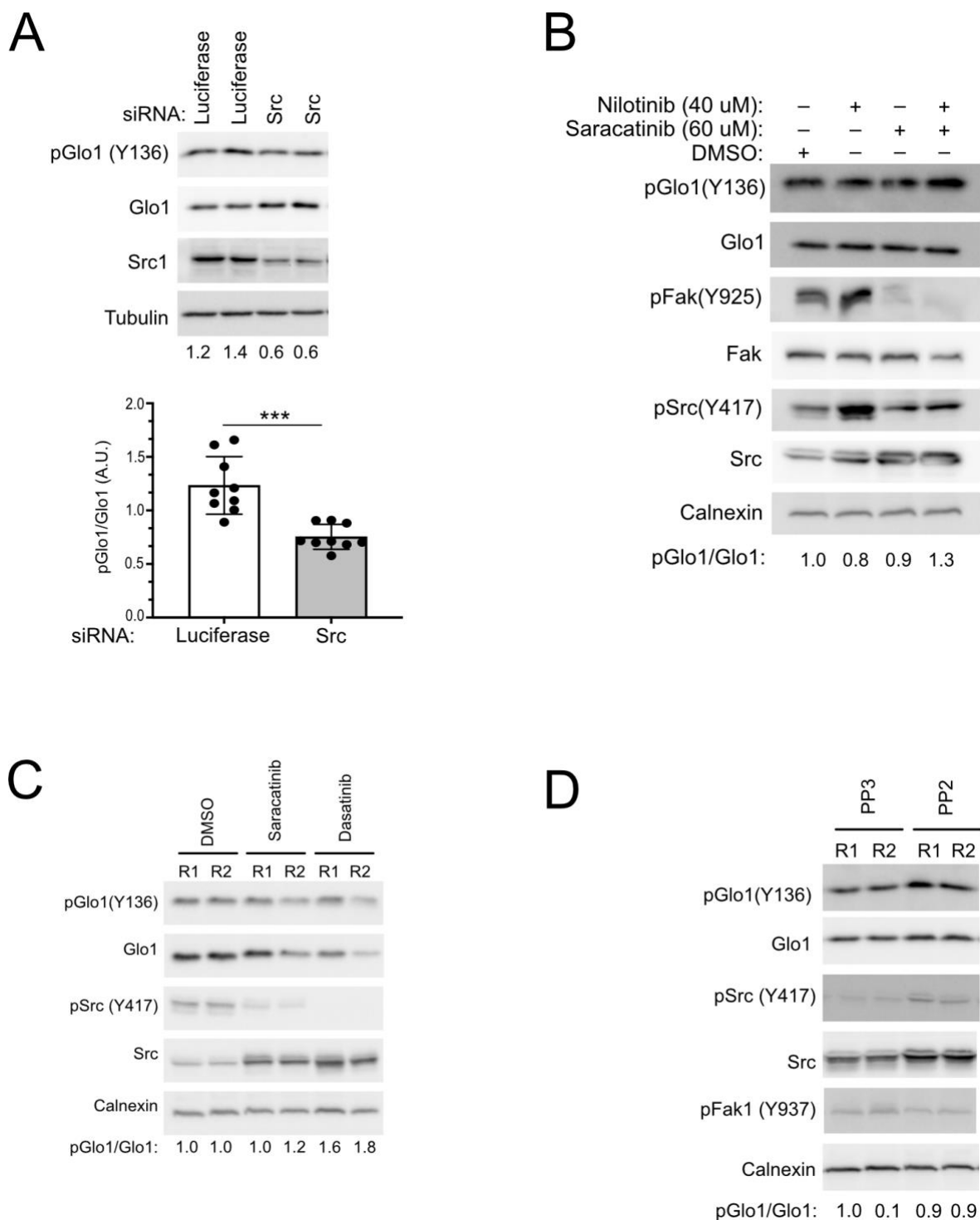


Figure 16. Validation of Src kinase family as responsible for Glo1(Y136) phosphorylation. (A) I knocked down Src kinase using a pool of 4 siRNAs either targeting Src kinase or luciferase as a negative control. Biological replicates n=9, ***p=0.002 determined, by two-sided unpaired Student's t-test. (B) I incubated HeLa cells for 30 minutes with either the Src inhibitor Saracatinib and/or the Abl1 inhibitor Nilotinib. (C) I incubated HeLa cells overnight with either Saracatinib or Dasatinib, (D) or the Src family inhibitor PP2 I used PP3 the inactive analogue of PP2 as negative control. I validated the inhibition of the Src kinase family using pSrc(Y417) or pFak(Y925) antibodies. This is published data [149].

3.1.5. Phosphorylation of Glo1(Y136) increases its activity

Having identified Y136 of Glo1 as necessary for its activity in loss-of-function experiments (Figure 11 and 12A), I then determined whether phosphorylation at this residue would be sufficient to increase Glo1 activity. To this end, I phosphorylated recombinant hGlo1 *in vitro* using either Src or Lyn and then performed a Glo1 activity assay (Figure 17A, upper panel). The phosphorylation of Glo1 by either Src or Lyn kinase increased its activity compared with the non-phosphorylated Glo1 (Figure 17A, lower panel). I then further validated the contribution of Y136 phosphorylation to this increased activity in a similar assay using purified recombinant Y136F Glo1 so as to prevent phosphorylation at this residue (Figure 17B). The Y136F mutation blunted the increase in Glo1 activity observed upon phosphorylation by Src, indicating that phosphorylation by Src at this residue mediates at least in part this effect. However, I could still detect a mild increase in Glo1 activity in the Y136F mutant upon phosphorylation by Src, suggesting that phosphorylation at other tyrosines could also contribute. Thus, I demonstrated for first time that the activity of Glo1 increases when its phosphorylated on Y136.

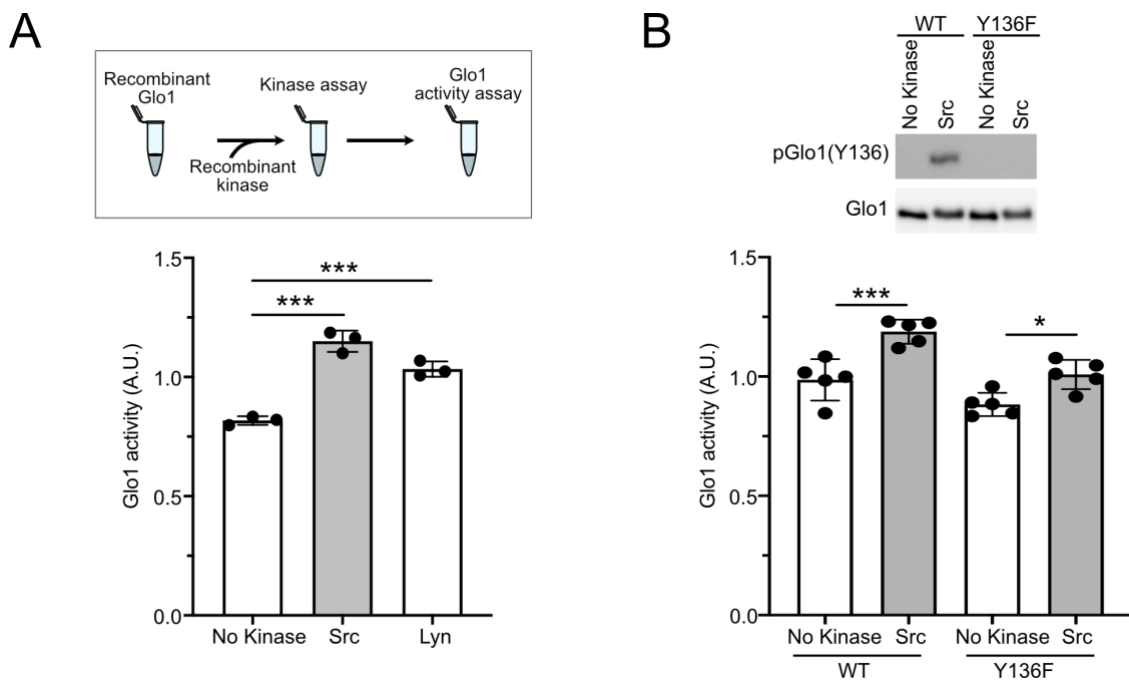


Figure 17. Phosphorylation of Glo1 on Y136 by Src kinases increases its activity. (A-B) I performed an *in vitro* kinase assay followed by a Glo1 activity assay. For the assays, I incubated recombinant non-phosphorylated WT or mutant Y136F Glo1 with either Src (A-B) or Lyn (A) kinases. Then I measured Glo1 activity. (B top panel) Immunoblot of WT or mutant Y136F Glo1 *in vitro* phosphorylated or not with Src kinase. Biological replicates n=3 for (A), n=5 for (B). For all panels, *p<0.05 and ***p<0.001, determined by one-way ANOVA (multiple comparison). This is published data [149].

3.1.6. Cellular conditions that regulate Glo1(Y136) phosphorylation in cell culture

It is of great importance to identify the cellular conditions affecting Glo1(Y136) phosphorylation and activity in order to understand its possible role in the development of pathologies like diabetes. Therefore, I assessed the status of Glo1(Y136) phosphorylation under different stimuli, MG and glucose (Glc). I decided to not only use HeLa but also HepG2 cells, a hepatocellular carcinoma cell line. The liver plays an important role in Glc homeostasis and in diabetes liver functions are dysregulated. Therefore, assessment of how Glo1 phosphorylation is regulated in liver cells would be more relevant for a better understanding of metabolic pathologies as diabetes. I started by studying whether MG has an effect on Glo1(Y136) phosphorylation. Regulation of Glo1 activity by MG would allow the cell to adjust its detoxification rate to the rate of MG production. I incubated HeLa or HepG2 cells with different concentrations of MG for 30 minutes and assessed Glo1(Y136) phosphorylation by immunoblotting. There were no significant changes in Glo1(Y136) phosphorylation upon MG treatment (Figure 18A-B). Thus, MG has no evident effect on Glo1(Y136) phosphorylation in HeLa or HepG2 cells.

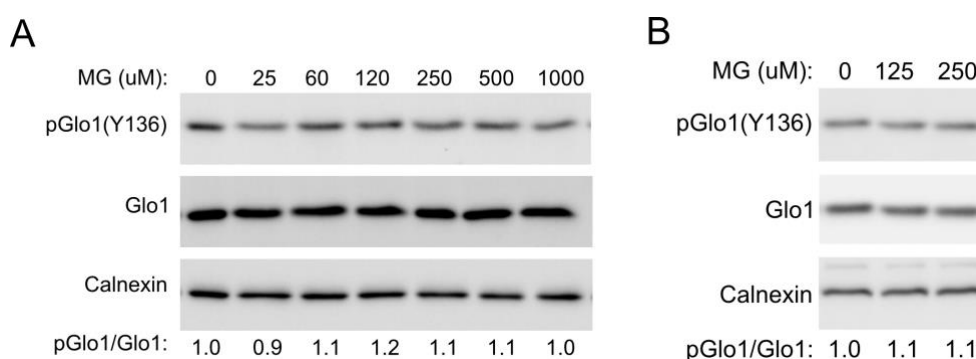
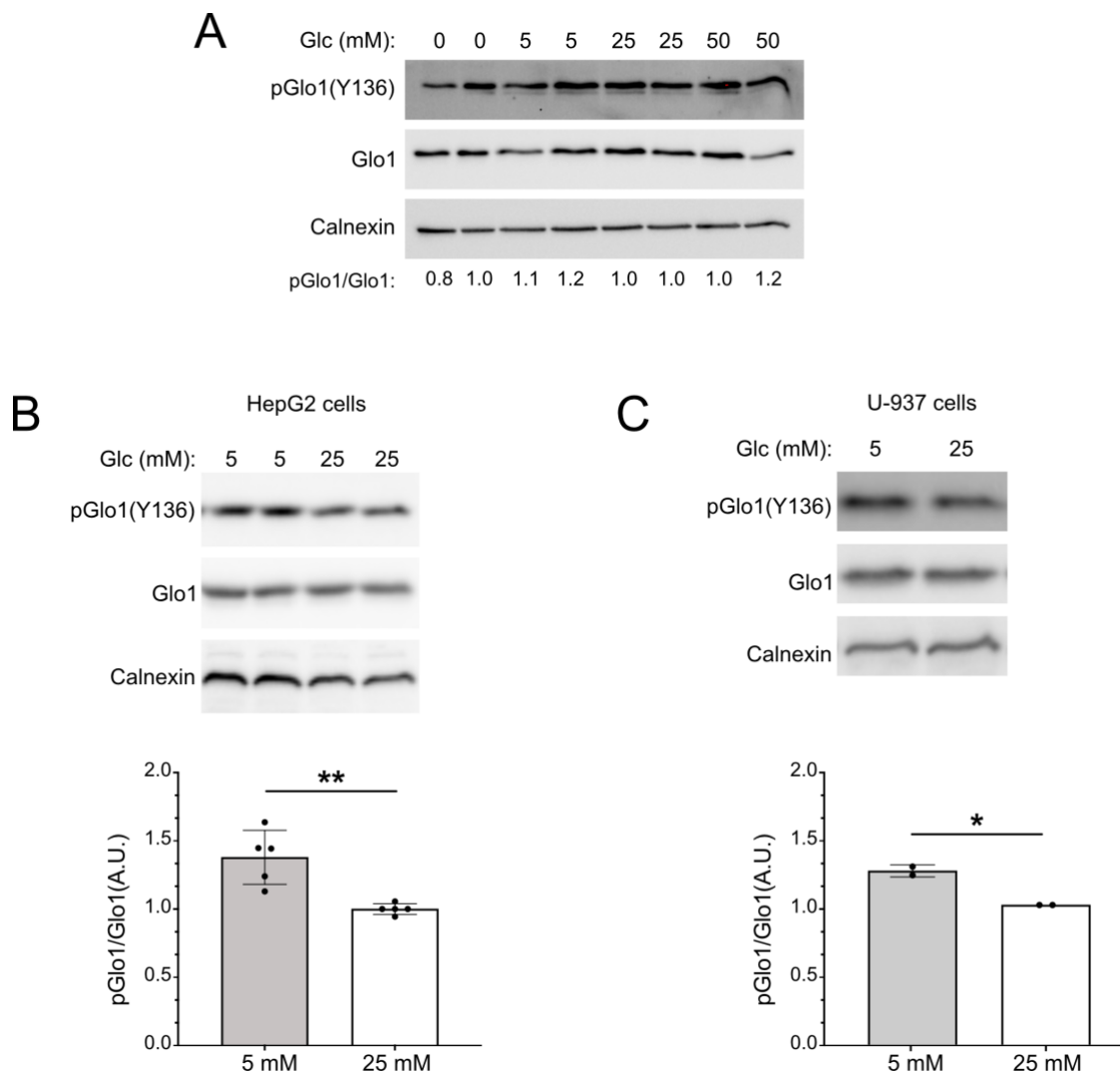


Figure 18. Glo1(Y136) phosphorylation does not respond to MG in HeLa or HepG2. I incubated (A) HeLa or (B) HepG 2 cells with increasing concentrations of MG for 30 minutes and assessed Glo1 phosphorylation by immunoblotting. This is published data [149].

Dysregulation in Glc usage and clearance lead to hyperglycemia and diabetes. Diabetic patients have elevated MG levels in plasma, suggesting a clear relationship between hyperglycemia and MG production [91, 115, 116]. Because of this, I decided to test the effect of Glc on Glo1(Y136) phosphorylation. Hence, I incubated HeLa cells overnight with different concentrations of Glc, but no Glc concentration changed Glo1(Y136) phosphorylation significantly (Figure 19A). Thus, Glc does not affect Glo1(Y136) phosphorylation in HeLa cells. Interestingly, however, Glc did have an impact on Glo1(Y136) phosphorylation in two other cell lines. Overnight incubation of either liver HepG2 or

myeloid U-937 cells with 5 mM Glc caused an increase in Glo1(Y136) phosphorylation as compared to high Glc condition (25 mM) (Figure 19B-C), indicating that Glc regulates Glo1 phosphorylation at this residue in these cell lines. The observed differences in Glo1(Y136) phosphorylation levels upon glucose stimulation between these different cell lines could be explained by the fact that HepG2 is a human liver cancer cell line and the liver plays an important role in systemic Glc metabolism. Thus, changes in Glc levels are especially relevant in this tissue. In fact, it has been reported that hyperglycemic conditions cause HepG2 cells to develop steatosis, commonly seen in diabetes [150]. Additionally, U-937 cells are also highly sensitive to hyperglycemic conditions. It has been reported that hyperglycemia leads to cell death in this cell line, indicating its high sensitivity to Glc-induced changes [151, 152].



I then assessed Glo1 activity in HepG2 or U-937 cells incubated with either 5 or 25 mM Glc overnight. Consistent with the effect of high Glc on Glo1 phosphorylation, Glo1 activity decreased in both cell lines incubated with 25 mM Glc when compared with their 5 mM Glc controls (Figure 20A-B). These results support the observation that Glo1(Y136) phosphorylation activates the enzyme and suggest that an increase of Glc levels beyond the physiological range, 5.5 to 7 mM Glc, paradoxically negatively affects Glo1(Y136) phosphorylation and activity and may thus cause a buildup of MG. It is worth noting that, although the decrease in Glo1 activity for both cell lines was only around 20%, MG is a highly reactive molecule and a small rise in its levels may be enough to cause significant amount of modifications on proteins, leading to important changes in the function of these macromolecules.

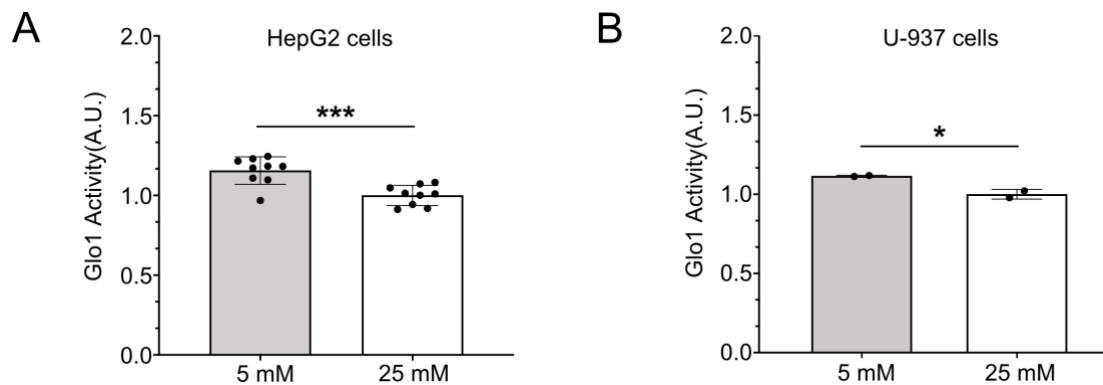


Figure 20. Glo1 activity is decreased in hyperglycemic conditions in HepG2 and U-937. I cultured (A) HepG2 or (B) U-937 cells overnight in physiological (5 mM) or high (25 mM) Glc concentrations. Then, I assessed Glo1(Y136) Glo1 activity. Biological replicates; (A) n=10 and (B) n=2. For all panels, *p<0.05 and ***p<0.001, determined by two-sided, unpaired Student's t-test. This is published data [149].

3.1.7. Assessment of Glo1 phosphorylation levels in tissues from diabetic and healthy mice

It was reported before that liver and kidney tissue from diabetic mice display high MG levels and reduced Glo1 activity compared to non-diabetic mice, but the underlying mechanism is still unclear [132, 153]. Based on my observations that phosphorylation of Y136 regulates Glo1 activity and is decreased under hyperglycemic conditions, I hypothesized that hyperglycemia could cause a decrease in Glo1(Y136) phosphorylation during diabetes. Thus, I decided to assess the status of Glo1(Y136) phosphorylation in a broad range of animal models of diabetes. Administration of streptozotocin (STZ) causes a depletion of

pancreatic beta cells and hence, leads to reduced insulin secretion and hyperglycemia. Consistent with the *in vitro* results, I observed that liver samples from STZ mice did indeed show a significant decrease in Glo1(Y136) phosphorylation compared to the respective controls (Figure 21).

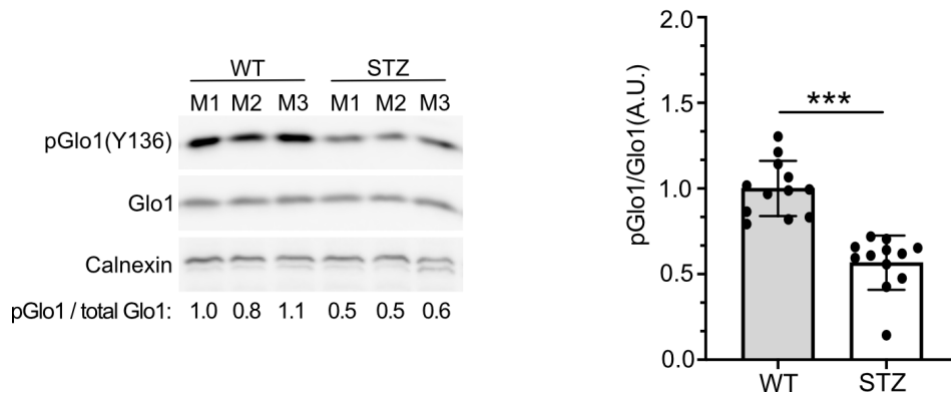


Figure 21. Glo1(Y136) phosphorylation is decreased in STZ mice. (A) I assessed Glo1 Y136 phosphorylation in liver of control or STZ mice by immunoblotting and I quantified immunosignal. n=3 biological replicates x 4 technical replicates. ***p<0.001, determined by two-sided, unpaired Student's t-test. Mouse (M). This is published data [149].

I also studied Ins2Akita mice, which represent a genetic mouse model of diabetes caused by a dysfunctional insulin 2 gene. At 3 and 6 months Ins2Akita mice showed a decrease in Glo1(Y136) compared to their respective controls (Figure 22B-C), consistent with the results from the STZ model (Figures 21). Unexpectedly, at 1 month of age Glo1(Y136) phosphorylation was higher rather than lower in Ins2Akita mice (Figures 22A) despite the presence of hyperglycemia. One possibility is that other factors different from glucose might be regulating Glo1(Y136) phosphorylation in an opposite manner, possibly as an initial compensatory mechanism that subsequently fails in the later stages of the disease.

Finally, I evaluated Glo1(Y136) phosphorylation in a mouse model with hypercholesterolemia and hyperglycemia (HGHCi). In this mouse model, the animals express the gain of function variant of murine PCSK9 in the liver. PCSK9 plays an important role in lipoprotein metabolism and its hyperactivation leads to hypercholesterolemia [154, 155]. The animals were also injected with streptozotocin to generate hyperglycemia and fed a high-fat diet to enhance the production of cholesterol [154]. In the case of HGHCi mice, Glo1(Y136) phosphorylation was lower than in control animals (Figures 23A), supporting what I saw in other diabetes mouse models (Figures 21-22). Similarly, also high-fat diet alone caused some reduction in Glo1(Y136) phosphorylation, although not significant

(Figure 23B), consistent with the alterations in glucose homeostasis often observed in high-fat dietary regimens. Together, these *in vivo* data in combination with the *in vitro* results discussed above indicate that Glo1(Y136) phosphorylation enhances Glo1 activity and is itself affected by glucose levels, in that high glucose causes less phosphorylation at this residue and hence lower Glo1 activity. This mechanism could at least in part explain the origin of the buildup of MG often observed in hyperglycemic conditions.

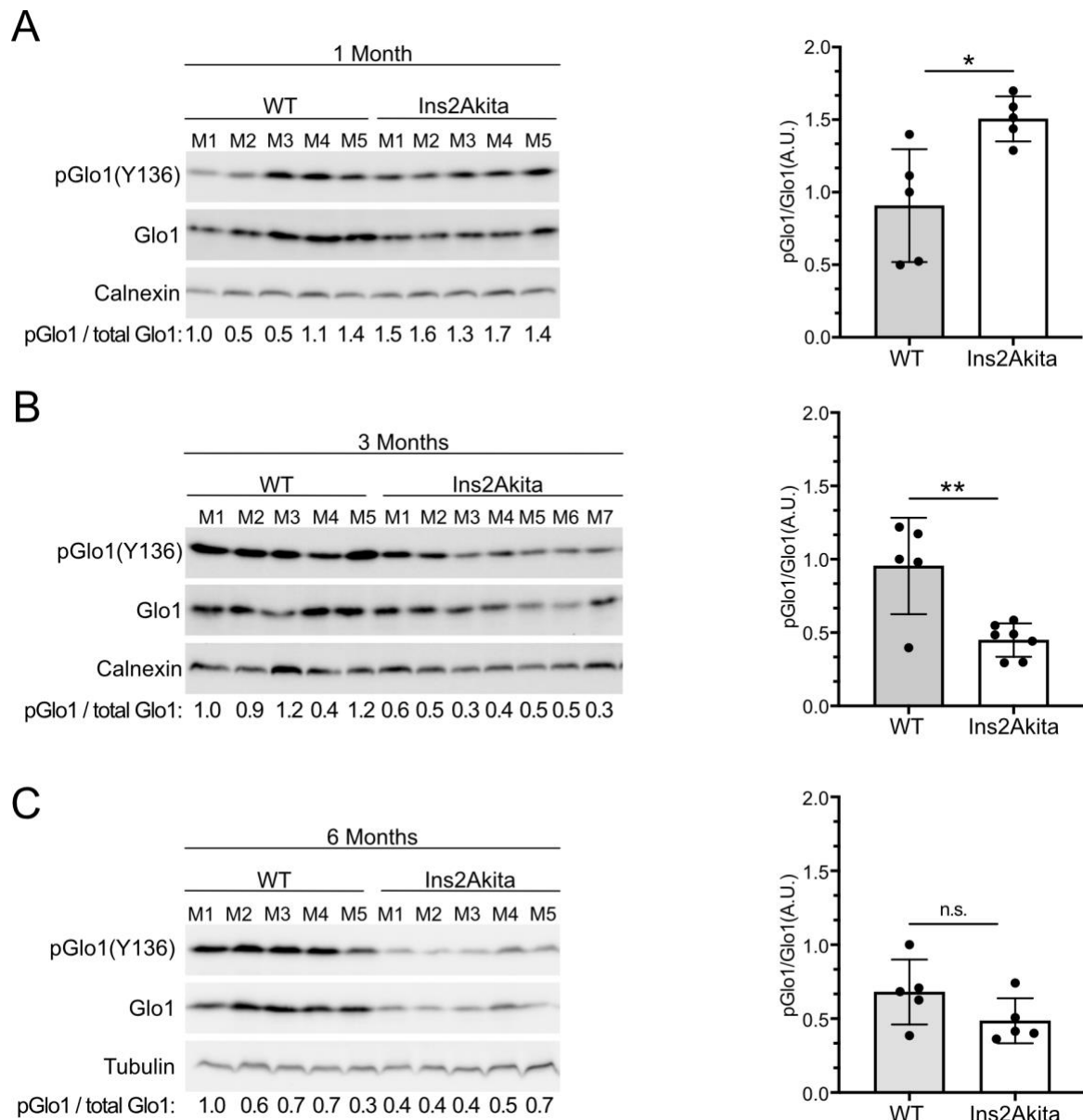


Figure 22. Glo1(Y136) phosphorylation is decreased in Ins2Akita mice. I assessed Glo1(Y136) phosphorylation in liver of ins2akita mice (A) 1-month old, (B) 3-months old and (C) 6-months old. (A-B) In all cases, the representative immunoblot are shown on the left and the respective quantification are on the right side. Biological replicates for (A) n=5, for (B) n=5 for WT and n=7 for Ins2Akita, and for (C) n=5. For all panels, *p<0.05, **p<0.01 and ***p<0.001, determined by two-sided, unpaired Student's t-test. Mouse (M), not significant (ns). This is published data [149].

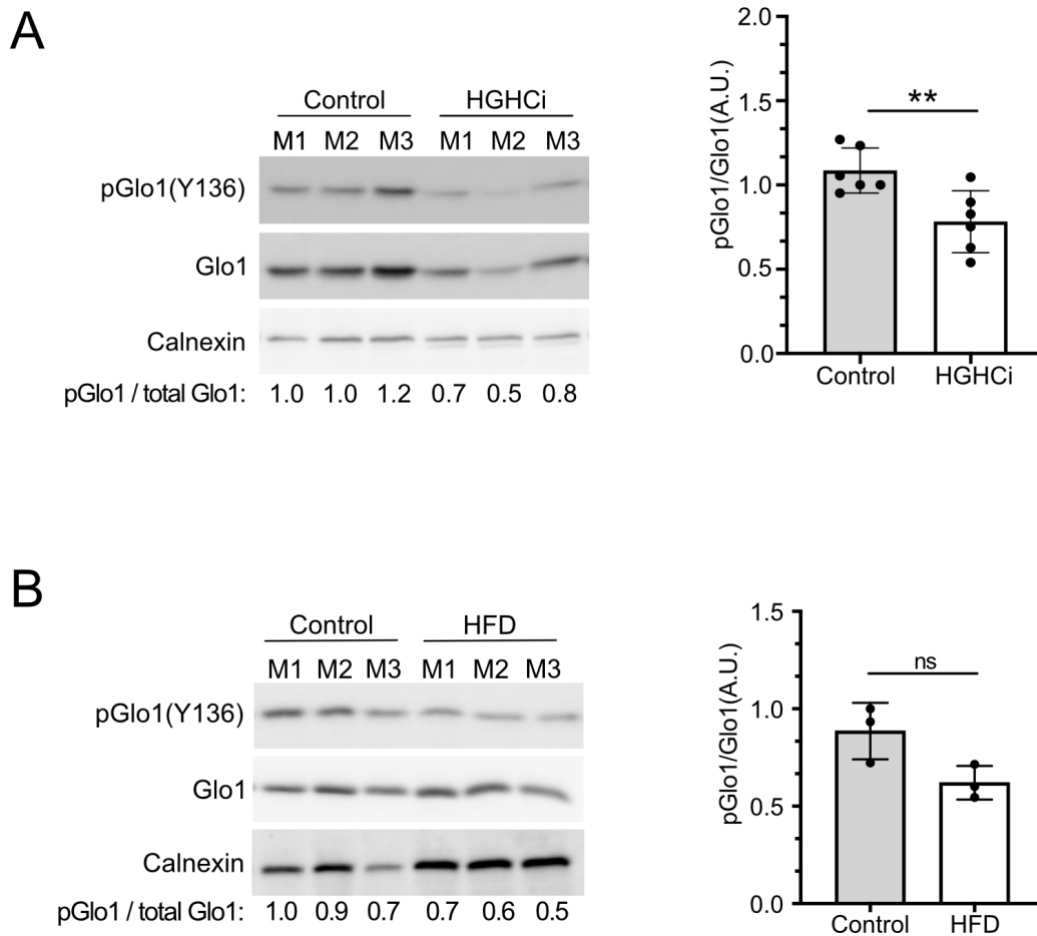


Figure 23. Glo1(Y136) phosphorylation is decreased in HGHCi mice and possibly in HFD mice. I assessed Glo1(Y136) phosphorylation in liver extracts of control or (A) HGHCi or (B) HFD mice. In panel (A) I re-hybridized the phospho-Glo1 membrane with total-Glo1 blot. Biological replicates for (A) n=3 x 2 technical replicates and for (B) n=3. *p<0.05, **p<0.01 and ***p<0.001, determined by two-sided, unpaired Student's t-test. Mouse (M). Not significant (ns). This is published data [149].

3.2. The impact of MG on cellular metabolism

3.2.1. Strategies for the study of MG impact on cellular metabolism

Dysregulation of Glo1 activity could lead to elevated levels of MG, protein modifications and changes in their canonical function. Moreover, dysregulation of protein activity due to MG adducts could cause important changes in cellular metabolism. In particular, our lab has previously shown that FASN is directly modified by MG and that its activity is increased in Glo1 KO flies and accompanied by increased total body triglyceride levels [101], raising the possibility that MG might be acting as a signaling molecule capable of selectively modifying proteins and triggering changes in the cellular state and metabolism. Building on these findings, I wanted to determine which metabolic pathways are affected by MG and how.

I first sought to determine the optimal conditions to study the impact of MG on cellular metabolism. I used two approaches, one based on different Glo1 KO cell lines to mimic a more stable increase in MG levels and a second one where I incubated cells with MG to mimic a transient increase in MG levels. I started by phenotyping the HEK293T and HeLa Glo1 KO cells I previously generated (Figures 9-10). I assessed MG levels in WT and Glo1 KO HeLa and HEK293T cell lines in collaboration with Thomas Fleming (Laboratory of Mechanism of Chronic Diseases at the University Hospital Heidelberg). However, there were no significant changes in the levels of intracellular MG between the WT and KO cell lines (Figure 24A-B), possibly because the method used for MG measurement involves extensive processing of the samples, including lysis and deproteination, which could cause small difference in MG levels to be undetected [156].

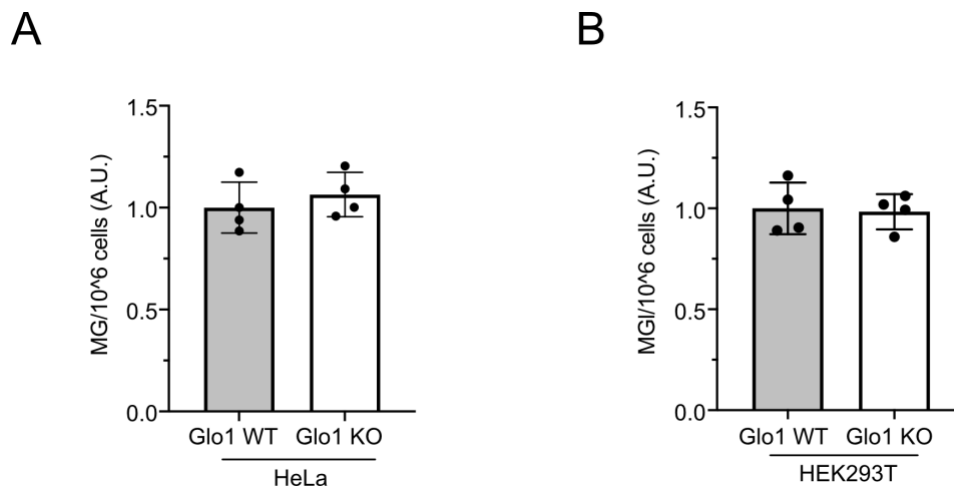


Figure 24. Free intracellular MG is not increased in Glo1 KO cells. (A) I seeded 0.5×10^6 cells HeLa cells and (B) 10^6 cells HEK293T cells, the next day I wash the cells once and then snap froze them for posterior measurement of intracellular levels of free MG. (A-B) Biological replicates $n=4$. Determined by two-sided, unpaired Student's t-test.

The MG measurements mentioned above (Figure 24) reflect only free levels of the metabolite and do not include adducts formed by MG with proteins. The main type of MG adducts on arginine is MG-H1, while CEL is formed by the interaction of MG with lysine residues. Therefore, I next assessed the presence of MG-H1 and CEL adducts in Glo1 WT and KO HeLa cells (Figure 25). As MG has been reported to interact substantially with DNA and mitochondrial proteins [157-159], I evaluated the presence of MG adducts in various cellular compartments. No substantial increase in MG-H1 or CEL adducts was observed in the input or cytosolic fraction. However, a band around 35 kDa detected by the antibody against CEL adducts was increased in both mitochondrial and nuclear fractions of Glo1 KO cells compared

with the WT (Figure 25, upper panel). Additionally, a band above 250 kDa detected by the antibody against MG-H1 adducts was increased in the nuclear fraction of Glo1 KO HeLa cells, (Figure 25, second panel). Together, these results indicate that, in basal conditions, Glo1 KO HeLa cells experience a mild, probably chronic, increase in MG levels which causes selected protein adducts to form, but that do not correspond to a detectable increase in overall free MG levels.

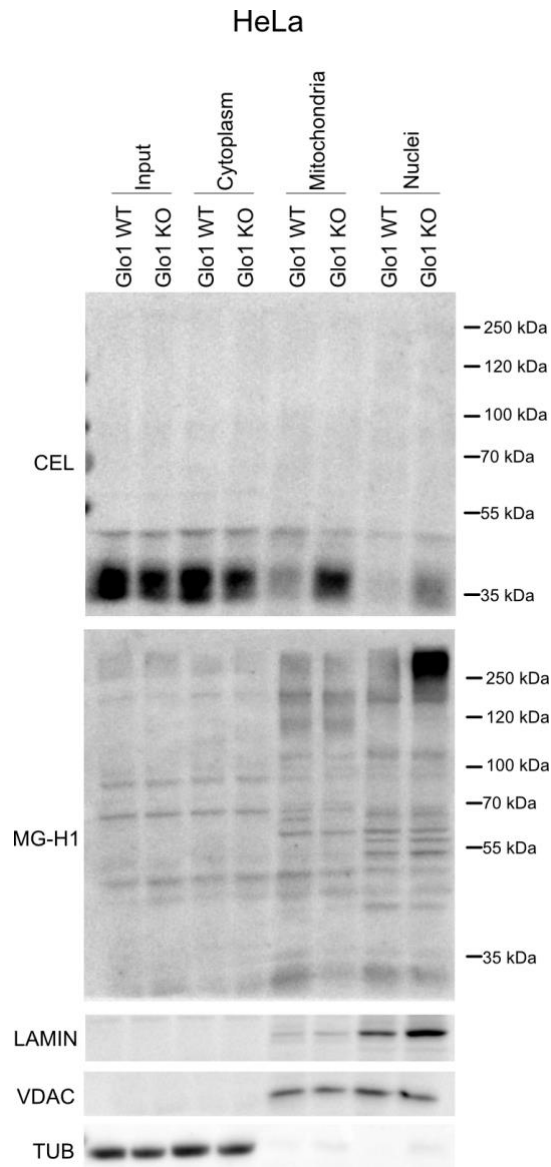


Figure 25. Increased levels of MG adducts in mitochondrial and nuclear fraction of Glo1 KO HeLa cells. I performed cell fractionation of WT or Glo1 KO HeLa cells. Then, I assessed levels of lysine CEL adducts (first immunoblot) and arginine MG-H1 adducts (second immunoblot). The three lower immunoblots show the loading controls for the different cellular compartments, LAMIN (nuclear), VDAC (mitochondrial) and TUB (cytosolic and input).

I also investigated whether MG adducts were increased in different cellular compartments of Glo1 KO HEK293T cells (Figure 26). Consistent with the results observed in HeLa cells, a band around 35 kDa detected by the antibody against CEL adducts was increased in the mitochondrial fraction of Glo1 KO cells when compared with WT HEK293T cells (Figure 26, first panel). In contrast to Glo1 KO HeLa cells (Figure 25), no increase in MG-H1 immunosignal for high molecular weight proteins was detected in the nuclear fraction of the Glo1 KO HEK293T cells (Figure 26, second panel). Nevertheless, the immunosignal detected by the antibody against MG-H1 adducts was increased for low molecular weight proteins in the Glo1 KO HEK293T mitochondrial fraction but not the WT one (Figure 26, second panel). These results suggest that Glo1 KO HEK293T cells have elevated MG levels in comparison to WT cells.

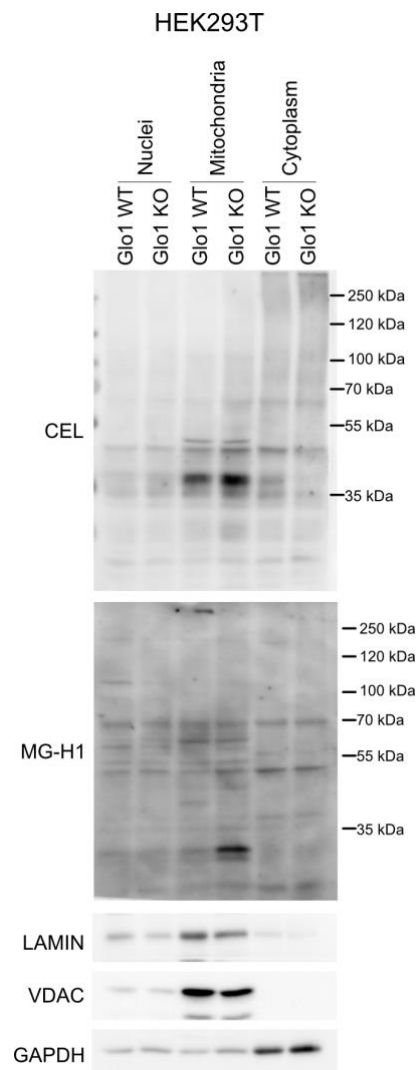


Figure 26. Increased levels of MG adducts in mitochondrial fraction of GLO1 KO HEK293T cells. I performed cell fractionation of WT or Glo1 KO HEK293T cells. Then, I assessed levels of lysine CEL adducts (upper immunoblot) or arginine MG-H1 adducts (second immunoblot). The three lower immunoblots show the loading controls for the different cellular compartments, LAMIN (nuclear), VDAC (mitochondrial) and TUB (cytosolic and input).

It is known that incubation of cells with MG causes reactive oxygen species (ROS) levels to raise, linking elevated MG levels with enhanced ROS production [160, 161]. Thus, I decided to assess ROS levels in the Glo1 KO HeLa and HEK293T cells. In both cases, the Glo1 KO cells showed higher ROS levels than the WT cells, suggesting a link between MG levels and ROS production in the Glo1 KO cells (Figure 27). Hence, I decided that this result together with the mild increase in MG adducts (Figures 25 and 26) were enough evidence that Glo1 KO cells suffer from chronic MG increase. Consequently, I used both Glo1 KO cell lines to study the impact of MG on cellular metabolism.

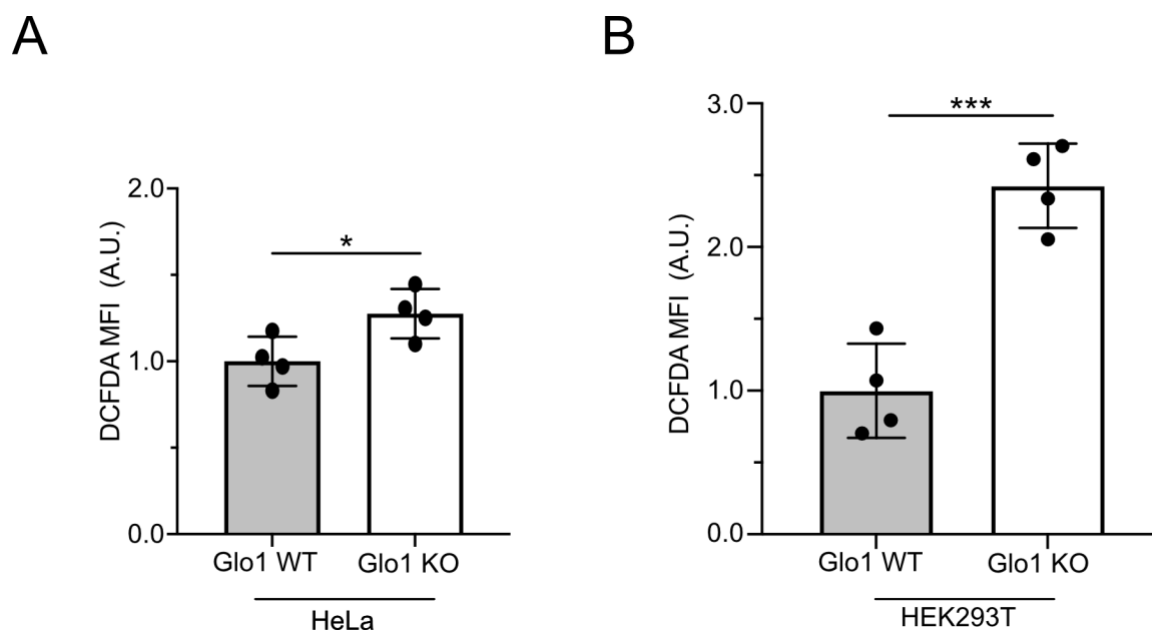


Figure 27. ROS levels are increased in Glo1 KO HeLa and HEK293T cells. I measured levels reactive oxygen species (ROS) in WT and Glo1 KO (A) HeLa and (B) HEK293T cells by flow cytometry using DCFDA. (A-B) Biological replicates n=4. For all panels, *p<0.05, **p<0.01 and ***p<0.001 determined by two-sided, unpaired Student's t-test.

Next, I standardized the experimental conditions for the transient MG increase, regarding MG concentration and treatment duration. I was seeking a MG concentration that corresponded to a significant intracellular MG increase within the physiological range, corresponding to what is observed in diabetic patients, i.e. 2 to 5 times higher plasma MG levels than in healthy patients [116, 162]. To this end, I incubated HeLa and HEK293T cells with 25 μ M MG for different periods of time and then measured intracellular and extracellular MG concentrations in collaboration with Thomas Fleming (Laboratory of Mechanism of Chronic Diseases at the University Hospital Heidelberg) (Figure 28). Despite some differences between the two cell lines, addition of MG generally caused intracellular and extracellular MG levels to transiently peak and then progressively decrease again. Peak levels in the HeLa cell line were

approximately 3 times higher than base levels and hence, within the pathophysiological range. In contrast, the HEK293T cell line seemed to be more efficient in detoxifying MG and as a consequence 25 μ M MG was not enough to cause the desired increase in intracellular MG. Therefore, I decided to increase the MG concentration to 100 μ M for the HEK293T cell line to achieve a similar increase in intracellular MG levels as observed in the HeLa cell line.

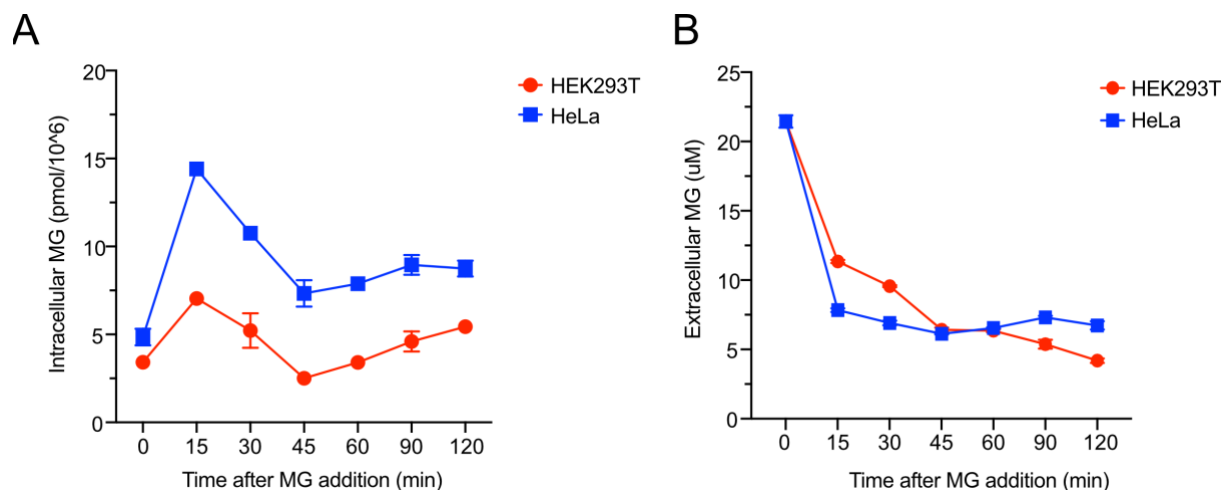


Figure 28. Optimization of experimental conditions to generate a transient MG increase. I treated HeLa and HEK293T cells (10^6 cells) with 25 μ M MG for the indicated amount of time, and both (A) intracellular and (B) extracellular free MG levels were determined by LC-MS/MS.

To confirm the increased MG levels, I incubated WT HEK293T cells with 100 μ M MG for 60 minutes and then assessed the presence of MG adducts in different cellular compartments (Figure 29). I used untreated WT HEK293T cells to determine the baseline MG adduct levels and MG untreated Glo1 KO HEK293T cells as a positive control, as they previously showed increased MG adduct levels (Figure 26). In general, when I incubated WT HEK293T with MG there was an increase of MG adducts in the nuclear and mitochondrial fractions that mimicked the one in Glo1 KO HEK293T. The CEL adducts (Figure 29, first panel), even when mild, showed a band above 35 kDa that was increased in the nuclear and mitochondrial fraction from WT cells incubated with MG and Glo1 KO cells in comparison with the WT control cells. Additionally, the MG-H1 adducts were significantly increased in two bands below 35 kDa in the mitochondrial fraction of the cells incubated with 100 μ M MG and the Glo1 KO cells compared with the WT cells (Figure 29, second panel). These results show that incubation of WT HEK293T cells with 100 μ M MG is enough to cause an increase in MG levels similar to the MG concentration in Glo1 KO HEK293T cells. As a consequence, I used these experimental conditions in my following experiments with HEK293T cells.

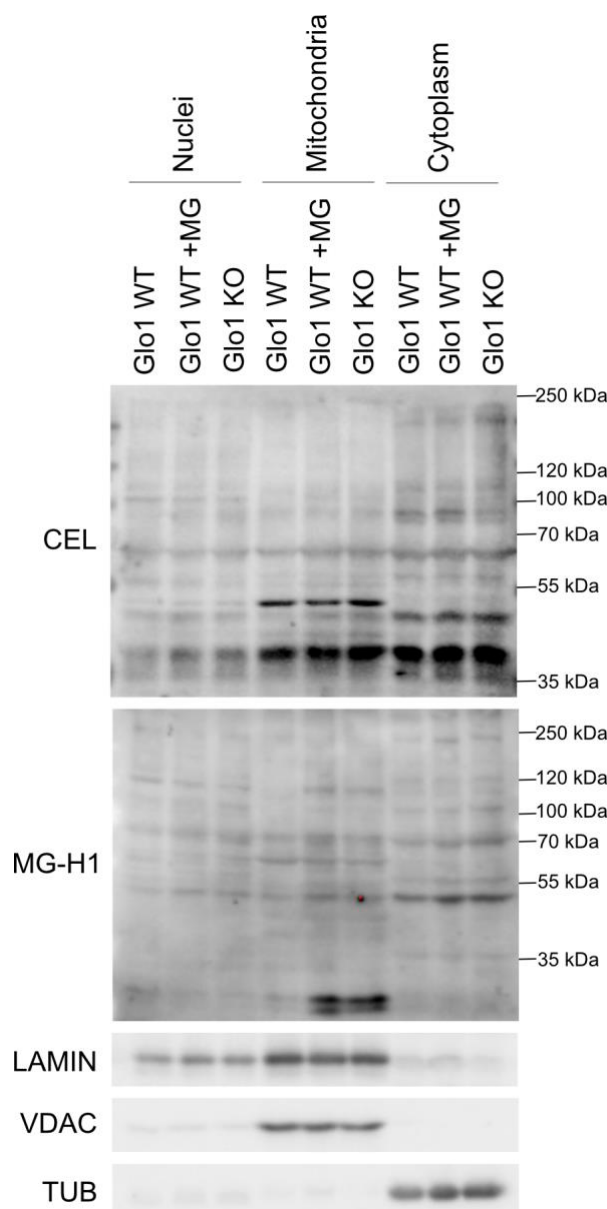


Figure 29. MG treatment of HEK293T causes an increase in MG adducts. I incubated HEK293T WT cells (4×10^6 cells) with 100 μ M MG for 60 minutes. Then, I performed cell fractionation of the cells and I assessed levels of lysine CEL adducts (upper immunoblot) or arginine MG-H1 adducts (second immunoblot). The three lower immunoblots show the loading controls for the different cellular compartments, LAMIN (nuclear), VDAC (mitochondrial) and TUB (cytosolic and input).

3.2.2. MG increases L-lactate production

While culturing the Glo1 KO cell lines I noticed that their culture medium, which contains phenol red as a pH indicator, turned yellow faster than the medium of their WT counterparts, despite similar cell number. I therefore suspected that the KO cells might produce and excrete more lactate causing a faster decrease in the pH of the medium. Hence, I measured L-lactate in the media of WT and Glo1 KO cells (Figure 30). Indeed, levels of extracellular L-lactate were

increased in the Glo1 KO cell line compared with WT HeLa cells. Notably, I was able to rescue the increased L-lactate levels by re-expression of WT Glo1 (Figure 30A). Similar to HeLa cells, the absence of Glo1 in HEK293T cells causes an increase in extracellular levels of L-lactate (Figure 30B). These results indicate that Glo1 is necessary to prevent excessive L-lactate production and suggest that MG is the responsible molecule for the increase in L-lactate production.

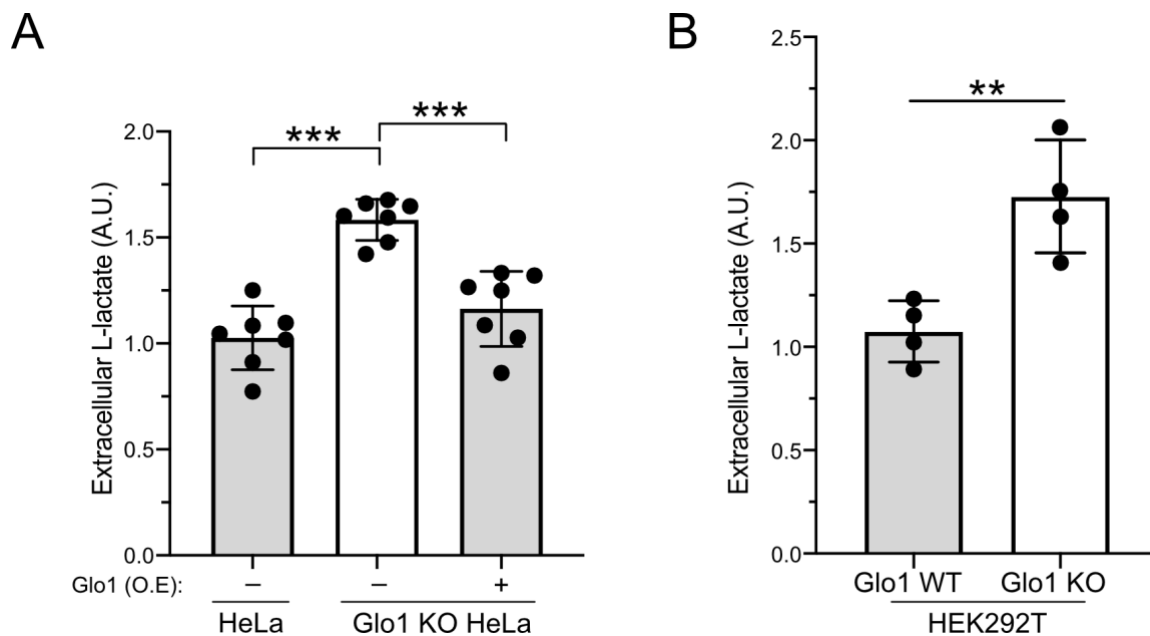


Figure 30. L-lactate production is increased in Glo1 KO cells. I measured extracellular L-lactate levels in (A) WT, or Glo1 KO HeLa cells transiently expressing WT Glo1, and in (B) WT or KO HEK293T cells. (A) Biological replicates n=7. *p<0.05, **p<0.01 and ***p<0.001, determined by one-way ANOVA (multiple comparison). (B) Biological replicates n=4. *p<0.05, **p<0.01 and ***p<0.001, determined by two-sided, Student’s t-test. Over-expression (O.E).

To test if MG levels affect L-lactate production in HeLa cells, I measured extracellular L-lactate levels after 60 and 120 minutes of incubation with 25 uM MG (Figure 31A). Of note, I changed the media for all conditions 24 hours before the experiment. There was no increase in extracellular L-lactate levels after 60 or 120 minutes of MG treatment in WT HeLa cells. In contrast, Glo1 KO cell line showed increased extracellular MG levels in line with my previous data (Figure 30). However, the increase of extracellular L-lactate reflects the accumulation of excreted lactate over 24 hours, suggesting that longer incubation times with MG could lead to an increase in extracellular L-lactate. The effect of MG levels on L-lactate production was evident when I measured intracellular L-lactate levels. In this case, 25 uM MG treatment for 120 minutes caused a significant increase in intracellular L-lactate levels

compared with control (Figure 31B). This data supports the conclusion that MG increases L-lactate production in HeLa cells. To confirm the increase in intracellular MG levels upon MG treatment, I measured extracellular D-lactate levels (Figure 31C). In contrast to its stereoisomer L-lactate, which is the main end product of glycolysis, D-lactate is produced during the detoxification of MG via the glyoxalase pathway. The levels of D-lactate were already considerably higher after 60 minutes of MG treatment suggesting that the added MG is getting detoxified.

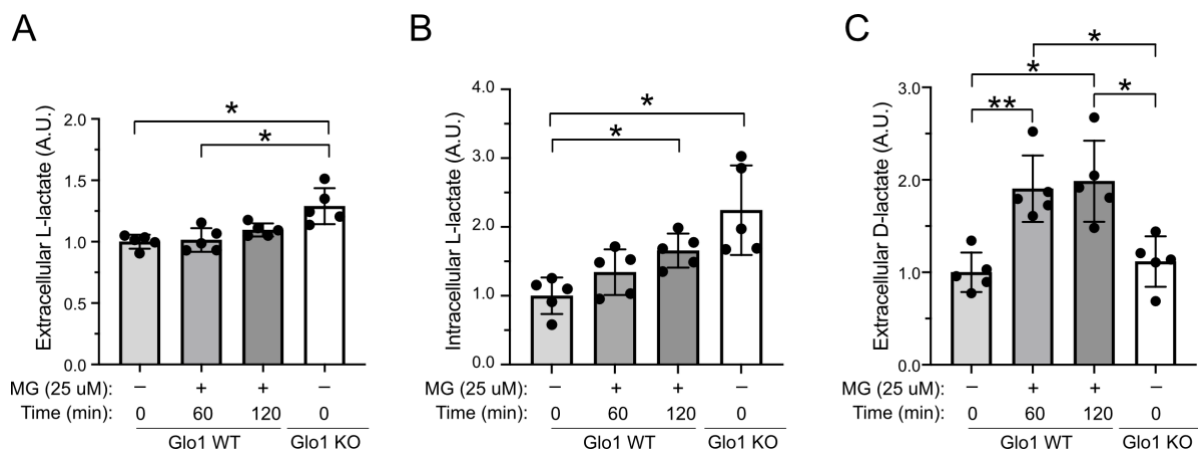


Figure 31. MG treatment increases L-lactate production in WT HeLa cells. I incubated WT HeLa cells (10^6 cells) with 25 uM MG for 60 minutes. Then, I measured extracellular (A) and intracellular (B) L-lactate, as well as (C) extracellular D-lactate levels. Biological replicates $n=5$. * $p<0.05$ and ** $p<0.01$, determined by Brown-Forsythe and Welch ANOVA (multiple comparison).

In contrast to HeLa cells, when I incubated WT HEK293T with 100 uM MG for 60 minutes, extracellular L-lactate levels were significantly increased (Figure 32A), while intracellular L-lactate levels only showed a slight increase in comparison with untreated WT cells (Figure 32B). This finding suggests a more efficient excretion of L-lactate in HEK293T in comparison with HeLa cells. Moreover, the addition of 100 uM MG to WT HEK293T cells caused a significant increase in D-lactate levels when compared with untreated Glo1 WT or KO cells (Figure 32C), hinting that 60 minutes incubation with 100 uM MG is enough to cause a significant increase in intracellular MG levels. These results support the hypothesis that MG causes an increase in L-lactate production in both cell lines.

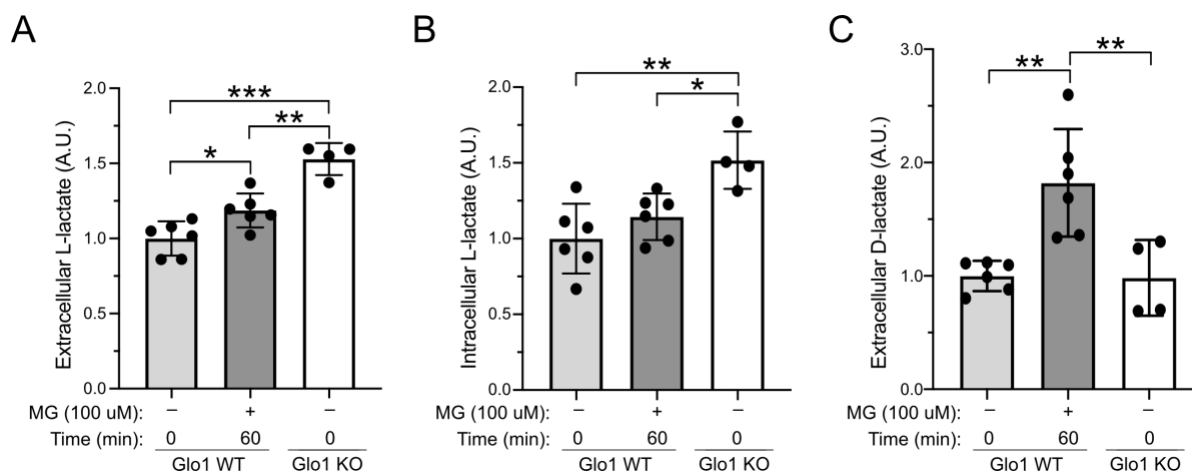


Figure 32. MG treatment increases L-lactate in HEK293T cells. I incubated WT HEK293T cells (10^6 cells) with 100 uM MG for 60 minutes. Then, I measured extracellular (A) and intracellular (B) L-lactate, as well as (C) extracellular D-lactate. Biological replicates: WT HEK293T and MG incubated $n=6$, Glo1 KO 293T $n=4$. For all panels, * $p<0.05$, ** $p<0.01$ and *** $p<0.001$, determined by one-way ANOVA (multiple comparison).

3.2.3 Impact of MG on glucose metabolism

The increase in L-lactate production observed in the Glo1 KO cell lines could be caused by different molecular mechanisms which are not mutually exclusive: (I) increased glucose uptake and flux through glycolysis (Figure 33A), (II) increased LDH activity and/or (III) decreased PDH activity. First, I tested whether HeLa Glo1 KO cells took up more glucose than WT cells. For this purpose, I measured glucose levels in the cell medium before and after 24 hours. The differences in the amount of glucose between the two time points reflected the amount of glucose taken up by the cells. Consistent with the first potential mechanism, the Glo1 KO cell line showed increased glucose uptake compared to WT cells that was blocked by the re-expression of WT Glo1 in these cells (Figure 33B). The same was true for Glo1 KO HEK293T cells, which also showed increased glucose uptake compared with WT cells (Figure 33C). These findings suggest that Glo1 is capable of regulating glucose metabolism.

Increased LDH activity could also be a cause for high L-lactate levels in the Glo1 KO cells (Figure 34A). Hence, I assessed the activity of LDH in both WT and Glo1 KO HeLa and HEK293T cells. The Glo1 KO cells had significant higher LDH activity than their WT controls (Figure 34B-C). The changes in activity were not a consequence of changes in LDH expression between the Glo1 WT and KO HEK293T, as shown by Western Blot analysis (Figure 34C, right panel). These results suggest that Glo1 is playing a role in regulating LDH activity.

Additionally, the elevated LDH activity and increased glucose uptake in Glo1 KO cells (Figure 33) strongly suggest that the lack of Glo1 increases glycolytic flux.

Lastly, these results strongly suggest that MG is able to cause important changes in glycolysis by stimulating glucose uptake and L-lactate production. Moreover, MG is a byproduct of glycolysis, thus, higher glycolytic flux could lead to more MG production [16], which, in turn, increases glycolytic flux. Hence, it is then possible that a potentially hazardous positive feedback loop exists in which MG leads to more MG production. This mechanism could contribute to the high MG levels observed in the plasma of diabetic patients [115, 116]. Therefore, MG could mediate metabolic reprogramming associated with diabetes, although additional experiments, including treatment of WT HeLa and HEK293T cells with MG, are still required to further validate the role of MG in regulating glucose metabolism.

3.2.4. Impact of MG on PDH activity

The enhanced anaerobic glycolysis phenotype I observed in the Glo1 KO cells could also be a consequence of decreased PDH activity, causing pyruvate flux to redirect towards L-lactate production instead of acetyl-CoA, similar to what is observed during the Warburg effect (Figure 35A). Thus, I assessed whether Glo1 KO cells had decreased PDH activity. Indeed, both HeLa and HEK293T cells lacking Glo1 showed a significant decrease in PDH activity compared with the WT cells (Figure 35B-C). The transient expression of Glo1 in HeLa cells, rescued in tendency the decrease in PDH activity (Figure 35B). A significant rescue in PDH activity was observed upon stable transfection of Flag-tagged WT Glo1 (WT) but not a catalytically inactive mutant (CI) Glo1 that I generated by substituting glutamic acid in position 172 with glutamine [163] (Figure 35C). As expected, the HEK293T cell line stably transfected with the mutant Glo1 expressed the protein (Figure 36, left panel) but did not show any Glo1 activity (Figure 36, right panel), while the cell line stably transfected with WT Glo1 expressed Flag-Glo1 protein and showed Glo1 activity levels similar to the WT HEK293T cell line (Figure 36). The higher molecular weight of Glo1 in the stably transfected cell lines is due to the Flag tag. These results suggest that it is MG and not the lack of Glo1 that causes PDH activity to decrease in the Glo1 KO cells.

PDH is an important metabolic node, as it catalyzes the oxidation of pyruvate to acetyl-CoA which is used for energy production via the TCA cycle, or indirectly for lipid synthesis, then

dysregulation of PDH activity have important metabolic repercussions. Therefore, I decided to focus on characterizing the impact of MG on PDH activity. Firstly, I assessed whether knocking down Glo1 would have an effect on PDH activity (Figure 37). Analogous to the Glo1 KO results, PDH activity decreased upon knockdown of Glo1 in HeLa or HEK293T cells (Figure 37). Consequently, a decrease in Glo1 activity or protein level has a strong effect on PDH activity.

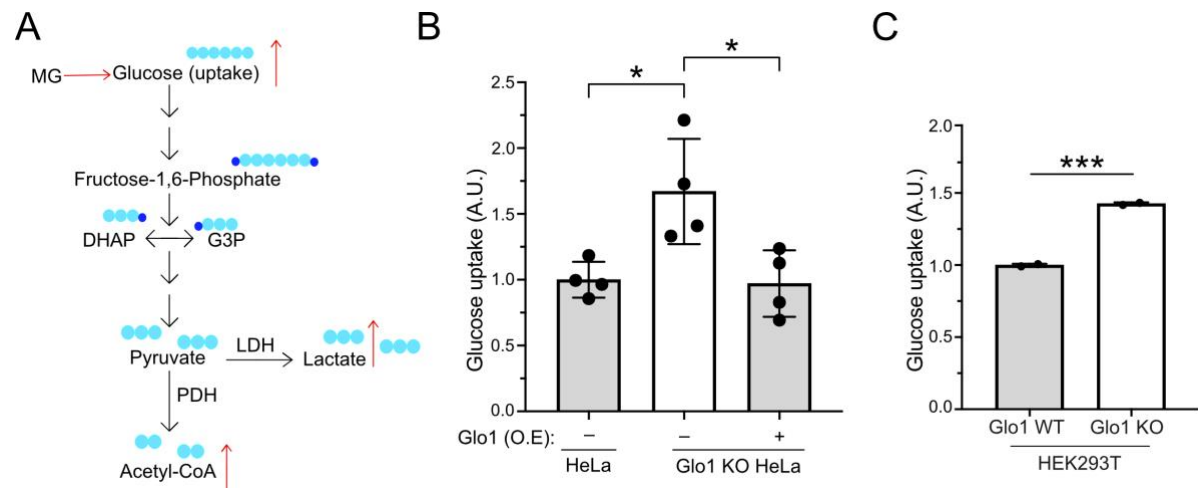


Figure 33. Glo1 is necessary for normal glucose uptake. (A) A raise in the glycolytic flux due to an increase in glucose uptake could lead to the elevated L-lactate. (B) I measured glucose uptake in WT or Glo1 KO HeLa cell lines transiently expressing WT Glo1. Biological replicates n=4. For (B), *p<0.05, determined by one-way ANOVA (multiple comparison). (C) I measured glucose uptake in WT or Glo1 KO HEK293T. Biological replicates n=2. For(C), ***p<0.001, determined by two-sided, unpaired Student's t-test. Over expression (O.E).

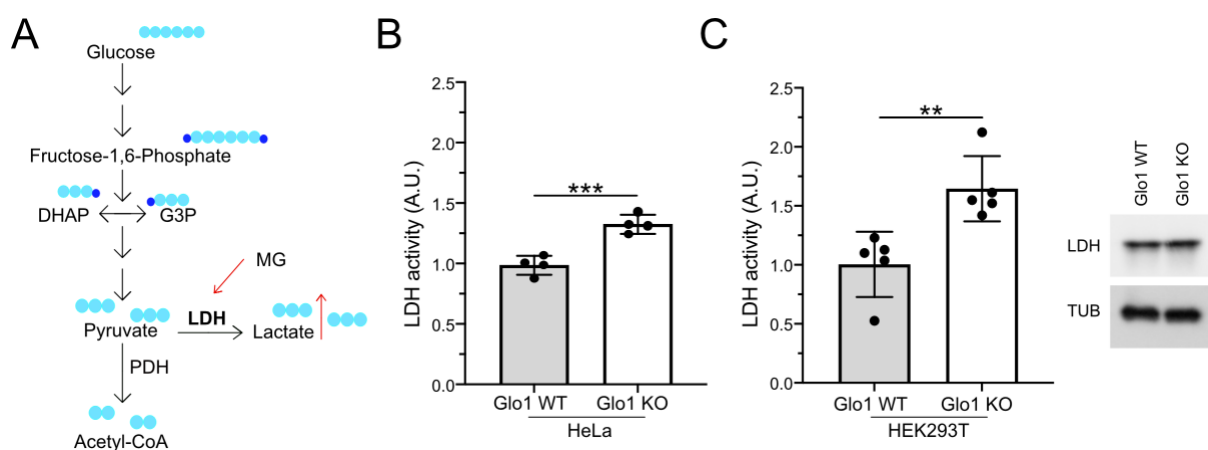


Figure 34. Loss of Glo1 increases LDH activity. (A) MG could stimulate LDH activity causing an increase in L-lactate levels. I measured LDH activity in (B) WT and Glo1 KO HeLa cells biological replicates n=4, as well as (C) WT and Glo1 KO HEK293T cells, biological replicates n=5. For all panels, **p<0.01 and ***p<0.001, determined by two-sided, unpaired Student's t-test. Over expression (O.E).

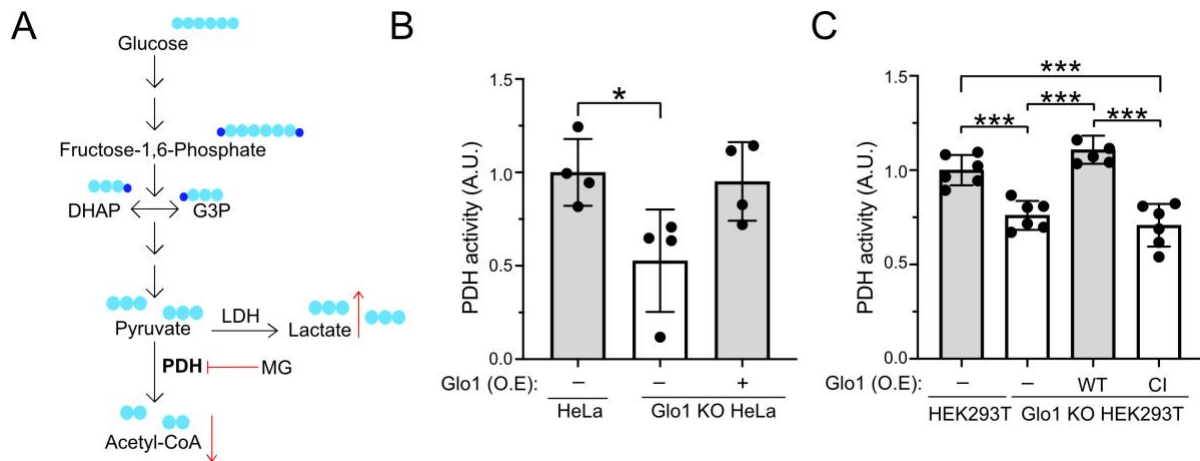


Figure 35. Loss of Glo1 decreases PDH activity. (A) MG could inhibit PDH activity causing re-direction of the pyruvate towards L-lactate production. (B) I measured PDH activity in WT, and Glo1 KO HeLa cells transiently expressing WT Glo1. Biological replicates n=4. (C) I measured PDH activity in WT, Glo1 KO or stably transfected Glo1 HEK293T with either flag tagged WT or catalytic dead Glo1, biological replicates n=6. For all cases, *p<0.05, **p<0.01 and ***p<0.001, determined by one-way ANOVA (multiple comparison). Over expression (O.E), catalytically inactive (CI).

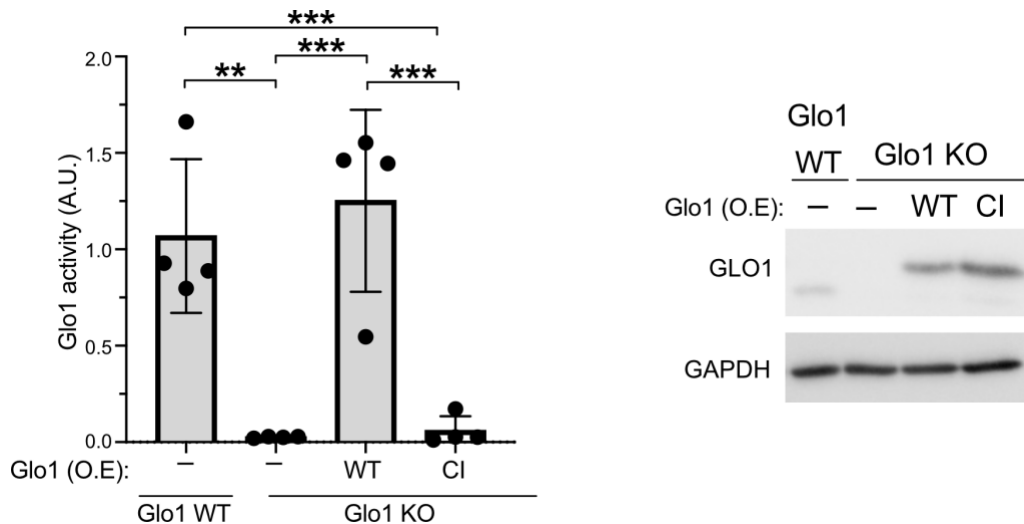


Figure 36. Characterization of WT or CI Glo1 stably transfected HEK293T. I stably transfected Glo1 HEK293T cells with Flag-tagged WT or CD Glo1 and I assessed Glo1 activity or Glo1 presence by immunoblot. Biological replicates n=4. *p<0.05, **p<0.01 and ***p<0.001, determined by one-way ANOVA (multiple comparison). Over expression (O.E), catalytically inactive (CI).

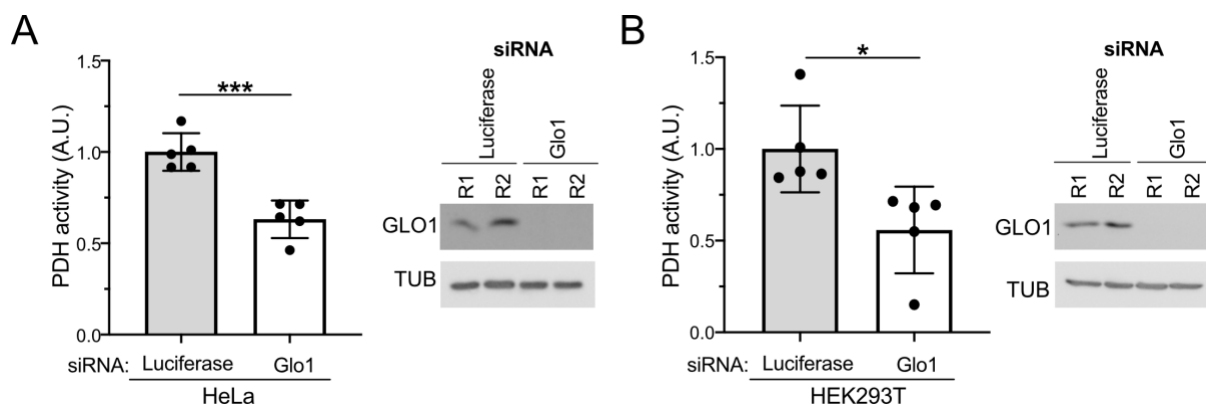


Figure 37. PDH activity is decreased in Glo1 knockdown HeLa and HEK293T cells. I knocked down Glo1 in HeLa (A) or (B) HEK293T cells using siRNAs and assessed the KD efficiency by immunoblotting (left panel), as well as PDH activity by enzymatic assays (right panel). Biological replicates n=5. For all panels, *p<0.05 and ***p<0.001, determined by two-sided, unpaired Student's t-test.

To validate that the observed decrease in PDH activity upon Glo1 knockout/knockdown is a direct effect of increased MG levels (Figure 35 and 37), I incubated WT HEK293T cells for 60 minutes with 100 μ M MG and assessed PDH activity. This caused a decrease in PDH activity similar to the one observed in the Glo1 KO cells, suggesting that an increase in MG levels is enough to trigger the decrease in PDH activity (Figure 38A). Finally, I incubated purified porcine PDH with 100 μ M MG for 60 minutes and assessed its activity. I observed that incubation of PDH with 100 μ M MG for 60 minutes also decreased PDH activity (Figure 38B), hinting at a direct interaction between MG and PDH. Nevertheless, the influence of MG on PDH activity was milder in the *in vitro* experiments probably due to other factors playing a part in the *in vivo* inhibition of PDH. For example, cellular conditions like elevated ROS or GSH levels that facilitates MG interaction with PDH in the Glo1 KO cells could play a role *in vivo*. There is also a chance that 100 μ M MG was stoichiometrically not enough for the amount of porcine PDH I used, and higher MG concentration are needed to accomplish a similar inhibition. Still, these results validate that MG causes PDH activity to decrease and the inhibition is in part mediated via direct interaction.

Hyperglycemia is known to increase AGE and MG levels in endothelial cells in culture [16]. As I always cultured my WT and Glo1 KO HEK293T cells in high glucose medium, I wondered if different Glc concentrations would affect PDH activity. Thus, I incubated WT or Glo1 KO HEK293T either in 5 mM or 25 mM Glc overnight and then I assessed enzymatic activity. Upon lower Glc I observed stronger differences in PDH activity between WT and Glo1 KO cells (Figure 39). Additionally, PDH activity in WT cells cultured in low Glc was

higher than when cells were grown under high Glc concentrations, suggesting that high Glc has an inhibitory effect on PDH. In sharp contrast, PDH activity in Glo1 KO was always lower than in WT cells and unaffected by the concentration of Glc. These results suggest that there is a correlation between conditions with high MG, either high Glc or Glo1 KO, and low PDH activity.

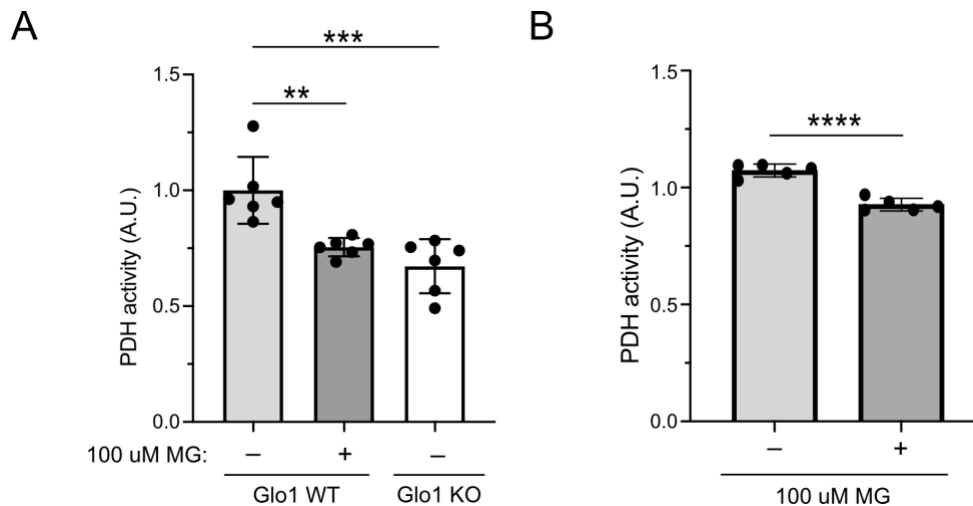


Figure 38. MG inhibits PDH activity *in vivo* and to a lesser degree *in vitro*. (A) I incubated HEK293T cells with 100 uM MG for 60 minutes and assessed PDH activity. Biological replicates n=6. For (A), *p<0.05, **p<0.01 and ***p<0.001, determined by one-way ANOVA (multiple comparison). (B) I incubated purified porcine PDH with 100 uM MG for 1hour. Biological replicates n=5. For (B), **p<0.01 and ***p<0.001, determined by two-sided, unpaired Student's t-test.

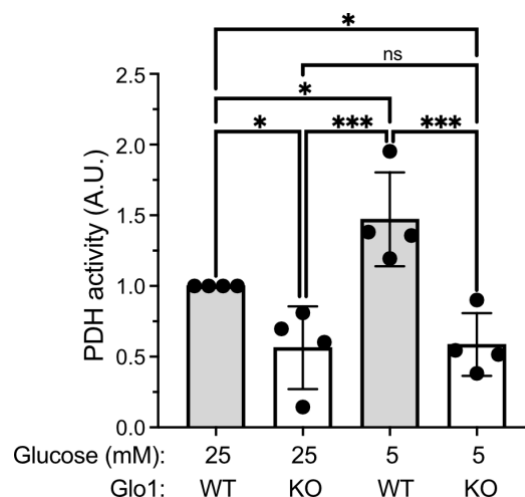


Figure 39. Low glucose condition causes an increase in PDH activity in WT but not in Glo1 KO HEK293T cells. I isolated PDH containing mitochondrial fractions from WT or Glo1 KO HEK293T cells grown in medium containing either 25 mM glucose (Glc), and 2 mM glutamine or 5 mM Glc and 2 mM glutamine and assessed PDH activity. Biological replicates n=4. *p<0.05, **p<0.01 and ***p<0.001 determined by one-way ANOVA (multiple comparison). Over expression (O.E), not significant (ns).

To this point I showed that the absence of Glo1 or the incubation of cells with MG cause inhibition of PDH activity, probably enhancing glucose uptake and L-lactate production, which fit with my observations using Glo1 KO cells. As impairments in PDH activity are linked to metabolic inflexibility and development of diabetes [70], I postulate for the first time that elevated levels of MG inhibit PDH activity leading to development of diabetes.

3.2.5. Regulation of PDH activity by MG is not mediated via canonical mechanisms

Up to now regulation of PDH activity has been mainly attributed to PDH post-translational modifications, specifically PDH activity is known to be negatively regulated via phosphorylation of its E1 subunit (PDHA1) on serine 232 (S232), serine 293 (S293) and serine 300 (S300) [75, 164]. Hence, I first tested whether MG affects the phosphorylation of any of these residues. However, there were no significant changes in the phosphorylation levels of the serine residues of PDHA when comparing Glo1 KO and WT HEK293T cells (Figure 40A). Additionally, MG caused no evident increase in PDHA1 phosphorylation in WT HEK293T cells after 100 uM MG addition for up to 6 hours (Figure 40B). Together, these results indicate that the decrease in PDH activity caused by MG does not depend on phosphorylation of PDHA1 on S232, S293 or S300.

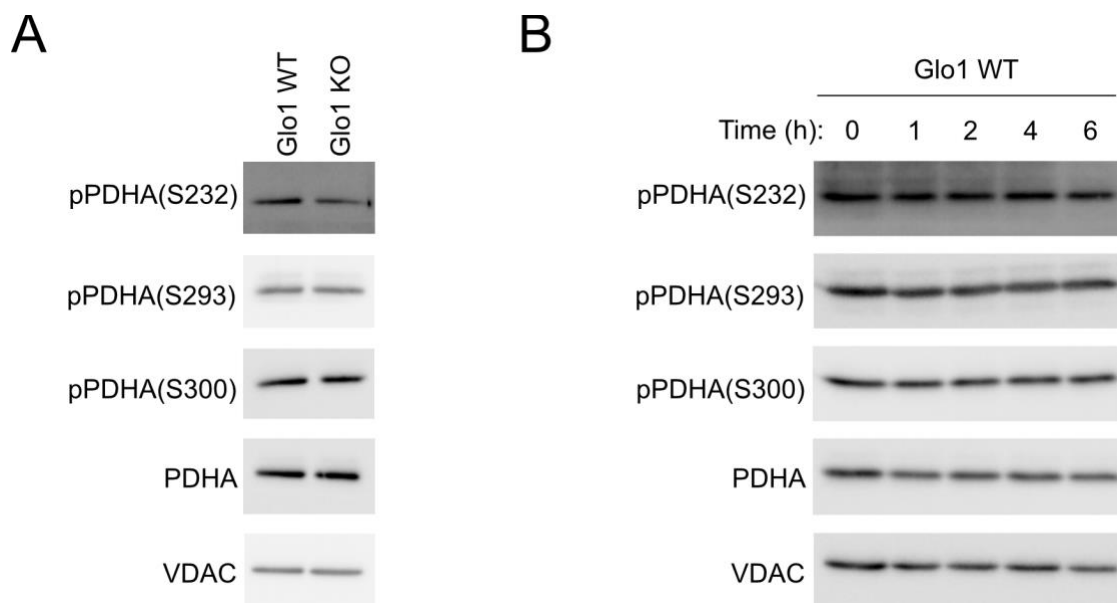


Figure 40. MG does not affect PDHA1 phosphorylation. (A) I assessed phosphorylation of PDHA in WT or Glo1 KO HEK293T cells. (B) I incubated WT HEK293T with 100 uM MG for up to 6 hours, purified the mitochondrial fraction and assessed the phosphorylation of PDHA1 during the time course. These immunoblots are representative images of 2 biological replicates.

Next, I asked whether changes in the abundance of the three subunits of the PDH complex (Figure 41A) could be responsible for the reduced PDH activity caused by MG. To this end, I purified mitochondrial fractions of WT or Glo1-KO HEK293T cells and assessed the levels of the components of the PDH complex by immunoblot. No change in the levels of any component of the PDH complex was detectable (Figure 41B), indicating that the decrease in PDH activity is not due to changes in the levels of PDH. Thus, the regulation of PDH activity by MG does not seem to involve the canonical mechanisms of PDH regulation.

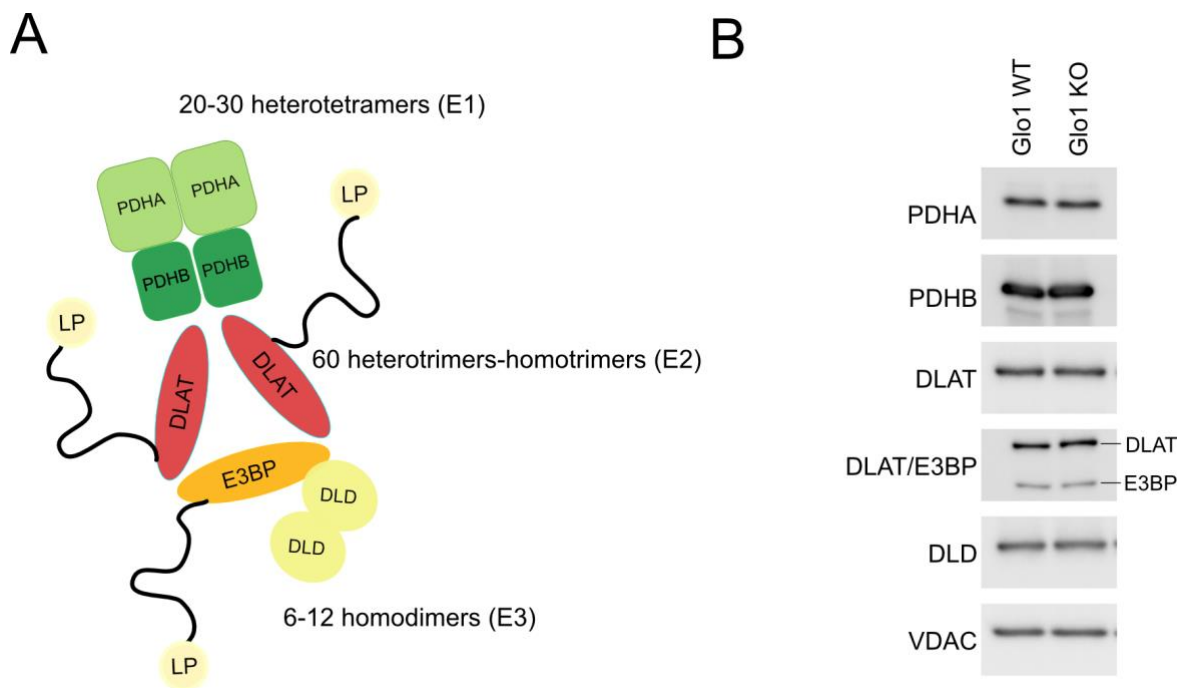


Figure 41. MG does not affect the expression of PDH subunits. (A) Schematic representation of the subunit composition of PDH. E1 is composed of 20-30 PDHA and PDHB heterotetramers, E2 consists of in total 60 dimers, either heterotrimers of E3BP/DLAT alone or in combination with DLAT homodimer, and E3 is formed from 6-12 homodimers of DLD. (B) I evaluated the expression of the different PDH subunits on WT and Glo1 HEK293T by immunoblot. This immunoblot is a representative image of 2 biological replicates.

3.2.6. MG interacts with several PDH subunits

After discarding the known mechanisms that regulate PDH activity, I continued studying how MG could regulate PDH activity. As the structure of MG resembles that of pyruvate (Figure 42A), I hypothesized that a competitive inhibition between MG and the physiological substrate of PDH could be taking place. Thus, I assessed the Michaelis-Menten kinetics of PDH to characterize the type of inhibition caused by MG. PDH from Glo1 KO HEK293T cells showed a 41% increase in its K_m compared to WT cells, while the V_{max} was 18% lower than in WT

samples (Figure 42B). The conventional models to categorized the inhibitors postulate that a higher K_m would fit with a competitive inhibitor, while the decrease in V_{max} would fit with non-competitive inhibitor behavior. However, Michaelis-Menten conventional classification excludes the possibility of an inhibitor affecting both the affinity of the enzyme for its substrate, K_m , and the catalytic turnover, V_{max} . MG is a highly reactive metabolite and the fact that both K_m and V_{max} are changed in Glo1 KO HEK293T cells hints at the possibility of MG interacting with different subunits of PDH and causing multiple effects.

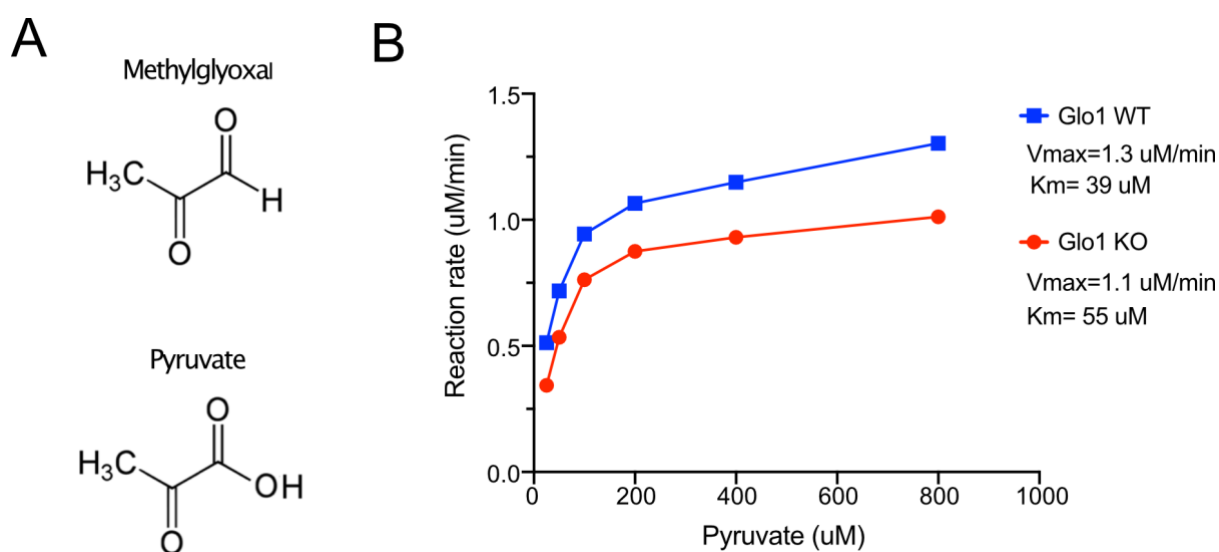


Figure 42. MG interacts with PDH causing a mixed inhibition effect. (A) Structural formula of methylglyoxal and pyruvate. (B) Michaelis-Menten graph based on PDH activity in WT or Glo1 KO HEK293T cells. This is a representative assay of 3 replicates.

To determine if and how MG covalently interacts with PDH, I then employed a click chemistry approach taking advantage of an MG analogue harboring an alkyne group (Figure 43A), which was synthesized for us by the group of Aubry Miller (Cancer Drug Development, Dkfz). The click chemistry technique is based on two groups of molecules that rapidly react with each other in a copper catalyzed reaction. I used alkyne MG and azide biotin for my click chemistry experiments. First, I incubated Glo1KO HEK293T cells with 200 uM MG analogue for 1 hour, then I isolated all proteins modified by MG through a click reaction with biotin azide and a subsequent pull-down using streptavidin beads (Figure 43B). To validate the MG click pull down method, I first analyzed two proteins previously reported to be modified by MG, KEAP1 and FASN [101, 102]. After normalization for the input levels of these proteins, I indeed found that both proteins were enriched in the click-MG pull downs (Figure 44). Importantly, although some interaction with MG was detectable also for a

number of other proteins analyzed, GAPDH and VDAC were completely de-enriched in the pull down (Figure 44 and 45), attesting to the specificity of this approach.

Excitingly, when I tested the presence of PDH subunits in the MG pull down, I could detect a particular enrichment for PDHA, DLAT and DLD (Figure 44). The presence of different PDH subunits in the click it pull downs could also explain the mixed inhibition observed with the Michaelis-Menten experiments (Figure 42B). The click-MG results suggest that MG is able to interact with PDH and this might cause the change in its activity.

Worth mentioning is that LDH was also present in the click-MG pull downs and it had a click it/input ratio similar to PDH (Figure 44). This result indicates that LDH could also be directly modified by MG. This could explain the change in LDH activity observed in Glo1 KO HeLa and HEK293T cells (Figure 34). However, further experiments are necessary to validated this possibility.

While analyzing the click it MG pull downs, I noticed that high molecular weight proteins such as mTOR, Acetyl-CoA carboxylase (ACACA) and FASN were highly modified by MG (Figures 44 and 45). This effect could depend on the fact that larger proteins could simply have more amino acid residues capable of reacting with MG, in particular arginine, cysteine, and lysine residues. To test this possibility, I counted the number of these amino acids for each protein (Table 2) and determined the correlation between the click it/input ratio and the number of reactive amino acids (Figure 46). For each of these amino acids, there was a clear correlation between their absolute number per protein and the pulldown enrichment. Thus, the number of amino acids capable of reacting with MG does likely play a role in the degree of interaction between the metabolite and the protein. It is important to notice, that PDH is composed of medium molecular weight subunits forming a megadalton complex and as a consequence would be extremely susceptible to MG modifications. Together, these results and the Michaelis-Menten characterization suggest that MG could interact with PDH in more than one way. It is possible then that the effects on PDH activity is due to a combination of inhibitory interactions on different subunit of PDH.

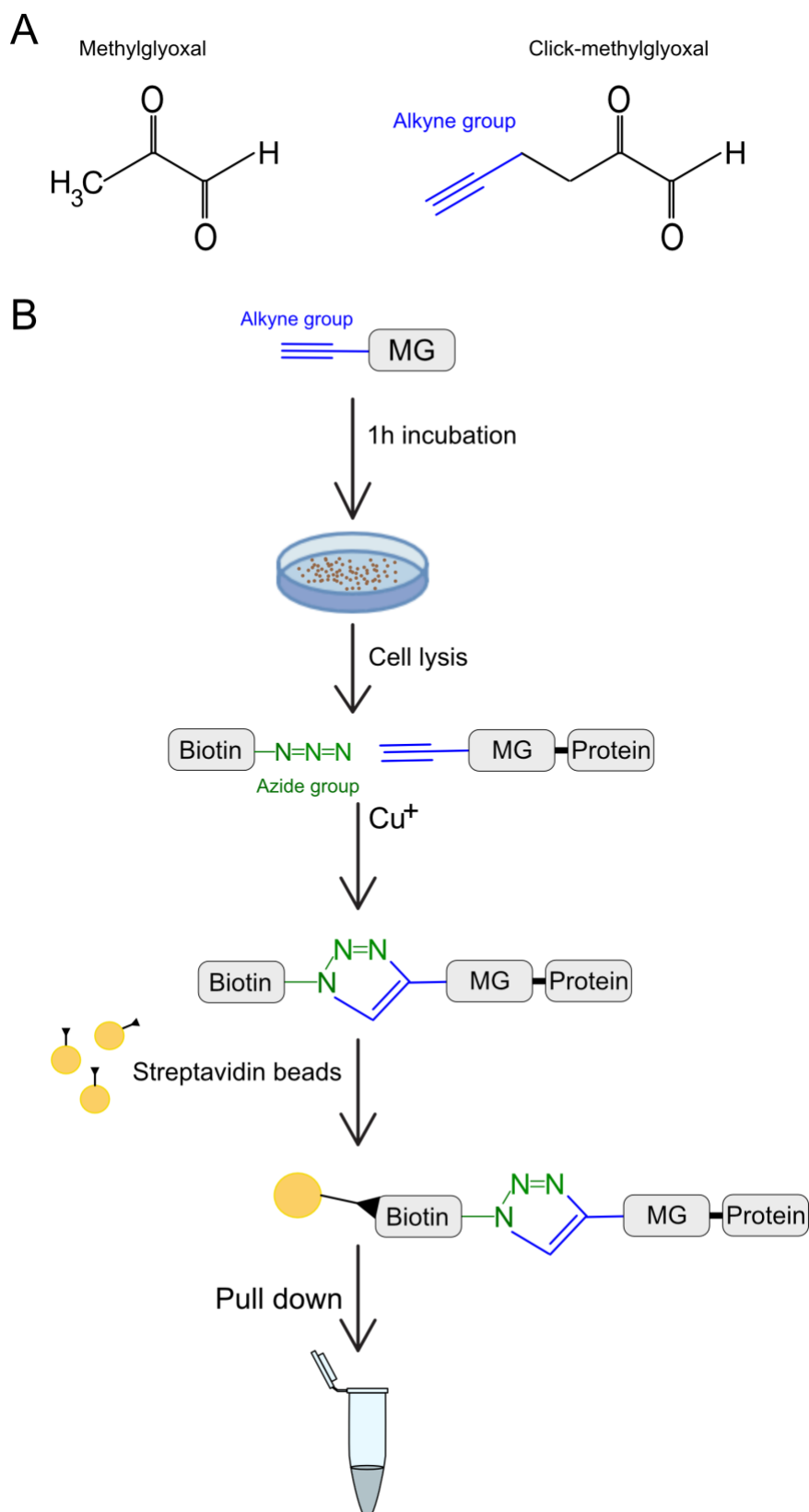


Figure 43. Schematic representation of MG click chemistry based pull downs. (A) Structural formula of the MG analogue harboring an alkyne group. (B) I incubated HEK293T cells with MG analog (harboring an alkyne group), then I lysed the cells and used the lysates in a click chemistry reaction with biotin azide, during which a 1,3-dipolar cycloaddition took place between the azide and alkyne groups, forming a 1,2,3-triazole. Subsequently I pulled down the MG modified proteins using streptavidin beads and assessed the samples by immunoblot.

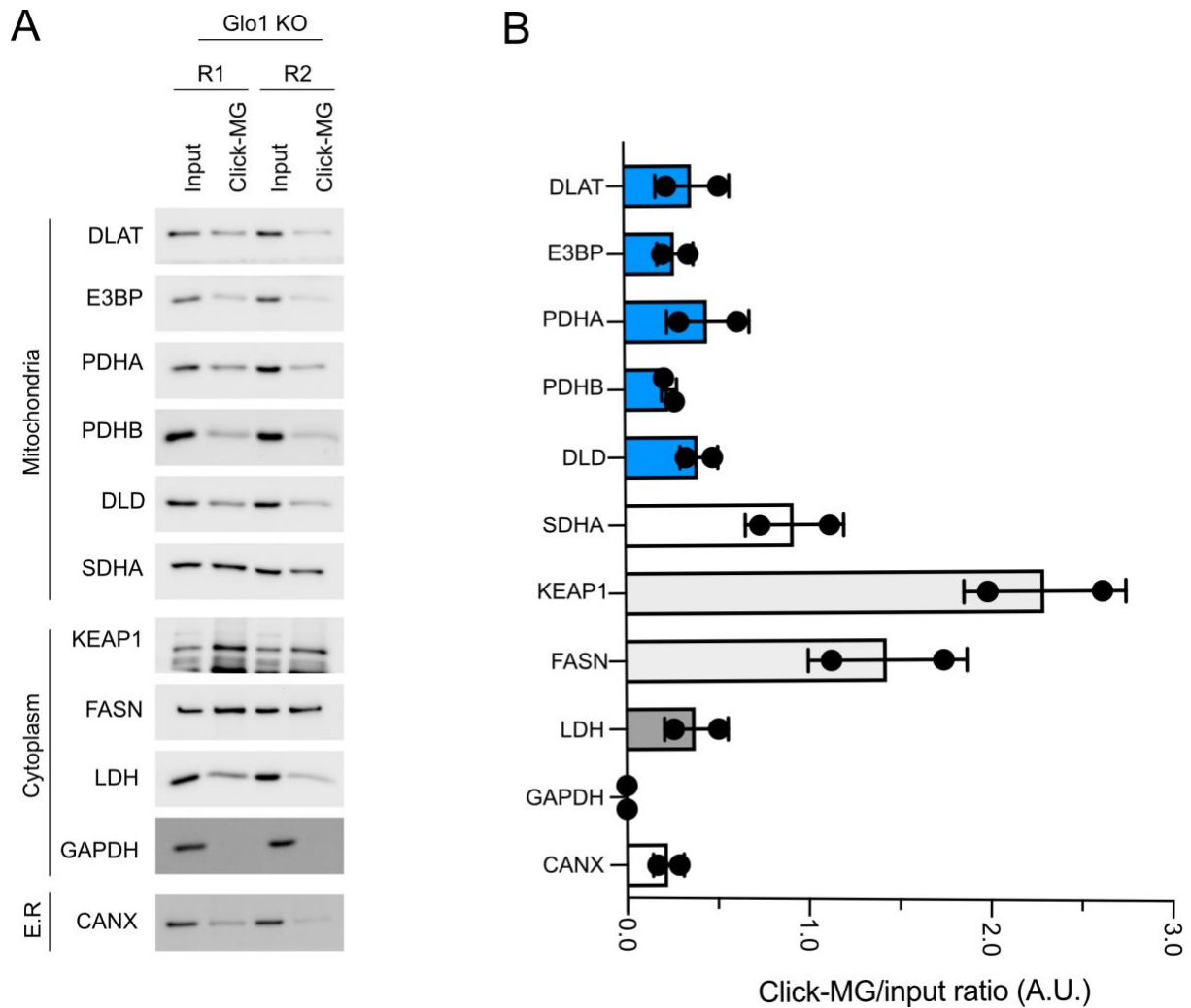


Figure 44. MG interacts with different components of PDH complex. (A) I incubated HEK293T cells with 200 μ M MG analog (harboring an alkyne group), then I lysed the cells and used the lysates in click chemistry reaction with biotin azide. Subsequently, I pulled down the MG modified proteins using streptavidin beads and I assessed the pull downs by immunoblotting. (B) I first quantified the immunoblots and the I normalized the click pull down levels of each protein by its input levels (click-MG/input ratios). Endoplasmic reticulum (E.R). PDH subunits are indicated in blue, proteins previously reported to be modified by MG are indicated in light grey and LDH is indicates in dark grey.

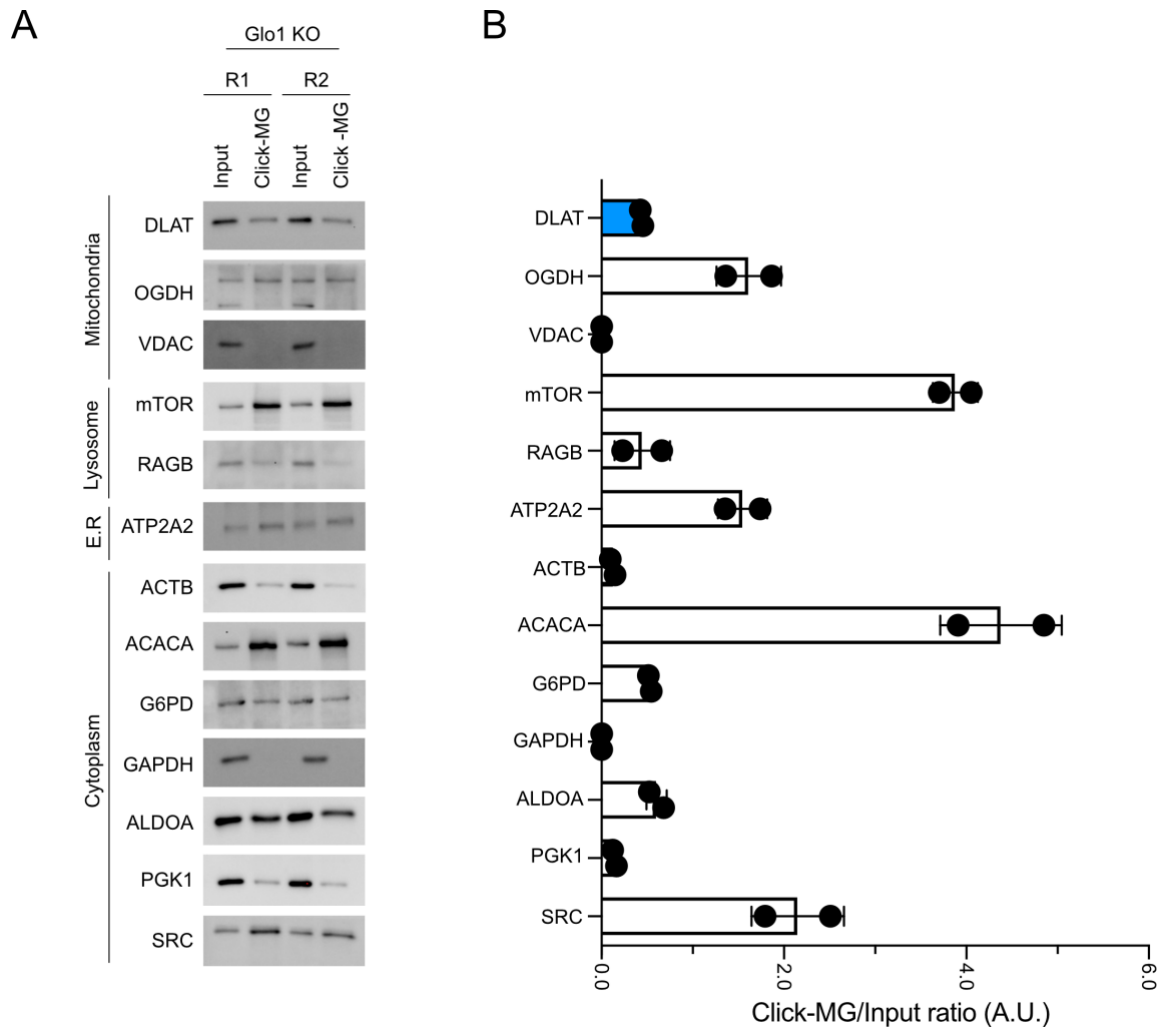


Figure 45. MG does not interact with all proteins. (A) I incubated HEK293T cells with 200 μ M MG analog (harboring an alkyne group), then I lysed the cells and used the lysates in click chemistry reaction with biotin azide. Subsequently, I pulled down the MG modified proteins using streptavidin beads and I assessed the pull downs by immunoblotting. (B) I first quantified the immunoblots and the I normalized the click pull down levels of each protein by its input levels (click-MG/input ratios). Endoplasmic reticulum (E.R). DLAT subunit of PDH is indicated in blue.

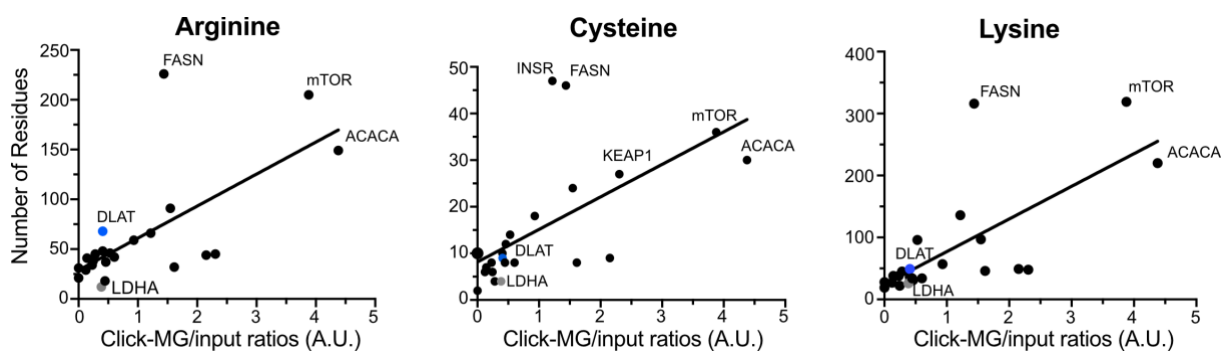


Figure 46. MG click it interactions with proteins depend on number of arginine, cysteine and lysine residues. Correlation between Click-MG/input ratio from figures 44 and 45 and number of arginine (left), cysteine (middle) or lysine (right) residues. DLAT subunit of PDH is indicated in blue.

Table 2. Protein with click it/input ratio and number of arginine, cysteine, and lysine residues present.

Gene	Gene ID	Transcript ID	Click it/Input	Arg	Cys	Lys
SDHA	ENSG00000073578	ENST00000264932	0.930791836	59	18	57
CANX	ENSG00000127022	ENST00000247461	0.228771873	34	8	38
DLD	ENSG00000091140	ENST00000205402	0.406517057	48	10	36
PDHX	ENSG00000110435	ENST00000227868	0.281258256	45	4	45
DLAT	ENSG00000150768	ENST00000280346	0.407295739	68	9	49
PDHB	ENSG00000168291	ENST00000302746	0.244489278	38	6	22
PDHA1	ENSG00000131828	ENST00000422285	0.459632344	37	12	31
FASN	ENSG00000169710	ENST00000306749	1.43742641	226	46	316
KEAP1	ENSG00000079999	ENST00000171111	2.305168317	45	27	48
LDHA	ENSG00000134333	ENST00000227157	0.384301669	12	4	26
MTOR	ENSG00000198793	ENST00000361445	3.878536643	205	36	319
ACACA	ENSG00000278540	ENST00000616317	4.379098987	149	30	220
ALDOA	ENSG00000149925	ENST00000412304	0.602541254	42	8	34
ATP2A1	ENSG00000196296	ENST00000395503	1.546926222	91	24	97
OGDH	ENSG00000105953	ENST00000449767	1.61381669	32	8	46
G6PD	ENSG00000160211	ENST00000393562	0.529218549	46	14	96
RRAGB	ENSG00000083750	ENST00000374941	0.445823669	18	8	34
ACTB	ENSG00000075624	ENST00000493945	0.122317991	29	6	27
PGK1	ENSG00000102144	ENST00000373316	0.142663357	41	7	38
SRC	ENSG00000197122	ENST00000373578	2.150340609	44	9	49
INSR	ENSG00000171105	ENST00000302850	1.216920036	66	47	136
GAPDH	ENSG00000111640	ENST00000229239	0	31	10	19
VDAC1	ENSG00000213585	ENST00000265333	0	21	2	28

3.2.7. MG modifies PDHA via a CEL adduct

After confirming that PDH is directly modified by MG, I went on to determine in more detail the identity of the modifications via mass spectrometry. To this end, I immunoprecipitated an N-terminally Flag-tagged PDHA subunit and submitted it for mass spectrometric analysis by the DKFZ proteomics core facility, after confirming that all PDH components were present in the Flag-PDHA IP of both WT and Glo1KO cell lines (Figure 47). It is important to notice that the mass spectrometry analysis only included parameters that allowed the detection of MG adducts on Arg and Lys residues. Therefore, no MG adducts on Cys residues or MICA adducts were assessed in this experiment. Among the Arg and Lys modifications caused by MG, only a CEL modification on PDHA1 was increased in the Glo1 KO HEK293T IP compared with WT (Table 3).

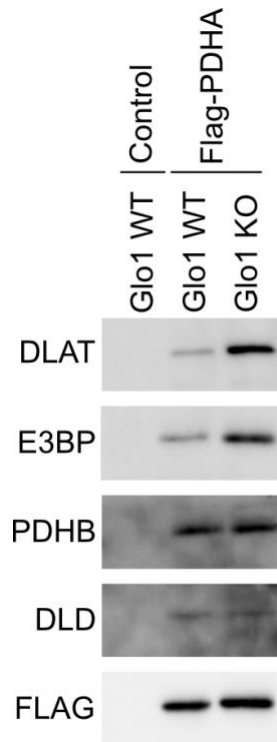


Figure 47. Flag-PDHA immunoprecipitation pulled down all PDH components. I transfected or not WT or Glo1 KO HEK293T cells with Flag-PDHA and performed an immunoprecipitation and I eluted the proteins with Flag-peptide. I used not transfected WT HEK293T cells as a negative control. I assessed eluates for all PDH subunits by immunoblotting.

Table 3. PDHA1 and DLAT are modified by MG in Glo1 KO HEK293T cell. The modified residues are indicated in red.

Protein	Type of modification	Peptide
PDHA1	Carboxyethyl-lysine	SKSDPIMLLKDR
PDHA1	Missed cleavage	PCIFICENNRYGMGTSV
DLAT	Missed cleavage	LAVEK ^R GIDLTQVK ^R GTGPDGR

I then validated the mass spectrometry results by immunoblotting the Flag-tagged PDHA IP with a CEL antibody. The Flag-tagged PDHA from the Glo1 KO HEK293T showed a 40% increased on CEL adducts when compared with the WT cells, corroborating that this adduct is preferentially formed on PDHA from Glo1 KO cells (Figure 48). Thus, MG modification of PDHA via CEL adduct formation could be mediating the decrease in PDH activity observed in the Glo1 KO cells.

Interestingly, mass spectrometric analysis also identified two different missed cleavages, one in PDHA and the other one in DLAT, which were significantly elevated in Glo1KO cells (Table 3). Since missed cleavages can be produced by the presence of an amino acid modification that causes the enzyme to skip the cleavage site, it is possible that these two missed cleavages are consequence of MG adducts. This possibility is currently being tested.

The mass spectrometry results validate that MG directly modifies PDH via a CEL adduct on PDHA. This subunit is mediating the first catalytic step in the oxidation of pyruvate to acetyl-CoA [43, 62, 63], thus, a MG modification in PDHA is likely to cause defects in PDH activity. Additionally, the DLAT subunit also showed a missed cleavage, raising the possibility that a MG modification is taking place in this subunit preventing the protein digestion at that position. These findings are consistent with the click-MG results, where DLAT was pulled down.

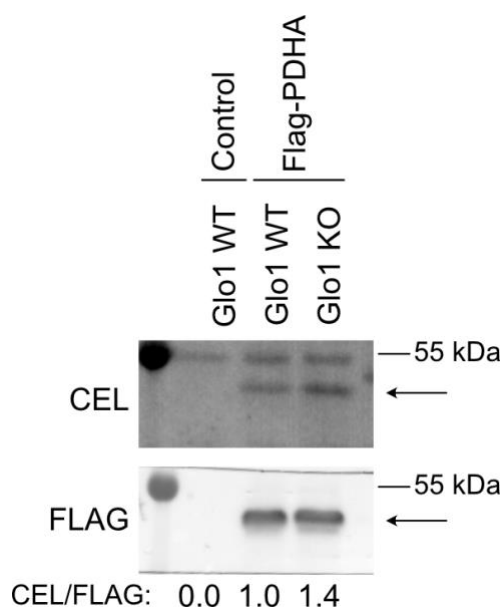


Figure 48. Levels of MG CEL adduct of PDHA are increased in Glo1 KO HEK293T cells. I transfected WT or Glo1 KO HEK293T cells with Flag-PDHA and performed an immunoprecipitation with FLAG beads. Proteins were eluted with Flag-peptide. I used not transfected WT HEK293T cells as a negative control. I assessed the presence of CEL adducts in the eluates by immunoblotting.

3.2.8. MG triggers the oligomerization of DLAT

I decided to further assess the impact of MG on DLAT, because my data indicated that DLAT is modified by MG and, hence, its activity could be affected: (I) I pulled down DLAT in the click MG experiments, (II) the mass spectrometry data showed a missed cleavage in DLAT,

and (III) the Michaelis-Menten experiments hinted at a mixed inhibition. Moreover, (IV) I noticed that more DLAT and E3BP were pulled down by FLAG-PDHA in the Glo1 KO cell lines compared with WT cells (Figure 47). This raised the possibility that in Glo1 KO cells a more stable interaction is taking place between PDHA and the components of the E2 subunit, DLAT and E3BP. It is known that PDH components display salt-lability and the ionic strength of the buffer affects the stability of the PDH complex [165]. To explore further the possibility of an MG-mediated stabilization of the interactions between the PDH subunits, I tested the effect of increasing NaCl concentration in the wash buffer of the immunoprecipitation. Consistent with previous observations, I also confirmed that higher NaCl concentrations caused a progressive loss of all subunits of PDH co-immunoprecipitating with PDHA, this was true for both WT and Glo1 KO HEK293T cells (Figure 49). This result disproves the hypothesis that MG is causing a covalent crosslinking modification between PDHA and the E2 subunit proteins, DLAT and E3BP.

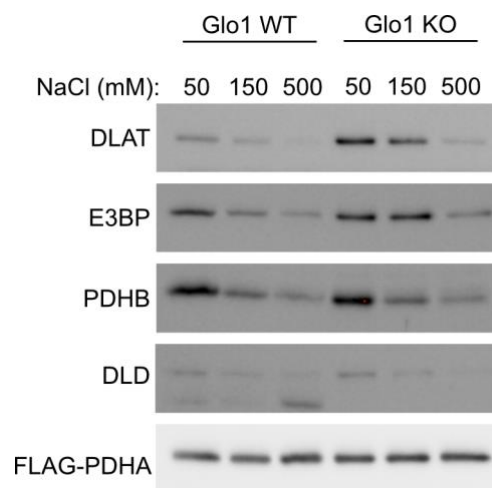


Figure 49. MG does not cause stabilizing interactions between PDHA and the E2 subunit components DLAT and E3BP. I transfected WT or Glo1 KO cells with Flag-PDHA and performed an immunoprecipitation with FLAG beads. I supplemented the wash buffer with increasing concentrations of NaCl.

Next, I hypothesized that MG could cause oligomerization of DLAT through protein crosslinking, thus explaining why more DLAT is pulled down with PDHA in the Glo1 KO HEK293T IP (Figure 47). Therefore, I incubated WT and Glo1 KO cells with different concentrations of MG for 60 minutes and blotted for DLAT under non-reducing conditions, to not exclude redox-sensitive interactions, e.g. crosslinking via disulfide bond formation (Figure 50). Intriguingly, MG treatment caused a concentration-dependent increase in the intensity of a 210 kDa band corresponding to a potential trimer of DLAT (Figure 50).

Analogously, the same 210 kDa band was stronger in the Glo1 KO cells compared with WT ones (Figure 50, line1 and 6). These results suggest that MG causes the formation of a 210 kDa oligomer of DLAT with a molecular weight corresponding to a DLAT trimer. Nevertheless, the 210 kDa oligomer of DLAT could also be a product of DLAT interacting with other proteins.

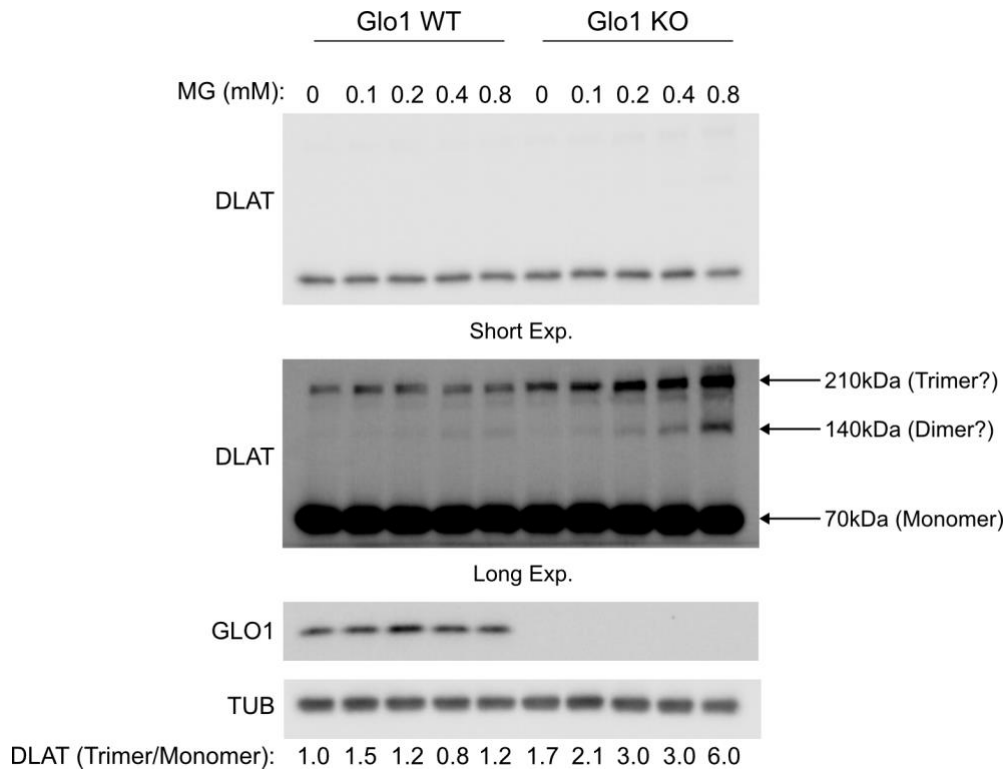


Figure 50. MG causes oligomerization of DLAT. I incubated WT or Glo1 KO HEK293T cells with increasing concentrations of MG for 60 minutes, before lysing the cells and assessing the presence of oligomers of DLAT by immunoblotting. Exposure (Exp.).

The E2 subunit of the PDH complex is composed of either homotrimers of DLAT and/or heterotrimers of DLAT and E3BP [32, 166]. Since the molecular weight of a heterotrimer composed of DLAT and E3BP would be difficult to distinguish from that of a homotrimer of DLAT (190 kDa vs 210 kDa, respectively), I tested whether the band described above could represent such a heterotrimer of DLAT with E3BP. To this end, I blotted MG-treated samples from WT and Glo1KO HEK293T cells for E3BP under non-reducing conditions, similar to what I described above for DLAT (Figure 50). Contrary to the DLAT results, I did not observe a high molecular weight E3BP band in the WT cells, and the Glo1 KO cells only showed a high molecular weight band upon treatment with high concentration of MG (Figure 51). These findings suggest that MG causes the formation of a high molecular weight oligomer of DLAT and not a heterotrimer of DLAT and E3BP. Additionally, since I observed that the decrease

in PDH activity of Glo1 KO cells happens independent of any MG treatment (Figure 35), while crosslinked heterotrimers of DLAT and E3BP seem to form only upon MG treatment, it is unlikely that they are the cause for the decreased PDH activity.

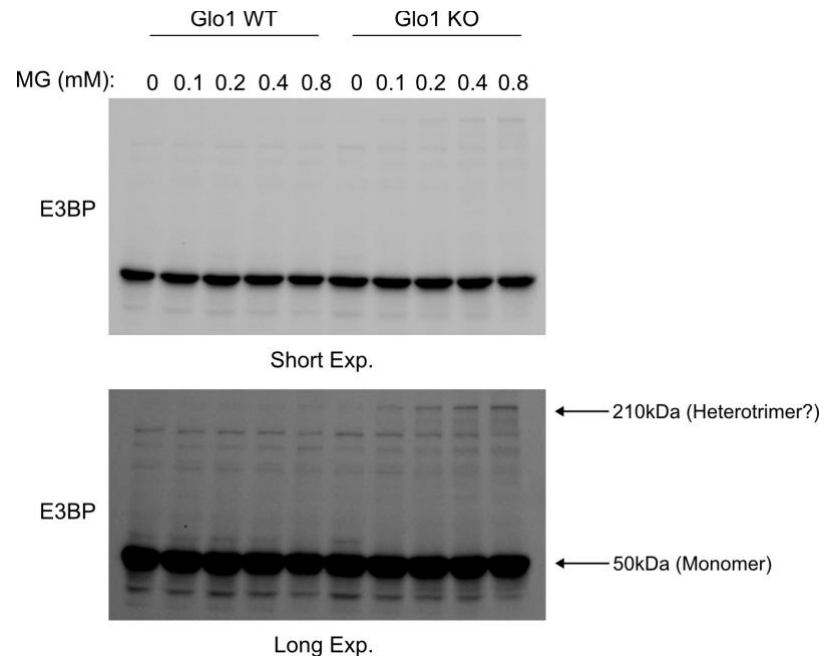


Figure 51. MG does not crosslink of DLAT and E3BP. I incubated WT or Glo1 KO cells with increasing concentrations of MG for 60 minutes, before lysing the cells and assessing the presence of oligomers of DLAT/E3BP by immunoblotting. Exposure (Exp.).

To further confirm the existence of a 210 kDa DLAT band and rule out any unspecificity of the antibody, I repeated the MG incubations for 60 minutes but I assessed WT or Glo1 KO cells with or without knockdown for DLAT. Reassuringly, knockdown of DLAT reduced the intensity of both the 70 and the 210 kDa bands, confirming that the latter is indeed a high molecular form of DLAT (Figure 52). This result hints at MG triggering the formation of a high molecular weight oligomer of DLAT. The identity of the proteins involved in the 210 kDa DLAT band is currently being assessed.

The formation of the 210 kDa oligomer of DLAT in presence of MG could be either via a redox sensitive bond like a disulfide bond, or via a more stable crosslink. MG can directly act as a protein crosslinking agent, by interacting first with a cysteine residue and then with a proximal arginine, generating a stable crosslink known as MICA adduct. This was first reported for the dimerization of KEAP1 [102]. Thus, I assessed whether the oligomerization of DLAT was redox sensitive by testing if supplementing the sample buffer with DTT would prevent the complex formation. Indeed, the addition of DTT caused a substantial decrease in

the DLAT high molecular weight band (Figure 53), indicating that oligomerization of DLAT is not dependent on a stable crosslinking such as a MICA adduct, but rather due to redox sensitive interaction like a cysteine disulfide bond.

The 210 kDa oligomer of DLAT could be at least in part responsible for the altered PDH activity in Glo1KO cells or upon MG treatment. Hence, I wanted to further validate that MG causes the formation of 210 kDa DLAT band. To this end, I tested whether the oligomerization of DLAT could be reversed by reconstitution of Glo1KO cells with Flag-tagged WT or inactive Glo1, similar to what I did before for PDH activity (Figure 35C). Consistent with the activity experiments, in one replicate DLAT trimerization was at least partially rescued upon Flag-WT Glo1 expression, but not by Flag-CI Glo1 mutant (Figure 54, replicate 1). While on the second replicate, there was no different in the trimmer levels between Flag-tagged WT or CI Glo1 (Figure 54, replicate 2). The variability of these results suggests that additional factors apart from MG could be playing a role in the oligomerization of DLAT.

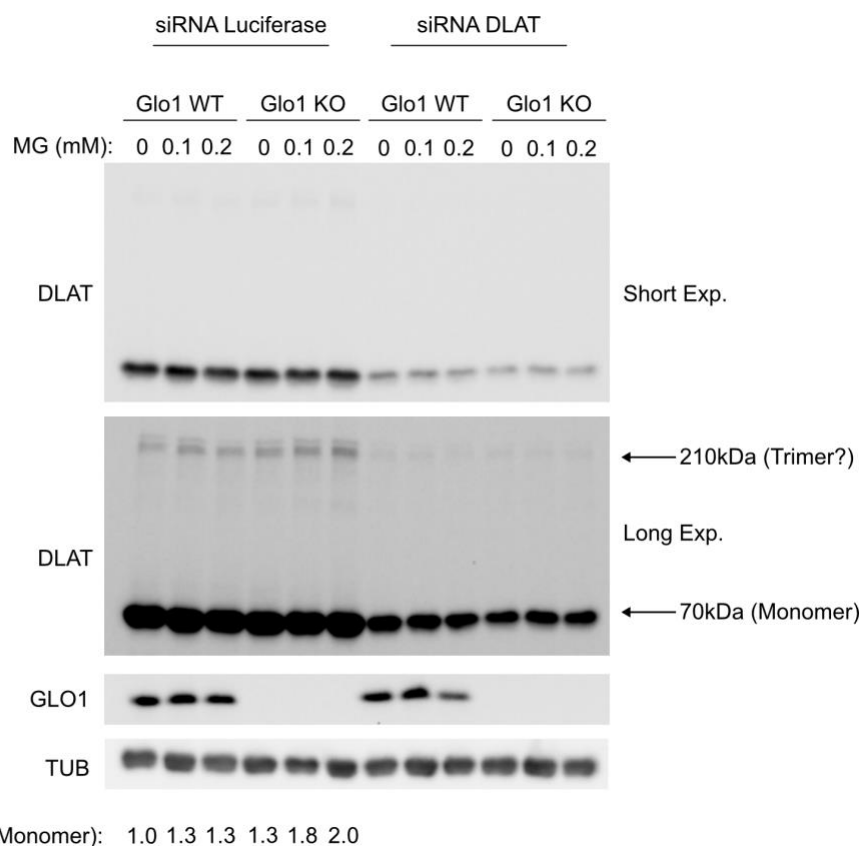


Figure 52. DLAT antibody specifically recognized the formation of DLAT oligomers. I knocked down DLAT or luciferase (control) in WT or Glo1 KO HEK293T cells. After 4 days, I incubated the cells with increasing concentrations of MG for 60 minutes, before lysing the cells and assessing the presence of oligomers of DLAT by immunoblotting. Exposure (Exp.).

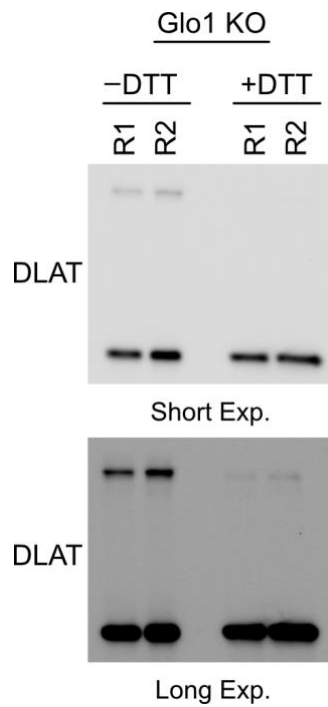


Figure 53. DLAT oligomerization is DTT-sensitive. I lysed Glo1 KO cells and prepared the samples in Laemmle with or without DTT and assessed the presence of DLAT homotrimers by immunoblotting. Exposure (Exp), replicate (R).

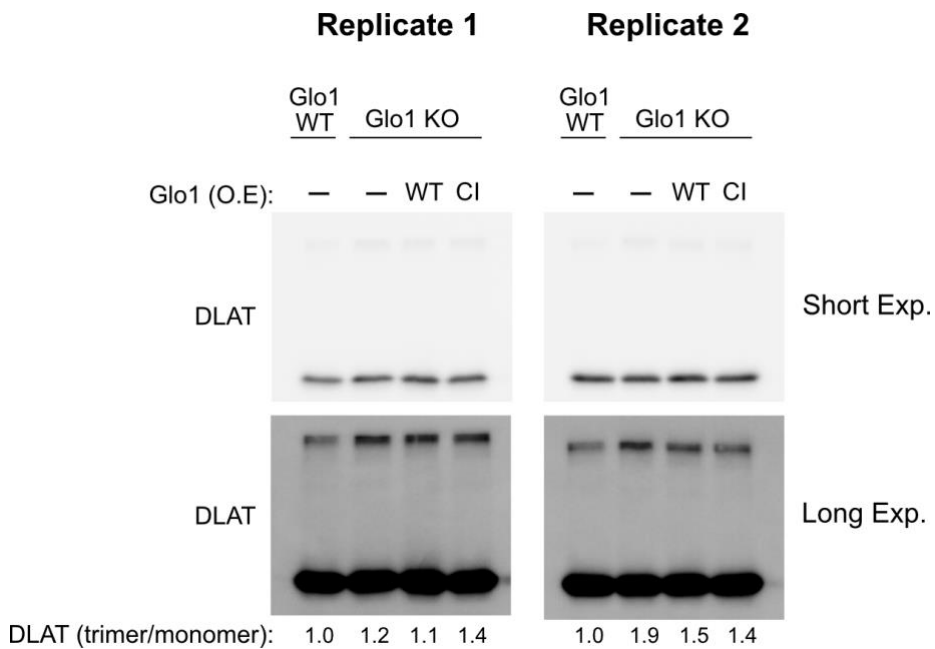


Figure 54. DLAT oligomerization in Flag-tagged WT and CI Glo1-expressing cells shows contradicting results. I lysed WT or Glo1 KO HEK293T cells, as well as Glo1 KO cells stably transfected with Flag-Tag WT or catalytically inactive Glo1 (CI) and assessed the presence of DLAT homotrimers by immunoblotting.

3.2.9. MG causes a redox sensitive modification on DLAT

It is worth noting, that the assessment of the 210 kDa oligomer of DLAT requires significant protein concentrations and long exposure times for the immunosignal detection. Therefore, to further study the characteristics of this DTT susceptible modification on DLAT, I devised an alternative assay based on the same principles as acyl-PEG exchange (APE) (Figure 55). In this assay, the free thiol groups on cysteines are first blocked using N-methylmaleimide in a reaction that causes their alkylation. Next, DTT is applied to disrupt susceptible modifications, such as glutathionylations or disulfide bonds on cysteine, causing a free, new thiol group. Finally, the free thiol groups react with methoxy-polyethylene glycol-maleimide (mPEG) generating a mPEG-protein. The mPEG modification is detected by immunoblot due to a shift in the molecular weight of the protein [167, 168]. The number of mPEG modifications can be inferred from the exact increase in the molecular weight. Using this assay, I studied the presence of DTT susceptible modifications on all PDH subunits from WT and Glo1 KO HEK293T cells (Figure 56 and 57). DLAT was the only subunit for which the assay showed a difference between Glo1 KO and WT cells, indicating the presence of one cysteine residue substantially more modified in Glo1KO cells (Figure 56), while no major difference was observed for the other PDH subunits (Figure 57). These results further validate the previous conclusions that DLAT is likely modified by MG in a DTT-sensitive manner. Additionally, I observed stronger and more evident differences in the levels of MG modification of DLAT between WT and Glo1 KO HEK293T using the APE assay than by assessing its oligomerization (Figure 50-54). Thus, additional experiments based on the APE assay, including treatment of WT HeLa and HEK293T cells with MG, are still required to further validate the effect of MG on DLAT.

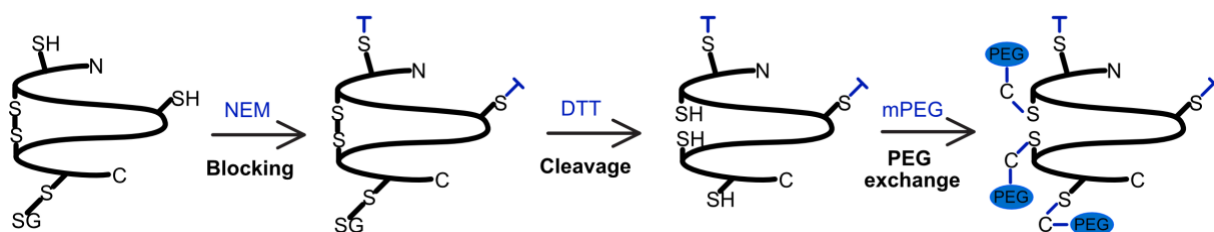


Figure 55. Acyl-PEG exchange assay. A schematic representation of the essential steps of the APE assay I performed to study DTT-sensitive modifications of PDH. I first blocked the free thiols groups on unmodified cysteine residues using N-methylmaleimide, then I reduced disulfide bonds or other redox-sensitive modifications with DTT. Finally, I incubated the sample with m-PEG that reacts with the free thiol group on proteins, causing a shift in the molecular weight of the protein, and I assessed the molecular weight shift by immunoblotting.

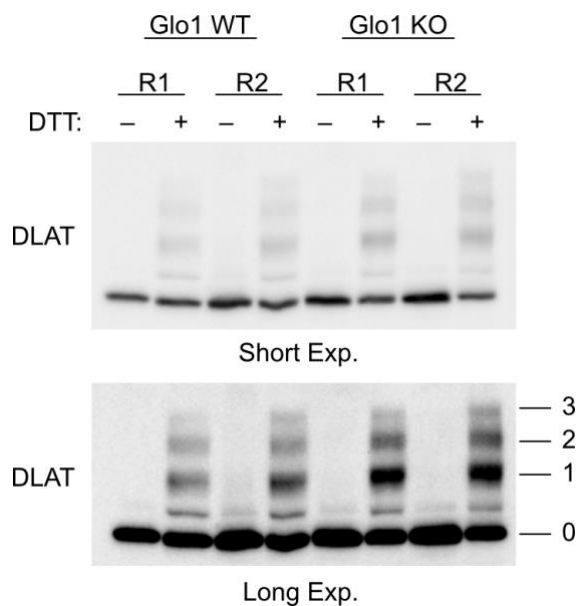


Figure 56. DLAT shows a DTT sensitive cysteine modifications in Glo1 KO cells. I use WT or Glo1 KO HEK293T cells in an adapted APE assay. I assessed the molecular weight shift in the DLAT subunit of PDH by immunoblotting. Exposure (EXP) and replicate (R).

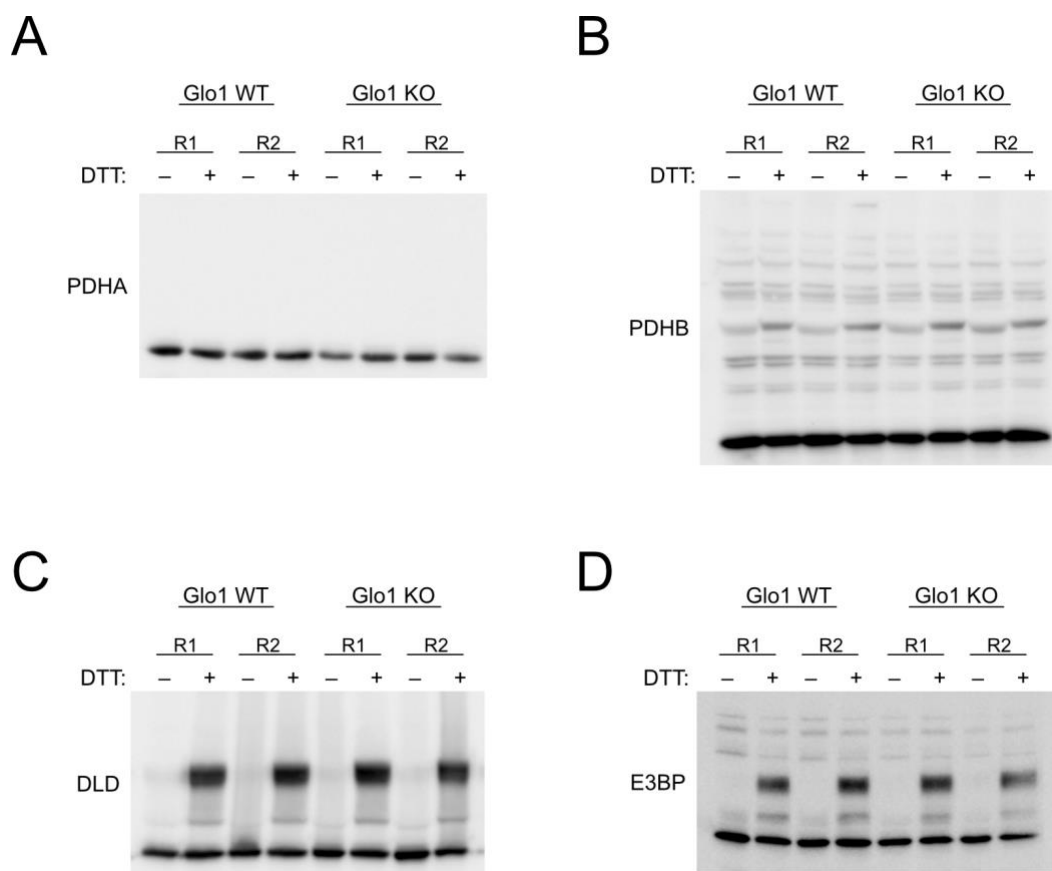


Figure 57. Other PDH subunits do not show DTT sensitive modifications. I use WT or Glo1 KO HEK293T cells in an adapted APE assay. I assessed the molecular weight shift on (A) PDHA, (B) PDHB, (C) DLD and (D) E3BP subunit by immunoblotting. Exposure (EXP) and replicate (R).

Next, I wondered whether the MG-dependent DTT-sensitive modification on DLAT plays an important mechanistic role in the inhibition of PDH (Figure 58). Based on this hypothesis, I assessed if the decrease in PDH activity in Glo1 KO HEK293T cells could be rescued by DTT. To this end, I purified the mitochondrial fraction in a buffer supplemented with 50 mM DTT, I then washed the mitochondrial fraction and subsequently performed the assay in PDH buffer without DTT. DTT addition during cell fractionation caused PDH activity to increase in both WT and Glo1 KO cells (Figure 58A). However, when I independently compared WT and Glo1 KO cells with DTT or without DTT, the PDH activity of Glo1 KO cells with DTT is a partial rescue (figure 58B). This result suggests that DTT susceptible modifications on DLAT are partially regulating PDH activity in the Glo1 HEK293T cells, supporting the model of mixed inhibition observed with the Michaelis-Menten experiments (Figure 42B).

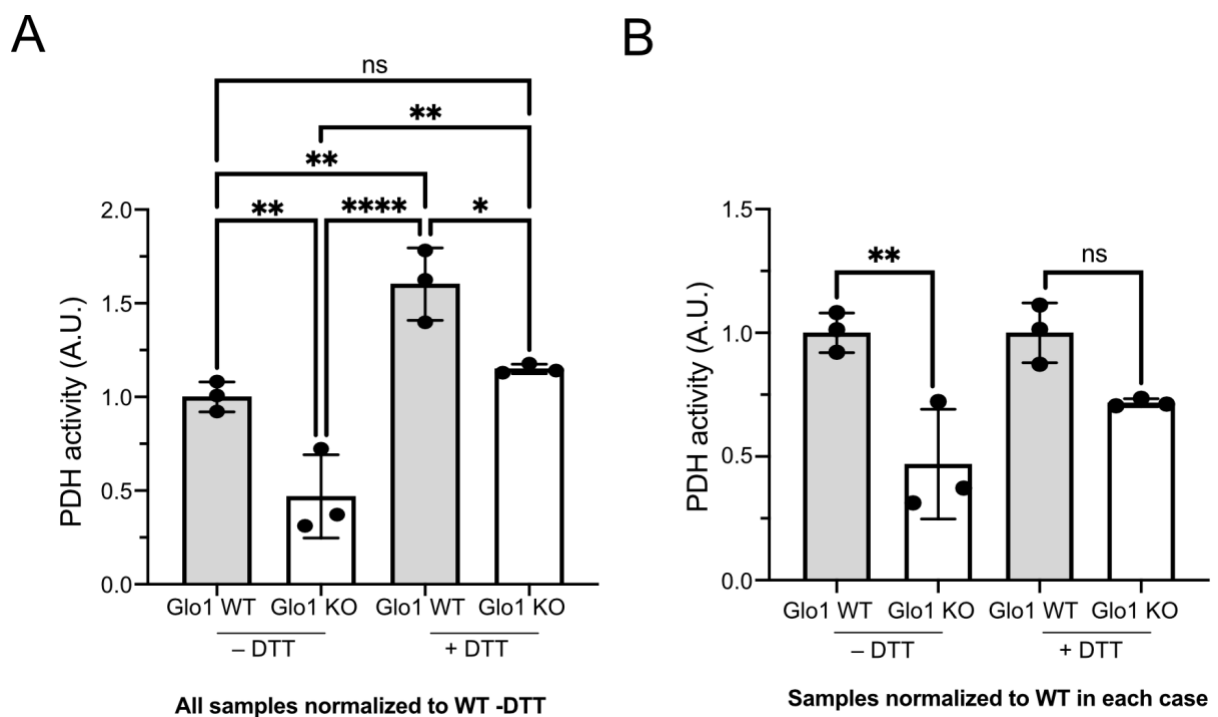


Figure 58. DTT treatment partially rescues the decrease in PDH activity in Glo1 KO HEK293T. I cultured WT or Glo1 KO HEK293T cells in low Glc conditions and cell fractionated them in a lysis buffer with or without DTT (50 mM). Then, I isolated the mitochondrial pellet and resuspended it in PDH assay buffer without DTT. (A) PDH activity is normalized to average activity of Glo1 WT without DTT. (B) I normalized the samples in (A) to average activity of Glo1 WT within the same treatment group (-/+ DTT). For all the cases the activity was first normalized to total levels of mitochondrial proteins. Biological replicates n= 3, *p<0.05, **p<0.01 and ***p<0.001 determined by one-way ANOVA (multiple comparisons). Not significant (ns).

My results then proposed that MG modifies PDH in more than one way, via direct interaction with PDHA forming a CEL adduct and also generating DTT susceptible modifications on DLAT. As consequence, MG inhibition of PDH might be more complex than I initially hypothesized and additional characterization of both mechanisms is still required to fully understand how they function, as well as their role on pathologies as diabetes.

3.2.10. Impact of MG on mitochondrial respiration

A decrease in PDH activity would be expected to affect the levels of its product, acetyl-CoA, and as a consequence the pathways depending on it, in particular the TCA cycle and oxidative phosphorylation (Figure 59A). Based on this, I measured acetyl-CoA levels in WT and Glo1 KO HeLa cells, but unexpectedly, Glo1 KO cells had even higher acetyl-CoA levels than WT HeLa cells (Figure 59B). This could be due to the increase in glucose uptake (Figure 33), possibly compensating for the decrease in PDH activity.

To further characterize the metabolic changes caused by MG, I assessed glycolytic and respiratory capacity with a combination of glycolysis and mito stress test using the Seahorse platform (Figure 60). The basal glycolytic capacity, measured as the rate of extracellular acidification (ECAR) after addition of glucose, was higher in Glo1 KO cells compared with WT, while maximum glycolytic capacity after addition of oligomycin, which inhibits ATP synthase (complex V), was only slightly higher in Glo1 KO cells (Figure 60A). These results are in line with the previous observations of increased glucose uptake and L-lactate excretion in Glo1 KO cells (Figure 30 and 33) and suggest a compensatory increase in glycolytic flux following decreased PDH activity.

One main fate of glycolytic acetyl-CoA is to fuel the TCA cycle which enables OXPHOS, cellular respiration (Figure 59A). The Seahorse mito stress test measures the respiration rate as the rate of oxygen consumption (OCR). Under basal conditions, before oligomycin addition, the OCR was higher in Glo1 KO HeLa cells compared with WT. The addition of FCCP, an uncoupling agent, allows uninhibited flow through the electron transport chain and hence, to determine the maximum oxygen consumption rates. Glo1 KO cells had also higher maximal respiration capacity than WT cells (Figure 60B), in line with the higher levels of acetyl-CoA in Glo1 KO cells (Figure 59B). In contrast, the spare capacity, i.e. the difference between basal respiration and maximal respiration, was not changed between WT and Glo1 KO cells, suggesting both cells could respond in the same way to energetic demands (Figure 60B).

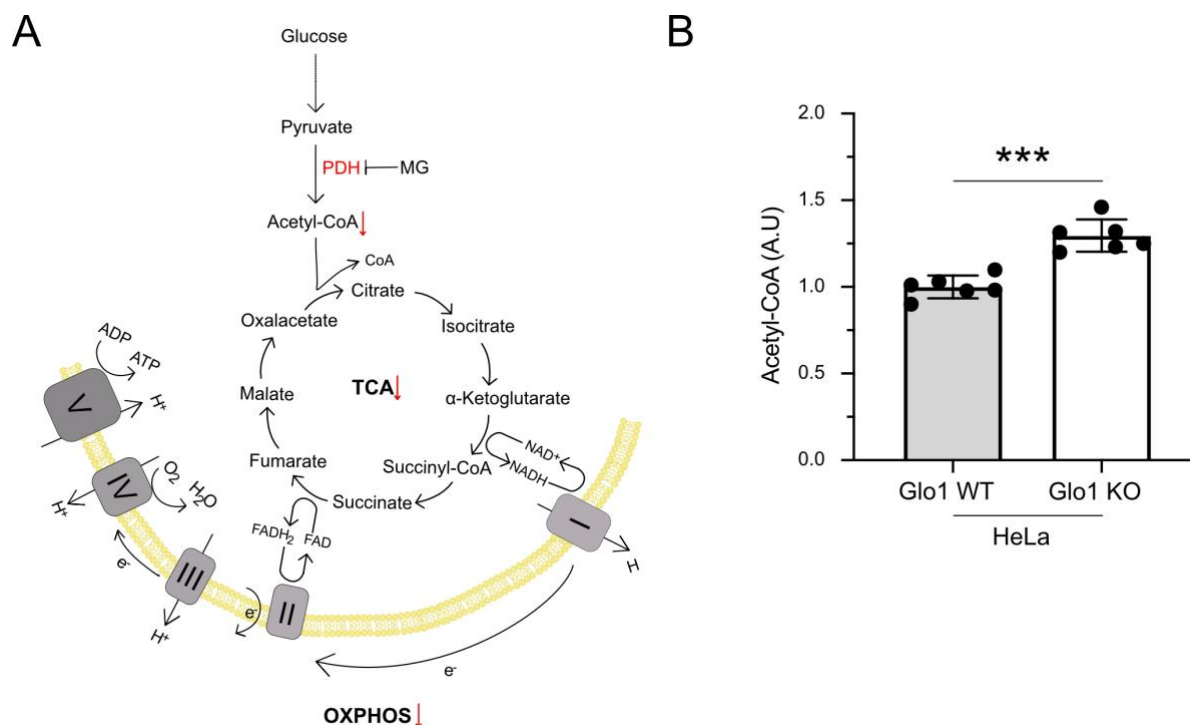


Figure 59. Glo1 KO HeLa cells produced more Acetyl-CoA. (A) Schematic representation of glycolysis, TCA cycle, and OXPHOS. The effect of MG on metabolism is indicated in red. (B) I measured acetyl-CoA levels in HeLa cells. * $p < 0.05$, ** $p < 0.01$ and *** $p < 0.001$ determined by two-sided, unpaired Student's t-test.

Besides from pyruvate, acetyl-CoA is also produced by β -oxidation of long chain fatty acids such as palmitate (Figure 61A). To further assess the origin of the higher acetyl-CoA levels of Glo1KO cells, I then performed a Seahorse palmitate oxidation stress test after addition of palmitate as substrate for respiration in medium containing only 0.5 mM Glc and using etomoxir as negative control, an inhibitor of CPT1 and thus, of β -oxidation (Figure 61A). As expected, minimal levels of respiration were observed in both cell lines in the absence of palmitate (BSA only) or upon etomoxir incubation (Figure 61B). WT cells were more efficient in the use of palmitate when compared with Glo1 KO HeLa cells. These results suggest that Glo1 KO HeLa cells have an impairment in the use of long chain fatty acids as source of respiration and thus, fatty acid β -oxidation is likely not the main source of acetyl-CoA in these cells.

All these results validate that Glo1 dysregulations lead to metabolic remodeling of glucose and lipid metabolism. Therefore, elevated levels of MG could impair the metabolic flexibility of the cell, leading to deficiencies associated with diabetes and obesity.

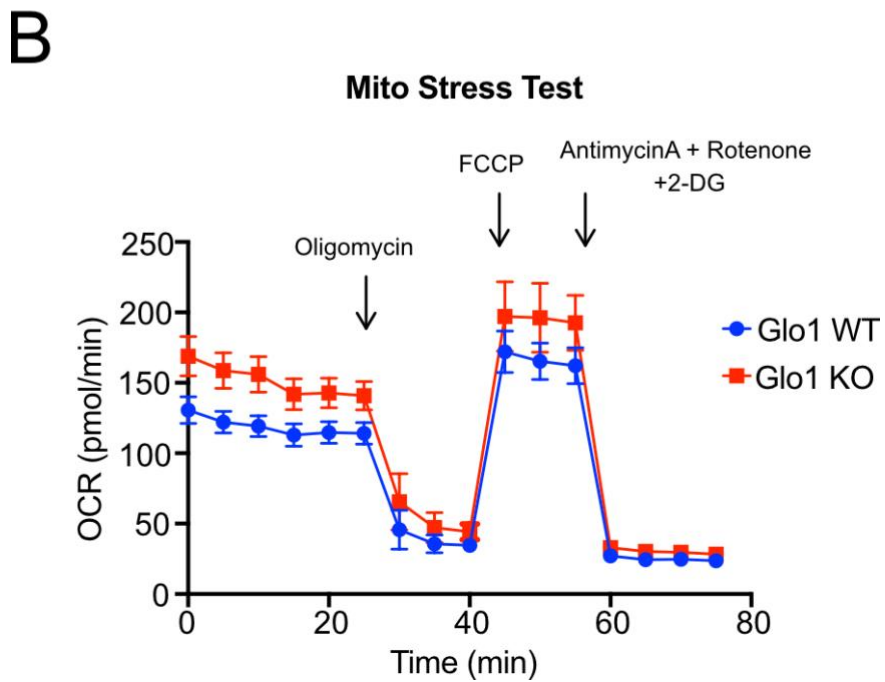
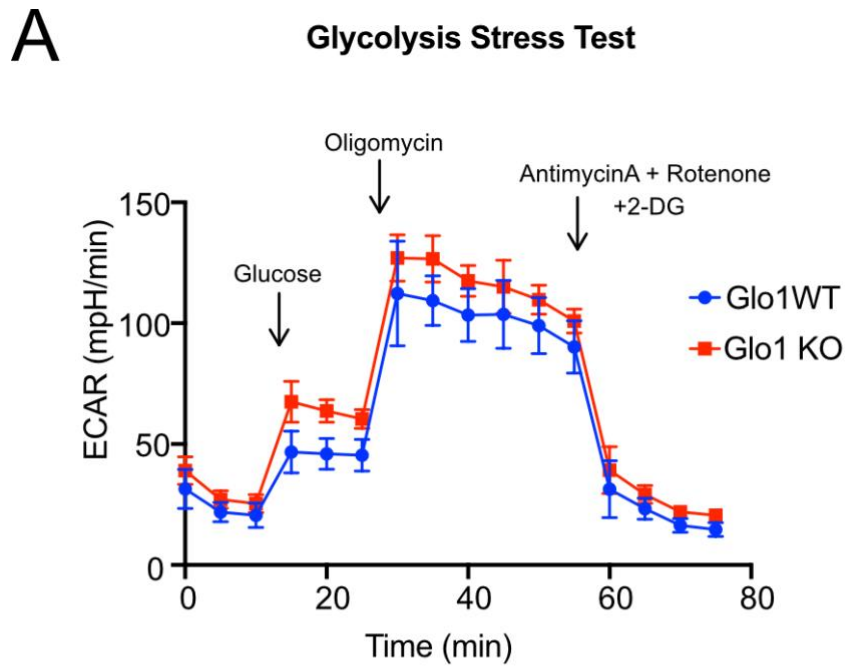


Figure 60. Glo1 KO HeLa cells are metabolically more active. I performed a combination of (A) Seahorse glycolysis stress test and (B) mito stress test in HeLa WT or Glo1 KO cells. Extracellular acidification rate (ECAR), oxygen consumption rate (OCR).

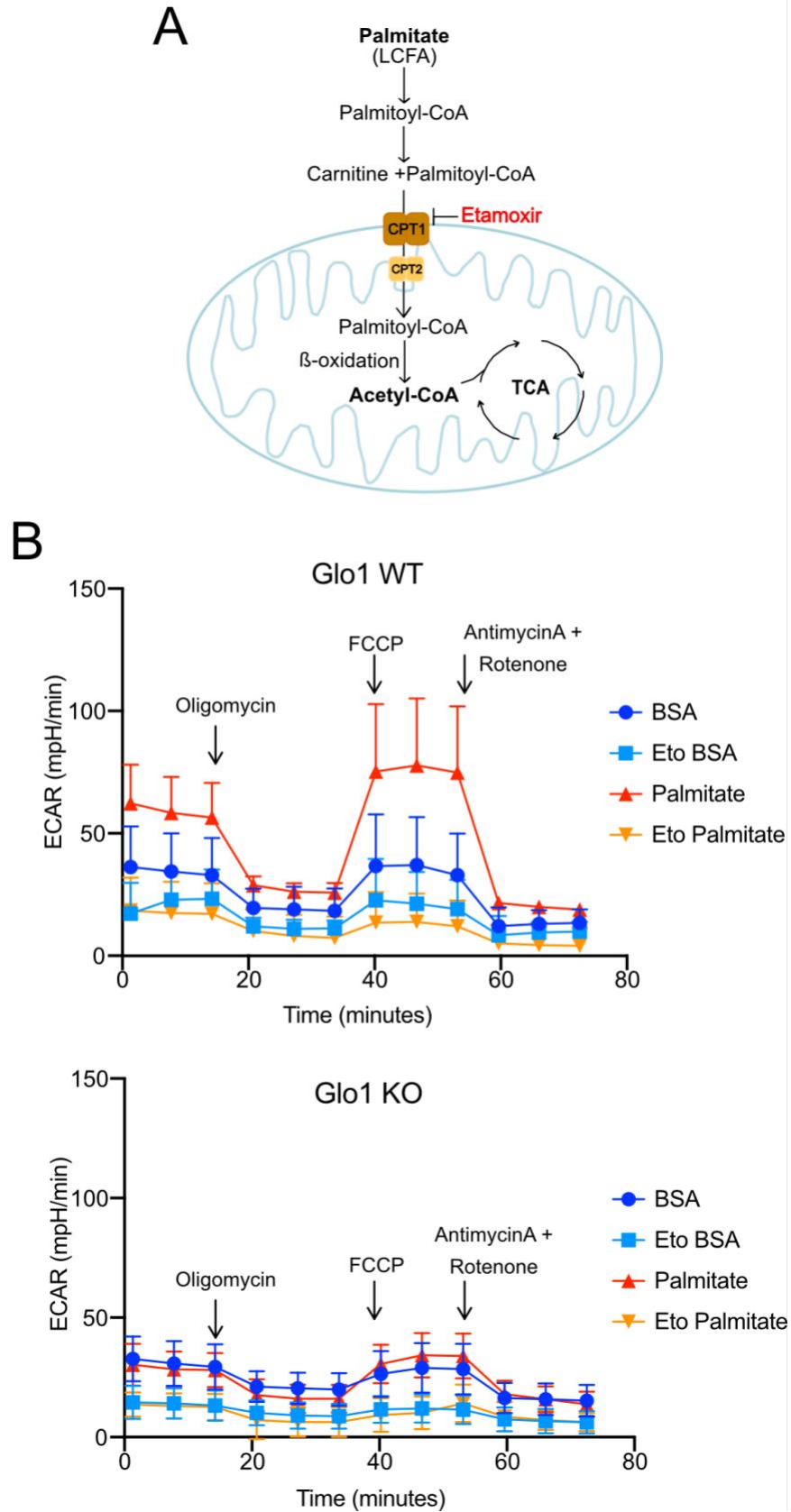


Figure 61. Glo1 KO HeLa cells are incapable of using Palmitate as substrate for respiration. (A) Schematic representation of long chain fatty acid uptake (LCFA) and β -oxidation to acetyl-CoA. (B) I performed a Seahorse palmitate oxidation stress test in WT (upper panel) or Glo1 KO HeLa cells (lower panel). Bovine serum albumin (BSA), Extracellular acidification rate (ECAR), Etomoxir (Eto).

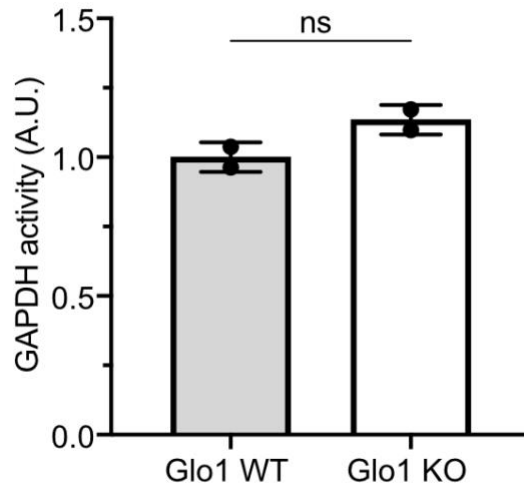
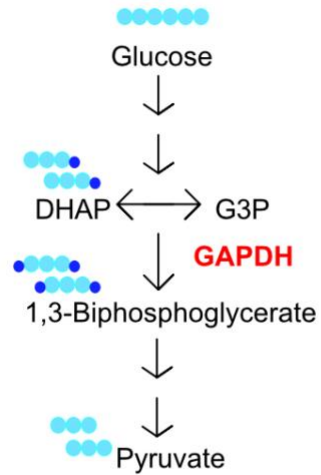
3.2.11. MG does not impact the activity of other metabolic enzymes

As MG caused changes in glucose metabolism (Figure 33 and 60), I then assessed whether the activity of another important glycolytic enzyme, glyceraldehyde-3-phosphate dehydrogenase (GAPDH), was altered in Glo1 KO HEK293T cells. GAPDH is responsible for the oxidative phosphorylation of glyceraldehyde-3-phosphate to yield 1,3-biphosphoglycerate, the 6th step of glycolysis (Figure 62A, left panel). Changes in GAPDH activity would not only have an impact on the glycolytic flux but also on the levels of trioses phosphate, the main source of MG from glycolysis. However, there were no changes in the activity of GAPDH in Glo1 KO cells when compared to WT cells (Figure 62A, right panel). This observation is also in line with the click-MG pull downs showing that GAPDH was not modified by MG (Figure 44 and 45).

KGDH is an important regulatory node in the Krebs cycle catalyzing the conversion of α -ketoglutarate into succinyl-CoA (Figure 62B, left panel). Interestingly, KGDH shares the same E3 subunit, dehydrolypoil dehydrogenase, as PDH and in both cases lipoate is the catalytic cofactor. Despite these similarities, KGDH activity was not significantly changed in Glo1 KO HEK293T cells, suggesting the effect of MG on PDH is rather specific and that it is likely independent of the E3 subunit or the lipoate cofactor, as they are shared with KGDH (Figure 62B, right panel). Additionally, OGDH and DLD subunits of KGDH were present in the click-MG pull downs, suggesting that not all MG modifications lead to changes in activity (Figure 44).

The fact that GAPDH and KGDH activities were not affected in the Glo1 KO HEK293T cells (Figure 62), suggest a rather specific effect of MG on proteins as PDH and LDH. These results also raised the possibility that even when MG modifies a broad range of proteins, not all MG modifications lead to a functional consequence. In other words, the activity of only a set of enzymes could be disturbed by MG, controlling also specific processes.

A



B

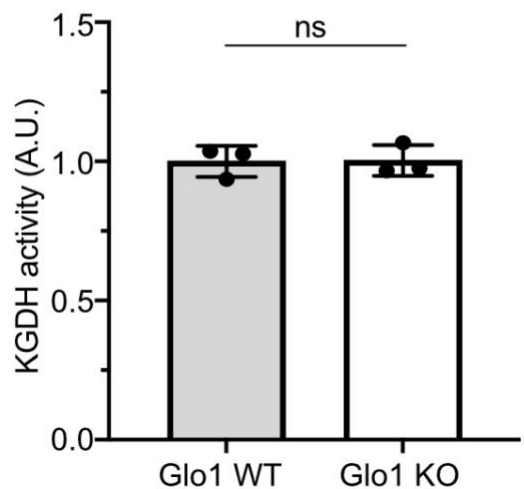
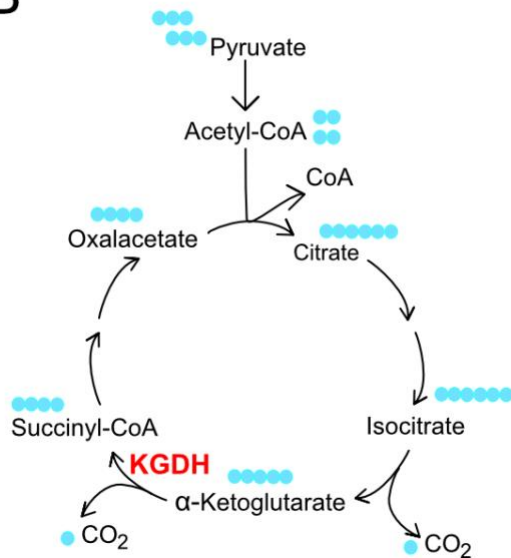


Figure 62. GAPDH and KGDH activities are unchanged in Glo1 KO HEK293T cells. (A, left panel) Schematic representation of GAPDH reaction in glycolysis. (A, right panel) GAPDH activity assay performed on the cytosolic fraction of Glo1 WT or KO HEK293T cells. Biological replicates n=2. (B, left panel) Schematic representation of KGDH reaction in TCA cycle. (B, right panel) KGDH activity assay performed on the cytosolic fraction of Glo1 WT or KO HEK293T cells. Biological replicates n=3. In both cases *p<0.05, **p<0.01 and ***p<0.001 determined by two-sided, unpaired Student's t-test. Not significant (ns).

3.2.12. MG does not impair PDH activity in kidneys of HGHCi mice

PDH is an important metabolic node whose activity has been reported to decrease in diabetic animals [90, 169]. Based on the results above showing that MG impairs PDH activity (Figure 35-39), I thus wondered whether MG could similarly affect PDH activity also *in vivo*. To this end, I analyzed kidney samples from WT and Glo1 KO mice kindly provided by the laboratory of Marc Freichel at the Pharmacology Institute of the University of Heidelberg. Although not significant, samples from Glo1 KO animals showed a tendency towards lower PDH activity (Figure 63A), without any detectable change in PDHA or DLAT expression, as assessed by WB (Figure 63B). Since these animals were fed a standard diet that does not challenge the metabolism, it is possible that under these conditions the levels of MG are low and additional detoxification mechanism such as ARK and ALDH are enough to compensate for the loss of Glo1.

Encouraged by the tendency towards lower PDH activity upon deletion of Glo1, I then wondered whether a metabolic challenge could further enhance the effect of MG on PDH. To this end, I analyzed kidney samples from a high glucose and high cholesterol (HGHCi) mouse model, generated by the laboratory of Marc Freichel by combining expression of the D377Y variant of murine PCSK9 in the liver, injection of streptozotocin and high-fat diet [154]. Importantly, Freichel laboratory's data suggests that HGHCi mice have higher MG levels than control mice (data not showed). Unfortunately, I was not able to observe any significant change in PDH activity between the different treatments (Figure 64A). Interestingly, however, HGHCi mice displayed decreased PDH activity as compared to the untreated ones, both for WT and Glo1 KO mice (Figure 64A), indicating that the high glucose/high cholesterol condition has a negative impact on PDH activity.

PDH activity can be regulated by phosphorylation of three key serine residues on PDHA: S300, S293 and S232. Thus, I decided to test whether the changes in PDH activity under HGHCi conditions were due to changes in PDHA phosphorylation. Independently of Glo1 expression, the HGHCi condition caused an increase of pS300 and pS232 when compared with the respective controls (Figure 64B-C). These results hints towards phosphorylation being the main cause of the decreased PDH activity in the HGHCi kidneys. As my results in cell culture suggested that MG does not affect PDH activity (Figure 40), it is unlikely that MG modulates the decrease in PDH activity observed in HGHCi kidneys.

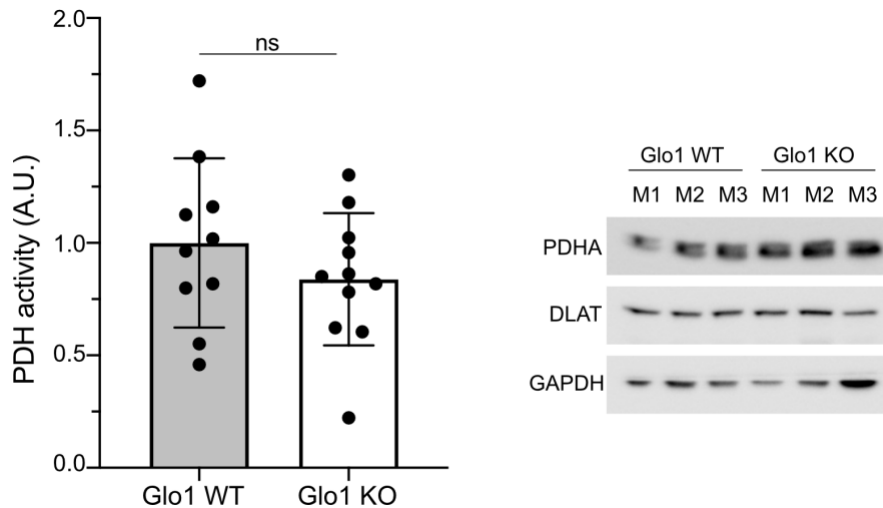


Figure 63. Kidneys of Glo1 KO mice showed a trend towards decreased PDH activity. I homogenized kidneys of Glo1 WT or KO mice and I determined (left panel) PDH activity or (right panel) I assessed expression levels of two of its subunits, DLAT and PDHA, by immunoblotting. Biological replicates n=10 (left panel), n=3 (right panel). Determined by one-sided, unpaired Student's t-test. Not significant (ns), mouse (M).

3.2.13. MG impairs PDH activity in livers of HGHCi mice

Given the important metabolic functions of the liver, including systemic glucose homeostasis, I then went on to perform analogous experiments using liver samples from WT or Glo1 KO HGHCi mice. Excitingly, in contrast to the experiments with kidney samples, loss of Glo1 caused a significant decrease in PDH activity in the liver under high glucose/high cholesterol conditions (Figure 65A), indicating that MG could also inhibit PDH activity *in vivo* and suggesting that this effect could be tissue specific.

Importantly, although some samples showed higher phosphorylation of PDHA, the overall phosphorylation state of PDH was not significantly altered in the liver of Glo1KO mice after normalization for the total levels of PDHA (Figure 65B-C). Additionally, PDHA and PDHB levels were not decreased in Glo1KO samples, but rather increased as compared to controls (Figure 66), indicating that lower expression of PDH subunits is not the reason for the reduced PDH activity. The higher expression of these PDH subunits could suggest a compensatory mechanism taking place upon deletion of Glo1 and, given the overall lower PDH activity measured in liver samples, indicates an even lower activity per PDH molecule. Consistent with my cell culture experiments, lack of Glo1 in the liver of HGHCi mice caused reduce PDH activity, hinting that MG could also modified and decreased PDH activity in these animals.

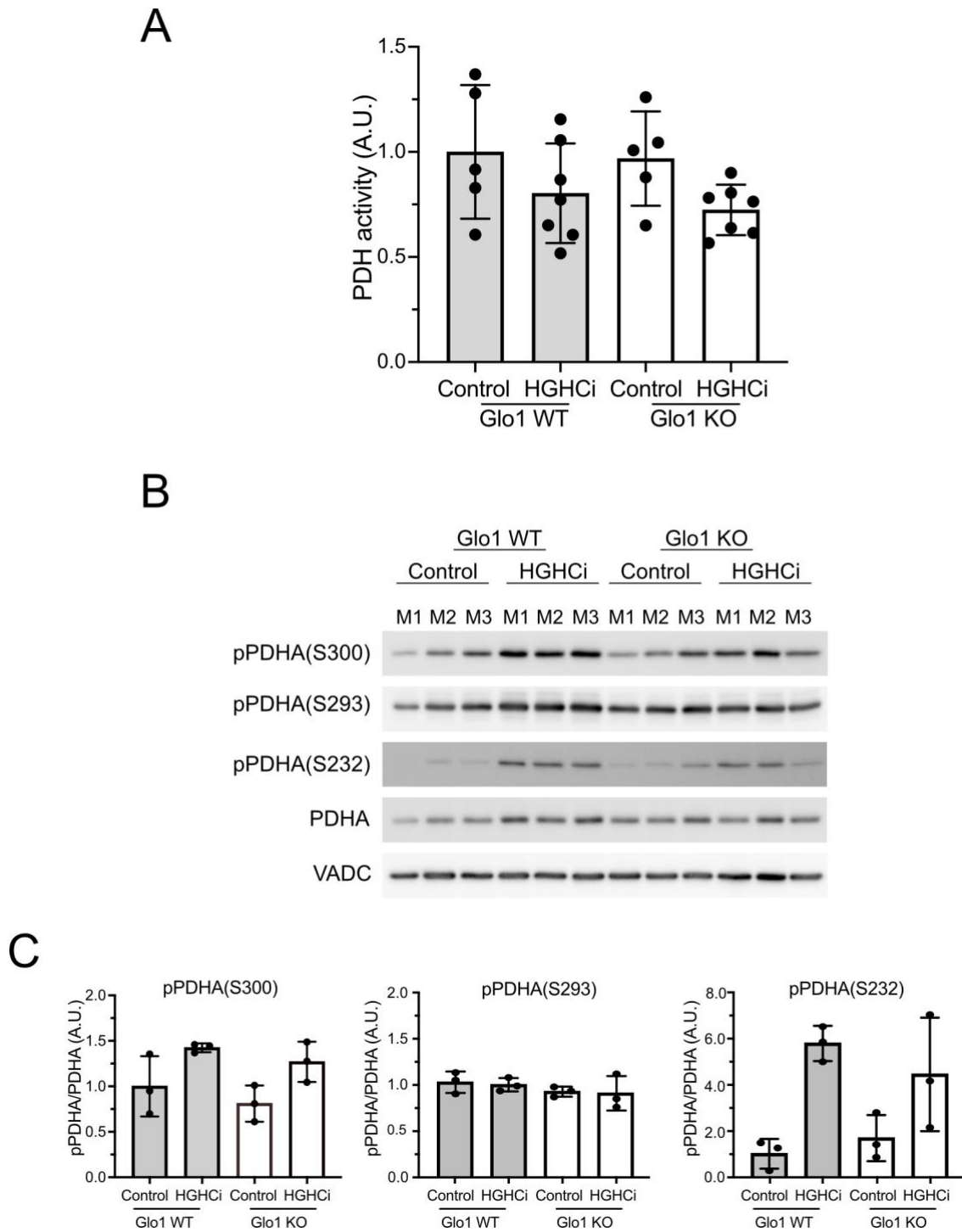


Figure 64. HGHCi kidney samples show decreased PDH activity due to increased phosphorylation of PDHA. I homogenized kidneys of control or HGHCi Glo1 WT or KO and I assessed (A) PDH activity or (B) PDHA phosphorylation. (C) I quantified the ratio of pPDH to PDH for pS300, pS293, and pS232. For (A) Biological replicates n=5 for control mice and n=7 for HGHCi mice, for (B-C) biological replicates n=3. Mouse (M). (A) Determined by one-way ANOVA (multiple comparisons).

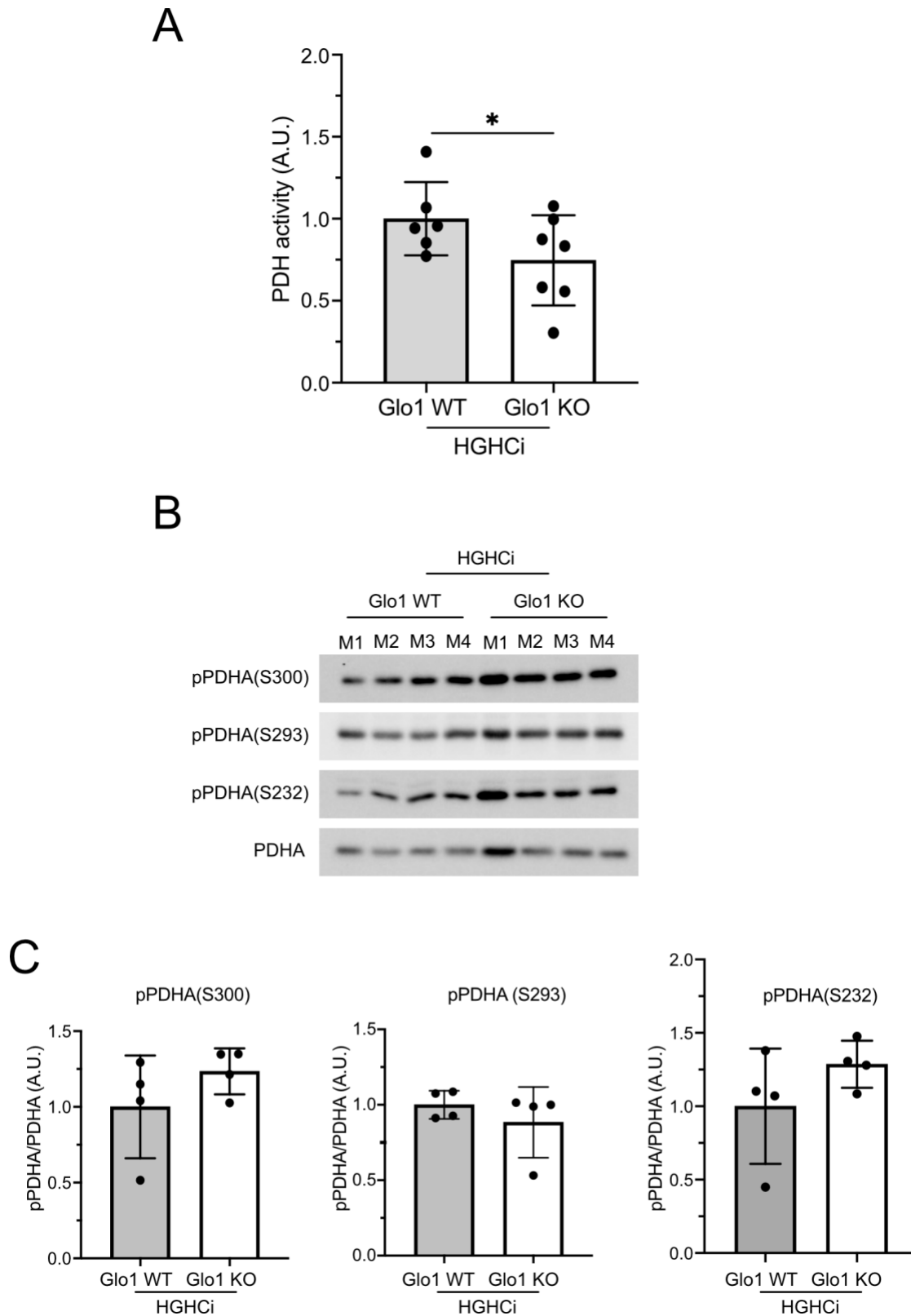


Figure 65. Loss of Glo1 in livers of HGHCi mice causes decreased PDH activity independently of PDHA phosphorylation. I homogenized livers of HGHCi Glo1 WT and KO mice. I then purified the mitochondrial fraction and assessed (A) PDH activity or (B) phosphorylation of PDHA. (C) I quantified the ratios of pPDHA to PDHA for pS300, pS293, and pS232. Biological replicates for (A) WT n=6 and and KO n=7 and for (B-C) n=4. For all cases *p<0.05, determined by one-sided, unpaired Student's t-test. Mouse (M).

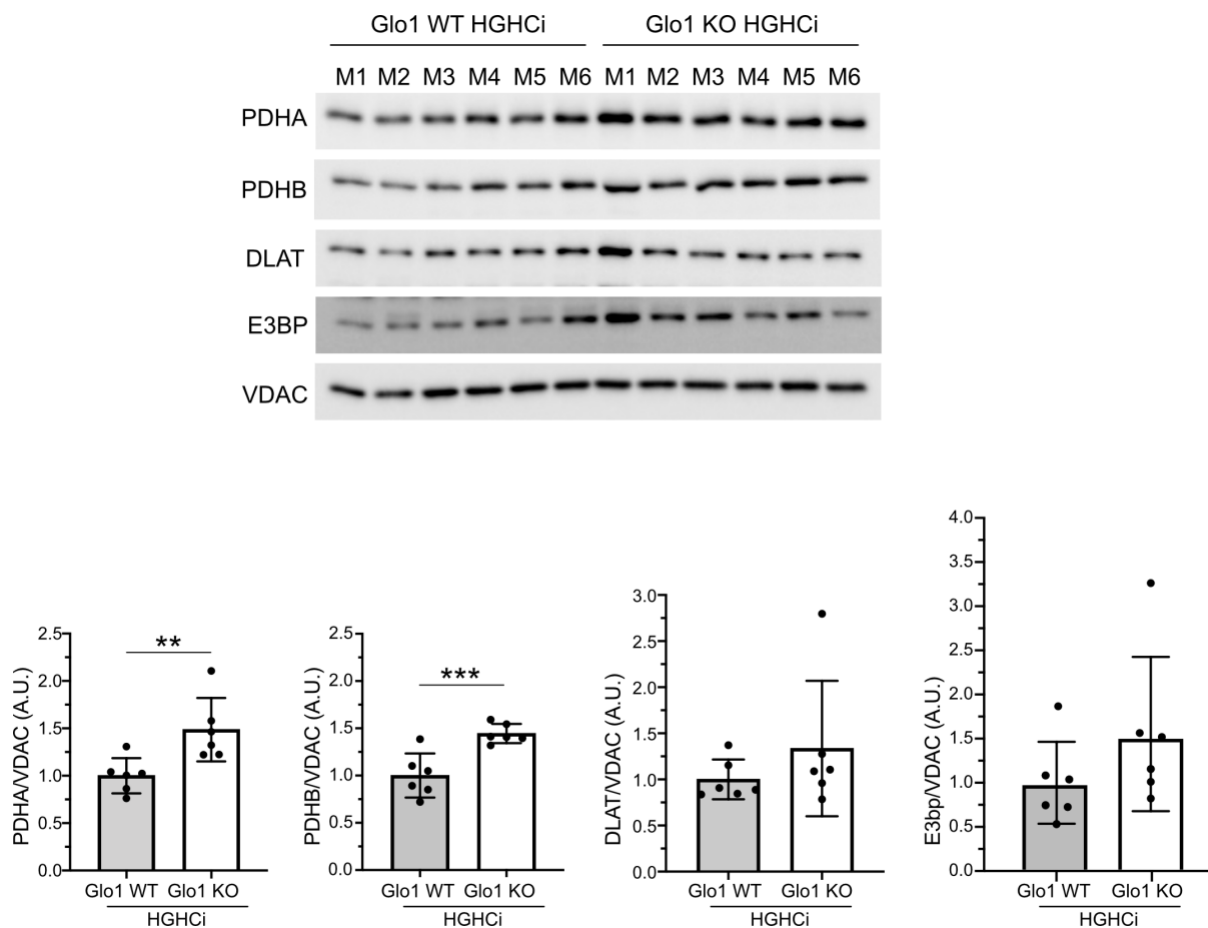


Figure 66. Lack of Glo1 in liver from HGHCi mice causes an increase in the expression of PDHA and PDHB subunits. I homogenized livers of HGHCi Glo1 WT and KO mice. I then purified the mitochondrial fraction and assessed the expression levels of different PDH subunits. Biological replicates n=6. For all cases **p<0.01, and ***p<0.001 determined by one-sided, unpaired Student's t-test. Mouse (M).

3.2.14. Low Glo1 expression correlates with decreased PDH activity in Ins2Akita mice

As high MG levels have been associated with diabetes, I then assessed PDH activity in a mouse model of type 1 diabetes. I previously observed that as Ins2Akita mice aged the Glo1 phosphorylation at Y136 decreased in comparison with their WT control counterparts (Figure 22), suggesting decreased Glo1 activity. Additionally, I also noticed that old Ins2Akita mice expressed lower levels of Glo1, with the lowest Glo1 expression observed in 6 months old Ins2Akita mice (Figure 67A). These two observations predict diminished Glo1 activity, making the Ins2Akita mice an interesting system to study PDH activity. Thus, I performed activity assays in kidney samples from Ins2Akita mice as they aged and compared them to age-matched control mice. Similar to Glo1 phosphorylation and expression, PDH activity was also decreased in old Ins2Akita mice, with the lowest PDH activity observed in 3 and 6 months old

Ins2Akita mice (Figure 67B). These results suggest that Glo1 activity and expression could play a role in regulating PDH activity also *in vivo* in diabetic conditions.

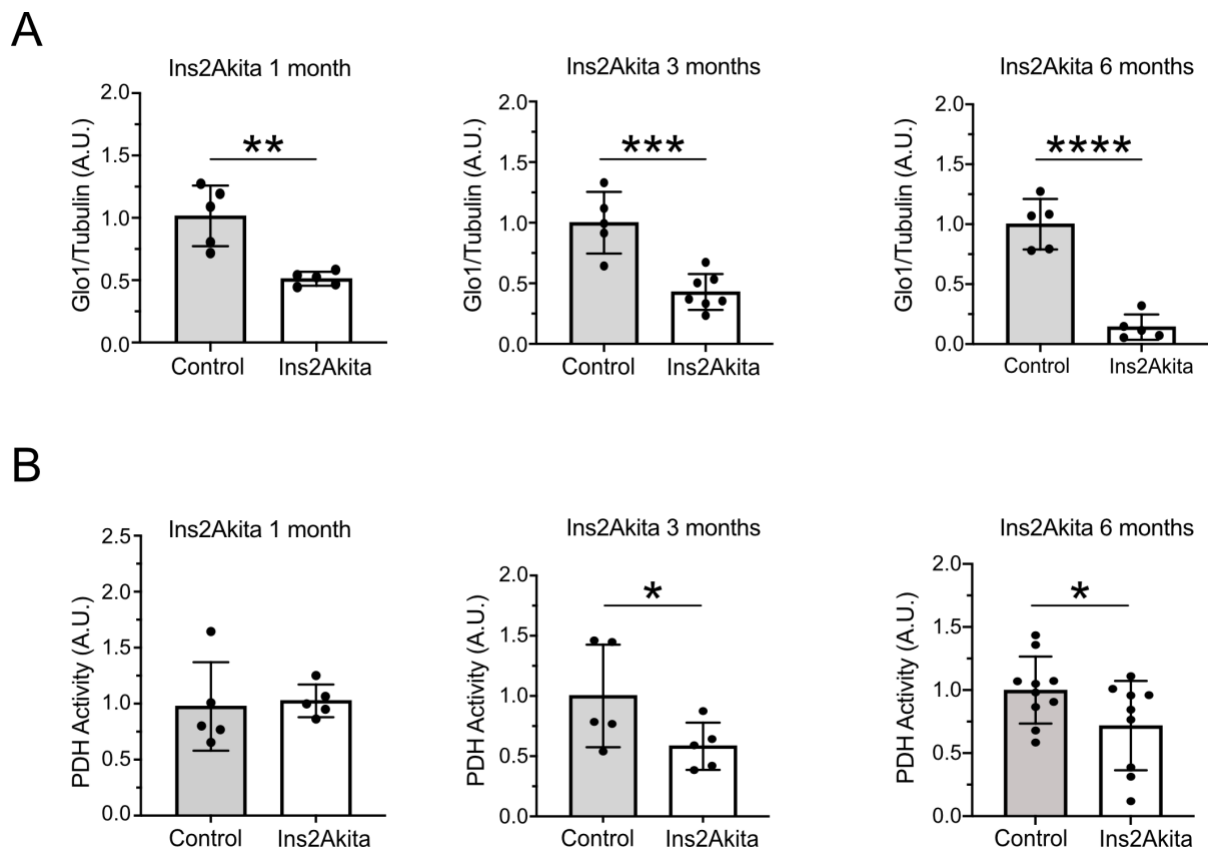


Figure 67. Low Glo1 expression correlates with decreased PDH activity in Ins2Akita mice. (A) I quantified Glo1 protein levels from the immunoblots in figure 22. (B) I purified the mitochondrial fraction from homogenized kidneys of 1-month, 3-month, and 6-month old control or Ins2Akita mice and I measured PDH activity. Biological replicates (B) 1-month and 3-month old n=5, 6-month old control n=10 and Ins2Akita n=10. For all cases *p<0.05, **p<0.01, and ***p<0.001 determined by one-sided, unpaired Student's t-test.

As phosphorylation of PDHA has been reported to be increased in diabetes [87], I then evaluated whether changes in PDHA phosphorylation were responsible for the decrease in PDH activity observed in 6 months old Ins2Akita mice kidneys (Figure 68). Overall, no significant changes were detectable in the phosphorylation of any of the three serine residues that regulate PDH activity after normalization for total PDHA levels. Although not significant, the S300 and S232 phosphorylation were increased in tendency in some Ins2Akita mice (Figure 68), suggesting that phosphorylation of PDHA at S300 and S232 could be playing a small role in PDH activity regulation. Nevertheless, these results suggest that dysregulation of Glo1 activity and expression could lead to decrease PDH activity in Ins2Akita mice.

Lastly, my results hint that in mouse models dysregulation on Glo1 activity and hyperglycemic conditions cause a decrease in PDH activity. Moreover, consistent with my cell culture data, low PDH activity in these diabetic mice was not mediated by phosphorylation of PDHA or changes on the PDH subunits. Therefore, it is possible that in diabetic mice models MG regulates PDH activity via PDHA CEL adduct formation and DTT sensitive modifications on DLAT. Nevertheless, further studies are still necessary to fully characterized the role of MG in mouse models of diabetes.

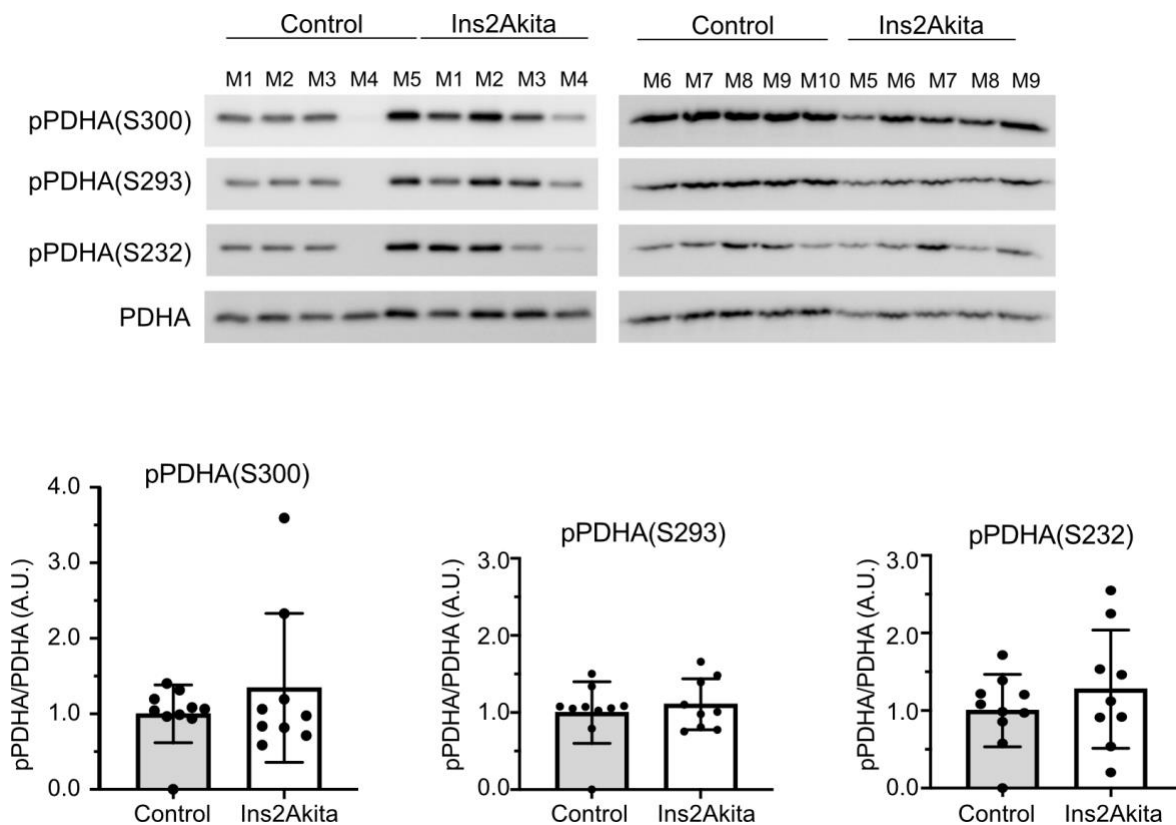


Figure 68. PDH activity decrease in kidneys of 6-month old Ins2Akita mice is not due to increased PDHA phosphorylation. I homogenized kidneys of control or Ins2Akita mice. I purified the mitochondrial fraction and I assessed PDHA phosphorylation of S300, S293, and S232. Biological replicates n=10 for control and n=9 for Ins2Akita. For all cases *p<0.05, **p<0.01 and ***p<0.001 determined by one-sided, unpaired Student's t-test. Mouse (M).

4. Discussion

4.1. Glo1 KO cells have higher levels of MG

Increased MG levels and MG adducts are associated with diabetes and the development of diabetic complications. This is indicated by the observation that diabetic patients with complications have the highest levels of MG in plasma [115, 116] and that Glo1 KO *Drosophila melanogaster* and *Danio rerio* develop features of type 2 diabetes, like insulin resistance, obesity, and hyperglycemia [101, 130]. Understanding how MG affects cellular metabolism and how Glo1 activity is regulated could therefore give very important insights into the pathogenesis of diabetes.

Glo1 KO HeLa and HEK293T cells have increased MG-H1 and CEL adducts mainly in the mitochondrial and nuclear fraction. These are considered the most common MG adducts and closely reflect MG levels [114]. Besides MG-H1 and CEL, other adducts such as argpyrimidines or MICA are also likely to be increased in Glo1 KO cells, although their levels were not measured due to technical limitations. The observation that MG adducts were increased only in the mitochondrial and nuclear fraction raises the possibility that these two compartments might be more susceptible to modifications by MG or that, alternatively, cytosolic proteins might be degraded faster following modification by MG.

In addition to adducts, higher ROS levels have been frequently reported upon MG accumulation [170, 171]. In hippocampal neurons, MG treatment caused oxidative-stress mediated cell death, which could be abrogated by the antioxidant *N*-acetylcysteine (NAC) [172]. Higher ROS levels were also observed in HepG2 and HEK293 cells incubated with MG for 24 hours [160, 161]. Additionally, adipose derived stem cells from diabetic patients have higher MG and ROS levels, which could be reduced by overexpression of Glo1 [173]. In line with these results, I also found elevated ROS levels in Glo1 KO cells, further confirming that these cells experience MG accumulation. Interestingly, high levels of both ROS and MG have been associated to the inflammatory response which is a critical problem in diabetic patients [174].

ROS can be produced as a byproduct of respiration, consequently a raise in metabolic activity could lead to more ROS production [175-177]. I observed that Glo1 KO cells suffered

important metabolic changes, higher glucose uptake, acetyl-CoA levels and basal respiration, all of which could increase ROS levels. Additionally, it is known that MG affects the activity of glutathione reductase (GR) in *in vitro* experiments performed with purified bovine GR, and in HT22 nerve cells incubated with MG [178, 179]. GR regenerates reduced glutathione, which is essential to fight oxidative and carbonyl stress [180]. Hence, high MG levels in the Glo1 KO could mediate ROS production via GR inhibition.

Surprisingly, despite having elevated ROS and MG adducts, the deletion of Glo1 did not cause an increase in free MG levels. Due to its high reactivity, MG is always in a dynamic equilibrium between the free state and the one bound to proteins and other biological macromolecules, which includes the adducts discussed above, but also more reversible interactions such as the hemithioacetals adducts formed between MG and cysteine residues [95]. In fact, based on both modeling and experimental evidence it has been estimated that only 1% of MG exist in a free form [98, 181]. It is thus possible that upon deletion of Glo1 the excess of free MG is promptly buffered by proteins and other molecules, as also indicated by the increase in MG adducts discussed above, without a concomitant measurable increase in free MG levels. Lastly, the current MG measurement techniques require extensive manipulation of the samples under harsh condition which can affect the sensitivity and reproducibility of the results [156].

My results provide evidence that Glo1 KO cell lines develop phenotypes associated with high MG levels such a MG adducts and ROS. More important, they highlight the importance of a proper function of Glo1 for MG detoxification and protection of the cell against carbonyl stress and oxidative stress. Dysregulation of Glo1 activity is known to cause pathological conditions in cells and animal model [53, 134, 135]. Therefore, the proper balance in MG levels is of vital importance against the development of pathologies such as diabetes and obesity.

4.2. MG regulates its own production

There is a clear interconnection between hyperglycemia and MG levels. On one hand, the trioses phosphate from glycolysis are the major source of MG production [92], which means that a mere increase in glycolytic flux causes more MG production. Consistent with this, endothelial cells cultured in 25 mM glucose for 3 days were reported to uptake more glucose and have elevated levels of MG as compared to cells cultured in 5 mM glucose [15]. Diabetic

patients are also known to have higher MG levels in plasma when compared with healthy individuals [115, 116]. On the other hand, multiple lines of evidence indicate that an increase in MG levels stimulates higher glucose uptake and glycolysis. HepG2 cells incubated with 50 μ M MG for 24 hours showed an increase in glucose uptake [160, 182]. Similar results were reported upon knockdown of Glo1 in L6 rat myoblasts, which showed increased glucose uptake and impaired internalization of GLUT4 transporters when cultured in high glucose media [183]. My results with HeLa and HEK293T cells also match this series of observations. Upon deletion of Glo1, both cell lines showed higher glucose uptake than their control counterparts. The mechanism behind the stimulation of glycolytic flux is thought to involve increased expression of GLUT1, hexokinase 2, phosphofruktokinase and LDH [160], which have been all shown to boost glycolytic flux in mouse cells [15].

Together, the fact that MG is produced during glycolysis and that MG causes an increase in glycolytic flux highlights a potentially dangerous positive feedback loop whereby more glycolysis leads to higher MG levels which in turn increase glycolytic flux further. It is tempting to speculate that such a feedback loop mechanism could be an important pathogenetic process at the basis of diabetes and its complications. An accumulation of MG due to failure of its detoxifying mechanism via Glo1 could be the initial triggering event, which highlights the importance of studying how Glo1 activity is regulated.

4.3. Glo1 activity is regulated via glucose sensitive phosphorylation of Y136

To date, little is known about the regulation of Glo1 via posttranslational modifications, as well as the identity of the protein responsible for them. According to the data base PhosphoSitePlus (<https://www.phosphosite.org/homeAction.action>), Glo1 can be phosphorylated on five different amino acids and acetylated on four others. However, it is only known that the phosphorylation of Glo1 on T106 is CaMKII dependent and causes changes in the stability and activity of the enzyme [141-143]. Additionally, several cysteine residues are known to be modified on Glo1, but only the S-nitroso-glutathinylation (GSNO) of Glo1 on C138 has an effect on Glo1 activity, this modification inhibits Glo1 under high nitric oxide and GSH conditions [144-146].

My results contribute an additional piece to the puzzle of how Glo1 activity is regulated by showing that phosphorylation at Y136 increases Glo1 activity. In the absence of this

phosphorylation, Glo1 activity is roughly 40% less active. The mechanism underlying this effect is however unclear. Interestingly, based on available structures of Glo1 (<https://www.rcsb.org/structure/3VW9>), Y136 is located in the proximity of a flexible loop proposed to have a dynamic position and possibly playing an important role in substrate accessibility to the active site of Glo1 [147, 184]. An exciting possibility is that, by introducing a negative charge, phosphorylation at Y136 could change the position of two positively charged amino acids, K156 and K158, located in the flexible loop and thus allowing better accessibility of the substrate to the catalytic pocket (Figure 69). Structural studies comparing phosphorylated and unphosphorylated Glo1 will be necessary to confirm this possibility.

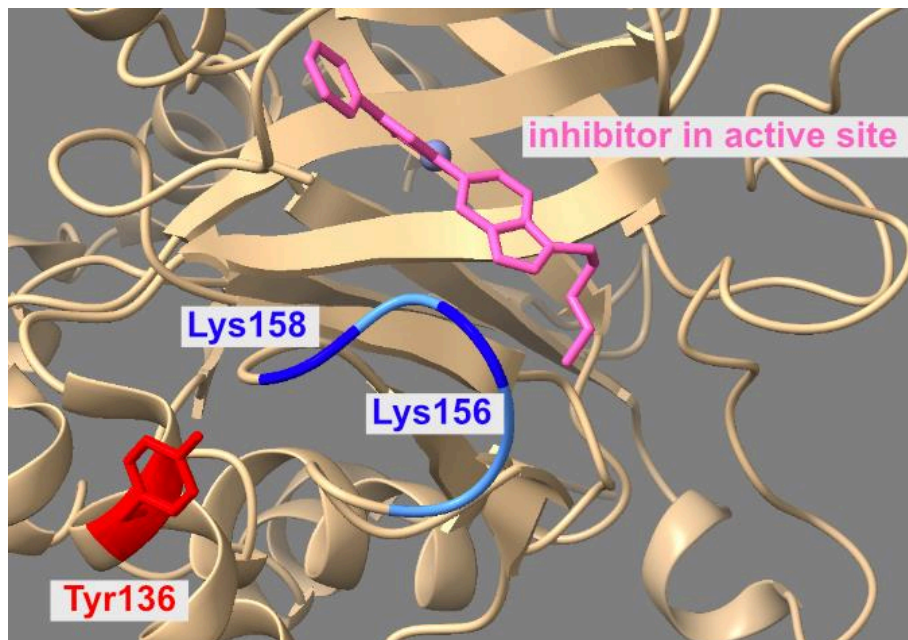


Figure 69. Location of Y136 in Glo1. Glo1 Y136 is located near a flexible loop (blue) by the catalytic site of the enzyme which allows the entry of substrate to Glo1. Glo1 structure was visualized using UCSF ChimeraX [185].

My results point to Glo1 Y136 phosphorylation as a glucose-responsive modification. Glo1 phosphorylation at Y136 decreases when cells are cultured in high glucose (25 mM) and in diabetic mouse models, while it was not affected directly by administration of MG. Consistent with this, I observed that Glo1 activity was also decreased when cells were cultured in high glucose as compared to cells incubated overnight in low glucose medium. These results are in line with previous observations showing that endothelial cells exposed to high glucose produce more MG due to increased hexokinase 2 levels and decreased Glo1 activity and expression [16]. In my cellular model, phosphorylation at Y136 did not alter Glo1 levels nor stability,

indicating that the decreased Glo1 expression observed in endothelial cells under hyperglycemic conditions likely represents an additional mechanism not related with Glo1 phosphorylation. Indeed, I observed an approximately 50% decrease in Glo1 phosphorylation at Y136 but not in total Glo1 levels in the liver of STZ diabetic mice, which have been shown to have high MG and AGEs levels that can be rescued by overexpression of Glo1, suggesting that in these mice hyperglycemia affects phosphorylation of Glo1 at Y136 and activity, but not Glo1 stability [127-129]. Intriguingly, this degree of reduction in Glo1 phosphorylation is in the same range as the 57% reduction in Glo1 activity previously reported for STZ mice [132], hinting at a link between phosphorylation and Glo1 activity also *in vivo*.

In *ins2akita* mice, Glo1 phosphorylation exhibited an interesting biphasic behavior. At one month, Y136 phosphorylation was increased as compared to controls, while at 3 and 6 months, it was decreased. These results suggest that, depending on the specific disease mechanism, an initial increase in Glo1 phosphorylation could take place possibly in an attempt to cope with the increased blood glucose levels, but that prolonged hyperglycemia eventually results in a maladaptive decrease in Glo1 phosphorylation and Glo1 activity. An analogous observation was also reported in Glo1 KO fruit flies, in which the decreased insulin sensitivity of tissues was compensated at early stages by higher insulin levels followed by a decrease in circulating insulin and hyperglycemia as the animal aged [101]. Despite likely representing two separate mechanisms, reduced Glo1 expression and reduced activity due to reduced Y136 phosphorylation could synergize to cause a failure in the MG detoxifying mechanism via Glo1 upon hyperglycemia. Consistent with this, I observed that both phosphorylation of Glo1 at Y136 and Glo1 protein levels were reduced in 3 and 6 months old *Ins2Akita* mice compared with WT mice, as well as in *HGHCi* mice compared with WT. More research is still needed to understand the interplay between the different mechanism that regulate Glo1 activity and expression.

This mode of regulation is in a certain way paradoxical, since it would decrease Glo1 activity when it is most needed, i.e. in hyperglycemic conditions. Since normal glucose levels in healthy individuals are around 5 mM during fasting and peak to about 7 mM after feeding, the decrease in Y136 phosphorylation is likely to represent a pathological phenomenon that could take place in diabetic conditions. In line with this, diabetic patients exhibit fasting blood glucose levels of around 7 mM and as high as 11 mM after feeding [186], while in mouse models of diabetes (e.g. STZ mice and *Ins2akita*) blood glucose levels are up to 3 times higher than control mice,

27 mM vs 9 mM [149]. Although hyperglycemia in diabetic patients rarely reaches the levels corresponding to the glucose concentration at which I observed inhibition of Glo1 phosphorylation, a chronic increase in glucose levels above 5 mM (30 to 50% higher) might also cause a similar decrease in Glo1 phosphorylation.

This maladaptive mechanism whereby hyperglycemia decreases Glo1 phosphorylation at Y136 could further exacerbate the deleterious feedback loop of glycolysis/MG production discussed above. In addition, elevated MG could also have a negative impact on insulin resistance through other mechanisms. For instance, MG has been shown to modify insulin directly causing it to be less efficient at stimulating glucose uptake in 3T3-L1 adipocytes and L8 skeletal muscle cells [119]. Other studies have also reported that elevated MG levels lead to insulin resistance and hyperglycemia [118-120, 130]. As a consequence, a vicious cycle may exist whereby elevated levels of MG lead to insulin resistance and hyperglycemia, decreasing Glo1 phosphorylation at Y136 and activity and looping back to enhance MG production (Figure 70).

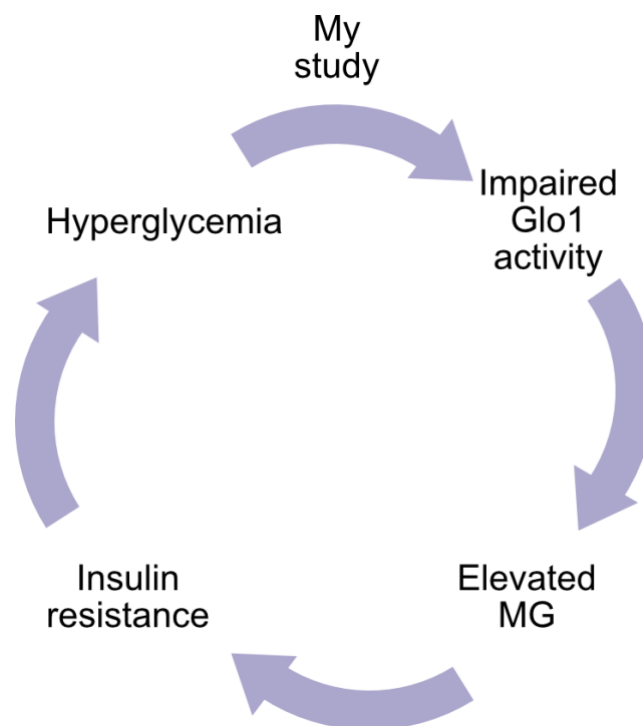


Figure 70. Schematic diagram of the positive feedback loop between MG and glucose. I found that hyperglycemia impairs Glo1 activity by reducing Y136 phosphorylation. Decrease Glo1 activity under hyperglycemic conditions will contribute to elevated MG levels. It has been reported that elevated MG can lead to insulin resistance and hyperglycemia.

4.4. Redundancy in the mechanism of Glo1 phosphorylation

To determine the kinase responsible for Glo1 phosphorylation at Y136, I conducted a CRISPR-Cas9 screen encompassing all known human tyrosine kinases. Interestingly, this screen revealed the existence of multiple kinases that could mediate Glo1 phosphorylation at this residue, pointing to the presence of a redundant mechanisms. Kinases capable of phosphorylating Glo1 at Y136 are all members of the Src family, Abl1, EphA5 and VEGFR3. As MG is a toxic and highly reactive metabolite, redundant phosphorylation of Y136 might be a protective mechanism to avoid that Glo1 phosphorylation relies on the activity of only one kinase pathway.

Among the kinases identified by the CRISPR-Cas9 screen, members of the Src family were also validated by siRNA and in vitro kinase assays. Surprisingly, I noticed a discrepancy between genetic versus pharmacological inhibition of Src kinase members with respect to Glo1 phosphorylation. While genetic depletion of Src kinases via sgRNAs or siRNAs reduced Glo1 phosphorylation, I failed to observe any decrease upon pharmacological inhibition of the Src kinases. One possible explanation is that the chemical inhibition of all Src kinase members would activate mechanism that would not be activated if only one member of the Src kinase family is inhibited at a time. Alternatively, Src phosphorylation of Glo1 is dependent on other variables that were not consistently controlled for between the different experiments. The cells in the CRISPR-CAS9 and siRNA experiments were kept in the same medium 4 days, while the cells in the chemical inhibitor experiments were kept for only 1 day in the same medium. As a consequence, other parameters such as amino acids or growth factors levels could affect the preferential pathway/kinase used to phosphorylate Glo1. Similar discrepancies in the effect of Src family inhibitor dasatinib were observed in mononuclear cells incubated or not with grow factors. Dasatinib only inhibited MAPK, Akt and STAT5 signaling in the absence of growth factors [187].

4.5. MG-dependent L-lactate production as a mediator of metabolic syndrome

L-lactate has gained more and more attention in the last few years, it is now clear that it plays an important role in the regulation of metabolic processes and dysregulation of its metabolism has been associated with diabetes, as well as carcinogenesis [188, 189]. It is known that fasting plasma lactate is higher in patients with diabetes compared with healthy controls [190-192]. Several studies have also shown that early stages of diabetes are characterized by elevated

levels of L-lactate [193-195] and lactate levels have even been proposed as predictor of future diabetes occurrence [22, 196]. Therefore, dysregulation of lactate metabolism and enhanced production could contribute to the development of diabetes and/or its progression.

My results point to a potential connection between the observation of dysregulated lactate metabolism in diabetes and MG accumulation, which is also a common occurrence in diabetes, as discussed above. Indeed, I showed that L-lactate production and excretion were enhanced upon addition of MG to HeLa and HEK293T cells, as well as upon deletion of Glo1 in both cell lines. This effect could be rescued by reconstitution of cells with Glo1, confirming a specific Glo1- and MG-dependent mechanism. These results are in line with previous studies showing that 3T3-L1 adipocytes and HepG2 cells also increase lactate secretion when incubated with MG. Although in these studies the effect of MG on lactate production had been attributed to increased LDH expression [160, 182], I was not able to detect changes in LDH protein levels in Glo1 KO cells. In contrast, I found that in the absence of Glo1 LDH activity was higher than in the corresponding control cells, suggesting that the increased lactate levels could be due at least in part to this mechanism. The higher activity of LDH could be caused by direct modification by MG. Indeed, a previous report showed the presence of MG-H1 adducts on Arg106 of the A subunit of LDH [105] and I could also detect a direct interaction between MG and LDH in the click chemistry pull downs I performed (Figure 44-45). In addition to increased LDH activity, elevated levels of L-lactate could also be caused by increased glucose uptake and glycolytic flux, as discussed above.

Glo1 KO flies suffer from alterations in lipid metabolism, such as higher TAG levels and increase FASN activity [101]. In line with this result, I observed that Glo1 KO HeLa cells were unable to use long chain fatty acids to respire. Interestingly, lactate acts as a signaling molecule able to affect lipid metabolism [30, 31] and I showed that L-lactate production and excretion were enhanced in the Glo1 KO HeLa cells, implying that L-lactate could at least in part underlie the alterations in lipid metabolism. Specifically, lactate acts as a signaling molecule in adipose cells by binding to GPR81 and decreasing lipolysis [33], while depletion of GPR81 in the liver caused a 3.5-fold increase in TAG levels [34, 182]. Additionally, GPR81 has been proposed to control β -oxidation by modulating CPT1 expression, the long fatty acid transporter located in the mitochondria [182]. Therefore, increased L-lactate levels in Glo1 KO cells could inhibit β -oxidation via GPR81. It will be interesting to see if the alterations in lipid metabolism I observed in Glo1 KO HeLa cells can be rescued by inhibiting GPR81 and/or correcting lactate production to normal levels.

4.6. MG decreases PDH activity with important metabolic repercussions

The capacity of an organism to respond to fuel availability, switching between lipids or carbohydrates as source of energy is known as metabolic flexibility. One of the main enzymes behind metabolic flexibility is PDH, linking glucose metabolism, the TCA cycle and lipid metabolism. Additionally, the inhibition of PDH underlies the Warburg effect observed in cancer cells, which is accompanied by increased lactate production [49, 197, 198]. Dysregulation of PDH activity has been associated with obesity and diabetes, highlighting the importance of a proper PDH function for a healthy state [36, 70, 199].

To understand the origin of the increased lactate levels upon deletion of Glo1, I thus assessed the activity of PDH and found that the absence of Glo1 or the incubation of cells with MG caused impaired PDH activity. This effect could be rescued by re-expression of WT Glo1, but not by a catalytically inactive mutant (E172Q) of Glo1, suggesting that it is MG and not the loss of Glo1 what causes PDH activity to decrease in the Glo1 KO cells. The effect of MG on PDH is remarkably specific. Although KGDH, also a mitochondrial dehydrogenase, shares the same DLD subunit with PDH [51], its activity was not altered in Glo1-depleted cells. MG however can modify also KGDH, as indicated by the observation that several subunits of KGDH could be pulled down by click MG, including DLD and OGDH, suggesting that while modification by MG could be a rather promiscuous phenomenon, this does not always result in altered protein function or activity.

Interestingly, altered PDH activity has been reported in diabetic and obese mice [83-85] and hyperglycemia and hyperlipidemia have been linked to impaired PDH activity in beta cells [200, 201]. Consistent with these results, I observed that in HEK293T WT cells PDH activity increased when cells were cultured in low glucose medium. In contrast, the impaired PDH activity of Glo1 KO HEK293T could not be restored by culturing the cells in low glucose medium, indicating that the absence of Glo1 is enough to cause impairments of PDH activity. It is possible that Glo1 absence causes an increase of MG levels regardless of glucose levels in the medium. Therefore, Glo1 dysregulation will lead to loss of metabolic flexibility due to inhibition of PDH.

A decrease in PDH activity could also affect the levels of acetyl-CoA, its direct product. Surprisingly, however, Glo1 KO HeLa cells had higher acetyl-CoA levels than WT cells. One possibility is that alternate sources of acetyl-CoA such as fatty acids and amino acids, which

do not depend on PDH, could compensate for the decreased PDH activity. Glo1 KO HeLa cells however showed lower levels of β -oxidation than WT cells, hinting that oxidation of fatty acids is unlikely to be responsible for the higher levels of acetyl-CoA in the Glo1 KO HeLa cells. Besides fatty acid β -oxidation, glutamine metabolism through glutaminolysis could be an additional source of acetyl-CoA, a possibility that I did not test. As Glo1 KO cells uptake more glucose, as discussed above, an alternative explanation is that, despite the partial inhibition of PDH activity, the increased availability of pyruvate is still sufficient to drive higher production of acetyl-CoA.

In vivo experiments further strengthen the link between accumulation of MG and impaired PDH activity. In Ins2akita mice, a well-known model of type 1 diabetes, high level of MG and MG adducts have been reported [202, 203] and I noticed that decreased PDH activity correlates with reduced levels of Glo1 expression and phosphorylation at Y136. Hence, it is possible that an impairment in Glo1 activity leads to elevated MG levels and, as a result, inhibition of PDH activity. Moreover, PDH activity was decreased also in Glo1 KO HGHCi mice liver, further showing that loss of Glo1 function and altered PDH activity are causally linked. Therefore, inhibition of PDH activity by MG could be a general pathological event occurring when detoxification through Glo1 is impaired and contributing to the development of diabetes or diabetic complications.

4.7. Decreased PDH activity caused by MG is not mediated via a canonical mechanism

The mechanism behind PDH inhibition by MG is likely to be complex and, despite all my efforts, still not completely clear. I could exclude that MG exerts its effect on PDH through canonical modalities of PDH regulation, in particular phosphorylation of PDHA, whose alterations have been described in several animal models of diabetes [85, 86, 90]. MG, however, did not affect PDHA1 phosphorylation in HEK293T cells nor did it change the expression of any PDH subunit. Similarly, I did not detect significant changes in PDHA phosphorylation in the liver of Glo1 KO HGHCi mice or in the kidney from Ins2Akita mice, pointing to a mechanism independent of PDHA phosphorylation.

Regulation of PDH via phosphorylation or MG modification are not mutually exclusive, but could rather be integrated by PDH to control its overall activity. Interestingly, a previous study reported distinct PDH kinetic profiles between diabetic animals and control ones upon inhibition of PDH phosphorylation by DCA, which acts on PDK. The response to DCA in the muscles of diabetic mice was 4 times slower than in control mice, even when the same degree

of activity was reached [90]. This points to the existence of an intrinsic alteration of PDH function in diabetes, which could indeed depend on direct modification by MG.

MG could affect PDH through direct interaction and AGE formation. Consistent with this possibility, I observed that porcine PDH incubated with MG had decreased activity and I detected an interaction between MG and several PDH complex subunits by click MG experiments. The exact identity of these interactions is however still matter of study. I was able to detect a CEL adduct on PDHA by mass spectrometry and immunostaining, although other types of modifications such as MICA adducts which were not possible to analyze in our mass spectrometry experiment could also occur.

The Michaelis-Menten analysis I performed showed changes in both V_{max} and K_m of PDH from Glo1 KO cells, indicating that MG could regulate PDH in more than one way. Apart from PDHA, DLAT could also be playing a role in the regulatory mechanism of MG. DLAT showed a DTT-susceptible modification that was particularly pronounced in Glo1 KO cells. DTT could also partially rescue the decreased PDH activity observed in Glo1 KO HEK293T. The observation that the modification in DLAT can be reversed by DTT suggests that either MG is interacting with DLAT directly and catalyzing the formation of a DTT-susceptible bond between thiol groups of cysteines, or that MG affects DLAT indirectly by altering the redox balance of the cell. Indeed, a link between ROS and MG has already been reported in studies where cells were incubated with MG for 24 hours and developed higher ROS levels [160, 161], and I also observed that Glo1 KO HeLa and HEK293T cells had elevated levels of ROS compared with WT cells.

Under oxidative stress, glutathionylation is used as a mechanism to protect free cysteines from oxidation. This modification generates a reversible mixed disulfide between cysteines in proteins and glutathione. The character of this modification makes it susceptible to reducing agents such as DTT [204]. Intriguingly, it has been reported that incubation of monocytes with lipopolysaccharides causes glutathionylation of DLAT, which is also accompanied by low PDH activity, high phosphorylation of PDHA and high ROS levels [205]. Lipopolysaccharides are also known to stimulate MG production in macrophages [206]. It is thus possible that the impairment of PDH activity by high MG could also depend on an analogous mechanism.

4.8. MG triggers important metabolic changes that could lead to diabetes

Overall, I have showed that MG has important repercussions on cellular metabolism. MG levels and adducts increase when the detoxification of MG or its production are dysregulated. Hyperglycemia caused decreased Glo1 phosphorylation at Y136 and decreased activity which leads to increased MG, possibly in addition to increased MG production because of higher glucose uptake or flow through glycolysis (Figure 71, step 1 and 2). Higher levels of MG would then further increase glucose uptake by altering the expression of important enzymes that are known to modulate the glycolytic flux [160, 183]. Such increase would then lead to more MG production in a deleterious positive feedback loop (Figure 71, step 2). Higher levels of MG would then increase LDH activity and decrease PDH activity, which together with the higher glucose uptake would cause lactate accumulation (Figure 71, step 3). Lactate accumulation impairs β -oxidation, while decreased PDH activity facilitates the usage of pyruvate for gluconeogenesis [80, 182], potentially leading to increased TAG levels (adipose tissue) and higher glucose production (liver) (Figure 71, step 4). As a consequence, obesity and hyperglycemia – both features of diabetes – could develop (Figure 71, step 5).

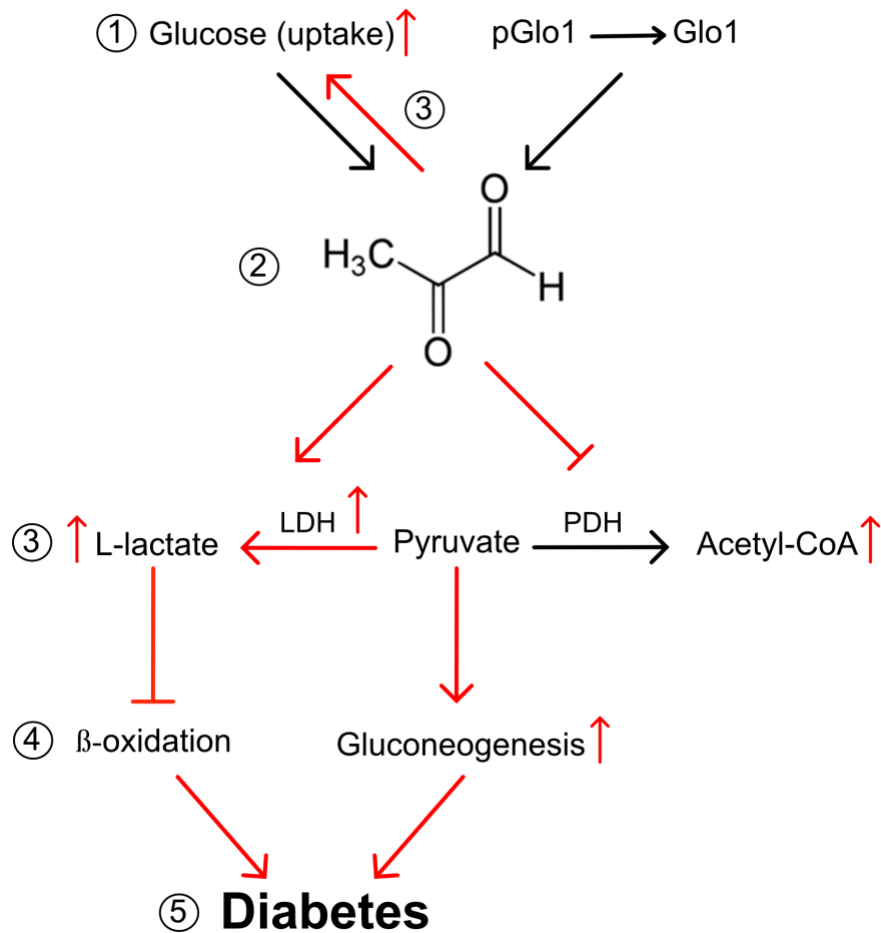


Figure 71. MG production leads to diabetes by mediating important changes in cellular metabolism. (1) Either an increased on the glycolytic flux or a decreased on the Glo1 capacity of detoxification lead to (2) elevated levels of MG. (3) There is a positive feedback loop between MG and glucose uptake, one increases the other. MG also causes changes to pyruvate metabolism, it decreased PDH activity and increases LDH activity. This in addition with a raise in the glycolytic flux cause redirection of some pyruvate to produce lactate and pyruvate (4) in liver cells could stimulated stimulate gluconeogenesis. (4) Lactate is also known to affect β-oxidization with decreases the usage of fatty acids and raises the TAG levels. (5) Dysregulation in the metabolism of both glucose and fatty acids are important factors on the development of diabetes.

5. Materials and Methods

5.1. Antibodies

The primary antibodies I used are listed in table 4. Additionally, the primary antibodies MG-H1(1:250) and total Glo1 [101] were made in Aurelio Teleman Laboratory.

The secondary antibodies I utilized are the following: anti-rabbit HRP (Jackson ImmunoResearch #111-035-003), anti-mouse HRP (Jackson ImmunoResearch #115-035-003), anti-guinea pig (Jackson ImmunoResearch #106-035-003). In all cases I diluted the secondary antibody 1:5000.

Table 4. List of commercial primary antibodies.

Antibody	Dilution	Source	Product Number
ACACA	1:1000	Cell Signaling Technology	3662
ACTB	1:1000	Hybridoma Bank	JLA20
ALDO	1:1000	Cell Signaling Technology	8060
ATP2A2/SERCA2	1:1000	Cell Signaling Technology	4388
CANX	1:1000	Enzo	ADI-SPA-960-D
CEL	1:500	Cell Signaling Technology	44358
DLAT	1:1000	Cell Signaling Technology	12362
DLD	1:1000	Santa Cruz Biotechnology	sc-365977
E3BP	1:1000	Santa Cruz Biotechnology	sc-393644
FAK	1:1000	Cell Signaling Technology	13009
FASN	1:1000	Invitrogen	PA5-22061
G6PDH	1:1000	Cell Signaling Technology	12263
GAPDH	1:5000	Cell Signaling Technology	2118
Her2/ErbB2	1:1000	Cell Signaling Technology	#4290
Insulin receptor β	1:1000	Cell Signaling Technology	#3025S
JAK2	1:1000	Thermo Scientific	#AHO1352
KEAP1	1:2000	Proteintech	10503-AP
Lamin A/C	1:1000	Santa Cruz Biotechnology	sc-7292
LDHA	1:1000	Cell Signaling Technology	#2012
mTOR	1:1000	Cell Signaling Technology	#2983
OGDH	1:1000	Cell Signaling Technology	#13407
PDHA	1:1000	Cell Signaling Technology	#3205
PDHB	1:1000	Proteintech	#14744-1-AP
PGK1	1:1000	Cell Signaling Technology	#68540

Phospho-FAK (Y397)	1:1000	Cell Signaling Technology	#8556
Phospho-FAK (Y925)	1:1000	Cell Signaling Technology	#3284
Phospho-PDHA(S232)	1:1000	Sigma	#AP1063
Phospho-PDHA(S293)	1:1000	Abcam	#ab92696
Phospho-PDHA(S300)	1:1000	Merck	#ABS194
Phospho-Src (Y417)	1:1000	Cell Signaling Technology	#6943
Phospho-Stat3 (Y705)	1:1000	Cell Signaling Technology	#9131
Phospho-Tyr Antibody	1:500	Santa Cruz Biotechnology	sc-7020
Pyruvate dehydrogenase E2/E3bp	1:1000	Abcam	#ab110333
RagB	1:1000	Cell Signaling Technology	#8150S
SDHA	1:1000	Cell Signaling Technology	#11998
Src	1:1000	Cell Signaling Technology	#21080
Stat3	1:1000	Cell Signaling Technology	#9139
TNK1	1:1000	Cell Signaling Technology	#4570
TUB	1:5000	Sigma	#T9026
VDAC	1:1000	Cell Signaling Technology	#4661

5.2. Generation of the phospho-Glo1(Y136) antibody

The company Seramun Diagnostica GmbH immunized rabbits with the peptide IAVPDV(phosphoY)SA(homoalanine)KRFC coupled to KLH. They used for the initial immunization Freund's complete adjuvant and then for the 3 booster injections, they changed to Freund's incomplete adjuvant. They collected the hyperimmune serum 7 days after the last booster injection. I precipitated the proteins from the serum by adding 0,452 g of $(\text{NH}_4)_2\text{SO}_4$ to 2 ml of serum, I then purified the antibody using a resin that I had previously coupled to the Y136 phospho-peptide. I generated the resin and performed the antibody purification with the SulfoLink Immobilization Kit for Peptides following the manufacturer's instructions (Thermo Scientific # 44999).

5.3. Cell culture conditions and treatments

I cultured HEK293T (Michael Boutros, DKFZ), HeLa (ATCC #CCL-2) and HepG2 (ATCC #HB-8065) cells in DMEM (Life Technologies #41965-062) containing 25 mM glucose, 4 mM L-glutamine, 1% penicillin/streptomycin (Life Technologies #15140-122), and 10% FBS. To culture U-937 (DSMZ #ACC5), I used RPMI 1640 (Life Technologies #52400-025) supplemented with 1 mM sodium pyruvate (Life Technologies #11360070), 2 mM L-glutamine (Life Technologies #25030024), 1x penicillin/streptomycin (Life Technologies #15140-122), and 10% FBS. I maintained all cell lines in 5% CO₂ at 37°C and I tested them for mycoplasma to exclude contamination.

I performed the glucose experiments in DMEM containing 5 mM glucose, which I prepared by combining DMEM high glucose, no glutamine, no phenol red (Life Technologies #31053028) and DMEM no glucose, no glutamine, no phenol red (Life Technologies # A1443001). Additionally, I added 2 mM L-glutamine (Life Technologies #25030024) and 10% FBS to the media. The day before the experiment, I seeded the cells in regular medium and the day of the experiment, I incubated the cells overnight with either fresh high (25 mM) or low (5 mM) glucose medium.

For HeLa and HepG2 inhibitor or MG treatments, I seeded the cells the day before the experiment, before adding the inhibitor or MG directly to the well the next day. Duration of the treatments and concentration of the inhibitors and MG are indicated in the figures. Also, for MG experiments in HEK293T, I seeded 4×10^6 cells in a 10-cm dish before adding 100 μ M MG directly to the plate for 60 minutes on the next day.

5.4. RNA extraction, reverse transcription, and qPCR

I extracted the RNA from cultured cells with Trizol (Life Technologies #15596018) following the manufacturer's instructions. I reverse transcribed 2 μ g RNA with Maxima H Minus reverse transcriptase (ThermoFisher #EP0753) and oligo-dT primer. I performed the quantitative PCR using a SYBRGreen-based master mix (primaQUANT CYBR 2x qPCR SYBRGreen Master Mix with LOW ROX, Streinbrenner, #SL-9913).

5.5. Plasmids

I PCR-amplified the coding sequences of Glo1 and PDHA1 from HeLa cDNA using Phusion High-Fidelity Polymerase (New England Biolabs #M0530). I then cloned Glo1 into a pcDNA3.1(+)-based vector and PDHA into pRK5-based vector. I added tags by subcloning the inserts into pcDNA3.1(+) or pRK5-based plasmids containing the tag of interest, respectively. I generated point mutations of Glo1 by PCR-based site-directed mutagenesis using the oligos shown in table 5. I verified all plasmids by Sanger sequencing.

5.6. Plasmids transfections and siRNA knockdowns

I transfected HeLa cells using Lipofectamine 2000 Reagent (ThermoScientifica #11668030) and HEK293T using PEI (Polysciences #23966-1). In both cases I followed the manufacturer's instruction and I always performed the transfections one day after I seeded the cells.

I performed siRNA-mediated knockdowns by reverse-transfection with 15 nM pools of four siRNAs targeting human Glo1 (siGENOME, Horizon Discovery #MU-012277-01-0002), human DLAT (siGENOME, Horizon Discovery #LQ-008490-01-0002) or renilla luciferase as a negative control (siGENOME, Horizon Discovery #P-002070-01-50). For all experiments I waited three days after transfection to lyse and analyze the cells by immunoblotting.

5.7. Generation of Glo1 knockout cells and HEK293T stably transfected cell lines

I generated monoclonal Glo1 knockout HeLa and HEK293T cell lines via CRISPR-Cas9-mediated genome editing using the PX459 plasmid expressing both Cas9 and the sgRNAs. I designed the sgRNA, I used for HeLa cells, with the website CHOP-CHOP (<https://chopchop.cbu.uib.no/>) [207], while for HEK293T, I used the sgRNAs sequences from the Brunello and Brie library [208] (Table 5). Finally, I validated the KO cell lines by PCR-amplifying the target genomic locus, TOPO cloning, and sanger sequencing (Life Technologies #450640). I also validated the Glo1 KO by immunoblotting for Glo1 protein, Glo1 activity assays, and qPCR.

I made the cell lines stably expressing flag-tagged WT or CI Glo1 by transfection of linearized plasmids into Glo1 KO HEK293T cells, before performing puromycin selection. Lastly, I validated the cell lines by immunoblotting and Glo1 activity assays.

5.8. CRISPR-CAS9 screening

I generated a library of 180 gRNAs targeting 90 kinases with 2 sgRNAs per kinase. I used the sgRNAs sequences from the Brunello and Brie library [208] (Table 5). I cloned all sgRNAs individually into the PX459 plasmid. I transfected HeLa cells with 2 gRNAs targeting the same kinase or the empty vector. Then, I incubated the cells with 1.5ug/ml puromycin, before adding fresh puromycin free medium on the fourth day. Afterwards, I waited 2 days for the cells to recover. Finally, I lysed the cells and assessed Glo1 phosphorylation by immunoblotting. I assigned a number to each kinase I targeted (Table 6).

5.9. Recombinant human Glo1 protein purification

In order to purify human Glo1 protein, I cloned the human Glo1 coding sequence into the pEMT-11 plasmid (EMBL protein expression/purification facility, Heidelberg). I then expressed the plasmid in Rosetta™(DE3) Competent Cells (Novagen #70954) and induced the

protein expression by addition of 0.5 mM IPTG to the growing culture. After I incubated the culture for 4 hours at 37°C, I spun down and lysed the bacteria. Lastly, I purified the recombinant protein under native conditions with a Ni-NTA agarose affinity resin according to manufacturer's instruction (Quiagen #R90101).

5.10. Cell lysis, immunoblots, and immunoprecipitations

I performed the cell lysis by washing the cells with Dulbecco's phosphate buffer saline (DPBS) (Life Technologies #14040117), adding lysis buffer (50 mM Tris pH 7.4, 150 mM NaCl, 1% triton X-100, 1x Roche Complete protease inhibitor cocktail with EDTA, and 1x Roche PhosSTOP phosphatase inhibitors) to the well/dish, and scraping the cells. I precipitated cell debris centrifuging the lysates for 10 minutes, 10000g at 4°C. I measured protein concentration of each lysate using Bradford reagent (Biorad #500-0006). Followingly, I mixed 15-20 ug of proteins with sample buffer (250 mM Tris-HCl pH 6.8, 50% glycerol, 5% SDS, 100 mM DTT, and 0.1% Bromophenol Blue) and I separated the proteins by tris-glycine SDS-PAGE.

For immunoblotting, I transferred the proteins onto nitrocellulose membranes, blocked the membranes for 1 hour in PBS-T containing 5% skim milk powder, and incubated them with the primary antibody (1:1000 in 5% BSA) overnight. Next, I washed the membrane with PBS-T and incubated it with the secondary antibody (1:5000 in 5% milk) for 1 hour. Finally, I detected the chemiluminescent signal using ECL substrates (Western Lightning Plus-ECL, PerkinElmer #NEL105001EA, or Supersignal West Femto, ThermoFisher #34095) with a ChemiDoc imager (Bio-Rad). I quantified the immunoblots using Image Lab (Bio-Rad).

For Flag-PDHA1 co-immunoprecipitations (co-IP), I used two 15-cm dishes per condition and lysed the cells in each plate with 300 ul of lysis buffer (40 mM HEPES pH 7.4, 5 mM MgCl₂, 1% triton X-100, 1x Roche Complete EDTA-free protease inhibitor cocktail, and 1x Roche PhosSTOP phosphatase inhibitors). I precipitated cell debris by centrifugation of the lysates for 10 minutes, 10000g at 4°C, before using the same concentration of protein per condition (4-6 mg in 1ml final volume) and incubated the lysates with 30ul pre-washed anti-DYKDDDDK affinity resin beads (ThermoFisher #A36803) for 2 hours gently rotating. Next, I washed the immunoprecipitates three times with lysis buffer supplemented with 150 mM NaCl and eluted with 300 ul of 5 mg/mL FLAG-peptide. I concentrated the elution to a final volume of 50 ul in a Vivaspin-500 centrifugal concentrators MWCO 10.000DA (Sigma Aldrich #Z614033-100EA).

5.11. Chloroform methanol precipitation

For the acyl-PEG and the click chemistry assays, I needed to clean the samples for reagents that could interfere with the next step on the protocol. I then performed the precipitation by sequentially adding to the sample of interest 400 ul of methanol, 150 ul of chloroform, and 300 ul of H₂O, before mixing them by inversion and centrifuging for 5 minutes, 20000g at 4°C. Next, I removed the upper aqueous phase without disturbing the pellet located between the two phases. Followingly, I washed the pellet with 500 ul of methanol and centrifuged the sample for 3 minutes, 20000g at 4°C. I discarded the supernatant, washed once more the pellet with 800 ul methanol, and centrifuged for 3 minutes, 20000g at 4°C. Finally, I air dried the pellet and resuspend it in the buffer of interest depending on the assay I was performing.

5.12. Cellular fractionation

I utilized cellular fractionation as a tool for the study of proteins enriched on a specific compartment. For this, I first seeded 6x10⁶ HEK293T or 3x10⁶ HeLa cells per 10-cm dish. The next day, I washed the cells once with DPBS and harvested them by scraping the 10-cm dish containing 1 ml of mitochondria lysis buffer (10 mM tris-HCl pH 7.5, 1x Roche Complete EDTA-free protease inhibitor cocktail, and 1x Roche PhosSTOP phosphatase inhibitors). I then homogenized the cell lysates in a pre-cooled glass homogenizer (tight pestle; 20 strokes up and down), added 200 ul of 1.5 M sucrose and centrifuged the lysates for 5 minutes, 600g at 4°C. I kept the pellet containing the nuclear fraction and centrifuged the supernatant a second time for 10 minutes, 10000g at 4°C. The resulting supernatant contained the cytosolic fraction. I washed the pellet containing the mitochondrial fraction once more. Last, I resuspend the mitochondrial pellet in 100 ul of the buffer of interest.

5.13. Sources of mouse tissue samples, tissue lysis, and mitochondrial fraction purification

The STZ, ob/ob and HFD mice livers were provided by Dr. Thomas Fleming (Laboratory of Mechanism of Chronic Diseases at the University Hospital Heidelberg). While Dr. Hans-Peter Hammes shared the Ins2akita liver and kidney samples with us (Department of Endocrinology, University of Heidelberg, Mannheim, Germany). The Glo1 KO and WT HGHCi mice livers and kidneys were donated by Dr. Marc Freichel (Pharmacology Institute of the University of Heidelberg). All mice tissues samples were collected, snap-frozen in liquid nitrogen and stored at -80°C by the providing laboratory.

For the purification of the mitochondrial fraction, I covered each tissue sample with mitochondria lysis buffer 2 (10 mM tris-HCl pH 7.5, 2 mM EDTA, 1x Roche Complete protease inhibitor cocktail, and 1x Roche PhosSTOP phosphatase inhibitors). I used 1 ml of buffer per 5x5x5mm tissue sample or 4 ml for the whole organ. I next homogenized the tissues with a pre-cooled glass homogenizer (tight pestle; 20 strokes up and down). I added 1.5 M sucrose to reach a final concentration of 300 mM and centrifuged the lysates for 5 minutes, 800g at 4°C. I collected the supernatant and for the whole organ samples, I diluted the supernatant 1:2 using mitochondria lysis buffer 2. Next, I centrifuged the supernatants for 10 minutes, 8000g at 4°C. I washed the pellet containing the mitochondrial fraction twice with the buffer of interest, without disturbing the pellet. Lastly, I resuspend the pellet in 150 ul of the buffer of interest.

In order to prepare the mouse liver lysates for immunostainings, I added 4 ml of liver lysis buffer (40 mM Tris pH 7.4, 1% triton X-100, 10 mM β -glycerophosphate, 10 mM sodium pyrophosphate, 30 mM NaF, 2x Roche Complete protease inhibitor cocktail with EDTA, and 2x Roche PhosSTOP phosphatase inhibitors) to each liver before grounding them on dry ice using a glass homogenizer. I precipitated cell debris by centrifugation of the lysates for 15 minutes, 14000 rpm at 4°C. Finally, I transferred the supernatant to a new tube and I added sample buffer to the samples.

5.14. Enzymatic assays

I performed the pyruvate dehydrogenase activity assays using either a commercially available colorimetric activity assay kit (Sigma Aldrich MAK183) or an assay protocol adapted from Chretien *et al.*[209]. For the second assay, I resuspended the mitochondrial pellets in PDH/LDH sample buffer (10 mM KH₂PO₄, 5 mM MgCl₂, 10% triton, and 1x Roche Complete protease inhibitor cocktail with EDTA). I mixed 10 ul of the sample with 170 ul of assay buffer (10 mM potassium phosphate buffer pH 7.4, 10 mM KCl, 5 mM MgCl₂, 0.5 mM NAD⁺, 0.2 mM CoenzymeA, 0.2 mM Thiamine pyrophosphate, 1 mM Cysteine and 0.2 mM GNE-140), before adding 4 mM pyruvate or H₂O as a control and measuring NADH production by monitoring the absorbance at 340 nm for 60 minutes.

LDH uses pyruvate to produce lactate in a reaction that consumes NADH. Then, I also measured LDH activity following (Chretien et al., 1995) methodology [209], but I modified several parameters. I used 10 ul of cytosolic fractions diluted 1/10 and I added 170 ul of LDH

assay buffer (10 mM potassium phosphate buffer pH 7.4, 5 mM MgCl₂, 0.5 mM NADH, 1 mM Cysteine). Last, I assessed NADH usage by monitoring the decreased in the absorbance at 340 nm.

I used a commercially available colorimetric assays for the measurements of GAPDH (Sigma Aldrich MAK277) and KGDH activity (Sigma Aldrich MAK189). For both enzymes, I first performed cellular fractionation using one 10-cm dish of cells before measuring enzyme activity in the cytosolic fraction for GAPDH or the mitochondrial fraction for KGDH.

For measuring Glo1 activity, I seeded cells in a 6-well plate the day before the experiment. I homogenized the cells in 400 μ L of Glo1 lysis buffer (10 mM sodium phosphate buffer pH 7.0 and 0.02% Triton X-100) by sonication for 15 seconds with 10% amplitude using a Branson sonifier. Next, I centrifuged the lysates at 14000 rpm for 30 minutes at 4°C. Before the assay, I incubated the Glo1 assay mix at 37°C for 10 minutes (50 mM sodium phosphate buffer pH 6.6, 20 μ M methylglyoxal (Sigma Aldrich M0252), and 20 μ M reduced L-Glutathione (Sigma Aldrich G6013)). Finally, I mixed 10 μ l of lysate with 190 μ l Glo1 assay mix and I measured the formation of Glo1 product S-lactoylglutathione by monitoring absorbance changes at 235 nm for 15 minutes.

For the *in vitro* kinase assays, I mixed recombinant human Glo1 with 600 ng of recombinant human kinase (ProQinase, in kinase assay buffer (50 mM HEPES pH 7.4, 6 mM MgCl₂, 6 mM β -glycerophosphate, and 1 mM DTT) and 500 μ M ATP in a total volume of 25 μ l. I performed the assay at 30°C for 1 hour before stopping the phosphorylation reaction by adding 2x sample buffer and boiling the sample for 5 minutes at 95°C.

I performed all enzymatic assays in a 96-well plate format, using the SPECTROstar Omega plate reader (BMG LABTECH). I normalized enzyme activity either to total protein in the cellular fraction measured by Bradford assay or for Glo1 activity to total Glo1 protein analyzed by immunoblotting.

5.15. Measurements of glucose, lactate, and acetyl-CoA

For the measurements of glucose and lactate, I seeded 3×10^6 HEK293T or 1.5×10^6 HeLa cells per 10-cm dish. When analyzing glucose uptake, I collected a sample of fresh medium the day I seeded the cells and another one after 2 days. I assessed glucose consumption by measuring

the difference in the glucose levels between the two samples using a colorimetric glucose assay kit (Abcam ab65333) following the manufacturer's instructions. Similarly, I performed intracellular and extracellular lactate measurements with a commercial D-lactic acid/L-lactic acid kit (R-Biopharm #1112821035) following the manufacturer's instructions. For extracellular measurements of lactate, I seeded the cells and after 2 days collected an aliquot of medium. While for intracellular lactate measurements, I washed the cells twice with DPBS and scraped them in 210 ul PBS with 0.05% Tween. I used 10 ul of the lysates for protein quantifications by Bradford assay, while I added 200 ul of chloroform to the rest of the cell lysates. Next, I vortexed the lysates for 20 seconds and centrifugated them for 15 minutes, 14000g at 4°C. After centrifugation, I utilized 10 ul of the upper liquid phase to determine intracellular lactate levels. I normalized the result of both glucose and lactate to total protein levels.

I assessed acetyl-CoA levels with a commercially available kit (Sigma Aldrich MAK039). I seeded 0.5×10^6 HeLa cells per well of a 6-well plate and the next day I harvested them in the acetyl-CoA assay buffer. I sonicated the samples for 15 seconds with 10% amplitude and centrifuged the lysates for 10 minutes at 10000g at 4°C. I deproteinized the lysates by centrifugation in a Vivaspin-500 centrifugal concentrators MWCO 10.000DA (Sigma Aldrich #Z614033-100EA). Then, I collected the flow through and assessed acetyl-CoA levels following the manufacturer's instructions. I normalized the results to total protein concentration measured by Bradford.

5.16. Acyl-PEG assay

To study DTT-sensitive modifications on PDH, I adapted the acyl-PEG assay described by Percher *et al.* [210]. To do so, I seeded 2×10^6 HEK293T cells per well of a 6-well plate. The next day, I washed the cells twice with DPBS before lysing them in 200 ul TAE lysis buffer (5 mM thioethanolamine, 15 mM NaCl, 4% SDS, 5 mM PMSF, 1x Roche Complete EDTA-free protease inhibitor cocktail, and 1500 units/ml benzonase, pH 7.3). When the lysate became clear, I added 5 mM EDTA. Next, I added 2.5 ul 1M N-ethylmaleimide to 92.5 ul of lysate and incubated the mixture for 2 hours in rotation. After incubation, I performed 3 rounds of chloroform-methanol precipitation. After the first two precipitation steps, I resuspended the pellet in TAE buffer (5 mM thioethanolamine, 15 mM NaCl, and 4% SDS, pH 7.3), and after the third in 60 ul TAE buffer supplemented with 5 mM EDTA. Subsequently, I added 1 ul of 100 mM DTT or TAE-EDTA buffer (negative control) to 60 ul of the sample before incubation

for 30 minutes in rotation. Afterwards, I performed again 3 rounds of chloroform-methanol precipitation. Finally, I incubated the 60 ul of sample with 90 ul 1.33 mM methoxy polyethylene glycol maleimide (mPEG-mal) 5 kDa for 2 hours, before performing one last chloroform-methanol precipitation and resuspension of the pellet in 2x sample buffer. I assessed all the samples by immunoblotting.

5.17. Metabolic characterization by Seahorse XF assays

I used the Seahorse XFe96 analyzer to measure in parallel the glycolytic and respiratory capacity of WT and Glo1 KO HeLa cells. For this purpose, I combined the glycolysis stress test kit (Agilent Seahorse XF, 100-103020) and the mito stress test kit (Agilent Seahorse XF, 100-103015). During the whole assay, extracellular acidification rate (ECAR) as well as oxygen consumption rate (OCR) were measured by the analyzer, 3 to 4 times per 9 minutes interval. Hence, I set a 9 minutes interval between the addition of each compound during the assay. I first incubated the cells in medium without glucose and pyruvate for 30 minutes, then, I inserted the plate in the analyzer. After 9 minutes of measurements, 10 mM glucose was added to the cells, followed by 20 uM oligomycin. Next, the medium was supplemented with 20 uM FCCP and the assay ended by adding a combination of 1 M 2-deoxy glucose (2-DG), 10 uM rotenone, and 5 uM antimycin A.

Additionally, I assessed the ability of WT and Glo1 KO HeLa to use palmitate as a source of acetyl-CoA for respiration with the palmitate oxidation stress test kit (Agilent Seahorse XF, 100-103693) following the manufacturer's instructions.

5.18. Click chemistry

In order to test whether MG interacted with PDH, I seeded 8×10^6 HEK293T cells in a 10-cm dish. The next day, I incubated the cells for 1 hour with 200 uM of a MG analogue containing an alkyne group. This molecule was synthesized by the group of Aubry Miller (Cancer Drug Development, DkFz). Afterwards, I lysed the cells in 500 ul (50 mM tris pH 7.4, 1% triton) and centrifuged the lysates for 2 minutes, 4000 rpm at 4°C. I performed the click chemistry reaction by following the manufacturer's instructions (Click-iT Protein Reaction Buffer Kit, Thermo Fisher #C10276). To do so, I added 40 uM biotin azide (Thermo Fisher, #B10184) to the MG alkyne treated lysates. The alkyne group of MG reacts with the biotin azide to form an alkyne-azide cycloaddition. After the click chemistry reaction, I cleaned the samples by methanol chloroform precipitation and I air dried the pellet before resuspending it in 50 ul buffer A (30

mM Tris pH 8 and 1% SDS). For the pull-down, I added 450 ul of IP buffer (50 mM tris pH 7.4 and 150 mM NaCl) to the pellet and incubated the samples with streptavidin-coupled beads (Life Technologies 65001 Dynabeads MyOneStreptavidin C1) for 2 hours by end-over-end rotation at 4°C. I washed the beads with wash buffer 1 (50 mM tris pH 7.5 and 2% SDS) and afterwards with wash buffer 2 (50 mM tris, pH 7.5, 500 mM NaCl, 1 mM EDTA, and 1% Triton X-100). Finally, I eluted the proteins using 2X sample buffer containing 1mM biotin for 15 minutes at room temperature and then boiled the samples for 15 minutes at 95°C. I analyzed click chemistry inputs and pull-downs by immunoblotting.

5.19. Statistical analysis

I visualized and analyzed the data using GraphPad Prism (version 9.5.0) and Microsoft Excel (version 16.16.27). For all quantifications, I considered the data to be normally distributed, although I did not formally test this. When I compared two conditions, I used two-tailed, unpaired Student's t-test unless specified otherwise. When comparing more conditions, I performed one- or two-way ANOVA with Šídák's multiple comparison test.

Table 5. Oligonucleotides.

Oligonucleotides sequences	Description
CGACGCGGACCCAGTACCA	sgRNA exon 1 human Glo1
GCAGACCATGCTACGAGTGA	sgRNA exon 2 human Glo1
AGGCGTAGTGTGGGTGACTC	genotyping PCR exon 1 human Glo1 (forward)
TTCCATCACACTCCCGTCC	genotyping PCR exon 1 human Glo1 (reverse)
TTGGACTIONGCATCACACAGG	genotyping PCR exon 2 human Glo1 (forward)
ACGAGAGAAGCCCTGTCCAG	genotyping PCR exon 2 human Glo1 (reverse)
GCGCAGCCATGGCAGAAC	PCR human Glo1 coding sequence (forward)
ATCGGGACAGTGATCCATCAGT	PCR human Glo1 coding sequence (reverse)
GAATTCATGGCAGAACCGCAGCCCC	Cloning human Glo1 into pcDNA3.1(+) vector, EcoRI restriction site (forward)
GCGGCCGCCTACATTAAGGTTGCCATTTTGTAGG	Cloning human Glo1 into pcDNA3.1(+) vector, NotI restriction site (reverse)
TTTCTATTGCAGCAGGCCATGCTACGAGTGA	site direct mutagenesis human Glo1 T25A (forward)

AAGGATCCTAAGAAGGCCCTGGATTTTATACT	site direct mutagenesis human Glo1 S45A (forward)
ACACACAATTGGGGCGCCGAAGATGATGAGACC	site direct mutagenesis human Glo1 T107A (forward)
GATGTATACAGTGCTTGTAGAAGGTTTGAAGAAGCTGGGA	site direct mutagenesis human Glo1 K140R (forward)
GAAGAAGCTGGGAGTCAGATTTGTGAAGAAACCT	site direct mutagenesis human Glo1 K148R (forward)
AACCTGATGATGGTAGAATGAAAGGCCTGGC	site direct mutagenesis human Glo1 K157R (forward)
ATGATGGTAAAATGAGAGGCCTGGCATTATTC	site direct mutagenesis human Glo1 K159R (forward)
GTCCTGATGTATACGCCGCTTGTAAGGTTT	site direct mutagenesis human Glo1 S137A (forward)
CTGTCCTGATGTAGCCAGTGCTTGTAAGG	site direct mutagenesis human Glo1 Y136A (forward)
CTGTCCTGATGTATTCAGTGCTTGTAAGG	site direct mutagenesis human Glo1 Y136F (forward)
ACCCTCGAGGATTCGGTCATATTG	Glo1 Q PCR oligo (forward)
TCCAGTAGCCATCAGGATCTTGAA	Glo1 Q PCR oligo (reverse)
GATGGCTACTGGATTCAAATTTGAATCCTAAC	site direct mutagenesis human Glo1 E172Q (forward)
GAATTCTCCTGGGTTGTGAGGAGTCG	PCR human PDHA coding sequence from cDNA, EcoRI restriction site (forward)
GAATTCTCCTGGGTTGTGAGGAGTCG	PCR human PDHA Coding sequence from cDNA, Not1 restriction site (reverse)
GTATAGTCGACgATGAGGAAGATGCTCGCC	PDHA, cloning into pRK5 vector, Sal1 restriction site (forward)
GTATAGCGGCCGCTTAACTGACTGACTTAAACTTG	PDHA, cloning into pRK5 vector, Not1 restriction site (reverse)
CTTAGGCTATAATCACAATG	sgRNA1 gainst ABL1 exon 3
GGTTCATCATCATTCAACGG	sgRNA2 gainst ABL1 exon 4
GGTCAACATCACAACCATA	sgRNA1 gainst ABL2 exon 3
TGTACACCATCACTCCACAG	sgRNA2 gainst ABL2 exon 5
TATGAGTATGACTTTGAACG	sgRNA1 against BTK exon 2
CTGTGTTTGCTAAATCCACA	sgRNA2 against BTK exon 11
GGGAAGACTTCCTGACTGG	sgRNA1 against BMX exon 7
GGGGTTACCCCTTATCTCTG	sgRNA2 against BMX exon5
ATACTTTGAAGATCGTCATG	sgRNA1 against ITK exon1
ATCCTCAGGAACTCGCACTG	sgRNA2 against ITK exon6
AGAACATCTATTGAGACAAG	sgRNA1 against TXK exon6
GGAAGGCAAGAGACCGTTTG	sgRNA2 against TXK exon4
AAACACTTACTTCACTGCGG	sgRNA1 against TEC exon9
CATGATCTCAGATTAGAGAG	sgRNA2 against TEC exon7
AGCTTGGATTGAGTCAACAG	sgRNA1 against FGR exon5

AGGGGACTTCAGAAGCTACG	sgRNA2 against FGR exon3
TGTCCTTCAAGAAAGGCGAG	sgRNA1 against SRC exon5
GACCTGGAACGGTACCACCA	sgRNA2 against SRC exon10
TCCAAAAGGCGTTACCCCTG	sgRNA1 against YES1 exon2
AGAGAGAGTGAAACAATAA	sgRNA2 against YES1 exon5
ACGGGGACCTTGCGTACGAG	sgRNA1 against FYN exon4
TTGTCCTTTGGAAACCCAAG	sgRNA2 against FYN exon7
GACCCACTGGTTACCTACGA	sgRNA1 against LCK exon3
CTACAACGGGCACACGAAGG	sgRNA1 against LCK exon9
GCTCGTGAGGCTCTACGCTG	sgRNA1 against LYN exon9
TGAAAGACAAGTCGTCCGGG	sgRNA2 against LYN exon4
AATGGCCTCGTAATCATAACA	sgRNA1 against HCK exon4
ATGTATTGCCTCCGACCTGG	sgRNA2 against HCK exon2
ACTCGGGCCACAAAGTTACT	sgRNA1 against BLK exon5
CAGGTCCCGATCATTACATAG	sgRNA2 against BLK exon4
CTATATTCCTTCTAACTACG	sgRNA1 against FRK exon1
AGTTGCGGTCTATCTCCCAT	sgRNA2 against FRK exon4
CGCACCCGACAGGACGTAGT	sgRNA1 against PTK6/BRK exon2
CGTGGAAGACGTCCCCCGCG	sgRNA2 against PTK6/BRK exon1
CGCTCTATGACTTCACGGCG	sgRNA1 against SRMS exon1
TTGCAGCTGGTACTTTAGCG	sgRNA2 against SRMS exon2
ACACGGCCTCATCGATTGTG	sgRNA1 against MATK exon6
CGCGTCAAGCACCACACCAG	sgRNA2 against MATK exon5
CATTAACCAAAGGTCATGG	sgRNA1 against CSK exon6
CGCACAGCGTGTAGTCTCCG	sgRNA2 against CSK exon5
CGGTCCAACAACGATCCCAG	sgRNA1 against TNK2/AcK exon6
G TTCAGTGGAAAGCGACTGG	sgRNA2 against TNK2/AcK exon4
CCTCTGGGATCAGACACTTG	sgRNA1 against TNK1 exon4
TGGGCCTAAGTCTAAGAACT	sgRNA2 against TNK1 exon3
AGAAAACGATCAAACCCAC	sgRNA1 against JAK2 exon6
CTGCCACTGCAATACCAACG	sgRNA2 against JAK2 exon5
TGACGCGGAGGCGTATTCGG	sgRNA1 against JAK3 exon6
ACTCTCCAGGCTTAACACAG	sgRNA2 against JAK3 exon15
CCGGAAGTAGCCATCTACCA	sgRNA1 against JAK1 exon9
TGGTTTCATTGCAATGACGG	sgRNA2 against JAK1 exon7
TGAATGACGTGGCATCACTG	sgRNA1 against TYK2 exon6
TTGGGCCTGAGCATCGAAGA	sgRNA2 against TYK2 exon4
GTCTGCGTACTCCAGACCA	sgRNA1 against EGFR exon15
TGTCACCACATAATTACCTG	sgRNA2 against EGFR exon8
AACTACCTTTCTACGGACGT	sgRNA1 against ERBB2/HER2 exon8

TCATCGCTCACAACCAAGTG	sgRNA2 against ERBB2/HER2 exon3
AGCGGCGACACGACAGACAT	sgRNA1 against ERBB4/HER4 exon13
ATAGAGTACTCTTCCACCAA	sgRNA2 against ERBB4/HER4 exon11
ACCATTGCCCAACCTCCGCG	sgRNA1 against ERBB3/HER3 exon3
TGTCGAAATTATAGCCGAGG	sgRNA2 against ERBB3/HER3 exon13
TCTGATGATAAATGACTGCG	sgRNA1 against PTK2/FAK exon12
ACTTAAAGCTCAGCTCAGGT	sgRNA2 against PTK2/FAK exon22
GCAGTACGCCTCGCTCAGGG	sgRNA1 against PTK2B/Pyk2 exon13
TTGGTAAAAATAGAGCAGCG	sgRNA2 against PTK2B/Pyk2 exon9
CGAGCGCAAACCTTACTCTG	sgRNA1 against ZAP70 exon4
GCCGGCGGCAAAGCGCACTG	sgRNA2 against ZAP70 exon3
ATCCGAGCCAGAGACAACAA	sgRNA1 against SYK exon4
CACACCACTACACCATCGAG	sgRNA2 against SYK exon2
AAGCCAAAATGGAGTGTC	sgRNA1 against EPHA1 exon6
CTCCAATTGGATCTACCGCG	sgRNA2 against EPHA1 exon3
CTGCACGTCACACACTTCGT	sgRNA1 against EPHB4 exon3
CTTCCGGGTGAGATGCTCCG	sgRNA2 against EPHB4 exon4
ACCAAGTTTATCCGGCGCCG	sgRNA1 against EPHB2 exon3
AGGTCCTGATGTAAATGCG	sgRNA2 against EPHB2 exon5
AGGATCCTGGGACATTAGGG	sgRNA1 against EPHB1 exon3
TCGGACCGTTATTACCGAG	sgRNA2 against EPHB1 exon4
AGAGGTGAGTGGCTACGATG	sgRNA1 against EPHB3 exon3
TTCACGGCCGCATAACGAGG	sgRNA2 against EPHB3 exon5
TGTAATTGGTATGAGCTAGG	sgRNA1 against EPHA4 exon5
TGTGCCAAAATGTAAGTGTG	sgRNA2 against EPHA4 exon3
ACTCCAGTCCAGGATAACTG	sgRNA1 against EPHA3 exon5
ATTGCAGGAACACTTGCCAA	sgRNA2 against EPHA3 exon5
GGTGAGGCTTTGAAGAACCC	sgRNA1 against EPHA5 exon4
TAGAACTCAAATTTACCCTG	sgRNA2 against EPHA5 exon3
GAAAACATATCCATTAATG	sgRNA1 against EPHA6 exon2
TGGTACATGCCATAGAAGGT	sgRNA2 against EPHA6 exon4
CACCTGGTATGTTTCGTATCG	sgRNA1 against EPHA7 exon3
TTGTGCACGCAACGTATGGT	sgRNA2 against EPHA7 exon4
GCTCACGTATCCGGCTCATG	sgRNA1 against EPHA8 exon2
CCTCAAAATCGACACCATTG	sgRNA2 against EPHA8 exon3
CACACACCCGTATGGCAAAG	sgRNA1 against EPHA2 exon2
CTGGTGCGGGTCAGTCCGTG	sgRNA2 against EPHA2 exon5

CCGCAAATCGACACGATCG	sgRNA1 against EPHA10 exon3
TTTACAAGGTGTCCCCGCGG	sgRNA2 against EPHA10 exon4
CTGACGGTAGTAAAGGGTGA	sgRNA1 against EPHB6 exon4
TGAGAGCCGAGTGTAGTGG	sgRNA2 against EPHB6 exon6
TCCAGACAACCCATTTTCGAG	sgRNA1 against ALK exon5
CTGTAGCACTTTCAGAAGCG	sgRNA2 against ALK exon8
AGCACGTACCCGAAAACGT	sgRNA1 against LTK exon5
CTCACCCGGAGAATTCAGCG	sgRNA2 against LTK exon2
CTGGGCTGGAAAGACATATG	sgRNA1 against ROS1 exon15
GTGCACACCATACTCCATG	sgRNA2 against ROS1 exon6
TGTGGGAATAAGCCCCCAA	sgRNA1 against IGF1R exon2
TTCCGAAATTTACCGCATGG	sgRNA2 against IGF1R exon6
GGATGAACGCCGGACCTATG	sgRNA1 against INSR exon8
TGTTGTGAATGACGTAAGG	sgRNA2 against INSR exon3
GATGCCACATCTGCGTGACG	sgRNA1 against INSR exon2
GGCCATCACGCTAACCCTG	sgRNA2 against INSR exon8
ATGACTGAGCCATTACTCAG	sgRNA1 against MERTK exon7
TCAGGCTGCTTAGTAAAGTG	sgRNA2 against MERTK exon4
CCCGAAGCCAATGTACCTCG	sgRNA1 against AXL exon2
CGAAGCCATAACGCCAAGG	sgRNA2 against AXL exon5
CCTACCTTGAAGGTGAACAG	sgRNA1 against TYRO3 exon5
TGCGCTGTGCCAATGCCTTG	sgRNA2 against TYRO3 exon7
AGCTGTGGCAGCGTCAACAG	sgRNA1 against MET exon2
CTCACTGATATCGAATGCAA	sgRNA2 against MET exon2
CTGCCCACCTAAGCTTACTG	sgRNA1 against MST1R exon4
GTGGCATGTTAGTCACGGTG	sgRNA2 against MST1R exon6
CGTGAGTCTCTACCTGAGCG	sgRNA1 against RYK exon1
TGAACAGAAATGTTGACCTG	sgRNA2 against RYK exon3
AGTTCAAATGCCCTTCCAGT	sgRNA1 against FGFR1 exon5
GTTGCCCGCCAACAAAACAG	sgRNA2 against FGFR1 exon7
GGTGCTGAATGCCTCCCACG	sgRNA1 against FGFR3 exon3
AAGAACGGCAGGGAGTTCCG	sgRNA2 against FGFR3 exon5
CTTAGTCCAACCTGATCACGG	sgRNA1 against FGFR2 exon3
GCCGGCAAATGCCTCCACAG	sgRNA2 against FGFR2 exon7
TGGTGGCCACTGGTACAAGG	sgRNA1 against FGFR4 exon3
GGTAACTGTGCCTATTCGAG	sgRNA2 against FGFR4 exon4
CCCGGTGACCGTGTACGACG	sgRNA1 against RET exon4
CTAGATCGGAAAGTCTGTG	sgRNA2 against RET exon7
CTCACCTCTCACGAACACGT	sgRNA1 against FLT4 exon3
CATACCATGCACAATGACCT	sgRNA2 against FLT4 exon7

CTTACCATATATATGCACTG	sgRNA1 against FLT1 exon7
AGGTTGAGGGATACCATATG	sgRNA2 against FLT1 exon10
CAAGAACTGAACTAAATGTG	sgRNA1 against KDR exon6
TAATGTACACGACTCCATGT	sgRNA2 against KDR exon4
TCAGACTTAATAGTCCGCGT	sgRNA1 against KIT exon2
GAAAGAAGACAACGACACGC	sgRNA2 against KIT exon3
ACGCTACCTTCCAAAACACG	sgRNA1 against CSF1R exon2
GTTGGAAATCTACTTGATCG	sgRNA2 against CSF1R exon5
AAATAATCCGTCATTCTAG	sgRNA1 against PDGFRA exon4
TAAGTCAGGGGAAACGATTG	sgRNA2 against PDGFRA exon5
CTCCCGTGTCTAGCCCAGTG	sgRNA1 against PDGFRB exon3
GTCCCCTATGATCACCAACG	sgRNA2 against PDGFRB exon4
GGGGTCTCAACGCACACCCG	sgRNA1 against FLT3 exon3
GGTGCTTTGCGATTACAGG	sgRNA2 against FLT3 exon5
TACTCGGCCAGGTATATAGG	sgRNA1 against TEK exon4
TGGCACAGGAACACCCATAG	sgRNA2 against TEK exon6
CTGTCCGCAAGAACCAAGCG	sgRNA1 against TIE1 exon9
ACGTGACGTTAATGAACCTG	sgRNA2 against TIE1 exon11
GCAGCCAGTACACATGTACC	sgRNA1 against PTK7 exon2
GCTCTGACCATCAGAAAGGG	sgRNA2 against PTK7 exon4
GGGCTAGGCCAATTGACCGA	sgRNA1 against DDR2 exon9
GTAATTGATCTTGTACATGG	sgRNA2 against DDR2 exon6
ACCTATGACGGACATACCGT	sgRNA1 against DDR1 exon7
GGGGGTAGAAGCGAACCAGT	sgRNA2 against DDR1 exon6
AGGGCACAAGAACAGTGCAG	sgRNA1 against NTRK1 exon5
CTGGAGCTCCGTGATCTGAG	sgRNA2 against NTRK1 exon2
TCTTCACACGCTCAACGCCG	sgRNA1 against NTRK3 exon8
CGTCAACCTGACCGTACGAG	sgRNA2 against NTRK3 exon4
AACCTGCAGATACCCAATTG	sgRNA1 against NTRK2 exon8
TGAATGGAATGCACCAGTGG	sgRNA2 against NTRK2 exon11
CTTTGGAATATGCTGTCCCG	sgRNA1 against MUSK exon 5
TACCATTGTAGTACATGGT	sgRNA2 against MUSK exon 4
GAAACCCACCCCTAACGTG	sgRNA1 against ROR2 exon 3
GCTGGCAGAACCCATCCTCG	sgRNA2 against ROR2 exon 5
GTGCGTGGCAACAAACGGCA	sgRNA1 against ROR1 exon 3
TCATCGCGACACAAGTCACG	sgRNA2 against ROR1 exon 6
CTCCTCAAGTCCACAGACGT	sgRNA1 against AATK exon 4
GCATAGCAACCTGCTCGTCCG	sgRNA2 against AATK exon 9
CCCGTAGTCTCCGATGCGCA	sgRNA1 against LMTK3 exon 9

CGGGGAGTACACTCCCCCTG	sgRNA2 against LMTK3 exon 4
AAAGTTTGAGCTTTACCTG	sgRNA1 against STYK1 exon 4
GCCACTTAAGGAGACATCCG	sgRNA2 against STYK1 exon 5
AAAAGCAAGTGCCAACCCAA	sgRNA1 against LMTK2 exon 5
TCTGGAGCAGTCCATCGCAG	sgRNA2 against LMTK2 exon 9
GGCAGACAAGGACCGTGACA	sgRNA1 against FES exon 5
TGAGATCACCAGCCAAACTG	sgRNA2 against FES exon 3
TTATGTCAGCAACGTATCCA	sgRNA1 against FER exon 3
GTATGTATTGGCGTTGAAAG	sgRNA2 against FER exon 6
TGATCGTGAGGCTCATAATG	sgRNA1 gainst ATAT1 exon 5
TGATGCACTAGTGATAGGAG	sgRNA2 gainst ATAT1 exon 3
AGCTTAACCGGAGATCACAA	sgRNA1 gainst ESCO1 exon 4
TCGTAATAAGCCTAATTTAG	sgRNA2 gainst ESCO1 exon 4
AGATGACAGAGTTTCTTCAA	sgRNA1 gainst ESCO2 exon 4
AGTGATCTATAAGCCAATTG	sgRNA2 gainst ESCO2 exon 3
ATTAGACAAATCATTCCACC	sgRNA1 gainst HAT1 exon 5
CTCATCCCCAAAGAGTTGAT	sgRNA2 gainst HAT1 exon 3
ATGAGATAAACCGACTGCTG	sgRNA1 gainst KAT2A exon 3
CAAGGTCAATTACACCAGGT	sgRNA2 gainst KAT2A exon 5
ACCTCGGTACGAAACCACAC	sgRNA1 gainst KAT2B exon 6
GCGAGCGCGTACCTTGCAGG	sgRNA2 gainst KAT2B exon 1
CCGCAAATGACTGGTCACGC	sgRNA1 gainst CREBBP exon 2
CTTAGCCCACTGATGAACGA	sgRNA2 gainst CREBBP exon 8
ATGGTGAACCATAAGGATTG	sgRNA1 gainst EP300 exon 3
GTGGCACGAAGATATTACTC	sgRNA2 gainst EP300 exon 8
GACCAGGATTCTATTACTGG	sgRNA1 gainst TAF1 exon 4
TCTGGTATATGGACGCTGGG	sgRNA2 gainst TAF1 exon 9
AAAACAACCTGGTCATAGTG	sgRNA1 gainst ELP3 exon 7
TATTCCACCCAGTCTTACAC	sgRNA2 gainst ELP3 exon 5
AACAACGAATGCCGGGACGT	sgRNA1 gainst GTF3C4 exon2
GGATAGGGTGTTCAACCCTG	sgRNA2 gainst GTF3C4 exon2
ACTGCATTACTCATAACGC	sgRNA1 gainst NCOA1 exon7
GAGATACTAGGATTGACCGA	sgRNA2 gainst NCOA1 exon11
CAACGAGAATCGATATACTG	sgRNA1 gainst NCOA3 exon10
TCAGCCACGAGCTATGATGG	sgRNA2 gainst NCOA3 exon7
AGTGCATAGTTACTACCCTG	sgRNA1 gainst NCOA2 exon11
GGTCTGGCGAACCTCCGAGG	sgRNA2 gainst NCOA2 exon7
CTAGTGAAATTCGACAGGAC	sgRNA1 gainst CLOCK exon7
GTATCCTCTTCAGCACACAA	sgRNA2 gainst CLOCK exon11

AGTCCCTCAACAGTAATGAT	sgRNA1 gainst CSRP2BP exon5
GCACCTGAACGGAAGTACAT	sgRNA2 gainst CSRP2BP exon4
CAGTGTTCAAACCAATACTG	sgRNA1 gainst MCM3AP exon1
GTTCTGCTCAGTCTCAACAA	sgRNA2 gainst MCM3AP exon8
ATGAATGGGTGACGCATGAG	sgRNA1 gainst KAT5 exon4
CTGAGGGTACCGTTGAGCGG	sgRNA2 gainst KAT5 exon5
TGGCTGTTACAGACCCCACT	sgRNA1 gainst KAT6B exon8
TTACGACGCATACGTTTGGG	sgRNA2 gainst KAT6B exon8
ATGAACGAGTCTGCCGAAGA	sgRNA1 gainst KAT7 exon3
TTCATCGTGAGATACATTG	sgRNA2 gainst KAT7 exon4
CCATACTTACAGTTAACCGG	sgRNA1 gainst KAT8 exon3
TATGTGGACAAGATCCACAT	sgRNA2 gainst KAT8 exon5
TACGGAAGTCCAGCATTCGT	sgRNA1 gainst KAT6A exon2
TGATAGCCAATCGTAACTGC	sgRNA2 gainst KAT6A exon2

Table 6. List of kinase KOs in CRISPR-CAS9 screen. I assessed the effect of 90 kinases on Glo1(Y136) phosphorylation.

Number	Kinase name	Number	Kinase name
1	ABL1	46	EPHA2
2	ABL2	47	EPHA10
3	BTK	48	EPHB6
4	BMX	49	ALK
5	ITK	50	LTK
6	TXK	51	ROS1
7	TEC	52	IGF1R
8	FGR	53	INSR
9	Src	54	INSRR
10	Yes1	55	MERTK
11	Fyn	56	AXL
12	LCK	57	TYRO3
13	Lyn	58	MET
14	HCK	59	MST1R
15	BLK	60	RYK
16	FRK	61	FGFR1
17	PTK6/BRK	62	FGFR3
18	SRMS	63	FGFR2
19	MATK	64	FGFR4
20	CSK	65	RET
21	TNK2/Ack	66	FLT4/VEGFR3
22	TNK1	67	FLT1
23	JAK2	68	KDR
24	Jak3	69	KIT
25	JAK1	70	CSF1R
26	TYk2	71	PDGFRA
27	EGFR	72	PDGFRB
28	ERBB2/HER2	73	FLT3
29	ERBB4/HER4	74	TEK
30	ERBB3/HER3	75	TIE1
31	PTK2/FAK	76	PTK7
32	PTK2B/PyK2	77	DDR2
33	ZAP70	78	DDR1
34	SYK	79	NTRK1
35	EPHA1	80	NTRK3
36	EPHB4	81	NTRK2
37	EPHB2	82	MUSK
38	EPHB1	83	ROR2

39	EPHB3	84	ROR1
40	EPHA4	85	AATK
41	EPHA3	86	LMTK3
42	EPHA5	87	STYK1
43	EPHA6	88	LMTK2
44	EPHA7	89	FES
45	EPHA8	90	FER

6. List of abbreviations

2DG: 2 deoxy glucose

ACAT1: acetyl-coenzyme A acetyltransferase

ACAT1: acetyl-coenzyme A acetyltransferase

Acetyl-CoA: acetyl coenzyme A

ADP: adenosine diphosphate

AGEs: advance glycation end products

ALDH: aldehyde dehydrogenase

AMP: adenosine monophosphate

AMPK: AMP-activated protein kinase

APE: acyl-PEG exchange

ARK: aldose reductase

ATP: adenosine triphosphate

CamKII: Ca²⁺/calmodulin-dependent protein kinase class of enzyme II

CEL: 1-carboxyethyl lysine

CoA: coenzyme A

CPT1: carnitine palmitoyl transferase 1

DCA: dichloroacetate

DHAP: dihydroxyacetone phosphate

DLAT: dihydrolipoamide acetyltransferase

DPBS: dulbecco's phosphate buffered saline

DTT: dithiothreitol

EM: electron microscopy

ETC: electron transport chain

F6P: fructose 6 phosphate

FADH₂: flavin adenine dinucleotide

FoxO1: fork head box O1

GAP: glyceraldehyde 3 phosphate

GAPDH: glyceraldehyde 2 phosphate dehydrogenase

GD: gestational diabetes

Glc: glucose

Glo1: glyoxalase 1

Glo2: glyoxalase 2.

GPR81: G protein couple receptor 81

GR: glutathione reductase
GSH: reduced glutathione
GSNO: S-nitroso-glutathinylation
HAECs: human aortal endothelial cells
HGHCi: high glucose and high cholesterol
IA-alkyne: iodoacetamine alkyne
IMPDH2: inosine 5- monophosphate dehydrogenase 2
IP: immunoprecipitation
IRS-1: insulin receptor substrate 1
KD: knockdown
KEAP1: kelch-like ECH-associated protein 1
KO: knockout
LDH: lactate dehydrogenase
MG-H1: hydroimidazolone 1
MG: methylglyoxal
MOLD: N-lysino-4-methylimidazolium
NAD: amide adenine dinucleotide
Nfr2: NF-E2 related factor 2
NO: nitric oxide
OXPHOS: oxidative phosphorylation
PDH: pyruvate dehydrogenase complex
PDHA: pyruvate dehydrogenase α
PDHB: pyruvate dehydrogenase β
PDKs: pyruvate dehydrogenase kinases
PDPs: pyruvate dehydrogenase phosphatases
PI3K: phosphoinositide 3-kinase
PK: phosphofructokinase
qPC-MAP: quantitative protein cross-links discovered by migration analysis platform
SNPs: single nucleotide polymorphisms
STZ: streptozotocin
TCA: tricarboxylic acid cycle
TNF: tumor necrosis factor
TPP: thiamine pyrophosphate

7. References

1. Arneth, B., R. Arneth, and M. Shams, *Metabolomics of Type 1 and Type 2 Diabetes*. Int J Mol Sci, 2019. **20**(10).
2. Maraschin Jde, F., et al., *Diabetes mellitus classification*. Arq Bras Cardiol, 2010. **95**(2): p. e40-6.
3. Cole, J.B. and J.C. Florez, *Genetics of diabetes mellitus and diabetes complications*. Nat Rev Nephrol, 2020. **16**(7): p. 377-390.
4. Barnett, J.A., *A history of research on yeasts 5: the fermentation pathway*. Yeast, 2003. **20**(6): p. 509-43.
5. Patil, N., et al., *Monitoring and modelling the dynamics of the cellular glycolysis pathway: A review and future perspectives*. Mol Metab, 2022. **66**: p. 101635.
6. Dashty, M., *A quick look at biochemistry: carbohydrate metabolism*. Clin Biochem, 2013. **46**(15): p. 1339-52.
7. Petersen, M.C., D.F. Vatner, and G.I. Shulman, *Regulation of hepatic glucose metabolism in health and disease*. Nat Rev Endocrinol, 2017. **13**(10): p. 572-587.
8. Wu, C., et al., *Overexpression of 6-phosphofructo-2-kinase/fructose-2, 6-bisphosphatase in mouse liver lowers blood glucose by suppressing hepatic glucose production*. J Clin Invest, 2001. **107**(1): p. 91-8.
9. Wu, C., et al., *Increasing fructose 2,6-bisphosphate overcomes hepatic insulin resistance of type 2 diabetes*. Am J Physiol Endocrinol Metab, 2002. **282**(1): p. E38-45.
10. Matschinsky, F., et al., *Glucokinase as pancreatic beta cell glucose sensor and diabetes gene*. J Clin Invest, 1993. **92**(5): p. 2092-8.
11. Baltrusch, S., et al., *Characterization of glucokinase-binding protein epitopes by a phage-displayed peptide library. Identification of 6-phosphofructo-2-kinase/fructose-2,6-bisphosphatase as a novel interaction partner*. J Biol Chem, 2001. **276**(47): p. 43915-23.
12. Liberti, M.V. and J.W. Locasale, *The Warburg Effect: How Does it Benefit Cancer Cells?* Trends Biochem Sci, 2016. **41**(3): p. 211-218.
13. Parekh, N., et al., *Metabolic dysregulation of the insulin-glucose axis and risk of obesity-related cancers in the Framingham heart study-offspring cohort (1971-2008)*. Cancer Epidemiol Biomarkers Prev, 2013. **22**(10): p. 1825-36.

14. Rajas, F., A. Gautier-Stein, and G. Mithieux, *Glucose-6 Phosphate, A Central Hub for Liver Carbohydrate Metabolism*. *Metabolites*, 2019. **9**(12).
15. Tanner, L.B., et al., *Four Key Steps Control Glycolytic Flux in Mammalian Cells*. *Cell Syst*, 2018. **7**(1): p. 49-62 e8.
16. Irshad, Z., et al., *Activation of the unfolded protein response in high glucose treated endothelial cells is mediated by methylglyoxal*. *Sci Rep*, 2019. **9**(1): p. 7889.
17. Rabbani, N. and P.J. Thornalley, *Hexokinase-2 Glycolytic Overload in Diabetes and Ischemia-Reperfusion Injury*. *Trends Endocrinol Metab*, 2019. **30**(7): p. 419-431.
18. Hariton, F., et al., *Sulforaphane Delays Fibroblast Senescence by Curbing Cellular Glucose Uptake, Increased Glycolysis, and Oxidative Damage*. *Oxid Med Cell Longev*, 2018. **2018**: p. 5642148.
19. Rabinowitz, J.D. and S. Enerback, *Lactate: the ugly duckling of energy metabolism*. *Nat Metab*, 2020. **2**(7): p. 566-571.
20. Moreno-Sanchez, R., et al., *Energy metabolism in tumor cells*. *FEBS J*, 2007. **274**(6): p. 1393-418.
21. DiGirolamo, M., F.D. Newby, and J. Lovejoy, *Lactate production in adipose tissue: a regulated function with extra-adipose implications*. *FASEB J*, 1992. **6**(7): p. 2405-12.
22. Crawford, S.O., et al., *Association of blood lactate with type 2 diabetes: the Atherosclerosis Risk in Communities Carotid MRI Study*. *Int J Epidemiol*, 2010. **39**(6): p. 1647-55.
23. Schrauwen-Hinderling, V.B., et al., *Impaired in vivo mitochondrial function but similar intramyocellular lipid content in patients with type 2 diabetes mellitus and BMI-matched control subjects*. *Diabetologia*, 2007. **50**(1): p. 113-20.
24. Befroy, D.E., et al., *Impaired mitochondrial substrate oxidation in muscle of insulin-resistant offspring of type 2 diabetic patients*. *Diabetes*, 2007. **56**(5): p. 1376-81.
25. Cori, C.F. and G.T. Cori, *Carbohydrate metabolism*. *Annu Rev Biochem*, 1946. **15**: p. 193-218.
26. Pavlides, S., et al., *The reverse Warburg effect: aerobic glycolysis in cancer associated fibroblasts and the tumor stroma*. *Cell Cycle*, 2009. **8**(23): p. 3984-4001.
27. Bonvento, G., A.S. Herard, and B. Voutsinos-Porche, *The astrocyte--neuron lactate shuttle: a debated but still valuable hypothesis for brain imaging*. *J Cereb Blood Flow Metab*, 2005. **25**(10): p. 1394-9.
28. van Hall, G., *Lactate kinetics in human tissues at rest and during exercise*. *Acta Physiol (Oxf)*, 2010. **199**(4): p. 499-508.

29. Hui, S., et al., *Glucose feeds the TCA cycle via circulating lactate*. *Nature*, 2017. **551**(7678): p. 115-118.
30. Miller, H.I., et al., *Effect of Lactic Acid on Plasma Free Fatty Acids in Pancreatectomized Dogs*. *Am J Physiol*, 1964. **207**: p. 1226-30.
31. Rodahl, K., H.I. Miller, and B. Issekutz, Jr., *Plasma Free Fatty Acids in Exercise*. *J Appl Physiol*, 1964. **19**: p. 489-92.
32. Prajapati, S., et al., *Structural and Functional Analyses of the Human PDH Complex Suggest a "Division-of-Labor" Mechanism by Local E1 and E3 Clusters*. *Structure*, 2019. **27**(7): p. 1124-1136 e4.
33. Ahmed, K., et al., *An autocrine lactate loop mediates insulin-dependent inhibition of lipolysis through GPR81*. *Cell Metab*, 2010. **11**(4): p. 311-9.
34. Wagner, W., et al., *The lactate receptor (HCAR1/GPR81) contributes to doxorubicin chemoresistance via ABCB1 transporter up-regulation in human cervical cancer HeLa cells*. *J Physiol Pharmacol*, 2017. **68**(4): p. 555-564.
35. Roland, C.L., et al., *Cell surface lactate receptor GPR81 is crucial for cancer cell survival*. *Cancer Res*, 2014. **74**(18): p. 5301-10.
36. Sugden, M.C. and M.J. Holness, *Mechanisms underlying regulation of the expression and activities of the mammalian pyruvate dehydrogenase kinases*. *Arch Physiol Biochem*, 2006. **112**(3): p. 139-49.
37. Korkes, S., et al., *Enzymatic synthesis of citric acid. IV. Pyruvate as acetyl donor*. *J Biol Chem*, 1951. **193**(2): p. 721-35.
38. Reid, E.E., et al., *Pyruvate dehydrogenase complex activity in proplastids and mitochondria of developing castor bean endosperm*. *Biochem Biophys Res Commun*, 1975. **62**(1): p. 42-7.
39. Hiromasa, Y., et al., *Organization of the cores of the mammalian pyruvate dehydrogenase complex formed by E2 and E2 plus the E3-binding protein and their capacities to bind the E1 and E3 components*. *J Biol Chem*, 2004. **279**(8): p. 6921-33.
40. Ali, M.S., et al., *Identification of the tryptophan residue in the thiamin pyrophosphate binding site of mammalian pyruvate dehydrogenase*. *J Biol Chem*, 1995. **270**(9): p. 4570-4.
41. Eswaran, D., et al., *Arginine-239 in the beta subunit is at or near the active site of bovine pyruvate dehydrogenase*. *Biochim Biophys Acta*, 1995. **1252**(2): p. 203-8.

42. Ali, M.S., T.E. Roche, and M.S. Patel, *Identification of the essential cysteine residue in the active site of bovine pyruvate dehydrogenase*. J Biol Chem, 1993. **268**(30): p. 22353-6.
43. Harris, R.A., et al., *Regulation of the activity of the pyruvate dehydrogenase complex*. Adv Enzyme Regul, 2002. **42**: p. 249-59.
44. Brautigam, C.A., et al., *Subunit and catalytic component stoichiometries of an in vitro reconstituted human pyruvate dehydrogenase complex*. J Biol Chem, 2009. **284**(19): p. 13086-98.
45. Harris, R.A., et al., *Dihydrolipoamide dehydrogenase-binding protein of the human pyruvate dehydrogenase complex. DNA-derived amino acid sequence, expression, and reconstitution of the pyruvate dehydrogenase complex*. J Biol Chem, 1997. **272**(32): p. 19746-51.
46. Jilka, J.M., et al., *Properties of a newly characterized protein of the bovine kidney pyruvate dehydrogenase complex*. J Biol Chem, 1986. **261**(4): p. 1858-67.
47. Chen, G., et al., *Activated function of the pyruvate dehydrogenase phosphatase through Ca²⁺-facilitated binding to the inner lipoyl domain of the dihydrolipoyl acetyltransferase*. J Biol Chem, 1996. **271**(45): p. 28064-70.
48. Perham, R.N., *Swinging arms and swinging domains in multifunctional enzymes: catalytic machines for multistep reactions*. Annu Rev Biochem, 2000. **69**: p. 961-1004.
49. Stacpoole, P.W., *Therapeutic Targeting of the Pyruvate Dehydrogenase Complex/Pyruvate Dehydrogenase Kinase (PDC/PDK) Axis in Cancer*. J Natl Cancer Inst, 2017. **109**(11).
50. Smolle, M., et al., *A new level of architectural complexity in the human pyruvate dehydrogenase complex*. J Biol Chem, 2006. **281**(28): p. 19772-80.
51. Odievre, M.H., et al., *A novel mutation in the dihydrolipoamide dehydrogenase E3 subunit gene (DLD) resulting in an atypical form of alpha-ketoglutarate dehydrogenase deficiency*. Hum Mutat, 2005. **25**(3): p. 323-4.
52. Korotchkina, L.G. and M.S. Patel, *Site specificity of four pyruvate dehydrogenase kinase isoenzymes toward the three phosphorylation sites of human pyruvate dehydrogenase*. J Biol Chem, 2001. **276**(40): p. 37223-9.
53. Golej, J., et al., *Oral administration of methylglyoxal leads to kidney collagen accumulation in the mouse*. Life Sci, 1998. **63**(9): p. 801-7.
54. Roche, T.E., et al., *Distinct regulatory properties of pyruvate dehydrogenase kinase and phosphatase isoforms*. Prog Nucleic Acid Res Mol Biol, 2001. **70**: p. 33-75.

55. Huang, B., et al., *Isoenzymes of pyruvate dehydrogenase phosphatase. DNA-derived amino acid sequences, expression, and regulation.* J Biol Chem, 1998. **273**(28): p. 17680-8.
56. Turkan, A., Y. Hiromasa, and T.E. Roche, *Formation of a complex of the catalytic subunit of pyruvate dehydrogenase phosphatase isoform 1 (PDP1c) and the L2 domain forms a Ca²⁺ binding site and captures PDP1c as a monomer.* Biochemistry, 2004. **43**(47): p. 15073-85.
57. Mattevi, A., et al., *Atomic structure of the cubic core of the pyruvate dehydrogenase multienzyme complex.* Science, 1992. **255**(5051): p. 1544-50.
58. Wang, J., et al., *Structure and function of the catalytic domain of the dihydrolipoyl acetyltransferase component in Escherichia coli pyruvate dehydrogenase complex.* J Biol Chem, 2014. **289**(22): p. 15215-30.
59. Yu, X., et al., *Structures of the human pyruvate dehydrogenase complex cores: a highly conserved catalytic center with flexible N-terminal domains.* Structure, 2008. **16**(1): p. 104-14.
60. Vijayakrishnan, S., et al., *Solution structure and characterisation of the human pyruvate dehydrogenase complex core assembly.* J Mol Biol, 2010. **399**(1): p. 71-93.
61. Zhou, Z.H., et al., *The remarkable structural and functional organization of the eukaryotic pyruvate dehydrogenase complexes.* Proc Natl Acad Sci U S A, 2001. **98**(26): p. 14802-7.
62. Reed, L.J., et al., *Studies on the nature and reactions of protein-bound lipoic acid.* J Biol Chem, 1958. **232**(1): p. 143-58.
63. Skerlova, J., et al., *Structure of the native pyruvate dehydrogenase complex reveals the mechanism of substrate insertion.* Nat Commun, 2021. **12**(1): p. 5277.
64. Patti, M.E., et al., *Coordinated reduction of genes of oxidative metabolism in humans with insulin resistance and diabetes: Potential role of PGC1 and NRF1.* Proc Natl Acad Sci U S A, 2003. **100**(14): p. 8466-71.
65. Sparks, L.M., et al., *A high-fat diet coordinately downregulates genes required for mitochondrial oxidative phosphorylation in skeletal muscle.* Diabetes, 2005. **54**(7): p. 1926-33.
66. Morino, K., et al., *Reduced mitochondrial density and increased IRS-1 serine phosphorylation in muscle of insulin-resistant offspring of type 2 diabetic parents.* J Clin Invest, 2005. **115**(12): p. 3587-93.

67. Haythorne, E., et al., *Altered glycolysis triggers impaired mitochondrial metabolism and mTORC1 activation in diabetic beta-cells*. Nat Commun, 2022. **13**(1): p. 6754.
68. Rorsman, P. and F.M. Ashcroft, *Pancreatic beta-Cell Electrical Activity and Insulin Secretion: Of Mice and Men*. Physiol Rev, 2018. **98**(1): p. 117-214.
69. Maechler, P. and C.B. Wollheim, *Mitochondrial function in normal and diabetic beta-cells*. Nature, 2001. **414**(6865): p. 807-12.
70. Zhang, S., et al., *The pivotal role of pyruvate dehydrogenase kinases in metabolic flexibility*. Nutr Metab (Lond), 2014. **11**(1): p. 10.
71. Foster, D.W., *Malonyl-CoA: the regulator of fatty acid synthesis and oxidation*. J Clin Invest, 2012. **122**(6): p. 1958-9.
72. Stacpoole, P.W., *The pyruvate dehydrogenase complex as a therapeutic target for age-related diseases*. Aging Cell, 2012. **11**(3): p. 371-7.
73. Park, S., et al., *Role of the Pyruvate Dehydrogenase Complex in Metabolic Remodeling: Differential Pyruvate Dehydrogenase Complex Functions in Metabolism*. Diabetes Metab J, 2018. **42**(4): p. 270-281.
74. Patel, M.S. and L.G. Korotchkina, *Regulation of mammalian pyruvate dehydrogenase complex by phosphorylation: complexity of multiple phosphorylation sites and kinases*. Exp Mol Med, 2001. **33**(4): p. 191-7.
75. Korotchkina, L.G. and M.S. Patel, *Mutagenesis studies of the phosphorylation sites of recombinant human pyruvate dehydrogenase. Site-specific regulation*. J Biol Chem, 1995. **270**(24): p. 14297-304.
76. Fuller, S.J. and P.J. Randle, *Reversible phosphorylation of pyruvate dehydrogenase in rat skeletal-muscle mitochondria. Effects of starvation and diabetes*. Biochem J, 1984. **219**(2): p. 635-46.
77. Fan, J., et al., *Tyr-301 phosphorylation inhibits pyruvate dehydrogenase by blocking substrate binding and promotes the Warburg effect*. J Biol Chem, 2014. **289**(38): p. 26533-26541.
78. Wu, P., et al., *Starvation and diabetes increase the amount of pyruvate dehydrogenase kinase isoenzyme 4 in rat heart*. Biochem J, 1998. **329** (Pt 1)(Pt 1): p. 197-201.
79. Wu, P., et al., *Starvation increases the amount of pyruvate dehydrogenase kinase in several mammalian tissues*. Arch Biochem Biophys, 2000. **381**(1): p. 1-7.
80. Huang, B., et al., *Starvation and diabetes reduce the amount of pyruvate dehydrogenase phosphatase in rat heart and kidney*. Diabetes, 2003. **52**(6): p. 1371-6.

81. Ravindran, S., et al., *Lipoyl domain-based mechanism for the integrated feedback control of the pyruvate dehydrogenase complex by enhancement of pyruvate dehydrogenase kinase activity*. J Biol Chem, 1996. **271**(2): p. 653-62.
82. Lin, Y. and Z. Sun, *Current views on type 2 diabetes*. J Endocrinol, 2010. **204**(1): p. 1-11.
83. Katayama, Y., et al., *Dichloroacetate, a pyruvate dehydrogenase kinase inhibitor, ameliorates type 2 diabetes via reduced gluconeogenesis*. Heliyon, 2022. **8**(2): p. e08889.
84. Le Page, L.M., et al., *Increasing Pyruvate Dehydrogenase Flux as a Treatment for Diabetic Cardiomyopathy: A Combined ¹³C Hyperpolarized Magnetic Resonance and Echocardiography Study*. Diabetes, 2015. **64**(8): p. 2735-43.
85. Gopal, K., et al., *FoxO1 inhibition alleviates type 2 diabetes-related diastolic dysfunction by increasing myocardial pyruvate dehydrogenase activity*. Cell Rep, 2021. **35**(1): p. 108935.
86. Battiprolu, P.K., et al., *Metabolic stress-induced activation of FoxO1 triggers diabetic cardiomyopathy in mice*. J Clin Invest, 2012. **122**(3): p. 1109-18.
87. Zhang, Y., et al., *Regulation of hepatic pyruvate dehydrogenase phosphorylation in offspring glucose intolerance induced by intrauterine hyperglycemia*. Oncotarget, 2017. **8**(9): p. 15205-15212.
88. Zhang, M., et al., *Pyruvate dehydrogenase kinase 4 mediates lipogenesis and contributes to the pathogenesis of nonalcoholic steatohepatitis*. Biochem Biophys Res Commun, 2018. **495**(1): p. 582-586.
89. Cummings, B.P., et al., *Development and characterization of a novel rat model of type 2 diabetes mellitus: the UC Davis type 2 diabetes mellitus UCD-T2DM rat*. Am J Physiol Regul Integr Comp Physiol, 2008. **295**(6): p. R1782-93.
90. Park, J.M., et al., *Hyperpolarized NMR study of the impact of pyruvate dehydrogenase kinase inhibition on the pyruvate dehydrogenase and TCA flux in type 2 diabetic rat muscle*. Pflugers Arch, 2021. **473**(11): p. 1761-1773.
91. Ramasamy, R., S.F. Yan, and A.M. Schmidt, *Methylglyoxal comes of AGE*. Cell, 2006. **124**(2): p. 258-60.
92. Phillips, S.A. and P.J. Thornalley, *The formation of methylglyoxal from triose phosphates. Investigation using a specific assay for methylglyoxal*. Eur J Biochem, 1993. **212**(1): p. 101-5.

93. Richard, J.P., *Kinetic parameters for the elimination reaction catalyzed by triosephosphate isomerase and an estimation of the reaction's physiological significance*. *Biochemistry*, 1991. **30**(18): p. 4581-5.
94. Lai, S.W.T., et al., *Methylglyoxal and Its Adducts: Induction, Repair, and Association with Disease*. *Chem Res Toxicol*, 2022. **35**(10): p. 1720-1746.
95. Thornalley, P.J., *Dicarbonyl intermediates in the maillard reaction*. *Ann N Y Acad Sci*, 2005. **1043**: p. 111-7.
96. Ravandi, A., et al., *Isolation and identification of glycated aminophospholipids from red cells and plasma of diabetic blood*. *FEBS Lett*, 1996. **381**(1-2): p. 77-81.
97. Pamplona, R., et al., *Chromatographic evidence for Amadori product formation in rat liver aminophospholipids*. *Life Sci*, 1995. **57**(9): p. 873-9.
98. Lo, T.W., et al., *Binding and modification of proteins by methylglyoxal under physiological conditions. A kinetic and mechanistic study with N alpha-acetylarginine, N alpha-acetylcysteine, and N alpha-acetyllysine, and bovine serum albumin*. *J Biol Chem*, 1994. **269**(51): p. 32299-305.
99. Frye, E.B., et al., *Role of the Maillard reaction in aging of tissue proteins. Advanced glycation end product-dependent increase in imidazolium cross-links in human lens proteins*. *J Biol Chem*, 1998. **273**(30): p. 18714-9.
100. Acimovic, J.M., et al., *Influence of the microenvironment of thiol groups in low molecular mass thiols and serum albumin on the reaction with methylglyoxal*. *Chem Biol Interact*, 2010. **188**(1): p. 21-30.
101. Moraru, A., et al., *Elevated Levels of the Reactive Metabolite Methylglyoxal Recapitulate Progression of Type 2 Diabetes*. *Cell Metab*, 2018. **27**(4): p. 926-934 e8.
102. Bollong, M.J., et al., *A metabolite-derived protein modification integrates glycolysis with KEAP1-NRF2 signalling*. *Nature*, 2018. **562**(7728): p. 600-604.
103. Coukos, J.S. and R.E. Moellering, *Methylglyoxal Forms Diverse Mercaptomethylimidazole Crosslinks with Thiol and Guanidine Pairs in Endogenous Metabolites and Proteins*. *ACS Chem Biol*, 2021. **16**(11): p. 2453-2461.
104. Alhujaily, M., et al., *Studies of Glyoxalase I-Linked Multidrug Resistance Reveal Glycolysis-Derived Reactive Metabolite, Methylglyoxal, Is a Common Contributor in Cancer Chemotherapy Targeting the Spliceosome*. *Front Oncol*, 2021. **11**: p. 748698.
105. Donnellan, L., et al., *Proteomic Analysis of Methylglyoxal Modifications Reveals Susceptibility of Glycolytic Enzymes to Dicarbonyl Stress*. *Int J Mol Sci*, 2022. **23**(7).

106. Chen, X., et al., *Quantitative Chemoproteomic Profiling of Protein Cross-Links Induced by Methylglyoxal*. ACS Chem Biol, 2022. **17**(8): p. 2010-2017.
107. Coukos, J.S., et al., *Widespread, Reversible Cysteine Modification by Methylglyoxal Regulates Metabolic Enzyme Function*. ACS Chem Biol, 2023. **18**(1): p. 91-101.
108. Miziorko, H.M., *Enzymes of the mevalonate pathway of isoprenoid biosynthesis*. Arch Biochem Biophys, 2011. **505**(2): p. 131-43.
109. Dobler, D., et al., *Increased dicarbonyl metabolism in endothelial cells in hyperglycemia induces anoikis and impairs angiogenesis by RGD and GFOGER motif modification*. Diabetes, 2006. **55**(7): p. 1961-9.
110. Donnelly, R., et al., *ABC of arterial and venous disease: vascular complications of diabetes*. BMJ, 2000. **320**(7241): p. 1062-6.
111. Brownlee, M., *Biochemistry and molecular cell biology of diabetic complications*. Nature, 2001. **414**(6865): p. 813-20.
112. Duran-Jimenez, B., et al., *Advanced glycation end products in extracellular matrix proteins contribute to the failure of sensory nerve regeneration in diabetes*. Diabetes, 2009. **58**(12): p. 2893-903.
113. Berlanga, J., et al., *Methylglyoxal administration induces diabetes-like microvascular changes and perturbs the healing process of cutaneous wounds*. Clin Sci (Lond), 2005. **109**(1): p. 83-95.
114. Keilhauer, E.C., P.E. Geyer, and M. Mann, *HCD Fragmentation of Glycated Peptides*. J Proteome Res, 2016. **15**(8): p. 2881-90.
115. Wang, H., et al., *Proinflammatory and proapoptotic effects of methylglyoxal on neutrophils from patients with type 2 diabetes mellitus*. Clin Biochem, 2007. **40**(16-17): p. 1232-9.
116. Lu, J., et al., *Increased plasma methylglyoxal level, inflammation, and vascular endothelial dysfunction in diabetic nephropathy*. Clin Biochem, 2011. **44**(4): p. 307-11.
117. Bierhaus, A., et al., *Methylglyoxal modification of Nav1.8 facilitates nociceptive neuron firing and causes hyperalgesia in diabetic neuropathy*. Nat Med, 2012. **18**(6): p. 926-33.
118. Jia, X., et al., *Structural and functional changes in human insulin induced by methylglyoxal*. FASEB J, 2006. **20**(9): p. 1555-7.

119. Riboulet-Chavey, A., et al., *Methylglyoxal impairs the insulin signaling pathways independently of the formation of intracellular reactive oxygen species*. Diabetes, 2006. **55**(5): p. 1289-99.
120. Fiory, F., et al., *Methylglyoxal impairs insulin signalling and insulin action on glucose-induced insulin secretion in the pancreatic beta cell line INS-1E*. Diabetologia, 2011. **54**(11): p. 2941-52.
121. Racker, E., *The mechanism of action of glyoxalase*. J Biol Chem, 1951. **190**(2): p. 685-96.
122. Rabbani, N. and P.J. Thornalley, *Dicarbonyl proteome and genome damage in metabolic and vascular disease*. Biochem Soc Trans, 2014. **42**(2): p. 425-32.
123. Izaguirre, G., A. Kikonyogo, and R. Pietruszko, *Methylglyoxal as substrate and inhibitor of human aldehyde dehydrogenase: comparison of kinetic properties among the three isozymes*. Comp Biochem Physiol B Biochem Mol Biol, 1998. **119**(4): p. 747-54.
124. Baba, S.P., et al., *Reductive metabolism of AGE precursors: a metabolic route for preventing AGE accumulation in cardiovascular tissue*. Diabetes, 2009. **58**(11): p. 2486-97.
125. Thornalley, P.J., *Glyoxalase I--structure, function and a critical role in the enzymatic defence against glycation*. Biochem Soc Trans, 2003. **31**(Pt 6): p. 1343-8.
126. Ahmed, U., et al., *Reversal of hyperglycemia-induced angiogenesis deficit of human endothelial cells by overexpression of glyoxalase I in vitro*. Ann N Y Acad Sci, 2008. **1126**: p. 262-4.
127. Brouwers, O., et al., *Overexpression of glyoxalase-I reduces hyperglycemia-induced levels of advanced glycation end products and oxidative stress in diabetic rats*. J Biol Chem, 2011. **286**(2): p. 1374-80.
128. Brouwers, O., et al., *Glyoxalase-I overexpression reduces endothelial dysfunction and attenuates early renal impairment in a rat model of diabetes*. Diabetologia, 2014. **57**(1): p. 224-35.
129. Berner, A.K., et al., *Protection against methylglyoxal-derived AGEs by regulation of glyoxalase I prevents retinal neuroglial and vasodegenerative pathology*. Diabetologia, 2012. **55**(3): p. 845-54.
130. Lodd, E., et al., *The combination of loss of glyoxalase I and obesity results in hyperglycemia*. JCI Insight, 2019. **4**(12).

131. Wortmann, M., et al., *A Glyoxalase-1 Knockdown Does Not Have Major Short Term Effects on Energy Expenditure and Atherosclerosis in Mice*. J Diabetes Res, 2016. **2016**: p. 2981639.
132. Schumacher, D., et al., *Compensatory mechanisms for methylglyoxal detoxification in experimental & clinical diabetes*. Mol Metab, 2018. **18**: p. 143-152.
133. McLellan, A.C., et al., *Glyoxalase system in clinical diabetes mellitus and correlation with diabetic complications*. Clin Sci (Lond), 1994. **87**(1): p. 21-9.
134. Mey, J.T., et al., *Dicarbonyl stress and glyoxalase enzyme system regulation in human skeletal muscle*. Am J Physiol Regul Integr Comp Physiol, 2018. **314**(2): p. R181-R190.
135. Rodrigues, T., et al., *GLP-1 improves adipose tissue glyoxalase activity and capillarization improving insulin sensitivity in type 2 diabetes*. Pharmacol Res, 2020. **161**: p. 105198.
136. Li, X., et al., *Generation of a GLO-2 deficient mouse reveals its effects on liver carbonyl and glutathione levels*. Biochem Biophys Rep, 2021. **28**: p. 101138.
137. Tabler, C.T., et al., *Loss of glyoxalase 2 alters the glucose metabolism in zebrafish*. Redox Biol, 2023. **59**: p. 102576.
138. Ranganathan, S., et al., *Genomic sequence of human glyoxalase-I: analysis of promoter activity and its regulation*. Gene, 1999. **240**(1): p. 149-55.
139. Peculis, R., et al., *Identification of glyoxalase 1 polymorphisms associated with enzyme activity*. Gene, 2013. **515**(1): p. 140-3.
140. Wu, J.C., et al., *Association of two glyoxalase I gene polymorphisms with nephropathy and retinopathy in Type 2 diabetes*. J Endocrinol Invest, 2011. **34**(10): p. e343-8.
141. Van Herreweghe, F., et al., *Tumor necrosis factor-induced modulation of glyoxalase I activities through phosphorylation by PKA results in cell death and is accompanied by the formation of a specific methylglyoxal-derived AGE*. Proc Natl Acad Sci U S A, 2002. **99**(2): p. 949-54.
142. de Hemptinne, V., et al., *Phosphorylation on Thr-106 and NO-modification of glyoxalase I suppress the TNF-induced transcriptional activity of NF-kappaB*. Mol Cell Biochem, 2009. **325**(1-2): p. 169-78.
143. Morgenstern, J., et al., *Phosphorylation of T107 by CamKIIdelta Regulates the Detoxification Efficiency and Proteomic Integrity of Glyoxalase I*. Cell Rep, 2020. **32**(12): p. 108160.
144. Mitumoto, A., et al., *Glyoxalase I is a novel nitric-oxide-responsive protein*. Biochem J, 1999. **344 Pt 3**: p. 837-44.

145. Mitumoto, A., et al., *Nitric oxide inactivates glyoxalase I in cooperation with glutathione*. J Biochem, 2000. **128**(4): p. 647-54.
146. de Hemptinne, V., et al., *Tumour necrosis factor induces phosphorylation primarily of the nitric-oxide-responsive form of glyoxalase I*. Biochem J, 2007. **407**(1): p. 121-8.
147. Birkenmeier, G., et al., *Posttranslational modification of human glyoxalase I indicates redox-dependent regulation*. PLoS One, 2010. **5**(4): p. e10399.
148. Morgenstern, J., et al., *Loss of Glyoxalase I Induces Compensatory Mechanism to Achieve Dicarboxyl Detoxification in Mammalian Schwann Cells*. J Biol Chem, 2017. **292**(8): p. 3224-3238.
149. Cortizo, F.G., et al., *The activity of glyoxylase I is regulated by glucose-responsive phosphorylation on Tyr136*. Mol Metab, 2022. **55**: p. 101406.
150. Su, R.C., et al., *Hyperglycemia induces key genetic and phenotypic changes in human liver epithelial HepG2 cells which parallel the Leprdb/J mouse model of non-alcoholic fatty liver disease (NAFLD)*. PLoS One, 2019. **14**(12): p. e0225604.
151. Deragon, M.A., et al., *Mitochondrial ROS prime the hyperglycemic shift from apoptosis to necroptosis*. Cell Death Discov, 2020. **6**(1): p. 132.
152. McCaig, W.D., et al., *Hyperglycemia potentiates a shift from apoptosis to RIP1-dependent necroptosis*. Cell Death Discov, 2018. **4**: p. 55.
153. Maher, P., et al., *Fisetin lowers methylglyoxal dependent protein glycation and limits the complications of diabetes*. PLoS One, 2011. **6**(6): p. e21226.
154. Gaul, S., et al., *Novel Nongenetic Murine Model of Hyperglycemia and Hyperlipidemia-Associated Aggravated Atherosclerosis*. Front Cardiovasc Med, 2022. **9**: p. 813215.
155. Lu, H., et al., *Hypercholesterolemia Induced by a PCSK9 Gain-of-Function Mutation Augments Angiotensin II-Induced Abdominal Aortic Aneurysms in C57BL/6 Mice-Brief Report*. Arterioscler Thromb Vasc Biol, 2016. **36**(9): p. 1753-7.
156. Wang, T., et al., *A "turn-on" fluorescent sensor for methylglyoxal*. J Am Chem Soc, 2013. **135**(33): p. 12429-33.
157. Ahmed, E.K., et al., *Protein modification and replicative senescence of WI-38 human embryonic fibroblasts*. Aging Cell, 2010. **9**(2): p. 252-72.
158. Rabbani, N. and P.J. Thornalley, *Dicarboxyls linked to damage in the powerhouse: glycation of mitochondrial proteins and oxidative stress*. Biochem Soc Trans, 2008. **36**(Pt 5): p. 1045-50.

159. Frischmann, M., et al., *Identification of DNA adducts of methylglyoxal*. Chem Res Toxicol, 2005. **18**(10): p. 1586-92.
160. Sruthi, C.R. and K.G. Raghu, *Methylglyoxal induces ambience for cancer promotion in HepG2 cells via Warburg effect and promotes glycation*. J Cell Biochem, 2022. **123**(10): p. 1532-1543.
161. Cox, R.A. and K. Kanagalingam, *A study of the hydrolysis of unfractionated reticulocyte ribosomal ribonucleic acid by pancreatic ribonuclease and its relevance to secondary structure*. Biochem J, 1967. **103**(2): p. 431-52.
162. McLellan, A.C., S.A. Phillips, and P.J. Thornalley, *The assay of methylglyoxal in biological systems by derivatization with 1,2-diamino-4,5-dimethoxybenzene*. Anal Biochem, 1992. **206**(1): p. 17-23.
163. Ridderstrom, M., et al., *Involvement of an active-site Zn²⁺ ligand in the catalytic mechanism of human glyoxalase I*. J Biol Chem, 1998. **273**(34): p. 21623-8.
164. Patel, M.S. and L.G. Korotchkina, *Regulation of the pyruvate dehydrogenase complex*. Biochem Soc Trans, 2006. **34**(Pt 2): p. 217-22.
165. Lee, J., et al., *The plasticity of the pyruvate dehydrogenase complex confers a labile structure that is associated with its catalytic activity*. PLoS One, 2020. **15**(12): p. e0243489.
166. Zhou, Z.H., et al., *Direct evidence for the size and conformational variability of the pyruvate dehydrogenase complex revealed by three-dimensional electron microscopy. The "breathing" core and its functional relationship to protein dynamics*. J Biol Chem, 2001. **276**(24): p. 21704-13.
167. Alcock, L.J., M.V. Perkins, and J.M. Chalker, *Chemical methods for mapping cysteine oxidation*. Chem Soc Rev, 2018. **47**(1): p. 231-268.
168. Percher, A., et al., *Mass-tag labeling reveals site-specific and endogenous levels of protein S-fatty acylation*. Proc Natl Acad Sci U S A, 2016. **113**(16): p. 4302-7.
169. Gamble, J. and G.D. Lopaschuk, *Glycolysis and glucose oxidation during reperfusion of ischemic hearts from diabetic rats*. Biochim Biophys Acta, 1994. **1225**(2): p. 191-9.
170. Kim, D., et al., *Methylglyoxal-Induced Dysfunction in Brain Endothelial Cells via the Suppression of Akt/HIF-1alpha Pathway and Activation of Mitophagy Associated with Increased Reactive Oxygen Species*. Antioxidants (Basel), 2020. **9**(9).
171. Seo, K., S.H. Ki, and S.M. Shin, *Methylglyoxal induces mitochondrial dysfunction and cell death in liver*. Toxicol Res, 2014. **30**(3): p. 193-8.

172. Di Loreto, S., et al., *Methylglyoxal induces oxidative stress-dependent cell injury and up-regulation of interleukin-1beta and nerve growth factor in cultured hippocampal neuronal cells*. Brain Res, 2004. **1006**(2): p. 157-67.
173. Peng, Z., et al., *Glyoxalase-1 Overexpression Reverses Defective Proangiogenic Function of Diabetic Adipose-Derived Stem Cells in Streptozotocin-Induced Diabetic Mice Model of Critical Limb Ischemia*. Stem Cells Transl Med, 2017. **6**(1): p. 261-271.
174. Nowotny, K., et al., *Advanced glycation end products and oxidative stress in type 2 diabetes mellitus*. Biomolecules, 2015. **5**(1): p. 194-222.
175. Wong, H.S., B. Benoit, and M.D. Brand, *Mitochondrial and cytosolic sources of hydrogen peroxide in resting C2C12 myoblasts*. Free Radic Biol Med, 2019. **130**: p. 140-150.
176. Mazat, J.P., A. Devin, and S. Ransac, *Modelling mitochondrial ROS production by the respiratory chain*. Cell Mol Life Sci, 2020. **77**(3): p. 455-465.
177. Chen, Q., et al., *Production of reactive oxygen species by mitochondria: central role of complex III*. J Biol Chem, 2003. **278**(38): p. 36027-31.
178. Vander Jagt, D.L., et al., *Inactivation of glutathione reductase by 4-hydroxynonenal and other endogenous aldehydes*. Biochem Pharmacol, 1997. **53**(8): p. 1133-40.
179. Schmitz, A.E., et al., *Methylglyoxal-Induced Protection Response and Toxicity: Role of Glutathione Reductase and Thioredoxin Systems*. Neurotox Res, 2017. **32**(3): p. 340-350.
180. Carlberg, I. and B. Mannervik, *Glutathione reductase*. Methods Enzymol, 1985. **113**: p. 484-90.
181. Chaplen, F.W., W.E. Fahl, and D.C. Cameron, *Evidence of high levels of methylglyoxal in cultured Chinese hamster ovary cells*. Proc Natl Acad Sci U S A, 1998. **95**(10): p. 5533-8.
182. Wu, G., et al., *The lactate receptor GPR81 mediates hepatic lipid metabolism and the therapeutic effect of metformin on experimental NAFLDs*. Eur J Pharmacol, 2022. **924**: p. 174959.
183. Engelbrecht, B., et al., *Impact of GLO1 knock down on GLUT4 trafficking and glucose uptake in L6 myoblasts*. PLoS One, 2013. **8**(5): p. e65195.
184. Chiba, T., et al., *Design and evaluation of azaindole-substituted N-hydroxypyridones as glyoxalase I inhibitors*. Bioorg Med Chem Lett, 2012. **22**(24): p. 7486-9.
185. Pettersen, E.F., et al., *UCSF ChimeraX: Structure visualization for researchers, educators, and developers*. Protein Sci, 2021. **30**(1): p. 70-82.

186. Roy, H., et al., *VEGF-A, VEGF-D, VEGF receptor-1, VEGF receptor-2, NF-kappaB, and RAGE in atherosclerotic lesions of diabetic Watanabe heritable hyperlipidemic rabbits*. FASEB J, 2006. **20**(12): p. 2159-61.
187. Konig, H., et al., *Effects of dasatinib on SRC kinase activity and downstream intracellular signaling in primitive chronic myelogenous leukemia hematopoietic cells*. Cancer Res, 2008. **68**(23): p. 9624-33.
188. Perez-Tomas, R. and I. Perez-Guillen, *Lactate in the Tumor Microenvironment: An Essential Molecule in Cancer Progression and Treatment*. Cancers (Basel), 2020. **12**(11).
189. Wu, Y., et al., *Lactate, a Neglected Factor for Diabetes and Cancer Interaction*. Mediators Inflamm, 2016. **2016**: p. 6456018.
190. Avogaro, A., et al., *Intracellular lactate- and pyruvate-interconversion rates are increased in muscle tissue of non-insulin-dependent diabetic individuals*. J Clin Invest, 1996. **98**(1): p. 108-15.
191. Chen, Y.D., B.B. Varasteh, and G.M. Reaven, *Plasma lactate concentration in obesity and type 2 diabetes*. Diabete Metab, 1993. **19**(4): p. 348-54.
192. Woerle, H.J., et al., *Mechanisms for abnormal postprandial glucose metabolism in type 2 diabetes*. Am J Physiol Endocrinol Metab, 2006. **290**(1): p. E67-E77.
193. Hockaday, T.D., *Metabolic studies in unaffected co-twins on non-insulin-dependent diabetics*. Br Med J (Clin Res Ed), 1981. **283**(6284): p. 142-3.
194. Berhane, F., et al., *Plasma Lactate Levels Increase during Hyperinsulinemic Euglycemic Clamp and Oral Glucose Tolerance Test*. J Diabetes Res, 2015. **2015**: p. 102054.
195. Brouwers, M.C., et al., *Elevated lactate levels in patients with poorly regulated type 1 diabetes and glycogenic hepatopathy: a new feature of Mauriac syndrome*. Diabetes Care, 2015. **38**(2): p. e11-2.
196. Ohlson, L.O., et al., *Risk factors for type 2 (non-insulin-dependent) diabetes mellitus. Thirteen and one-half years of follow-up of the participants in a study of Swedish men born in 1913*. Diabetologia, 1988. **31**(11): p. 798-805.
197. McFate, T., et al., *Pyruvate dehydrogenase complex activity controls metabolic and malignant phenotype in cancer cells*. J Biol Chem, 2008. **283**(33): p. 22700-8.
198. Kaplon, J., et al., *A key role for mitochondrial gatekeeper pyruvate dehydrogenase in oncogene-induced senescence*. Nature, 2013. **498**(7452): p. 109-12.

199. Strumilo, S., *Short-term regulation of the mammalian pyruvate dehydrogenase complex*. Acta Biochim Pol, 2005. **52**(4): p. 759-64.
200. Liu, Y.Q., J.A. Moibi, and J.L. Leahy, *Chronic high glucose lowers pyruvate dehydrogenase activity in islets through enhanced production of long chain acyl-CoA: prevention of impaired glucose oxidation by enhanced pyruvate recycling through the malate-pyruvate shuttle*. J Biol Chem, 2004. **279**(9): p. 7470-5.
201. Xu, J., et al., *Regulation of PDK mRNA by high fatty acid and glucose in pancreatic islets*. Biochem Biophys Res Commun, 2006. **344**(3): p. 827-33.
202. Maresch, C.C., et al., *Hyperglycemia induces spermatogenic disruption via major pathways of diabetes pathogenesis*. Sci Rep, 2019. **9**(1): p. 13074.
203. Queisser, M.A., et al., *Hyperglycemia impairs proteasome function by methylglyoxal*. Diabetes, 2010. **59**(3): p. 670-8.
204. Giustarini, D., et al., *Assessment of glutathione/glutathione disulphide ratio and S-glutathionylated proteins in human blood, solid tissues, and cultured cells*. Free Radic Biol Med, 2017. **112**: p. 360-375.
205. Applegate, M.A., K.M. Humphries, and L.I. Szewda, *Reversible inhibition of alpha-ketoglutarate dehydrogenase by hydrogen peroxide: glutathionylation and protection of lipoic acid*. Biochemistry, 2008. **47**(1): p. 473-8.
206. Dhananjayan, K., et al., *Activation of Macrophages and Microglia by Interferon-gamma and Lipopolysaccharide Increases Methylglyoxal Production: A New Mechanism in the Development of Vascular Complications and Cognitive Decline in Type 2 Diabetes Mellitus?* J Alzheimers Dis, 2017. **59**(2): p. 467-479.
207. Labun, K., et al., *CHOPCHOP v3: expanding the CRISPR web toolbox beyond genome editing*. Nucleic Acids Res, 2019. **47**(W1): p. W171-W174.
208. Doench, J.G., et al., *Optimized sgRNA design to maximize activity and minimize off-target effects of CRISPR-Cas9*. Nat Biotechnol, 2016. **34**(2): p. 184-191.
209. Chretien, D., et al., *An improved spectrophotometric assay of pyruvate dehydrogenase in lactate dehydrogenase contaminated mitochondrial preparations from human skeletal muscle*. Clin Chim Acta, 1995. **240**(2): p. 129-36.
210. Percher, A., E. Thinon, and H. Hang, *Mass-Tag Labeling Using Acyl-PEG Exchange for the Determination of Endogenous Protein S-Fatty Acylation*. Curr Protoc Protein Sci, 2017. **89**: p. 14 17 1-14 17 11.

8. Own publications

During my PhD, I co-authored the following publications:

Cortizo FG, Pfaff D, Wirth A, Schlotterer A, Medert R, Morgenstern J, Weber T, Hammer HP, Fleming T, Nawroth P, Freichel M, Teleman AA. *The activity of glyoxylase 1 is regulated by glucose-responsive phosphorylation on Tyr136*. Mol Metab. 2022 Jan;55:101406.

doi: 10.1016/j.molmet.2021.101406.

Sulaj A, Kopf S, Von Rauchaupt E, Kliemank E, Brune M, Kender Z, Bartl H, **Cortizo FG**, Klepac K, Han Z, Kumar V, Longo V, Teleman AA, Okun GJ, Morgenstern J, Fleming T, Szendroedi J, Herzig S, Nawroth P. *Six-Month Periodic Fasting in Patients With Type 2 Diabetes and Diabetic Nephropathy: A Proof-of-Concept Study*. J Clin Endocrinol Metab. 2022 Jul 14;107(8):2167-2181. doi: 10.1210/clinem/dgac197

Gegner HM, Mechtel N, Heidenreich E, Wirth A, **Cortizo FG**, Bennewitz Katrin, Fleming Thomas, Andressen C, Freichel M, Teleman AA, Hell R, Poschet G. *Deep Metabolic Profiling Assessment of Tissue Extraction Protocols for Three Model Organisms*. Front Chem. 2022 Apr 25;10:869732. doi: 10.3389/fchem.2022.869732.

Morgenstern J, Katz S, Krebs-Hauptenthal J, Chen J, Saadatmand A, **Cortizo FG**, Moraru A, Campos MC, Teleman AA, Backs J, Nawroth P, Fleming T. *Phosphorylation of T107 by CamKII δ Regulates the Detoxification Efficiency and Proteomic Integrity of Glyoxalase 1*. Cell Rep 2020 Sep 22;32(12):108160. doi: 10.1016/j.celrep.2020.108160.

9. Acknowledgements

I am sincerely thankful to my supervisor Prof. Dr. Aurelio Teleman for giving me the opportunity to work in an excellent scientific environment, for his guidance, for always having the time to discuss my ideas and for allowing me to pursue them.

I am also grateful with the others member of my PhD committee, Dr. Wilhelm Palm and Prof. Dr. Marc Freichel, for their time and interest in my work, which was substantially improved by their invaluable inputs. Additionally, I would like to thank PD. Dr. Tobias Dick for agreeing to be part of my PhD committee and taking the time to evaluate my work.

I extend my gratitude to all our collaborators in the SFB118 project, that were always willing to share resources and ideas that substantially improved the quality of my work. Especially, Dr. Thomas Fleming for his constructive discussions, the MG measurements and for the endless supply of MG.

One important part of my work was also done thanks to Dr. Aubry Miller, who synthesized the click MG and took the time to review methodological strategies with us.

My sincere gratitude goes also to all the past and present member of Teleman laboratory, for always being willing to hear me, help me and teach me. Especially, to my friend Mykola Roiuk whose conversations and enthusiasm made my days joyful. A special thanks also goes to my friend Dr. Hana Nuskova who patiently helped me with all the FACS and SeaHorse experiments.

I am extremely thankful to my friend Dr. Philipp Willnow for his invaluable help and for all the scientific discussions.

I am most grateful to Dr. Gianluca Figlia for his time, for his scientific input, for his advice, for always encouraging me and for his sincere friendship.

My last thank you goes to my friend Oriana for her support and to my husband Ernesto who patiently listened to me and encouraged me during my PhD.